PLANT LIPID TRAFFICKING: THE CELL BIOLOGY OF CUTICULAR LIPID EXPORT AND MEMBRANE CONTACT SITES OF *ARABIDOPSIS THALIANA*

by

Heather McFarlane

B.Sc., The University of British Columbia, 2006

M.Sc., McGill University, 2008

A THESIS SUBMITTED IN PARTIAL FULFILLMENT OF

THE REQUIREMENTS FOR THE DEGREE OF

DOCTOR OF PHILOSOPHY

in

THE FACULTY OF GRADUATE STUDIES

(Botany)

THE UNIVERSITY OF BRITISH COLUMBIA

(Vancouver)

January 2013

Abstract

The plant cuticle coats the primary aerial tissues of all land plants to provide protection against non-stomatal water loss. Though the biosynthesis of cuticular lipids is now relatively well understood, the mechanisms of cuticular lipid export remain unclear. The objective of this thesis was to characterize several transporters required for cuticular lipid export and to determine the route of cuticular lipid export from their site of synthesis inside the cell to their site of accumulation on the cell surface. Based on interaction studies between two ATP-binding cassette transporters (ABCG11 and ABCG12) and the chemical phenotypes of their mutants, a model for the influence of ABC dimerization on subcellular localization and substrate specificity of these transporters is presented in the context of cuticular lipid export (Chapter 2). Analysis of several well-characterized secretory pathway mutants further indicates that at least some cuticular lipids reach these plasma membrane transporters via vesicular trafficking through the Golgi apparatus (Chapter 3). Furthermore, these mutant studies reveal a form and function relationship between the structure of the endoplasmic reticulum (ER) and its biosynthetic capacity, with respect to lipid synthesis (Chapter 3). Finally, ER-plasma membrane contact sites are investigated as a possible second route of cuticular lipid export (Chapter 4). While the frequency of contact sites is not correlated with cuticular lipid export, it remains possible that lipid trafficking may occur at these sites. Isolation and proteomic analysis of these membrane sub-fractions reveals a possible role for ER-plasma membrane contact sites in lipid remodeling or recycling, rather than cuticular lipid export. Taken together, these results build a complete model of cuticular lipid export from the site of synthesis to the site of lipid accumulation.

Preface

The bulk of Chapter 2 has been published as: McFarlane, H.E., Shin, J.J., Bird, D.A., and Samuels, A.L. 2010. Arabidopsis ABCG transporters, which are required for export of diverse cuticular lipids, dimerize in different combinations. *The Plant Cell* 22: 3066-3075 © Copyright American Society of Plant Biologists, 2010 (www.plantcell.org). The bulk of the text and many of the figures (where noted) were reproduced with permission. Dr. David Bird and Prof. Lacey Samuels identified the research question. Dr. David Bird and Prof. Lacey Samuels and Heather McFarlane designed the research. Dr. David Bird and John Shin performed the confocal localization of ABCG11 and ACBG12 in the double mutants (Figure 2.3 A-C and E-G; Figure 2.5 A-C and E-G). Heather McFarlane performed all other experiments, analyzed the data, and wrote the manuscript with the assistance of the other three coauthors.

For Chapter 3, Prof. Lacey Samuels and Heather McFarlane identified the research question. Prof. Lacey Samuels and Heather McFarlane designed the research. Yoshi Watanabe, an undergraduate student under the supervision of Heather McFarlane, performed the cryoSEM (Figure 3.3A) and confocal localization of ABCG11 and ABCG12 in the double mutants (Figure 3.4 and Figure 2.8C). Kristen Chan, an undergraduate student under the supervision of Heather McFarlane, provided technical assistance with genotyping. Heather McFarlane performed all other experiments and analyzed the data.

For Chapter 4, Prof. Lacey Samuels, Prof. Anna Stina Sandelius, and Heather McFarlane identified the research question. Prof. Lacey Samuels and Heather McFarlane designed the research. Brad Ross, UBC bioimaging technician, and Laura van Bezouwen, an MSc candidate under the supervision of Heather McFarlane, collected the tomograms. Prof. Mats Andersson and Dr. Roberto De Michele assisted with two-phase partitioning, and Dr. Susana Gonzalez Fernandez-Nino assisted with free-flow electrophoresis and performed the mass spectrometry of membrane fractions. Miranda Meents, an MSc student under the supervision of Heather McFarlane, assisted with the data analysis of proteomics results (represented in Figure 4.8 and 4.9). Heather McFarlane performed all other experiments and analyzed the data.

Table of Contents

List of Tables

List of Figures

List of Symbols and Abbreviations

35Spro	Cauliflower mosaic virus promoter
A	Amperes
A_{280}	Absorbance at 280 nm
ABC	ATP-binding cassette
ABCG	ATP-binding cassette transporter, subfamily G
ABRC	Arabidopsis Biological Resource Centre
ADP	Adenosine diphosphate
AHA	Autoinhibited H^+ ATPase
aka	also known as
ANOVA	Analysis of variance
ARF	ADP-ribosylation factor
AT	Arabdiopsis thaliana
ATP	Adenosine triphosphate
ATT	Aberrant induction of type three genes
BCIP	5-Bromo-4-chloro-3-indolyl phosphate
BiFC	Bimolecular fluorescence complementation
BiP	Binding immunoglobulin protein
BODIPY	4,4-difluoro-4-bora-3a,4a-diaza-s-indacene
BON	Bonzai
c	Centi (prefix) - $1000^{-2/3}$
C	Carbon
°C	Degrees Celsius
C2	Calcium-dependent phospholipid binding
Ca^{2+}	Divalent calcium ion
CCD	charge-coupled device
CD	Cutin deficient
cDNA	Complementary DNA
CER	eceriferum
CERT	Ceramide transfer protein

CFL	Curly flag leaf
CLASP	CLIP-associated protein
CLIP	Class II-associated invariant chain peptide
CoA	Coenzyme A
COF	Cuticular defect and organ fusion
Col-0	Columbia-0
COP	Coat protein
cv	Cultivar
cYFP	carboxy-terminus of yellow fluorescent protein
CYP	Cytochrome P450
Da	Daltons
DGAT	Acyl-CoA:diacylglycerol acyltransferase
DMSO	Dimethyl sulfoxide
DNA	Deoxyribonucleic acid
dT	Deoxy thymidine
DTT	dithiothreitol
E	Einstein
e.g.	*exempli gratia*
ECH	Echidna
EDTA	ethylenediaminetetraacetic acid
EGTA	ethylene glycol tetraacetic acid
ELO	Elongation defective
ER	Endoplasmic reticulum
et al.	*et alii*
EYPF	Enhanced yellow fluorescent protein
FAA	Fatty acid activation
FAE	Fatty acid elongase
FAPP	Phosphatidylinositol-four-phosphate adaptor protein
FAT	Fatty acid transporter
FATP	Fatty acid transfer protein

FFAT	Two phenylalanine, acidic tract domain
FFE	Free-flow electrophoresis
FID	flame ionization detector
FM4-64	N-(3-triethylammoniumpropyl)-4-(6-(4-(diethylamino) phenyl) hexatrienyl) pyridinium dibromide
FRET	Fluorescent resonant energy transfer
FYVE	Forms aploid and binucleate cells1/*Caenorhabditis elegans* protein ZK632.12/carboxypeptidase Y-deficient/early endosome associated1 domain
g	grams
g_{max}	Maximum gravitational acceleration
GAP	GTPase activating proteins
GC	Gas-liquid chromatography
GDP	Guanosine diphosphate
GDSL	Glycine - aspartic acid – serine - leucine motif
GEF	guanine nucleotide exchange factor
GFP	Green fluorescent protein
GNL	Gnom-like
GPAT	sn-glycerol-3-phosphate 2-O-acyltransferase
GPI	Glycosylphosphatidylinositol
GTP	guanosine triphosphate
H^+	proton
HCl	Hydrochloric acid
HDEL	Histidine - aspartic acid- glutamic acid - leucine
HDG	Homeodomain glabrous
HeLa	Henrietta Lacks human cell line
HEPES	4-(2-hydroxyethyl)-1-piperazineethanesulfonic acid buffer
HPLC	High-performance liquid chromatography
Hs	*Homo sapiens*
HSP	Heat shock protein

hyp	Hypocotyl
i.e.	*id est*
IP_3	Inositol 1,4,5-trisphosphate
Ist	Increased sodium tolerance
k	Kilo (prefix) - 1000^1
KCl	Potassium chloride
KCR	Beta-ketoacyl reductase
KCS	3-keto-CoA synthase
KOH	Potassium hydroxide
L	Litre
LACS	long chain acyl-CoA synthetase
LC	Liquid chromatography
Ler	Landsberg erecta
ln	Natural logarithm ($\log_e$)
log	Logarithm
LOPIT	Localization of organelle proteins by isotope tagging
LTI6b	Low-temperature induced protein 6b
LTP	Lipid transfer protein
LTPG	Glycosylphosphatidylinositol-anchored lipid transfer protein
µ	Micro (prefix) - 1000^{-2}
m	Meters
M	Molar
MAH	Midchain alkane hydroxylase
MASCP	Multinational Arabidopsis steering committee proteomics subcommittee
MES	2-(N-morpholino)ethanesulfonic acid
mRFP	Monomeric red fluorescent protein
MS	Mass spectrometry
MYB	Myeloblastosis
n	Nano (prefix) - 1000^{-3}
Na	Sodium

NaOH	Sodium hydroxide
NBD	7-nitrobenz-2-oxa-1,3-diazol-4-yl
NBT	nitroblue tetrazolium
NSF	N-ethylmaleimide sensitive fusion protein
NRT	Nitrate transporter
NVJ	Nucleus-vacuole junction
nYFP	Amino-terminus of yellow fluorescent protein
ORAI1	Calcium release-activated calcium channel protein 1
ORP	Oxysterol binding protein related protein
OSH	Oxysterol binding protein homologue
OSBP	Oxysterol binding protein
OX	Overexpression
PAGE	Polyacrylamide gel electrophoresis
PAS	Pasticcino
pBLAST	Protein Basic Local Alignment Search Tool
PCR	Polymerase chain reaction
PDI	Protein disulfide isomerase
PEG	Polyethylene glycol
PH	Pleckstrin homology
PI	Phosphatidylinositol
PIns4P	Phosphatidylinositol 4-phosphate
PIP	Plasma membrane intrinsic protein
PM	Plasma membrane
ppm	Parts per million
Psd	Phosphatidylserine decarboxylase
PVA	Plant VAMP-Associated
PVC	Pre-vacuolar compartment
pro	Promoter
Q-TOF	quadrupole time-of-flight
R	Disease resistance

RAB	Ras superfamily monomeric G protein
RDR	RNA-dependent RNA polymerase
RHD	Root hair defective
RNA	Ribonucleic acid
RT-PCR	Reverse transcription polymerase chain reaction
s	Seconds
SAR	Secretion-associated rat sarcoma-related
Sc	*Saccharomyces cerevisiae*
SC	Spectral count
Scs	Vesicle-associated membrane protein-associated protein/Choline sensitivity suppressor protein
SD	Standard deviation
SDS	Sodium dodecyl sulfate
SE	Standard error
Sec	Secretory
SecGFP	Secreted green fluorescent protein
SEM	Scanning electron microscopy
Sey1	Synthetic enhancement of YOP1
SGS	Suppressor of gene silencing
SIRT	Simultaneous iterative reconstruction technique
SMP	synaptotagmin-like-mitochondrial-lipid binding protein
SNARE	Soluble N-ethylmaleimide-sensitive factor attachment protein receptor
ST	Sialyltransferase
STR	Stunted arbuscule
STIM	Stromal interaction molecule
SUBA	Subcellular localisation database for Arabidopsis proteins
SYT	Synaptotagmin
T-DNA	Transfer-deoxyribonucleic acid
TAIR	The Arabidopsis Information Resource
TBS	Tris-buffered saline

TBST	Tris-buffered saline with Tween-20
Tcb	Tricalbins
TEM	Transmission electron microscopy
TGD	Trigalactosyldiacylglycerol
TGN	*trans*-Golgi network
TMD	Transmembrane domain
TRAPP	Transport protein particle
Tris	Tris(hydroxymethyl)aminomethane
TRS	Transport protein particle subunit
Tsc	tuberous sclerosis complex
TVP	T-SNARE affecting a late Golgi compartment vesicle protein
UBC	Ubiquitin carrier protein/ubiquitin conjugating enzyme
UPR	Unfolded protein response
v	volume
V	Volts
V-PPase	vacuolar-type inorganic pyrophosphatase
Vac	Vacuole related
VAMP	vesicle-associated membrane protein
VAP	vesicle-associated membrane protein-associated protein
VLCFA	Very long chain fatty acid
VHA	Vacuolar H^+-ATPase
w	weight
WBC	White brown complex
WIN	Wax inducer
WSD	Wax ester synthase/diacylglycerol acyltransferase
YFP	Yellow fluorescent protein
YIP	YPT/Rab interacting protein
Yop1	YIP one partner
YPT	Yeast protein two

Acknowledgements

First and foremost, I would like to thank my supervisor, Prof. Lacey Samuels. Lacey has supported me with exceptional mentorship, training, advice, and kindness throughout my PhD and will always be an extraordinary role model.

My supervisory committee, Prof. Christopher Loewen, Prof. Ljerka Kunst, and Prof. Geoff Wasteneys have provided guidance, stimulating discussion, and new perspectives throughout this project. Several collaborators were kind enough to host me in their laboratories. Prof. Anna Stina Sandelius and Prof. Mats Andersson were my hosts at Göteborgs Universitet, where I learned two-phase partitioning to isolate plasma membranes. Prof. Wolf Frommer was my host at the Carnegie Institution at Stanford University and Dr. Joshua Heazelwood was my host at the Joint BioEnergy Institute, where the proteomic analysis was conducted and where I learned free-flow electrophoresis with their postdocs, Dr. Roberto de Michele and Dr. Susana Gozales-Fernandez-Nino.

All of the members of the Samuels lab, past and present, and indeed many members of the UBC Botany and Cell Biology communities have been exceptional colleagues and friends during my time at UBC. A list of everyone who has supported this work with technical assistance, thoughtful feedback, shared materials, and friendship would cover several pages, but I would particularly like to thank Teagen Quilichini, who was patient and kind enough to provide helpful comments on this entire document. Several MSc and undergraduate students provided outstanding technical support to this project: Kristen Chan, Miranda Meents, Jessica Mazzarolo, John Shin, Laura van Bezoewen, and Yoichiro Watanabe. From outside the Samuels lab, Patricia Lam, Shabnam Tavassoli, Dr. Delphine Gendre, and Prof. Hugo Zheng provided helpful comments and unpublished materials, the UBC Bioimaging Facility provided technical support, and my colleagues at Let's Talk Science were inspiring examples of balancing science with community outreach.

Funding for this work was provided in the form of an NSERC Canada Graduate Scholarship D3, a L'Oréal-UNESCO for Women in Science fellowship, a UBC Four-Year Fellowship, an NSERC Michael Smith CGS Foreign Study Supplement, a UBC International Research Mobility Grant, and a Department of Botany Entrance Scholarship.

Finally, I would like to thank my friends and family for their continued patience, support, and love.

Chapter 1: Introduction

1.1 Structure, function, and composition of the plant cuticle

Due to their sessile nature, plants must adapt to changes in their environments. The plant cuticle, which coats the primary aerial tissues of all land plants, plays a crucial role in water relations (Riederer and Schreiber, 2001). The cuticle, along with stomata, intercellular air spaces, extended root systems, and vascular tissue form the necessary set of adaptations that allowed prolific land colonization by vascular plants (Riederer, 2006). The cuticle protects against non-stomatal water loss. It also mediates biotic interactions and protects the plant against ultraviolet radiation (Riederer, 2006). Although the direct relationship between the cuticle and drought stress is unclear, water deficiency, salinity stress, and the plant stress hormone, abscisic acid, can all induce transcription of cuticle synthesis genes and increase the cuticular lipid load of treated plants (Kosma et al., 2009). Based on phenotypes of several cuticle biosynthesis and secretion mutants, the cuticle also seems to play an important developmental role in separating tissue layers, as plants with cuticle defects often display fusions between organs (Sieber et al., 2000).

The cuticle is primarily composed of cutin and waxes, but may contain other compounds, such as cutan and phenolics (Jetter et al., 2006). Electron microscopy of a variety of plant cuticles reveals several layers of cuticular material, distinguishable by their different electron densities. Often, the cuticle is coated by a layer of epicuticular wax, which may organize into a variety of crystal structures (Jeffree, 2006). Chemical analysis of the intracuticular and epicuticular waxes has revealed that waxes are primarily composed of very long chain fatty acids (VLCFAs) and their derivatives, which are all greater than 20 carbons in length (C20). Waxes may also contain other hydrophobic substances such as triterpenoids (Jetter et al., 2000; Jetter et al., 2006). There is significant diversity in the wax makeup among species, and within a single species depending on tissue type and age. For example, the cuticular wax of Arabidopsis thaliana stems is primarily composed of 29 carbon alkane (nonacosane), ketone (nonacosan-15-one), and secondary alcohol (nonacosan-15-ol), while leaf wax is composed of a more heterogeneous mixture of compounds with diverse acyl chain lengths and lacks mid-chain oxygenated alkanes (Jetter et al., 2006). In contrast, cutin is a polyester of long chain fatty acids and derivatives,

including 16 and 18 carbon dicarboxylic acids, ω-hydroxy, and epoxy fatty acids. Glycerol may also be an important component of the cutin matrix (Graça, et al., 2002; Nawrath, 2006; Pollard et al., 2008; Yeats et al 2012).

1.2 Biosynthesis of cuticular lipids

In order to investigate the transport mechanisms involved in cuticular lipid export, it is necessary to understand the key steps in biosynthesis of these lipids. The subcellular localization of the final biosynthetic steps can lend insight into the mechanism of trafficking, as the end of the final step of synthesis defines the beginning of transport.

1.2.1 Regulation of cuticular lipid synthesis

To produce a cuticle that covers all aerial tissues of the primary plant body, cuticular lipid biosynthesis is tightly regulated to occur only in the epidermis of aerial tissues, and to occur at highest levels during cell elongation/expansion, in order to ensure even cuticle deposition (Suh et al., 2005). The WAX-INDUCER1 (WIN1) transcription factor was originally identified in a transcription factor overexpression screen as having an increased cuticular wax load (Broun et al 2004). Further studies of an inducible WIN1 overexpression line revealed that the short-term targets of this transcription factor are actually cutin biosynthesis genes, and that WIN1 can bind the promoter of at least one cutin biosynthetic gene (Kannangara et al., 2007). Three MYB family transcription factors, MYB30, MYB41, and MYB96, plus another transcription factor, HDG1, and a WW-domain protein, CFL1, have also been implicated in the regulation of cuticle biosynthesis, however only MYB30 and MYB96 have been shown to directly activate promoters of wax or cutin biosynthetic genes (Cominelli et al, 2008; Raffaele et al., 2008; Seo et al., 2011; Wu et al., 2011). Interestingly, it seems that wax biosynthesis is also regulated via a pathway dependent upon the exosome (an RNA degrading complex) and the small RNA biogenesis machinery, including SGS3 and RDR1 (Hooker et al., 2007; Lam et al., 2012). The exact species or sequence of the small RNA involved in cuticular wax biosynthesis has not yet been identified.

1.2.2 Cutin biosynthesis

The precursors to cutin and to waxes are long chain fatty acids, either 16 or 18 carbons long. These fatty acids are synthesized in the plastid, and then transported to the endoplasmic reticulum (ER) (Ohlrogge and Browse, 1995; Samuels et al., 2008). Fatty acids destined to become incorporated into the cutin matrix must be activated by esterification to Coenzyme A (CoA), hydroxylated, and transferred to glycerol (Pollard et al., 2008). The hydroxylation steps are catalyzed by ER-localized cytochrome P450 monooxygenases (CYPs), including CYP86A2 (ATT1) and CYP86A8 (LACERTA), (Wellesen et al., 2001; Xiao et al., 2004), while transfer to CoA is catalyzed by the long chain acyl-CoA synthases, LACS1 and LACS2 (Bessire et al., 2007; Lü et al., 2009). Acyl chains are subsequently transferred to glycerol to form mono-acylglycerols, which could be catalyzed by two glycerol-3-phosphate acyltransferases, GPAT4 and GPAT8, as their expression was directly correlated with cutin levels and loss of function lead to decreased cutin levels (Li et al., 2007). Recent characterization of a glycine-aspartic acid-serine-leucine motif lipase/hydrolase (GDSL), CD1, from tomato has demonstrated that this extracellular cutin synthase can catalyze sequential additions of mono-acylglycerol to form a linear cutin polymer, and it is likely that homologous GDSL lipases may play a similar role in Arabidopsis (Yeats et al 2012). Indeed, a number of GDSL proteins are upregulated in the stem epidermis (Suh et al., 2005), suggesting that at least some of these candidates may correspond to Arabidopsis cutin synthase genes. The additional steps required to form a complex cutin matrix are unknown, though export of cutin monomers must precede full assembly of the cutin matrix (Pollard et al., 2008). According to this model, the cutin precursors that must be transported from the ER to the cell surface include mono-acylglycerols and long chain (C16 and C18) dicarboxylic acids, ω-hydroxy, and epoxy fatty acids.

1.2.3 Wax biosynthesis

Fatty acids destined to become wax molecules are elongated to very long chain fatty acids via the fatty acid elongase (FAE) complex, which is localized within the ER membranes (Ohlrogge and Browse, 1995). This complex consists of four subunits, each encoded by a separate gene. Elongation begins with condensation of malonyl-CoA to a

plastid-derived acyl-CoA chain by a β-ketoacyl-CoA synthase (KCS) enzyme to produce a β-ketoacyl-CoA. The KCSs that catalyze this rate-limiting, committed step to fatty acid elongation may be limited by their structure to a narrow range of chain lengths (Denic and Weissman, 2007), which could explain the diversity of KCS enzymes in Arabidopsis (4 yeast-type ELOs, and 21 plant specific FAE1-like enzymes) (Kunst and Samuels 2009). Consistent with this hypothesis, a number of KCS enzymes are expressed in stem epidermal cells and/or in other wax-synthesizing tissues (Joubès et al., 2008). VLCFA elongation specifically for wax synthesis in Arabidopsis epidermal cells is primarily catalyzed by CER6, a FAE1-type KCS enzyme (Millar et al., 1999). Other, still uncharacterized condensing enzymes may also be involved, though the strong phenotype of *cer6* mutants suggests that these would play a relatively minor role (Millar et al., 1999). The β-ketoacyl-CoA intermediate is subsequently reduced, dehydrated, and reduced again to yield an acyl-CoA that has been elongated by two carbons during one cycle. In Arabidopsis, these steps are catalyzed by KCR1 (a β-ketoacyl-CoA reductase), PAS2 (a β-hydroxyacyl-CoA dehydratase), and CER10 (a enoyl-CoA reductase), respectively (Zheng et al., 2005; Bach et al., 2008; Beaudoin et al., 2009). Unlike *CER6*, the expression patterns of these genes are not tissue-specific, and they are required for VLCFA elongation throughout the plant, primarily for sphingolipid synthesis (Zheng et al., 2005). These core components of the elongase complex are capable of interacting with each other and with an immunophillin-like protein, PAS1, which may act to scaffold the elongase complex (Bach et al., 2001; Roudier et al., 2010). For acyl elongation past 28 carbons, CER2, a protein of unknown function, is required in addition to the core elongase enzymes (CER6, KCR1, PAS2, and CER10) (Haslam et al., 2012; Pascal et al., 2013).

Following elongation, waxes are generated by modification of VLCFAs by one of two pathways: the acyl reduction pathway, which generates primary alcohols and wax esters, and the alkane-forming pathway, which generates alkanes, aldehydes, secondary alcohols, and ketones (Kunst and Samuels, 2009). In the acyl reduction pathway CER4 catalyzes the two-step reduction of a VLCFA to a primary alcohol and WSD1 catalyzes the formation of wax esters (Rowland et al., 2004; Li et al., 2008). In contrast to the acyl reduction pathway, the exact nature of the alkane-forming pathway remains unclear. Many mutants displayed

a reduction in the products of the alkane pathway, but either these genes have not been cloned, or the sequence of the cloned gene has not suggested an obvious biochemical role for these gene products in alkane formation (Kunst and Samuels, 2009). Recent heterologous expression of CER1 and CER3 in yeast has indicated that both proteins are required for alkane formation and that co-expression of a cytochrome B5 oxygenase can increase the efficiency of this reaction (Bernard et al., 2012). These data support the hypothesis that alkane formation may be a redox-dependent reaction via an aldehyde intermediate, rather than a hydrolytic reaction, as had been previously proposed (Cheesbrough and Kolattukudy, 1984; Schneider-Belhaddad and Kolattukudy, 2000; Bernard et al., 2012). However, the exact mechanism of this reaction remains unknown (Bernard et al., 2012; Sakuradani et al., 2013). Only the end-point of the alkane pathway has been characterized in detail; the MAH1 cytochrome P450 monooxygenase catalyzes either one or two-step oxidation of alkanes to generate secondary alcohols or ketones, respectively (Greer et al., 2007). Interestingly, the enzymes that catalyze all characterized steps of wax biosynthesis, from the initial condensation reaction of VLCFA elongation to the end points of wax ester, primary alcohol, secondary alcohol, and ketone formation have all been localized to the ER (Millar et al., 1999; Greer et al., 2007; Li et al., 2008; Figure 1.1). This implies that all wax components, including very long chain (C26-C30) alkanes, ketones, primary and secondary alcohols, aldehydes and esters must be transported from the ER to the cell surface to form the protective plant cuticle

1.3 Export of cuticular lipids

Following hydroxylation of fatty acids to cutin precursors, or fatty acid elongation and modification of VLCFAs into wax components in the ER, cuticular lipids must be transported to the cell surface. Clearly, the hydrophobic nature of cutin and waxes necessitates facilitated transport, as they are immiscible in the cytoplasm and in the cell wall. Furthermore, waxes are predicted to preferentially partition into membrane bilayers, based on mathematical modeling of Arabidopsis stem wax components in a phosphatidylcholine bilayer model (Coll et al., 2007). The exact mechanism of cuticular lipid export to the plant cell surface is unknown, but several proteins required for wax export have been characterized in Arabidopsis, including ATP-Binding Cassette

transporters (ABCs) and lipid transfer proteins (LTPs). The role of other, yet uncharacterized, components of cuticular lipid export may be hypothesized based on information from lipid trafficking paradigms in yeast and animal cells, and on gene expression data from cells undergoing significant cuticular lipid export.

Together, studies on the ABCG subfamily of ABC transporters (ABCGs) and LTPs have contributed to a model of wax and cutin movement across the plasma membrane and through the cell wall (Figure 1.1). However, the intracellular trafficking mechanisms responsible for moving cuticular lipids from their site of synthesis in the ER to their site of secretion at the apical plasma membrane remain unknown (Kunst and Samuels, 2009). Careful measurements have indicated that stem epidermal cells elongate more than 80-fold during stem growth, but the wax load per cm^2 remains constant (Suh et al., 2005). Therefore, cuticular lipids must be synthesized and secreted at an extraordinary rate, especially in the first 3 cm of the stem measured from the shoot apical meristem, where the cell elongation rate is the highest (Suh et al., 2005). Indeed, lipid flux calculations estimate a rate of 1.1 μg of cuticular lipid exported per cm^2 of epidermal surface area per hour, representing more than 60% of the epidermal cells' lipid metabolism at a given time (Suh et al., 2005). This extraordinary rate of cargo export provides an excellent model for studying lipid traffic because all components of the export machinery should be highly up-regulated. Interestingly, components of both vesicular trafficking via the Golgi apparatus (e.g. SNAREs and components of the exocyst complex), and non-vesicular trafficking (e.g SEC-14 and PITP type LTPs) are up-regulated in the stem epidermis during the height of cuticular lipid synthesis and secretion (Suh et al., 2005), suggesting that both vesicle trafficking and single-molecular lipid transfer may contribute to cuticular lipid export.

1.3.1 Lipid export via vesicular trafficking

Though the initial stages of cuticular lipid synthesis occur in the plastid, which is not linked to the secretory pathway, the final stages occur in the ER. Therefore, one hypothesis of cuticular lipid export is that these lipids may traffic to the plasma membrane via a vesicular route through the Golgi apparatus (Bertho et al., 1991; Bird, 2008; Samuels et al., 2008). Historically, secretion of protein cargo has been more experimentally accessible

than lipid secretion so the bulk of information on the plant secretory pathway has come from studies of protein secretion (Hawes and Satiat-Jeunemaitre, 2005). In plants, protein secretion follows a vesicular trafficking route. If cuticular lipids are secreted via vesicular traffic, they would likely take the same route as secreted proteins. Secreted proteins are synthesized in the ER, and then transported to the Golgi apparatus via COPII-coated vesicles, which fuse with the cis-Golgi cisternae. ER resident proteins are returned via COPI vesicles. Cargo progresses through the Golgi, either by cisternal maturation, or by vesicle budding and fusion from cisterna to cisterna in a cis-to-trans direction (Staehelin and Moore, 1995). Cargo leaves the trans-Golgi via more vesicles, possibly passing through the transitional trans-Golgi network (TGN), and cargo vesicles fuse with the plasma membrane (Kang et al., 2011). Most cell wall material, including pectins and hemicelluloses, is synthesized in the Golgi and trafficked by secretory vesicles (Cosgrove, 2005). Excess lipids resulting from vesicle fusion at the plasma membrane during cell wall secretion are recycled at least in part by endocytosis (Bolte et al., 2004; Dhonukshe et al., 2007). The plant endocytic pathway remains somewhat ill defined, but involves both endosomal compartments and the TGN (Robinson et al., 2008; Viotti et al., 2010).

1.3.1.1 Transport between the ER and the Golgi apparatus

The plant ER is a motile, highly complex network of tubules and sheets that undergoes continuous remodeling (Staehelin, 1997; Sparkes et al., 2009b). In a mature, vacuolated cell, most of the ER is confined to the thin layer of cortical cytoplasm between the tonoplast and the plasma membrane, as well as the perinuclear ER, and several trans-vacuolar strands. In younger developing cells that do not yet have a large central vacuole, the ER is more evenly distributed throughout the cell (Ridge et al., 1999). Components of the ER-Golgi trafficking machinery are relatively well conserved between eukaryotes. In yeast, COPII vesicles transport cargo from the ER to the Golgi apparatus. The COPII coat consists of five main components: Sar1 GTPase, Sec23/Sec24 inner coat, and Sec13/Sec31 outer coat (Antonny and Schekman, 2001; Hawes et al., 2008). Sequences for all of these components have been detected in the Arabidopsis genome, however most of these gene families have undergone significant expansion (Sanderfoot and Raikhel, 2003). A dominant-negative mutant of Arabidopsis SAR1 results in ER accumulation of both Golgi-

resident and vacuolar proteins, implicating SAR1 in ER exit, similar to its role in yeast (Takeuchi et al., 2000; Batoko et al., 2000; Nielsen et al., 2008). Mutants in Sec24 result in defects in both ER-Golgi protein trafficking and in ER morphology, including ER vesiculation and fragmentation (Faso et al., 2009; Nakano et al., 2009). These phenotypes imply that the morphology of the ER and its biological function are closely related. In contrast, studies of Arabidopsis ER shaping proteins, such as Reticulon/Yop1p and Atlastin/Sey1p related proteins have demonstrated that significant changes can occur in ER morphology without affecting protein trafficking to the Golgi apparatus (Tolley et al., 2007; Sparkes et al., 2010; Chen et al., 2011c).

Retrograde traffic from the Golgi apparatus to the ER is similarly conserved among eukaryotes. Genes encoding components of COPI coated vesicles show a larger proliferation than those encoding components of COPII vesicles (Sanderfoot and Raikhel, 2003), implying that some of these components may have acquired novel functions in plants. For example, GNOM-LIKE1 (GNL1) is a guanine-nucleotide exchange factor (GEF) for ADP-ribosylation factor (ARF) (i.e. an ARF-GEF) that is homologous to Sec7p in yeast. Like its yeast counterpart, GNL1 is required for modulation of ARFs during retrograde trafficking from the Golgi apparatus to the ER (Richter et al., 2007; Teh and Moore, 2007). However, another Arabidopsis Sec7p homologue, GNOM, is required for endosomal/post-Golgi trafficking, indicating that some of the gene duplications in the plant secretory pathway have allowed neofunctionalization of these components (Mayer et al., 1993; Geldner et al., 2003; Richter et al., 2007; Teh and Moore, 2007). Furthermore, two different populations of COPI-coated vesicles have been observed in association with the plant Golgi apparatus, and their position relative to the Golgi stacks suggests that one population may be involved in retrograde Golgi to ER transport, while the other may be involved in retrograde transport within the Golgi (Donohoe et al., 2007).

1.3.1.2 Post-Golgi trafficking

In contrast to ER-Golgi traffic, the Golgi apparatus and post-Golgi trafficking in plants is drastically different from yeast and animals. Unlike in animal cells, the plant Golgi apparatus is comprised of many (dozens to hundreds) separate Golgi stacks. Each of these Golgi stacks has a complete complement of biosynthetic enzymes, maintains its own cis-to-

trans polarity, and is capable of traveling along actin microfilaments at remarkable rates (Boevink et al., 1998; Nebenführ et al., 1999). Furthermore, the plant TGN is involved in secretion to the plasma membrane, the cell wall, and the vacuole, and it also acts as an early endosome (Viotti et al., 2010). Secretory vesicles may bud from trans-Golgi cisternae or from the TGN individually or as secretory vesicle clusters, and then travel through the cytoplasm to fuse with the plasma membrane (Preuss et al., 2006; Toyooka et al., 2009; Kang et al., 2011). The complexity of the plant TGN and the different roles that this compartment can play (secretion to the plasma membrane, vacuolar trafficking, early endosomal recycling) have made dissecting these roles of the TGN and their molecular mechanisms extremely complicated. However, two TGN-localized protein complexes have recently been identified as key components in secretion from the TGN to the plasma membrane and cell wall. The multiprotein transport particle protein II (TRAPP II) complex is required for secretion from the TGN, where it may act as a GEF, to the plasma membrane and the cell plate, but it is not required for endocytosis (Qi et al., 2011). However, the role of the TRAPP II complex in vacuolar trafficking has not been investigated (Qi et al., 2011). ECHIDNA/Tvp23 is a trans-Golgi/TGN localized protein of unknown function that is functionally conserved between yeast and Arabidopsis (Gendre et al., 2011). In Arabidopsis, ECH forms a complex with two members of the YIP family of RAB-interacting proteins, which is specifically required for pectin secretion to the cell wall but not for the vacuolar trafficking or endocytic functions of the TGN (Drakakaki et al., 2011; Gendre et al., 2013). Whether these two complexes act in the same pathway for secretion from the TGN remains unknown. Several routes of vacuolar trafficking from the TGN exist, and both clathrin-coated vesicles and non-clathrin vesicles are required for transport from the Golgi/TGN to the vacuole (Hohl et al., 1996; Hinz et al., 1999; Kang et al., 2011).

Several mechanisms have been proposed for directed vesicle trafficking through the cytoplasm including passive movement with cytoplasmic streaming, facilitated movement via the cytoskeleton, and positioning of the Golgi apparatus near the site of secretion (Nebenführ and Staehelin, 2001; Esseling-Ozdoba et al., 2008; Yang, 2008). These mechanisms could be especially important for the secretion of cuticular lipids, since the cuticle is only on the outer periclinal cell wall of epidermal cells, implying that cuticular lipid secretion must be polarized to this region of the cell. Studies of polysaccharide polar

secretion in seed coat epidermal cells have revealed that polysaccharide producing Golgi stacks are evenly positioned throughout the cytoplasm and do not accumulate near regions of polar secretion (Young et al., 2008). Although microtubules preferentially accumulate at the site of polar secretion, microtubule disorganization does not lead to a loss of polar secretion (McFarlane et al., 2008). In contrast, defects in either the microtubule or the actin cytoskeleton can cause defects in polarized tip growth and directional cell expansion (Ketelaar et al., 2003; Whittington et al., 2001; Gutierrez et al., 2009; Sampathkumar et al., 2013). Inhibition of myosin motors can cause defects in polarized secretion (Peremyslov et al., 2008). Whether vesicles travel directly along actin filaments, or whether actin is simply required to facilitate cytoplasmic streaming remains unclear (Esseling-Ozdoba et al., 2008).

Vesicle fusion with the plasma membrane (and other target membranes) likely involves a variety of tethering and fusion factors. In yeast, these factors include SNAREs and the exocyst complex; however the roles of these elements remain poorly defined in plants. While components of the exocyst complex have been immunolocalized to vesicles in close proximity to the plasma membrane (Wang et al., 2010) and genetic studies have implicated several exocyst components in polar secretion of pectins and in tip growth of pollen tubes (Hála et al., 2008; Kulich et al., 2010), other genetic studies of exocyst mutants have implicated at least part of this complex in recognition and rejection of self-incompatible pollen (Samuel et al., 2009). Together, these results suggest that large expansion of exocyst component-encoding genes in plants may have led to neo-functionalization of some of these genes. Similarly, SNAREs have undergone a large gene family expansion in plants (Sanderfoot and Raikhel, 2003). Specific SNAREs have been implicated in cell plate formation (Waizenegger et al., 2000), vacuolar trafficking (Sanderfoot et al., 2001), and ER-Golgi traffic (Chatre et al., 2005; El-Kasmi et al., 2011). However, many SNAREs remain to be characterized and the complete mechanism of vesicle tethering and fusion at the plasma membrane remains elusive.

1.3.1.3 Organelle identity in the secretory pathway

The flux of cargo through the secretory system implies that organelles are dynamic, yet each organelle is able to maintain its specific identity. This identity is distinguishable by both lipid composition and by protein markers. Many specific protein markers of

secretory compartments have been isolated and characterized. Some of these have an obvious biological function (e.g. mannosidase I removes mannose residues from cargo proteins in the cis and medial Golgi cisternae during N-linked glycan processing), while others are useful markers whose biological function remains elusive (e.g. Arabidopsis RabA4b localizes to the TGN, but its role there remains ill-defined) (Staehelin and Moore, 1995; Preuss et al., 2006; Donohoe et al., 2007). The most conspicuous lipid gradient in the plant secretory system is the gradient of the ratio of sphingolipids and sterols to phospholipids. This ratio is relatively low in the ER, which is enriched in phosphatidylcholine, and much higher in the plasma membrane (Moreau et al., 1998; Sperling et al., 2005).

Different compartments of the secretory pathway are also defined by specific species of phosphoinositide phosphates (Munnik and Nielsen, 2011). Since the Arabidopsis genome lacks components of canonical phosphoinositide signaling, such as the inositol 1,4,5-trisphosphate (IP_3) receptor and protein kinase C, it is likely that these lipids play some other role in the secretory pathway (Munnik and Nielsen, 2011). Indeed, disrupting these phosphoinositide distributions, either by titrating them using specific lipid binding domains or by disrupting their biosynthesis via genetic mutations, results in defects in the function and morphology of the endomembrane system (Vermeer et al., 2006; Thole et al., 2008; Zhao et al., 2010). Presumably, the distribution of phosphoinositides is maintained by localized biosynthesis and catabolism by various phosphoinositide phosphatases, phosphoinositide kinases, and phospholipases (Munnik and Nielsen, 2011), but targeted lipid trafficking may also be involved.

Similarly, the pH of the secretory organelles varies across the secretory pathway, with the lowest pH found in the apoplast and the vacuole (Gao et al., 2004). Golgi pH and lipid compositions are usually intermediate between the ER and post-Golgi compartments, implying that the Golgi serves as an important transitional mediator in the secretory pathway (Moreau et al., 1998; Nishi and Forgac, 2002). Mutants in either subunits of the TGN-localized vacuolar-type H^+-ATPase or Na^+/H^+ antiporters demonstrate the crucial importance of this pH gradient since these mutants are defective in cell growth and Golgi morphology (Dettmer et al., 2006; Brüx et al., 2008; Bassil et al., 2011). Similarly, disrupting sterol or sphingolipid composition of the secretory pathway can have dramatic

effects on cell polarization, Golgi morphology, and plant development (Grebe et al., 2003; Willemsen et al., 2003; Zheng et al., 2005; Chen et al., 2006; Chen et al., 2008; Dietrich et al., 2008; Men et al., 2008; Markham et al., 2011).

1.3.1.4 Retrograde trafficking

In order to maintain the specific complements of resident proteins and lipids in each organelle of the secretory pathway there must be also retrograde trafficking. Experiments using inhibitors of clathrin-coated vesicle formation have demonstrated that recycling from the plasma membrane can occur by both clathrin-coated vesicles (Aniento and Robinson, 2005; Dhonukshe et al., 2007; Moscatelli et al., 2007), and via clathrin-independent pathways (De Caroli et al., 2011; Bandmann and Homann, 2012; Li et al., 2012). In plants, the TGN can act as an early endosome (Viotti et al., 2010), however other endosomal compartments, such as the one defined by the ARF-GEF GNOM, also exist (Geldner et al., 2003; Kleine-Vehn et al., 2006). Further recycling from the endosome/TGN to the Golgi/ER is required for some proteins, such as Golgi-resident proteins, and may be accomplished via a subset of COPI-coated vesicles (Donohoe et al., 2007).

1.3.1.5 Tools for studying lipid trafficking

The abundance of experimental tools available for studying proteins and polysaccharides, including GFP-fusion proteins, and protein-specific and polysaccharide-specific antibodies have led to many studies on secretion of proteins and polysaccharides. Similar markers are still lacking for most lipids, so few studies of lipid traffic in plant cells have been performed. Despite caveats concerning its use (Jelínková et al., 2010), an amphiphilic, steryl dye, FM4-64, is the most commonly employed lipid dye in plant research (Bolte, et al., 2004). Careful studies of FM4-64 uptake have demonstrated that it labels the endocytic pathway from the plasma membrane to the TGN/early endosome, to the vacuole, and that FM4-64 uptake is likely an active process since it is decreased upon cold stress or treatment with metabolic inhibitors (Bolte, et al., 2004; Viotti et al., 2010). However, it remains a topic of debate whether FM4-64 uptake is a clathrin-mediated process (Aniento and Robinson, 2005; Dhonukshe et al., 2007; Jelínková et al., 2010; De Caroli et al., 2011). Fluorescent resonant energy transfer (FRET) analysis of FM4-64 and

cytosolic GFP has demonstrated that this dye is not exchanged between membrane leaflets (Griffing, 2008) and microinjection of FM4-64 into plant cells has demonstrated that it will only partition into (and fluoresce in) the non-cytosolic face of membranes (van Gisbergen et al., 2008). Other studies have employed 7-nitrobenz-2-oxa-1,3-diazol-4-yl (NBD) and 4,4-difluoro-4-bora-3a,4a-diaza-s-indacene (BODIPY) tagged lipids. Since these fluorescent tags are incorporated into specific lipids (such as sphingomylein or phosphatidylcholine), they provide an opportunity to monitor these particular lipids (Grabski et al., 1993, Lisboa et al., 2008). Unfortunately, some of these probes are metabolized in plant cells, making studies of their localizations difficult to interpret. For instance, NBD-phosphatidylcholine, which seems to incorporate into the ER, is rapidly cleaved to NBD-diacylglycerol, thus drastically altering any interpretation of studies employing this probe (Grabski et al., 1993). The chemical simplicity of most lipids, especially cuticular lipids, makes them very difficult to visualize in live cells. However, genetically encoded fluorescent sensors have been developed for several specifically modified lipids by adding a fluorescent protein to a specific lipid-binding domain (Munnik and Nielsen, 2011). For example, YFP linked to two tandem FYVE domains has been used to detect phosphatidylinositol-3-phosphate, while YFP-PH domain can detect phosphatidylinositol-4-phosphate, and these probes have been used to determine the specific subcellular localizations of these lipids and to infer their function (Vermeer et al., 2006; Kusano et al., 2008; Thole et al., 2008; Vermeer et al., 2008). Other membrane probes, such as polyene-lipids and coumarins, are promising as future lipid probes but have not yet undergone rigorous testing in plant cells (Kuerschner, et al., 2004; Signore et al., 2010).

1.3.2 Lipid export via non-vesicular traffic

Recent studies of lipid trafficking have presented an alternate hypothesis to vesicular export of cuticular lipids: some lipids travel via non-vesicular pathways that do not require canonical vesicle budding and fusion machinery (Levine and Loewen, 2006; Benning et al., 2006). Even small molecule (e.g. Ca^{2+}) diffusion and lipid exchange between leaflets of a bilayer are included by the most general definition of non-vesicular traffic, since these movements do not require vesicle formation or fusion (Levine, 2004; Holthius and Levine, 2005). However, discussions of non-vesicular lipid trafficking are often more

narrowly defined as inter-bilayer transfer of lipids. The general model for non-vesicular lipid trafficking involves a lipid transfer protein (LTP) that binds a single lipid molecule in its hydrophobic pocket to facilitate lipid exchange across the cytosolic space between two bilayers (Figure 1.2). While lipids are certainly trafficked through the plant cell via vesicular traffic (see above), non-vesicular traffic likely also occurs in plant cells. Notably, there is no decisive evidence of vesicular traffic between the plastid, which is the primary site of fatty acid synthesis in plants (Ohlrogge and Browse, 1995), and the ER, which is a key site of membrane lipid synthesis; thus, non-vesicular lipid trafficking may be involved in fatty acid delivery from the plastid to the ER (Benning et al 2006).

It has been hypothesized that the efficiency of non-vesicular traffic could be improved if modification of the lipid at the destination membrane occurs in order to create a metabolic sink (Levine, 2004). In the context of cuticular lipid transport, this is the model that has been proposed for extracellular cutin monomer transport and polymerization into the cutin matrix (Yeats et al., 2012), and it may also apply to wax export and crystallization on the cell surface. Efficacy of non-vesicular trafficking would also be significantly increased if it occurs at regions of close association between membranes, called membrane contact sites (Levine, 2004). A variety of membrane contact sites are proposed to exist between the ER and many other organelles because the ER is highly dynamic, organized into discrete subdomains, and found throughout the cell (Hepler et al., 1990; Staehelin 1997; Holthius and Levine, 2005; Shockey et al., 2006; English et al., 2009; Sparkes et al., 2009b; Gidda et al., 2011; Figure 1.3). These contact sites are usually defined as gaps of 15 nm or less between membranes, and therefore involve ribosome exclusion from the surface of the ER (Toulmay and Prinz, 2011).

1.3.2.1 ER contact sites with endosymbiotic organelles

One of the best-characterized types of membrane contact sites in yeast and animals are ER-mitochondrion contact sites. These contact sites have been detected by fluorescence microscopy and TEM, and they have been modeled in three dimensions using both reconstruction of serial sections and tomography (Achleitner et al., 1999; de Brito and Scorrano, 2008). These subdomains of the ER presumably serve to connect the mitochondria to lipid trafficking because vesicular trafficking has not been detected

between the secretory pathway and endosymbiotic organelles (Levine and Loewen, 2006). Indeed, biochemical purification and characterization of these sites in yeast revealed that they were specifically enriched in enzymes that are required for synthesis of mitochondrial lipids (Gaigg et al., 1995). *In vitro* transport of phosphatidylserine from its site of synthesis in the ER to the mitochondria is not dependent on cytosolic factors or ATP, but is sensitive to proteinase treatment (Achleitner et al., 1999). This indicates that transport through ER-mitochondria contact sites is distinct from vesicle trafficking (which requires cytosolic factors and ATP) and that it is protein-mediated. Further studies have focused on characterizing the proteins that bridge these mitochondria to ER interactions, and a variety of proteins have been implicated in this process in both yeast and animals (Levine and Loewen, 2006). Most recently, a synthetic protein, consisting of GFP inserted between a mitochondrial targeting sequence and an ER targeting sequence, was employed in a screen for lethal or nearly lethal yeast mutants that can be complemented by this construct. This screen identified four proteins required for maintenance of ER-mitochondria contact sites. Interestingly, mutants in any one of these components phenocopied mutants in Psd2, a phospholipid biosynthetic gene, supporting the hypothesis that protein-mediated contact sites are involved in lipid transfer between the ER and the mitochondrion (Kornmann et al., 2009). Indeed, a recent study of ER-shaping proteins in yeast, such as reticulons and Sey1p, revealed that, together with the proteins identified by Kornmann et al. (2009), these proteins play a role in facilitating lipid exchange between the ER and mitochondria (Voss et al, 2013). However another study has implicated these genes in the unfolded protein response, implying that ER-mitochondria contact sites may play other roles in yeast, beyond lipid transport (Jonikas et al., 2009)

Similar to ER-mitochondria contact sites, ER-plastid contact sites are implicated in lipid transfer between these two organelles during lipid synthesis (Andersson et al., 2007). Plastid-specific thylakoid membrane lipids, which house the photosynthetic apparatus, are synthesized by two separate pathways, one that is entirely contained within the plastid, and a second that depends on lipid transfer from the plastid, to the ER, then back to the plastid (Ohlrogge and Browse, 1995). Therefore when the plastid-resident lipid synthesis pathway is disrupted, lipid transfer between the plastid and the ER is primarily responsible for thylakoid lipid biosynthesis (Kunst et al., 1988; Awai et al., 2006a). Because there is no

characterized vesicular traffic between the ER and the plastid, it has been hypothesized that all of this lipid transfer occurs via non-vesicular traffic though ER-plastid contact sites. Indeed, ER-plastid contact sites have been observed in TEM (Staehelin, 1997), and have been biochemically isolated (Andersson et al., 2007). Like ER-mitochondria contact sites, ER-plastid contact sites are biochemically distinct from the typical ER-derived microsomes (Andersson et al., 2007). Studies employing an optical scalpel and optical tweezers have demonstrated that the ER membranes that co-purify with plastids are strongly attached to the plastid, suggesting a protein-mediated attachment rather than an accidental association that may have occurred if plastids were simply contaminated with ER membranes (Andersson et al., 2007). An outer plastid membrane-localized protein of unknown function, Trigalactosyldiacylglycerol4 (TGD4) and a bacterial-type ABC transporter in the inner plastid membrane (TGD1, TGD2, and TGD3) are required for lipid exchange between the ER and the plastid (Xu et al., 2003; Awai et al., 2006a; Awai et al., 2006b; Lu et al., 2007; Xu et al., 2008). The current working model for this complex is that TGD4 transports phosphatidic acid from the ER to the outer plastid membrane and the TGD1/TGD2/TGD3 complex transfers it into the inner plastid membrane, where it is modified to a thylakoid membrane lipid (Roston et al, 2011; Roston et al, 2012; Wang et al., 2012). Consistent with a role for ER-plastid contact sites in lipid transfer, stromules (extensions of the plastid inner and outer membranes) are induced by stress treatments that may require lipid remodeling (Gray et al., 2012). These stromules extend along ER tubules, possibly to increase the surface area available for ER-plastid contact sites (Schattat et al., 2011). Curiously, mutant studies have inferred that the TGD1-4 proteins are involved only in lipid transfer from the ER to the plastid but not from the plastid to the ER (Xu et al., 2010). Since lipid transfer in both directions is required in plants, there may remain uncharacterized components of ER-plastid contact sites. Indeed, an ER localized ABC transporter, ABCA9, has been implicated in fatty acid transfer from the plastid to the ER during seed storage oil synthesis, though whether this protein functions at a ER-plastid contact site has not yet been investigated (Kim et al., 2013).

1.3.2.2 ER contact sites with non-endosymbiotic organelles

Contact sites have also been characterized between the ER and other organelles, including the Golgi apparatus, the vacuole, and the peroxisome. In yeast, non-vesicular lipid traffic between the ER and the peroxisome has also been characterized (Raychaudhuri and Prinz, 2008). The so-called nucleus-vacuole junction (NVJ) in yeast is a specific subdomain of the nuclear envelope, which is continuous with the ER and in physical contact with the vacuole. This contact site is maintained by an interaction between the vacuole membrane-localized Vac8p and the nuclear envelope-localized Nvj1p, but also contains Osh1p, an LTP that may also act as a lipid sensor, and Tsc3p, a yeast enoyl-CoA reductase (Pan et al., 2000; Elbaz and Schuldiner, 2011). Interestingly, the Arabidopsis enoyl-CoA reductase, CER10, does not localize to any analogous nuclear-vacuolar junction in plant cells, but when it is expressed in yeast its localization is confined to this region of the cell (Zheng et al., 2005).

In animals, contact sites between the ER and the trans-Golgi are enriched in three types of LTPs: ceremide transfer proteins (CERTs), oxysterol binding proteins (OSBPs), and four-phosphate adaptor proteins (FAPP2s), each of which presumably have targeting motifs for both compartments (D'Angelo et al., 2008). Ceramide, the precursor to all animal sphingolipids, is synthesized at the ER, but ceramide modification to the two most common classes of sphingolipids, sphingomyelin and glucosylsphingolipids, occurs only in the lumen of the Golgi apparatus (Levine, 2007) and synthesis of these lipids requires non-vesicular traffic via CERT or FAPP2, respectively (Hanada et al., 2003; D'Angelo et al., 2007; Halter et al., 2007; Hanada et al., 2009). An intracellular glycosphingolipid transfer protein has been identified in plants and has *in vitro* glycosphingolipid binding and transfer activity, however its biological role and *in vivo* activity remain uncharacterized (West et al., 2008). Despite the presence of vesicular traffic between the ER and the Golgi apparatus, contact sites between these organelles are also involved in lipid transfer between the ER and the Golgi apparatus, suggesting that non-vesicular trafficking may be a common paradigm of lipid transfer between membranes.

1.3.2.3 ER contact sites with the plasma membrane

Lipid transfer from the ER to the plasma membrane may also occur via a non-vesicular route. ER-plasma membrane (ER-PM) contact sites have been identified in yeast, animals, and plants. Reconstruction of TEM serial sections into a three dimensional model of yeast cells have revealed that thousands of these contact sites may occur in a single cell (Pichler et al., 2001; West et al., 2011). Biochemical characterization of ER-PM contact sites showed that they are enriched in enzymes required for synthesis of plasma membrane lipids (Pichler et al., 2001). Functionally, positioning of cortical ER has been implicated in creating zones of exclusion for both endocytosis and midplane selection during fission yeast cell division (Zhang et al., 2010; Stadalova et al., 2012; Zhang et al., 2012). In mammals, ER-PM contact sites, specifically between the sarcoplasmic reticulum and the plasma membrane, are required for Ca^{2+} dynamics during muscle contraction and contain the calcium channels stromal interaction molecule 1 (STIM1) in the ER and Calcium release-activated calcium channel protein 1 (ORAI1) in the PM (Orci et al., 2009; Carrasco and Meyer, 2011; Asghari et al., 2012).

In yeast, contact sites may also play an important role in sterol transport; using a transport screen that relied on the uptake of exogenously applied sterols and their subsequent esterification in the ER, both ABC transporters and oxysterol binding protein (OSBP)-related LTPs (OSHs) were identified as components of the sterol transport machinery (Li and Prinz, 2004; Raychaudhuri et al., 2006). This transport was independent of Sec18p (also known as NSF, which is essential for most vesicular trafficking) indicating that this pathway is non-vesicular (Li and Prinz, 2004; Raychaudhuri et al., 2006). Although the relationship between ABC transporters and LTPs in non-vesicular traffic remains poorly characterized (Sullivan et al., 2009), there is an interesting symmetry between working models for the activity of ABC transporters and LTPs in sterol uptake in yeast, and wax export in Arabidopsis (Samuels and McFarlane, 2012; see sections 1.4.3 below).

In addition to their putative role in non-vesicular traffic between the ER and the plasma membrane (Li and Prinz, 2004; Raychaudhuri et al., 2006), OSHs have also been implicated in lipid sensing (Beh et al., 2009) and polar secretion (Alfaro et al., 2011). A recent report has integrated these two functions by demonstrating that OSH proteins

participate in an ER-PM contact site complex that is required for an ER-localized phosphatase to convert plasma membrane-localized phosphatidylinositol-4-phosphate (PIns4P) to phosphatidylinositol (PI) (Stefan et al., 2011). For this lipid modification in *trans* to occur, at least one OSH and the yeast vesicle-associated membrane protein (VAMP)-associated proteins (VAPs), Scs2p and Scs22p, are required to form a bridge between the ER and the plasma membrane (Stefan et al., 2011). Scs2p and Scs22p are ER-localized proteins that can associate with LTPs (including members of the OSH family) via their FFAT domains (Loewen et al., 2003; Loewen and Levine, 2005). Mutants in these VAPs display defects in cortical ER association with the plasma membrane in both light and electron microscopy (Loewen et al., 2007) and an increase in PIns4P (Stefan et al., 2011). Thus, OSH proteins can interact with plasma membrane PIns4P (via their PH domains) and ER-localized VAPs (via their FFAT domains) and stimulate ER-localized phosphatase activity on plasma membrane-localized lipids (Stefan et al., 2011). Importantly, while the human homologue to Scs2p, HsVAP-A, can bind FFAT domains (Loewen et al., 2003) it can only partially complement *scs2 scs22* mutants, implying that VAPs play additional roles in yeast, compared to other eukaryotes (Loewen and Levine, 2005).

The Arabidopsis genome contains homologous proteins (12 OSH-related proteins, or ORPs, and 7 plant VAP homologues, or PVAs); ORP3a can bind plant sterols and interacts with PVA12 in the ER, suggesting that some OSH/VAP behaviour might be conserved between yeast and plants (Saravanan et al., 2009). Two plant ORPs have been implicated in interactions with protein kinases, implying that plant OSH proteins may be more closely involved in lipid sensing/signaling than lipid remodeling (Skirpan et al., 2006; Berendzen et al., 2012). However, under phosphate-limiting conditions plants must adjust their plasma membrane composition by increasing the proportion of galactolipids and other non-phosphorous-containing membrane lipids (Andersson et al., 2003; Andersson et al., 2005). The first step in this remodeling is the rapid cleavage of the phosphate head group to release diacylglycerol, which is rapidly transported to the ER (Grabski et al., 1993; Tjellström et al., 2008). Interestingly, this phospholipid remodeling occurs only on the cytosolic leaflet of the plasma membrane (Tjellström et al., 2010), which is predicted for non-vesicular trafficking and/or lipid remodeling in *trans* at membrane contact sites. Consistent with this hypothesis, another lipid remodeling enzyme, lyso-

phosphatidylcholine acyltransferase, is preferentially localized to regions of the plasma membrane that are associated with the ER (Larsson et al., 2007), but other components of these contact sites have not been identified.

To date, several protein-protein interactions bridging the plasma membrane and the ER have been identified, but the nature of these proteins suggest that these interactions may be transient, and therefore not responsible for anchoring the ER to the plasma membrane (Levine and Loewen, 2006; Stefan et al., 2011). Overexpression of a truncated version of yeast Ist2p in HeLa cells can induce cortical ER formation, suggesting that Ist2 may play a role in ER-PM contact site formation (Lavieu et al., 2010). Although it remains unclear whether Ist2p participates in ER-PM contact sites under normal conditions (Toulmay and Prinz, 2011; Wolf et al., 2012), overexpression of this domain can rescue the cortical ER defects of *Scs2 Scs22* double mutants (Zhang et al., 2012). Recently, proteins containing synaptotagmin-like-mitochondrial-lipid binding protein (SMP) domains have been localized exclusively to yeast membrane contact sites (Toulmay and Prinz, 2012). Of the seven SMP domain proteins in yeast, one localizes to the nuclear-vacuolar junction, three to ER-mitochondria contact sites (Kornmann et al., 2009), and three to ER-PM contact sites (Toulmay and Prinz, 2012). Consistent with the absence of a nuclear-vacuole junction in plants (Zheng et al., 2005) and the reduced importance of ER-mitochondria contact sites in favour of ER-plastid contact sites (Benning et al., 2006), a pBLAST search of the Arabidopsis genome (Altschul et al., 1997) reveals only homologues to the ER-PM contact site SMP proteins, called tricalbins in yeast, and annotated as synaptotagmins in plants. Functional characterization of plant synaptotagmins is limited, however they have been implicated in several processes that may require close communication between the ER and the plasma membrane, including cell-to-cell movement of viral particles via plasmodesmata, freezing tolerance, and maintenance of plasma membrane integrity (Schapire et al., 2008; Yamazaki et al., 2008; Lewis and Lazarowitz, 2010).

ER-PM contact sites have only been preliminarily characterized in plants; TEM has been employed to describe the morphology of these sites (Staehelin, 1997), and they have been biochemically isolated (Larsson et al., 2007). Though they have been hypothesized to play a role in membrane recycling from the plasma membrane, very little functional characterization of ER to plasma membrane contact sites has been undertaken in plants

(Staehelin and Chapman, 1987; Staehelin, 1997; Larsson et al., 2007). Because the main cuticular lipid species of Arabidopsis stems (C29 alkane) is hypothesized to partition into the hydrophobic phase of the bilayer (Coll et al., 2007), any lipid motifs that may interact with secretory vesicles and cargo-binding proteins might be shielded. In contrast, non-vesicular traffic via LTPs could extract specific lipids directly from bilayers and could therefore provide a mechanism to transport cuticular lipids from their site of synthesis in the ER to their site of secretion at the plasma membrane (Bird, 2008). Consistent with this hypothesis, a significant proliferation of ER, including ER extensions towards the site of wax secretion, has been observed during light-induced wax synthesis in *Sorghum bicolor* (Jenks et al., 1994). Furthermore, a number of putative non-vesicular trafficking components (e.g. LTPs) are up-regulated in the stem epidermis during cuticular lipid synthesis and secretion (Suh et al., 2005). Indeed, recent studies have demonstrated that several long chain acyl-CoA synthases (LACS) have the capacity to rescue yeast mutants that are defective in either LACS activity (*faa1Δ* and *faa4Δ*; defective in both *LACS* homologues in yeast) or non-vesicular traffic between the plasma membrane and the ER (*fat1Δ*; defective in the single fatty acid transporter homologue in yeast) (Pulsifer et al., 2012). These results imply that the *LACS* genes, which have previously been implicated in cuticular lipid synthesis (Lü et al., 2008), may actually be involved in non-vesicular trafficking of cuticular lipids. However, only circumstantial evidence currently exists in favour of non-vesicular trafficking of cuticular lipids from the ER to the plasma membrane.

1.3.3 Cuticular lipid export from the plasma membrane

1.3.3.1 Cuticular export across the plasma membrane via ABC transporters

Following trafficking to the plasma membrane, cuticular lipids must travel across the plasma membrane and through the cell wall before assembling into the cuticle and epicuticular waxes on the cell surface. To date, four ATP-binding cassette (ABC) transporters, ABCG11, ABCG12, ABCG13 and ABCG32 have been characterized as components of the cuticle export machinery (Pighin et al., 2004; Bird et al., 2007; Ukitsu et al., 2007; Lou et al., 2007; Panikashvili et al., 2007, Panikashvili et al., 2011; Bessire et al.,

2011). ABC family transporters bind and hydrolyze ATP in order to induce a conformational change to drive the transport of a substrate across a membrane. Each full transporter has two transmembrane domains (TMDs), consisting of several transmembrane helices, and two nucleotide-binding domains, consisting of characteristic ATP binding and hydrolysis motifs (Higgins, 2001). The ABC family in Arabidopsis contains more than 120 members belonging to 8 sub-families (Verrier et al., 2008; Figure 1.4). Interestingly, three of the four ABC transporters that have been implicated in cuticle export are members of the WBC-type ABCG sub-family. These ABCGs are half transporters, that is, they contain only one nucleotide binding domain and one TMD. Therefore, they must dimerize with other ABCGs, either as homodimers or as heterodimers, in order to form a functional transporter (Higgins, 2001). In contrast, ABCG32 is a full transporter of the same ABCG family; while *ABCG32* shares homology to the half-transporter *ABCG* genes, it encodes both TMDs and both nucleotide-binding domains as a single peptide. In animal systems, half- and full-transporter ABCGs have been implicated in lipid substrate transport. Drosophila WHITE, SCARLET, and BROWN half-transporters act together in different combinations to transport eye pigment precursors into pigment granules (Sullivan and Sullivan, 1975; Sullivan and Sullivan, 1979; Sullivan et al., 1980). Similarly human ABCG5 and ABCG8 dimerize to export sterols from the intestine (Berge et al., 2000), and human ABCG2/Breast Cancer Resistance Protein homodimerizes to confer multidrug resistance upon cells (Tarr et al., 2009).

Historically, the first characterized component of the cuticle export machinery was ABCG12 (also known as CER5) (Pighin et al., 2004). Mutants in this gene were originally isolated in the Koornneef lab as part of a screen for wax-deficient (or *eceriferum*, *cer*) plants (Koornneef et al., 1989). These mutants had a 55% decrease in stem epidermal surface wax, relative to wild type, but did not display any change in total wax load in epidermal whole-cell extracts (Pighin et al., 2004). These phenotypes indicate that *cer5* mutants are capable of synthesizing wild-type levels of wax components, but they are unable to export most of these waxes to the cell surface. Ultrastructural analysis using transmission electron microscopy (TEM) revealed that *cer5-1* mutant cells had rod-like cytoplasmic inclusions into the large central vacuole (Pighin et al., 2004). Nile red staining and confocal microscopy revealed that these inclusions are lipidic in nature, suggesting that the

inclusions are composed of the wax that is synthesized but not secreted in *cer5-1* mutants. The *cer5* mutation was mapped to a chromosomal region containing a gene encoding the ATP-binding cassette transporter ABCG12, and *cer5* mutants were subsequently complemented with *ABCG12* cDNA, indicating that the wax-deficient phenotype was caused by a defect in this transporter. Further characterization of *ABCG12* demonstrated that it was expressed at high levels in the stem epidermis and that a GFP:ABCG12 fusion protein is localized to the plasma membrane. Together, these data demonstrate that ABCG12 is required for wax accumulation at the cell surface (Pighin et al., 2004). However, the exact role of this transporter remains unknown because a direct transport assay has not been undertaken to determine whether ABCG12 can bind wax molecules and transport them across a lipid bilayer.

Based on the fact that *abcg12* knockout mutants display a reduction, but not a total loss of surface wax, other ABCG family members that are up-regulated in the stem epidermis were examined by mutant analysis. Mutants for *ABCG11* displayed all of the same wax export deficiency phenotypes as *abcg12* mutants, including a 50% reduction in surface wax and accumulation of intracellular lipid inclusions (Bird et al., 2007; Ukitsu et al., 2007; Lou et al., 2007; Panikashvili et al., 2007). Similar to *ABCG12*, *ABCG11* was expressed in the expanding stem epidermis, and YFP:ABCG11 was localized to the plasma membrane (Bird et al., 2007; Ukitsu et al., 2007; Lou et al., 2007; Panikashvili et al., 2007). These data indicated that ABCG11 might be the other wax transporter in Arabidopsis stem epidermis. However, unlike *ABCG12*, *ABCG11* expression was not restricted to the stem epidermis, and *abcg11* mutants displayed a range of phenotypes that seem unrelated to wax export. These phenotypes, including organ fusions and permeability to toluidine blue dye, are typically associated with defects in cutin accumulation at the cell surface (Nawrath, 2006; Pollard et al., 2008). Indeed, *abcg11* mutants had reduced levels of cutin on the stem epidermis, indicating that ABCG11 is required for both wax and cutin export (Bird et al., 2007; Panikashvili et al., 2007).

Another half-transporter, ABCG13, is required for cutin accumulation, specifically to form the cuticular ridges that decorate petals (Panikashvili et al., 2011). Double mutants between *abcg11* and *abcg13* closely resemble *abcg11* single mutants, implying that ABCG11 and ABCG13 may act in the same pathway in petal cutin export, but no physical

interaction has been demonstrated between these transporters (Panikashvili et al., 2011). Since *ABCG13* is not expressed in the stem epidermis, another, yet unidentified ABCG half-transporter likely acts with ABCG11 for stem cutin export (Suh et al., 2005). Three other ABCG family transporters, ABCG1, ABCG18, and ABCG19 are also significantly up-regulated in the epidermis of rapidly-elongating stem cells, suggesting that these half-transporters may be required for the low levels of wax export that persist in *abcg11* and *abcg12* mutants. Although single mutants for these transporters have been isolated, these mutants do not display any reduction in surface waxes or cutin defects (Mentewab and Stewart, 2005; D. Bird and L. Samuels, unpublished). This implies that they act redundantly in wax export or they may be involved in some other process. Indeed, other ABCG half-transporters have been implicated in transport of kanamycin, sporopollenin, and abscisic acid (Mentewab and Stewart, 2005; Kuromori et al., 2010; Quilichini et al., 2010).

A full-transporter from the ABCG family, ABCG32, is also required for cuticle formation in flowers, as well as leaves and stems, indicating that both half- and full-transporters are required for cutin export (Bessire et al., 2011). Interestingly, while ABCG11 and ABCG12 are evenly localized throughout the plasma membrane, ABCG32 is polarly localized to the apical surface of the plasma membrane, underlying the regions where cutin accumulates (Pighin et al., 2004; Bird et al., 2007; Bessire et al., 2011). As with ABCG12, the transport activity and substrate specificity of ABCG11, ABCG13, and ABCG32 have not yet been assayed, so the exact roles that these transporters play in wax and cutin export have not been clearly defined.

Given that both *abcg11* and *abcg12* mutants showed a reduction, but not a complete loss of surface waxes, double mutants were constructed to investigate whether these transporters interact genetically. Interestingly, *abcg11 abcg12* double mutants were identical to *abcg11* single mutants, suggesting that ABCG11 and ABCG12 act in the same complex or pathway in wax export (Bird et al., 2007). The most straightforward explanation of these data is that ABCG11 and ABCG12, which are both half-transporters, may heterodimerize to transport wax molecules across the plasma membrane. Because *abcg11* mutants also displayed cutin phenotypes, but *abcg12* mutants did not, this hypothesis assumes that ABCG11 dimerizes with another partner (either as a homodimer

with another ABCG11 molecule, or as a heterodimer with another, yet unidentified ABCG family member) for cutin export (Bird, 2008).

This dimerization-dependent effect on substrate specificity has been hypothesized in other ABCG transporter models and was first proposed in Drosophila eye pigment export. In this system, WHITE and SCARLET are hypothesized to dimerize to transport a brown, tryptophan-derived eye pigment, since both mutants lack brown eye colouring. Similarly, WHITE and BROWN half-ABCGs are hypothesized to dimerize to transport a red, guanine-derived eye pigment (Sullivan and Sullivan, 1975). This model is supported by genetic evidence that specific point mutations in the WHITE transporter, which is presumably required for transport of both components, can result in a defect in accumulation of only one pigment, implying a defect in dimerization with only one partner, or a specific alteration to substrate specificity (Mackenzie et al., 1999). Despite the wide acceptance of this long-standing model of dimerization affecting substrate specificity of ABCG family half-transporters, there is no *in vivo* evidence for WHITE-BROWN or WHITE-SCARLET dimerization, nor have substrate specificity assays been performed on these transporters. Indeed, previous attempts to characterize ABC transporter interactions in common yeast assay systems have demonstrated only that ABC transporters may behave unusually in these systems (e.g. they may be subject to mis-glycosylation and degradation) (Yang and Murphy, 2009). Biochemical isolation of ABC transporters to determine their interaction partners has demonstrated that only a subset of the interactions that can be detected with these methods are functional *in vivo* (Graf et al., 2002, Graf et al., 2004; Wang et al., 2006). In order to determine whether ABCG interaction partners can influence substrate specificity, and to understand roles of ABCG11 and ABCG12 in cuticular lipid export, these technical limitations must be overcome.

1.3.3.2 Cuticular lipid export across the cell wall

Following export across the plasma membrane, cuticular lipids must still traverse the cell wall to accumulate on the cell surface. Lipid transfer proteins (LTPs) are a second family of proteins that have been implicated in cuticle export to the cell surface. The working hypothesis was that these LTPs could facilitate cuticular lipid deposition on the cell surface by shielding cuticular lipids from the hydrophilic environment of the cell wall

during transport to the cell surface (Samuels et al., 2008). However, until very recently their role in wax export had not been conclusively demonstrated (DeBono et al., 2009; Lee et al., 2009; Kim et al., 2012). Plant-specific LTPs are a large family in Arabidopsis (at least 70 members) that are evolutionarily distinct from other families of intracellular LTPs that are conserved between plants, yeast, and animals, such as the Sec14 family (Vincent et al., 2005; Yates and Rose, 2008). Plant-specific LTPs are characterized as small (~100 amino acids), secreted proteins that contain an hydrophobic cavity composed of 4 α-helices and an 8-cysteine motif (Kader, 1997). Knockdown mutants for one particular LTP, called LTPG because of its predicted extracellular localization and glycosylphosphatidylinositol (GPI) anchor, had a 25% reduction in surface wax load. Like *ABCG12*, *LTPG* was up-regulated in the stem epidermis (but expression was not restricted to this area) and YFP:LTPG localized to the plasma membrane with a nonpolar distribution (DeBono et al., 2009; Lee et al., 2009). Recombinant LTPG was capable of binding a lipid analogue in its hydrophobic pocket, indicating that LTPG has the capacity to bind lipid substrates, such as waxes (DeBono et al., 2009). Similarly, mutants in a second plant-specific LTP, LTPG2, showed a very small (<5%) reduction in the primary component of Arabidopsis stem wax, 29-alkane, and a decrease in both 29-alkanes and total wax on siliques. Double *ltpg ltpg2* mutants were more severe than either single mutant, indicating that these two extracellular LTPs act in parallel in cuticle formation (Kim et al., 2012). Interestingly, like ABCG11 and ABCG12, LTPG is localized throughout the plasma membrane. Therefore, the mechanism by which cuticular lipids polarly accumulate only on the outside surface of the plant, and not all around the entire epidermal cell, remains unclear.

Together, ABCG11, ABCG12, and the two LTPs are required for wax accumulation on the cell surface. However, it remains unclear how these two half-size ABCG transporters are coordinated during lipid secretion, whether they interact together or with other ABCGs, and whether they interact with the LTPs. Furthermore, the mechanism of cuticular wax trafficking, from the site of synthesis in the ER to the plasma membrane-localized transporters, remains undefined.

1.4 Research objectives and significance of findings

The broad goal of this research is to determine the cellular pathway of lipid export from plant cells. I decided to use cuticular lipid export from the expanding stem of *Arabidopsis thaliana* as a model system to study lipid trafficking because of its extraordinary cargo export rates and its genetic tractability. Based on a review of current literature, there are two important questions in this area: 1) How do ABCG11 and ABCG12 interact to export cuticular lipids in the model system of the stem epidermis in Arabidopsis? 2) How are lipids trafficked from their site of synthesis in the ER to the PM for export by ABC transporters? There are two hypotheses as to how cuticular lipids may be trafficked to the ABC transporters at the cell surface. Hypothesis 1: Cuticular lipids are transported to the cell surface via the canonical ER-Golgi-plasma membrane transport pathway. Hypothesis 2: Cuticular lipids are transported to the cell surface via non-vesicular traffic, through ER to plasma membrane contact sites.

In order to address these questions, the three main objectives of my research were: 1) To define the interaction partners of the ABCG transporters, ABCG11 and ABCG12, in the context of cuticular lipid export. 2) To determine whether secreted cuticular lipids are transported to the cell surface via the Golgi, or via non-vesicular traffic. 3) To investigate the functional components of ER-plasma membrane contact sites and to define their role in cuticular lipid secretion.

Chapter 2 addresses the roles of ABCG11 and ABCG12 in cuticular lipid export. Using *in planta* techniques, I demonstrate that ABCG11 can both homodimerize and form a heterodimer with ABCG12, but that ABCG12 cannot homodimerize. Furthermore, I show that the trafficking of these proteins to the plasma membrane is dependent upon their successful dimerization in the ER. Although this flexible dimerization had been previously proposed, this is the first demonstration of an ABC half-transporter forming both a homodimer and a heterodimer *in vivo*. Based on the chemical phenotypes of *abcg11* and *abcg12* single mutants and *abcg11 abcg12* double mutants, I propose a model in which these flexible dimer parings of ABCG11 allow it to participate in transport of different compounds: the ABCG11 homodimer may be required for cutin transport while the ABCG11-ABCG12 heterodimer is required for wax export. These finding have implications for understanding the evolution and assembly of the plant cuticle, as well as the general

mechanism of ABC transporter function. My results were published in McFarlane et al., (2010), which has been cited in studies on plant, animal, and bacterial ABC transporters. Here, we also reported that cuticular lipids that are not exported in *abcg11* and *abcg12* mutants accumulate in the ER. This suggests that lipids might move from the ER to the plasma membrane via non-vesicular trafficking.

Chapter 3 investigates the role of vesicle trafficking via the Golgi apparatus in cuticular wax secretion. By exploiting several known mutants in the secretory pathway, *echidna*, gnom-*like1,* and *trs120-4*, I have shown that cuticular wax secretion depends in part on the secretory pathway. Interestingly, my results also reveal a close relationship between the structure of the ER and its biosynthetic capacity. These findings contribute to our understanding of lipid secretion in plants, which has implications for the export of cuticular lipids as well as commercially important essential oils. Additionally, the relationship between ER structure and function provides an important line of future investigation for biosynthesis of other ER-derived products, including monolignols, which are important components of wood.

Chapter 4 investigates the role of ER-PM contact sites in plants, given that results in Chapter 2 and Chapter 3 suggested that some cuticular lipid secretion may occur via direct, non-vesicular lipid trafficking from the ER to the plasma membrane. By measuring the frequency of ER-PM contact sites in cells undergoing different levels of cuticular lipid secretion and cell elongation, I demonstrate that ER-PM contact sites are correlated with cell elongation, rather than cuticular lipid synthesis and secretion. To determine what role ER-PM contact sites may play in elongating cells, I used a series of biochemical methods to purify these contact sites and then subjected them to proteomic analysis. While these methods were not able to identify a contact site-specific subfraction, high quality proteomics of plasma membrane fractions isolated using free-flow electrophoresis provide some intriguing plasma-membrane associated candidate proteins as potential components of contact sites.

The final chapter of this thesis, Chapter 5, revisits these key results and provides a broader context for the main conclusions that can be drawn from my work.

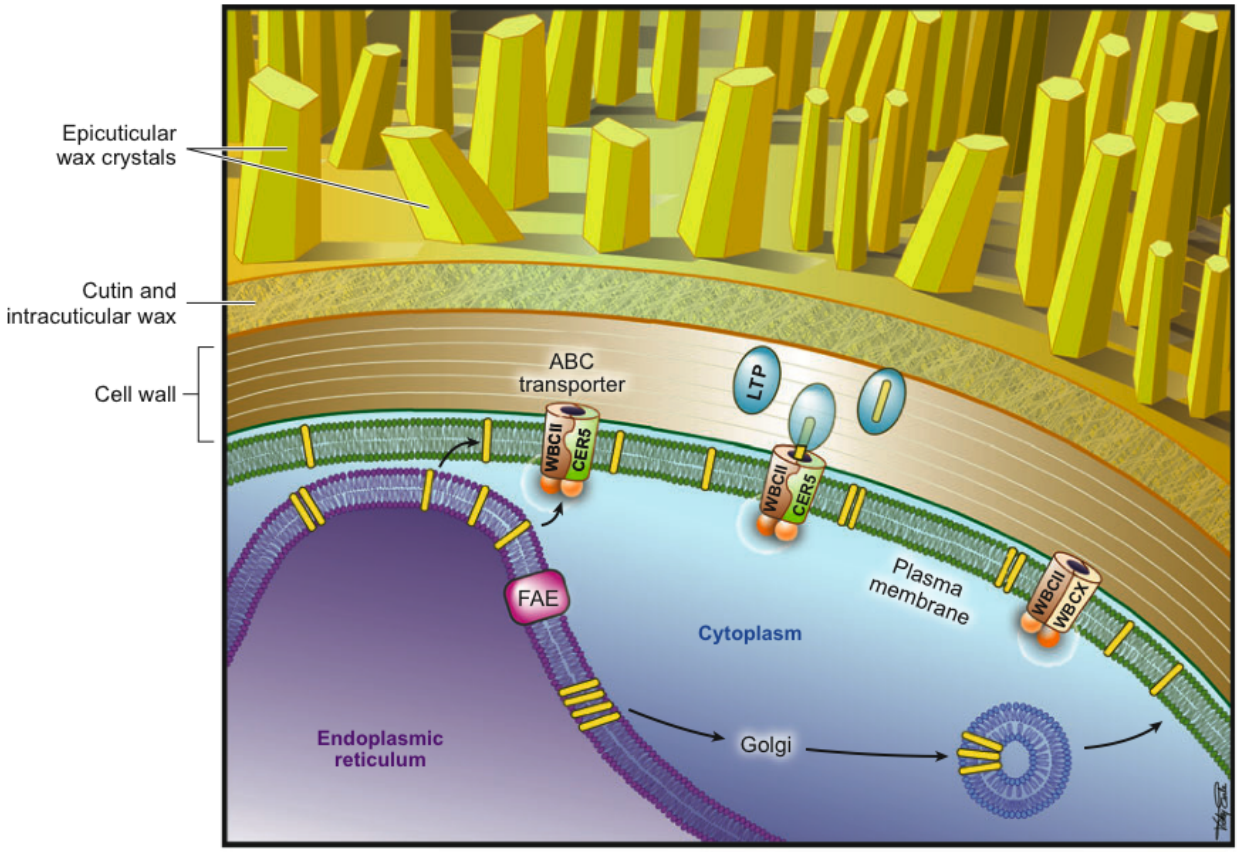

Figure 1.1: Overview of wax synthesis and export in a plant epidermal cell. FAE = fatty acid elongase complex, made of CER6, KCR1, PAS2, and CER10; WBC11 = ABCG11; CER5 = ABCG12; WBCx = unknown ABC transporter. Reproduced with permission from Samuels et al., 2008; Copyright © 2008, Annual Reviews Inc.

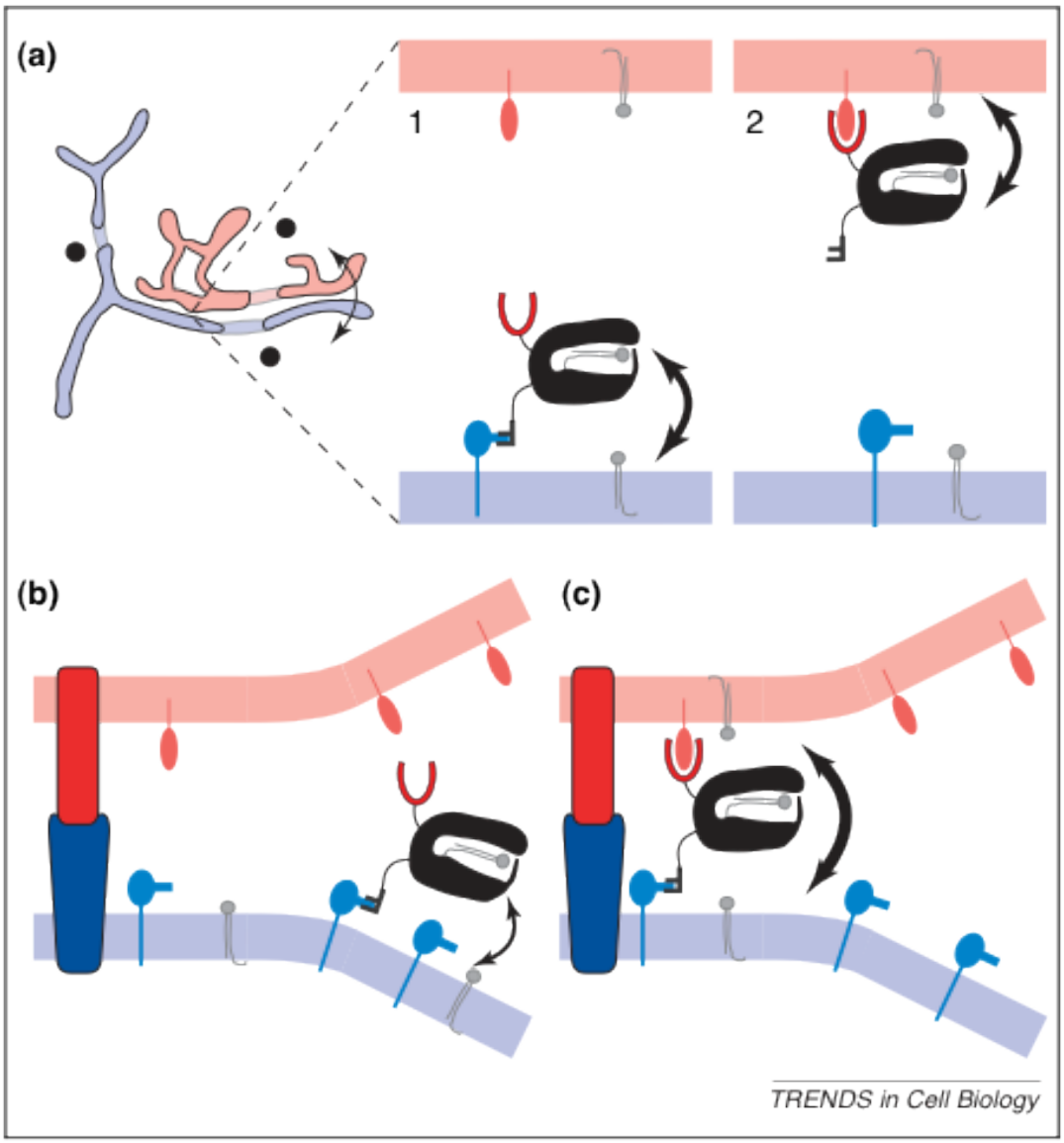

Figure 1.2: A model of non-vesicular lipid trafficking between two bilayers. A lipid transfer protein (black) that has signals for association with both the donor and acceptor membranes (blue and red, respectively) binds a single lipid (grey) to transfer it from the donor membrane to the acceptor membrane (a). The efficiency of this transfer is greatly improved if the two membranes are brought close together by a protein bridge (b). If the LTP can simultaneously associate with both bilayers, it may aid in bringing the donor and acceptor membranes closer together (c). Reproduced with permission from Levine, 2004; Copyright © 2004, Elsevier.

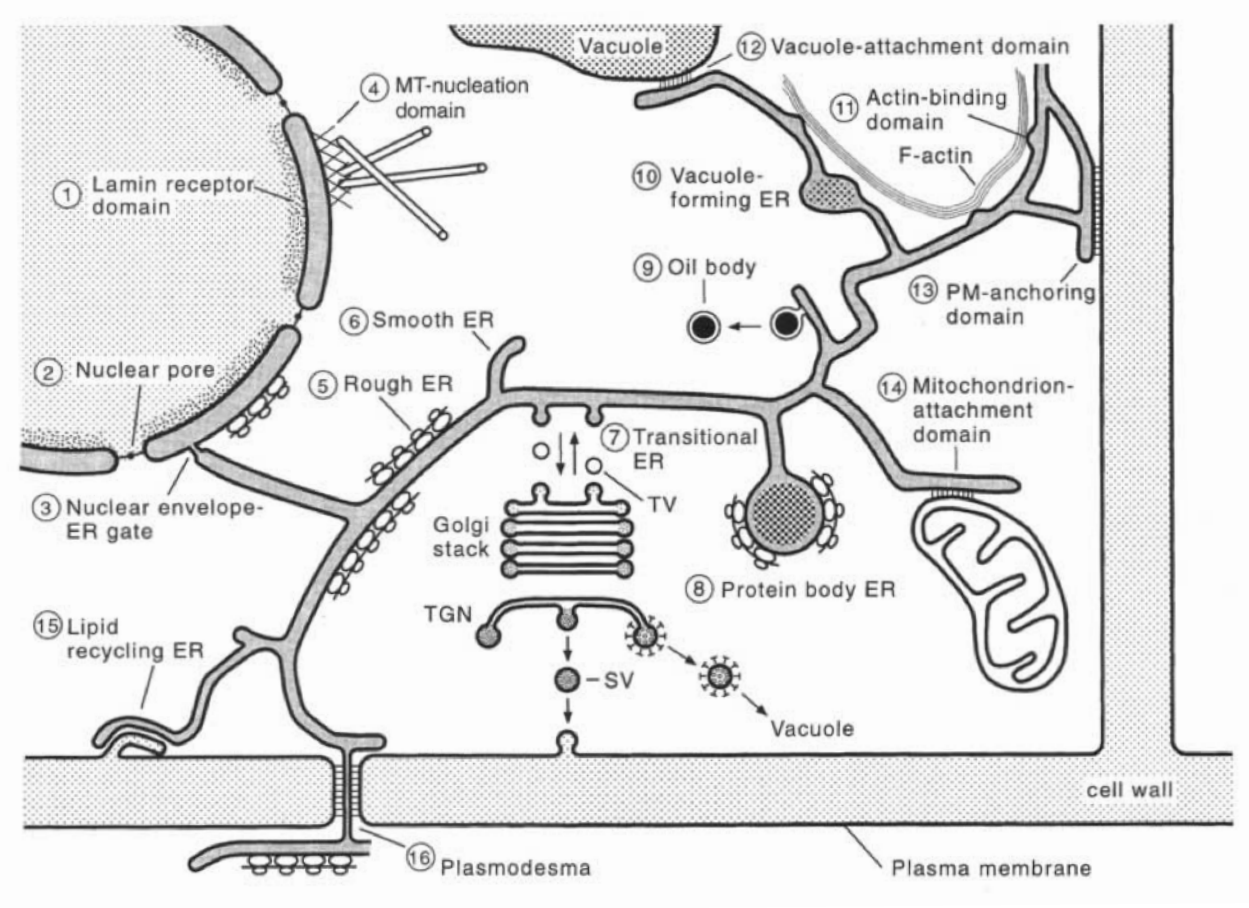

Figure 1.3: Schematic diagram of the plant endoplasmic reticulum. A number of different ER sub-domains that have been observed by electron microscopy, including ER-PM contact sites (13, 15) and ER-mitochondrion contact sites (14). Reproduced with permission from Staehelin, 1997; Copyright © 2002 John Wiley and Sons.

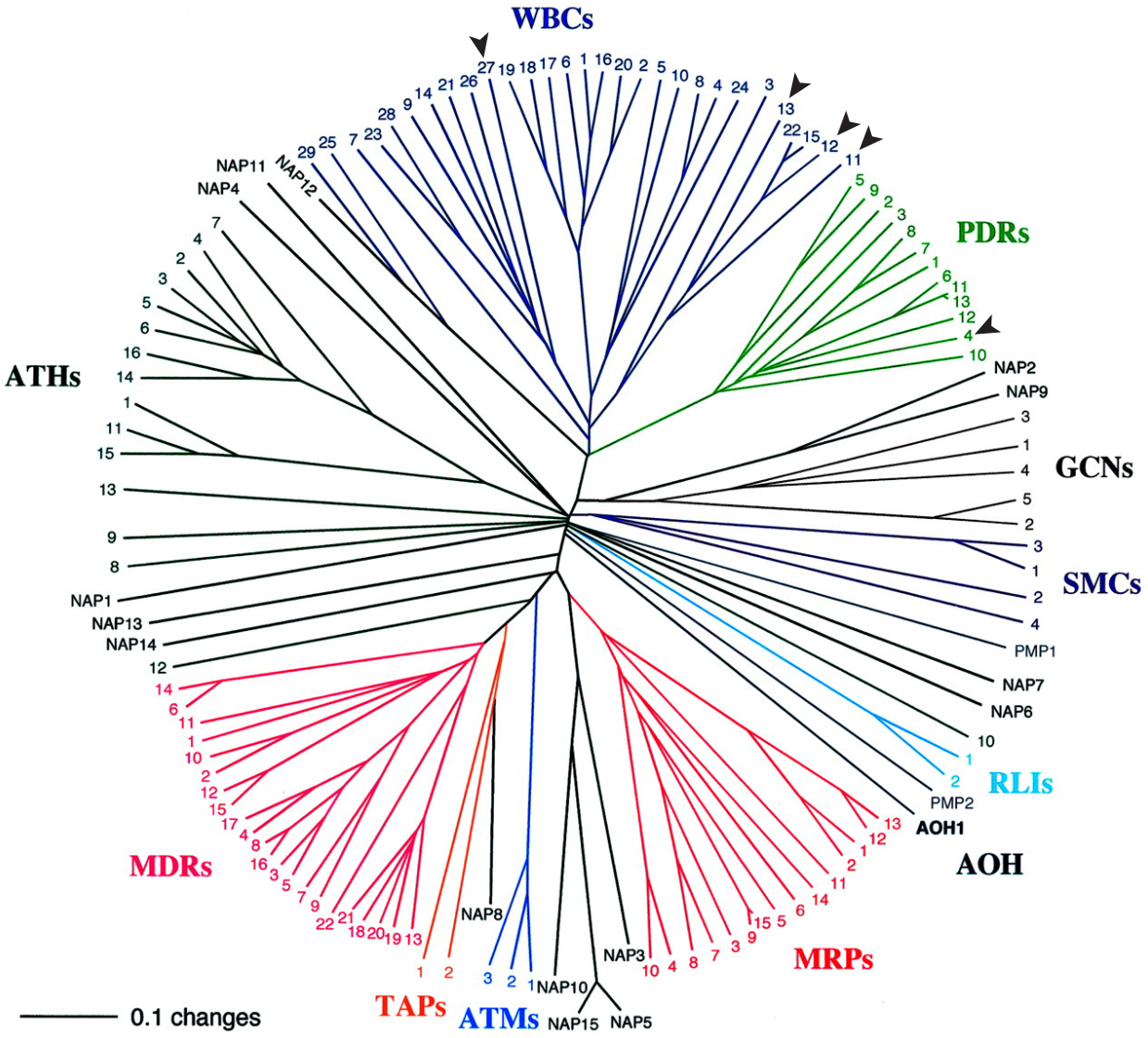

Figure 1.4: A phylogenetic tree of *Arabidopsis thaliana* ABC transporters. Protein sequences were aligned according to Sánchez-Fernández et al., 2001. The ABCG subfamily of half-transporters are also known as WBC transporters, while the ABCG subfamily of full transporters are also known as PDR transporters. ABCG members with known roles in surface lipid export (i.e WBC27 aka ABCG26, WBC11 aka ABCG11, WBC12 aka ABCG12, and PRD4 aka ABCG32) are highlighted by arrowheads. Reproduced with permission from Sánchez-Fernández et al., 2001; Copyright © 2001 American Society for Biochemistry and Molecular Biology.

Chapter 2: Arabidopsis ABCG transporters, which are required for export of diverse cuticular lipids, dimerize in different combinations

2.1 Introduction

ATP binding cassette (ABC) transporters are universal components of cells from all kingdoms that play diverse roles, including lipid transport. Many ABC transporters are encoded as fully functional units, consisting of two ATP-binding cassettes and two transmembrane domains. In contrast, some ABCG family members are encoded as half-transporters, that is, they consist of only one ATP-binding cassette and one series of transmembrane domains. Therefore, these half-transporters must dimerize to form a complete, functional ABC transporter. In *Arabidopsis thaliana,* the ABCG gene family contains 28 genes annotated as half-transporters (Verrier et al., 2008). In Arabidopsis, mutant phenotypes have implicated ABCG half-transporters in the transport of abscisic acid (Kuromori et al., 2010) and export of kanamycin (Mentewab and Stewart, 2005), sporopollenin (Quilichini et al., 2010; Xu et al., 2010; Choi et al., 2011; Dou et al., 2011; Kuromori et al., 2011), and cuticular lipids (Pighin et al., 2004; Bird et al., 2007; Luo et al., 2007; Panikashvili et al., 2007; Ukitsu et al., 2007). Whether these half-transporters function as homodimers or heterodimers is not known.

A model of ABCG half-transporters forming different heterodimers to perform multiple functions has been proposed in other eukaryotic systems. In *Drosophila melanogaster, WHITE, SCARLET,* and *BROWN* genes are involved in eye pigment accumulation and *WHITE* is also involved in cyclic GTP transport (Sullivan and Sullivan, 1975; Sullivan et al., 1979; Mackenzie et al., 2000; Evans et al., 2008). Mutant phenotypes have indicated that WHITE is required for accumulation of both guanine-derived (red) or tryptophan-derived (brown) eye pigments, as the eyes of *white* mutants lack any pigmentation (Sullivan et al., 1980; Ewart et al., 1994). Similarly, *brown* and *scarlet* mutant analyses indicated that these half-transporters are required for accumulation of guanine-derived or tryptophan-derived eye pigments, respectively (Ewart et al., 1994). This implies that the WHITE and BROWN half-transporters dimerize to transport guanine-derived pigments, while the WHITE and SCARLET half-transporters dimerize to transport

tryptophan-derived pigments. However, whether these gene products physically interact *in vivo* and whether they actually transport these substrates has not been tested.

ABCG transporters in mammals appear to form either obligate heterodimers, such as the ABCG5/ABCG8, or homodimers, such as ABCG2 (Tarr et al., 2009). While both ABCG5 and ABCG8 can interact promiscuously with other ABCG transporters tested *in vitro* (Graf et al., 2003), mouse ABCG5 and ABCG8 must heterodimerize with each other to exit the endoplasmic reticulum (ER), undergo posttranslational modification in the Golgi, and traffic to their site of biological activity at the plasma membrane (Graf et al., 2002, Graf et al., 2003). If either ABCG5 or ABCG8 is expressed individually, or if heterodimerization is disrupted by a point mutation in either transporter, both transporters are retained in the ER and degraded, indicating that formation of the ABCG5-ABCG8 heterodimer is a prerequisite for plasma membrane localization and activity (Graf et al., 2002, Graf et al., 2004). These studies suggest that only a subset of the ABCG transporter dimers that are detected by immunoprecipitation are capable of exiting the protein maturation machinery in the ER. Furthermore, these data imply that exit of these dimers from the ER can be used to assess the biological relevance of different dimers.

Two Arabidopsis ABCG half-transporters, ABCG11 and ABCG12, have been implicated in the export of lipids from the epidermis to the cuticle, which seals and protects the primary aerial tissues of the plant body (reviewed by Bird, 2008). The cuticle is a tough cross-linked cutin polyester scaffold composed of oxygenated-C16 and C18 fatty acids and glycerol (Pollard et al., 2008), surrounded by and covered with a hydrophobic wax mixture dominated by very long-chain fatty acid derivatives (Jetter et al., 2006; Samuels et al., 2008). ABCG half-transporters required for accumulation of both cutin and wax at the cell surface have been identified by mutant analysis in Arabidopsis. *abcg11/wbc11/desperado/cof1* mutants display reduced cutin and wax levels (Bird et al., 2007; Luo et al., 2007; Panikashvili et al., 2007; Ukitsu et al., 2007). Detailed analyses of these chemical phenotypes revealed that all wax and cutin constituents were decreased in *abcg11* mutants. Assuming that ABCG11 can directly transport cuticular lipids, these data imply that ABCG11 has a broad substrate specificity for a variety of structurally diverse cuticular lipids (Bird et al., 2007; Luo et al., 2007; Panikashvili et al., 2007; Ukitsu et al., 2007). The closely related ABCG12/CER5 transporter is required for wax (Pighin et al.,

2004), but not cutin, export (Bird et al., 2007). *abcg12* mutants exhibit a reduction only in wax components, suggesting that ABCG12 has a narrower substrate specificity than ABCG11 (Pighin et al., 2004). Fluorescently tagged ABCG11 or ABCG12 is localized to the plasma membrane and rescues cuticular lipid deficiencies of the knockout mutants in stably transformed lines (Pighin et al., 2004; Bird et al., 2007). Consistent with a role in cuticular lipid export, both genes are highly expressed in the stem epidermis, where wax and cutin synthesis and secretion are extremely high (Suh et al., 2005). However, *ABCG11* is also expressed in tissues in which cuticular lipids are not synthesized (e.g., emerging lateral roots), suggesting that it may play roles beyond cuticular lipid export (Bird et al., 2007; Luo et al., 2007; Panikashvili et al., 2007; Ukitsu et al., 2007). Indeed, *abcg11* mutants display pleiotropic phenotypes, including dwarfism, loss of apical dominance, and sterility, while *abcg12* mutants are phenotypically wild-type except for their glossy, wax-deficient stems (Pighin et al., 2004; Bird et al., 2007; Luo et al., 2007; Panikashvili et al., 2007; Ukitsu et al., 2007). Epidermal cells of both *abcg11* and *abcg12* mutants accumulate lipid inclusions, presumably due to the aggregation of cuticular lipid molecules that are synthesized, but not exported, from these mutants (Pighin et al., 2004; Bird et al., 2007; Panikashvili et al., 2007). *abcg11 abcg12* double mutants have the same levels of residual wax as either of the single mutants, suggesting that ABCG11 and ABCG12 act in the same pathway or complex in cuticular wax export (Bird et al., 2007).

Based on the pleiotropic phenotypes of *abcg11* mutants, we hypothesized that different dimerization combinations of ABCG transporters could account for the multiple functions of the ABCG11 half-transporter (Bird et al., 2007). In this study, ABCG11/ABCG12 heterodimers and ABCG11 homodimers were demonstrated *in planta* using bimolecular fluorescence complementation (BiFC), while ABCG12 homodimers were not. Heterodimerization between ABCG11 and ABCG12 was further supported by the behaviour of the ABC transporters during their biosynthesis and secretion in epidermal cells, which actively synthesize and export cuticular lipids to the plant surface. The different dimer combinations demonstrated by BiFC can account for the behavior of these half-transporters during their trafficking to the plasma membrane. ABCG12 was retained in lipid inclusions in the absence of ABCG11, and these inclusions were contiguous with the ER. This study emphasizes the flexibility of the half-transporter system of ABCG

transporters, in which specific dimer combinations perform specialized functions and different combinations of ABCG transporters allow a single gene product to perform multiple functions.

2.2 Results

2.2.1 ABCG11 and ABCG12 form a heterodimer, and ABCG11 can homodimerize

Given that ABCG11 and ABCG12 are both half-transporters (Verrier et al., 2008) and that the double mutant phenotype indicated that they likely act in the same pathway or complex in wax export (Bird et al., 2007), their physical interaction was tested *in vivo* using BiFC (Figure 2.1). This transient protoplast transformation approach was used because it has proven difficult, both in our hands and as documented by others (Geisler and Murphy, 2006; Yang and Murphy, 2009), to express plant ABC transporters in *Saccharomyces cerevisiae,* thus discouraging yeast protein–protein interaction studies. In the BiFC system, enhanced yellow fluorescent protein (EYFP) is split into two halves: N-terminal (nYFP) and C-terminal (cYFP), which are fused to the proteins of interest. Co-transformation of these constructs into a transient expression system in Arabidopsis leaf mesophyll protoplasts allows reconstitution of YFP if the two proteins are in close physical proximity, thereby allowing detection of YFP signal (Citovsky et al., 2006). A significant proportion of protoplasts co-transformed with *cYFP-ABCG11* and *nYFP-ABCG12,* or conversely, with *cYFP-ABCG12* and *nYFP-ABCG11,* displayed bright yellow fluorescence in the plasma membrane, indicating that these two proteins are capable of forming a heterodimer *in vivo* ($p < 0.05$) (Figures 2.1C, 2.1D, and 2.1I; Figure 2.2). This also confirms that ABCG BiFC constructs with either the C- or N-terminal pieces of YFP are capable of generating yellow fluorescence, regardless of the combination used.

When *cYFP-ABCG11* and *nYFP-ABCG11* were co-transformed into protoplasts, yellow fluorescence was observed in the plasma membrane of a significant proportion of these cells, indicating that ABCG11 can also homodimerize ($p < 0.05$) (Figures 2.1A, 2.1B, and 2.1I). In contrast, when *cYFP-ABCG12* and *nYFP-ABCG12* were co-transformed, only a small proportion of protoplasts fluoresced faintly when imaged under the same conditions

(Figures 2.1E, 2.1F, and 2.1I; Figure 2.2). To determine whether this signal was due to a genuine, low-level homodimerization of ABCG12 or whether it was an artifact of colocalization of two half-YFP constructs to the plasma membrane, each of the ABCG BiFC constructs were co-transformed with BiFC constructs for components of a plasma membrane–localized root nitrate transporter complex (Arabidopsis NRT2.1 or NRT3.1) (Yong et al., 2010), which are not predicted to interact with ABCG transporters. Protoplasts co-transformed with *NRT2.1-cYFP* and either *nYFP-ABCG11* or *nYFP-ABCG12* or with *NRT3.1-nYFP* and either *cYFP-ABCG11* or *cYFP-ABCG12* displayed the same faint fluorescence as *cYFP-ABCG12* with *nYFP-ABCG12* (Figures 2.1E to 2.1I; Figure 2.2). These proportions of fluorescent protoplasts were not significantly different from the proportion observed when the two ABCG12 constructs were co-transformed ($p > 0.35$). Thus, these low proportions of faintly fluorescing protoplasts are likely background signal due to chance associations between proteins that are plasma membrane localized, but do not legitimately interact.

2.2.2 ABCG11 trafficking to the plasma membrane is independent of ABCG12

Studies of ABCG half-transporters in mammalian cells indicate that both partners of a heterodimer must be present for the dimer to exit the ER and move to the plasma membrane (Graf et al., 2003; Graf et al., 2004). To test whether ABCG11 or ABCG12 can traffic normally only in the presence of their partners and to place these interactions into the context of cuticular lipid secretion in the epidermis, stably transformed plant lines expressing fluorescently tagged ABCGs (Pighin et al., 2004; Bird et al., 2007) were crossed into the single (*abcg11*) and double (*abcg11 abcg12)* knockout mutants. YFP-ABCG11 successfully trafficked to the plasma membrane in the presence of its wild-type ABCG12 partner (i.e. in the single *abcg11* mutant background; Figure 2.3A). Plasma membrane localization of YFP-ABCG11 was visualized as two distinct signals from neighboring cells lining the adjacent cell wall, which was labeled with propidium iodide (Figures 2.3B and 2.3C). In the absence of ABCG12 (i.e. in *abcg11 abcg12* double knockout mutant background), YFP-ABCG11 was also localized to the plasma membrane (Figure 2.3E), where it colocalized with the plasma membrane marker FM4-64 (Figures 2.3F and 2.3G). YFP-ABCG11 localization in the double mutant background was confirmed using

transmission electron microscopy (TEM) immunogold labeling of cryo-fixed, freeze-substituted stem epidermal cells, probed with an anti-green fluorescent protein (GFP) antibody (Figure 2.3D). The plasma membrane of epidermal cells was labeled by anti-GFP in transgenic plant lines carrying *YFP-ABCG11* (Figure 2.3H), but no signal above background was detected in wild-type control plants or in samples probed without a primary antibody (Figure 2.4). There was no evidence of polar localization of YFP-ABCG11 in stem epidermal cells using this high-resolution TEM technique, in contrast with previous reports using confocal microscopy, in which signal intensities may have been distorted by optical conditions or dissection (Panikashvili et al., 2007). These results demonstrate that ABCG11 is able to traffic to the plasma membrane even in the absence of ABCG12. This suggests that ABCG11 may heterodimerize with other ABCG half-transporters that are present in the stem epidermis, such as ABCG18 and ABCG19 (Suh et al., 2005). Alternatively, ABCG11 may form a homodimer in vivo, an interpretation that is consistent with the BiFC data.

2.2.3 ABCG12 trafficking to the plasma membrane is dependent upon ABCG11

If ABCG12 forms an obligate heterodimer with ABCG11, then ABCG11 is predicted to be required for normal traffic of ABCG12 to the plasma membrane. Therefore, GFP-ABCG12 was localized in *abcg12* and *abcg11 abcg12* mutants to investigate its trafficking in the presence and absence of its ABCG11 partner, respectively. In the single *abcg12* knockout mutants, GFP-ABCG12 signal was detected at the plasma membrane (Figure 2.5A), adjacent to the cell wall, which was visualized with propidium iodide (Figures 2.5B and 2.5C). Immunogold TEM labeling of the single *abcg12* mutant expressing the *GFP-ABCG12* construct revealed that anti-GFP signal was predominantly at the plasma membrane, with little intracellular and cell wall background label (Figure 2.5D; Figure 2.4). However, in the *abcg11 abcg12* double mutant background, GFP-ABCG12 signal was detected in a reticulate network resembling the ER and in large aggregations in the middle of the cells (Figure 2.5E). This signal had a low level of colocalization with FM4-64 (Figures 2.5F and 2.5G), which is not consistent with plasma membrane localization. In TEM, anti-GFP labeling was concentrated in the large aggregations of sheet-like inclusions that have been detected within the cytoplasm of *abcg11* and *abcg12* mutants (Figure 2.5H; Pighin et al., 2004; Bird

et al., 2007; Panikashvili et al., 2007). GFP-ABCG12 retention in the ER in the absence of ABCG11 is consistent with the prediction that ABCG12 dimerizes only with ABCG11 in the stem epidermal cells and that, as in mammals, ABCG half-transporter dimer formation is required for trafficking to the plasma membrane (Graf et al., 2003; Graf et al., 2004).

Accumulation of GFP-ABCG12 in the *abcg11 abcg12* mutant inclusions could be due to a nonspecific ER stress response and/or a general secretion defect in *abcg11* mutants. Therefore, as a control, a fluorescently-tagged plasma membrane-localized low temperature-induced protein 6b (GFP-LTI6b; line 29-1 from Cutler et al., 2000) was crossed into *abcg11* mutants. In wild type, this marker is localized to the cell periphery and colocalizes with FM4-64, confirming its plasma membrane localization (Figure 2.6A-C). This same plasma membrane localization and colocalization with FM4-46 was observed in *abcg11* mutants (Figure 2.6D-F), indicating that *abcg11* mutants do not suffer from genral large-scale endomembrane trafficking defects. Immunogold TEM labeling for another plasma membrane–localized protein, the plasma membrane intrinsic protein (PIP2A) aquaporin (Bots et al., 2005), detected PIP2A in the plasma membrane of wild-type and *abcg11* mutant cells (Figure 2.6G and H). However, no labeling above background was detected in the inclusions (Figure 2.6I; Figure 2.7). Together, these data confirm that the failure of GFP-ABCG12 to traffic to the plasma membrane in *abcg11* mutants is specific to ABCG12 and that the inclusions are not a general sink for plasma membrane–localized proteins.

Similarly, RT-PCR analysis of genes typically upregulated by the unfolded protein response (Martinez and Chrispeels, 2003; Kamauchi et al., 2005) confirmed that the presence of inclusions does not induce significant unfolded protein response (Figure 2.8). These data agree with a recent microarray analysis of gene expression changes in *abcg11* mutants (Panikashvili et al., 2010). Therefore, GFP-ABCG12 retention in inclusions is not due to a general protein or membrane trafficking defect in *abcg11* mutants. Rather, it is likely a result of the failure of ABCG12 to correctly dimerize with any other ABCG in the absence of ABCG11.

2.2.4 Membrane inclusions in *abcg11* mutants are contiguous with the ER

Because GFP-ABCG12 was retained in the ER and in the inclusions of *abcg11 abcg12* double mutants, the relationship between these inclusions and the ER was investigated further. TEM was used to examine the morphology of *abcg11* stem epidermal cells where inclusions protruded into the vacuole of epidermal cells (Figure 2.9). ER membranes are often closely associated with the inclusions, either layered between inclusions, or at the tips of the inclusions (Figures 2.9B and 2.9C).

To confirm the association of the ER with the inclusions, ER was positively identified with established markers in *abcg11* mutants. In wild-type epidermal cells, the ER marker GFP-HDEL (Batoko et al., 2000) labeled the ER network, including the cortical ER (Figure 2.10A). In *abcg11* mutant stem epidermal cells, GFP-HDEL labeled large aggregations in the center of these cells, in addition to the normal ER network (Figure 2.10E). This pattern is strikingly similar to the lipid inclusions labeled with Nile red detected in *abcg12* mutants (Pighin et al., 2004). In *abcg11* mutants, Nile red stained a similar pattern to GFP-HDEL (Figure 2.10F and G), suggesting that these ER accumulations are lipid rich and may be composed of cuticular lipids that are synthesized, but not exported, in *abcg11* mutants.

Since the ER was often layered between inclusions, the live-cell imaging with GFP-HDEL might reflect trapping of ER membranes between inclusions, rather than expansion of the ER membranes to form inclusions. To differentiate between these possibilities, TEM immunogold labeling was employed with anti-calreticulin, an established marker for the ER (Coughlan et al., 1997). In wild-type cells, anti-calreticulin labeled the electron-lucent ER lumen (Figure 2.10D; Figure 2.11). In *abcg11* mutants, anti-calreticulin labeled both ER lumen and inclusions (Figure 2.10H; 2.11). This confirms that the inclusions themselves contain *bona fide* ER markers.

In contrast to the ER defects observed in *abcg11* and *abcg12* mutants, no changes were observed to the Golgi apparatus in *abcg12-1* mutants, despite this drastic change to ER structure. In both confocal of the Golgi marker, sialyl transferase (ST)-mRFP, and TEM of the Golgi apparatus, no significant differences were observed between wild type and *abcg12-1* mutants (Figure 2.12A-D). Furthermore, the Golgi apparatus was unaffected in TEM of *abcg11* mutants (Figure 2.12E). Together, these data suggest that in *abcg11*

mutants, lipids are retained at their site of synthesis in inclusions that are associated with ER-derived membranes.

2.3 Discussion

Specific dimer pairings of ABCG half-transporters have been hypothesized to allow multiple functions for a single gene product in both Arabidopsis cuticular lipid export by ABCG11 and ABCG12 (Bird et al., 2007, Bird, 2008) and in Drosophila eye pigment accumulation by WHITE, BROWN, and SCARLET (Sullivan and Sullivan, 1975; Sullivan et al., 1979; Mackenzie et al., 2000; Evans et al., 2008). However, these dimer combinations have been hypothesized based on sequence analysis and mutant phenotypes and have not been directly tested, until now. Here, physical protein-protein interactions between Arabidopsis ABCG11 and ABCG12 were experimentally demonstrated by BiFC. BiFC data indicate which pairings are physically possible, assuming these gene products are expressed in the same cell at the same time. To place ABCG transporter dimerization in the context of the epidermal cell during lipid secretion, trafficking of ABCG transporters from the ER to the plasma membrane was examined in these cells. The behavior of these half-transporters during their biosynthesis and trafficking are consistent with the different dimer combinations demonstrated by BiFC. The consistency between these two data sets, together with functional data deduced from mutant phenotypes (Pighin et al., 2004; Bird et al., 2007; Luo et al., 2007; Panikashvili et al., 2007; Ukitsu et al., 2007), lead to the models proposed below for specific dimerization pairings of ABCG transporters in diverse functions.

2.3.1 ABCG11 is a promiscuous half-transporter

abcg11 mutants display pleiotropic phenotypes, including reduced surface wax and cutin loads, stunted growth, organ fusions, reduced fertility, and reduced apical dominance, indicating that ABCG11 is involved in processes in addition to wax export (Bird et al., 2007; Luo et al., 2007; Panikashvili et al., 2007; Ukitsu et al., 2007). Furthermore, the expression pattern of *ABCG11* extends beyond that of *ABCG12* to tissues in which neither cutin nor wax is being synthesized (e.g. emerging lateral roots) (Suh et al., 2005; Toufighi et al., 2005;

Bird et al., 2007; Luo et al., 2007; Panikashvili et al., 2007). Based on mutant phenotypes and expression pattern, I propose that ABCG11 acts as a generalist ABCG transporter, pairing with different half-transporters in different tissues to transport structurally diverse substrates. Consistent with this, ABCG11 was able to exit the ER and traffic to the plasma membrane independently of ABCG12, indicating that it can dimerize with itself or with other ABCG half-transporters that are expressed in epidermal cells (Suh et al., 2005). Additionally, homodimerization of ABCG11 was demonstrated in BiFC assays. These results are consistent with the model in which ABCG11 homodimerizes to export cutin precursors from the stem epidermis (Bird et al., 2007; Bird, 2008; Figure 2.13). Determining whether ABCG11 functions in cutin export as a homodimer will require further experiments. While analysis of several cutin biosynthesis mutants has revealed genes required for cutin monomer biosynthesis and assembly, the nature of cutin precursors that are exported for assembly in the cuticle is not known (Pollard et al., 2008). This gap in our understanding, as well as the problem that wax constituents are solid at biologically relevant temperatures, makes assessment of the possible substrates of ABCG11 challenging.

Both BiFC and trafficking data demonstrate that ABCG11 is capable of promiscuous pairing with multiple ABCG half-transporters. It is possible that ABCG11 dimerizes with multiple partners to form a variety of full transporters to perform diverse functions, as has been hypothesized in the Drosophila WHITE/BROWN/SCARLET model. Indeed, ABCG11 has been implicated in functions as diverse as maintenance of apical dominance, flower development, embryogenesis, root suberin export, and pollen coat/pollen wall formation (Panikashvili et al., 2010; T. Quilichini, L. Samuels, and C. Douglas, unpublished). Furthermore, preliminary results indicate that ABCG11 can dimerize with ABCG26, a tapetum-specific ABCG that is required for sporopollenin accumulation in the developing pollen wall (Quilichini et al., 2010; T. Quilichini, L. Samuels, and C. Douglas, unpublished). Together, these data imply a model in which the pleiotropic effects of *abcg11* mutation are due to the loss of a variety of full transporters that contain ABCG11.

2.3.2 ABCG12 interacts exclusively with ABCG11 for wax export

In contrast with the broad expression pattern of *ABCG11* and the pleiotropic phenotypes of *abcg11* mutants, mutants in *abcg12* display only wax-related phenotypes,

and expression of *ABCG12* is enriched in the stem epidermis where wax is actively being synthesized and secreted (Pighin et al., 2004; Suh et al., 2005; Toufighi et al., 2005). There is a precedent for strict ABCG heterodimerization in *Medicago truncatula* arbuscular mycorrhizal symbiosis (Zhang et al., 2010). During arbuscule formation, two ABCG half-transporter genes, *STUNTED ARBUSCULE1* (*STR1*) and *STR2,* are highly expressed. STR and STR2 heterodimerize and are incapable of forming homodimers. Their identical mutant phenotypes and expression patterns suggest that, like ABCG12, these two ABCG half-transporters are specialists (Zhang et al., 2010). Consistent with the hypothesis that ABCG12 is a specialist, GFP-ABCG12 was only able to exit the ER and move to the plasma membrane of stem epidermal cells in the presence of ABCG11, indicating that ABCG12 forms an obligate heterodimer with ABCG11 in stem epidermal cells. This is supported by the BiFC interaction data, which indicate that ABCG12 can heterodimerize with ABCG11 but is incapable of forming a homodimer. Therefore, defects in this heterodimer can account for the wax phenotypes of the *abcg11* and *abcg12* single mutants and the *abcg11 abcg12* double mutants (Figure 2.13).

Given that evolution of the protective plant cuticle was one of the key adaptations that allowed plant colonization on land, it is unsurprising that one ABCG transporter may be specifically required for wax export. Indeed, similar specific roles have been suggested for ABCG transporters in other key evolutionary adaptations. For instance, the tapeteum-specific ABCG26 is required for pollen wall development (Quilichini et al., 2010), ABCG32 is required for cutin accumulation on the cell surface (Bessire et al., 2011), and ABCG25 is required for abscisic acid-mediated stomata regulation (Kuromori et al., 2010). That some specific ABCGs play narrowly defined roles in plants, such as cuticle deposition, pollen wall development, and hormone transport, highlights the importance of these functions in plants.

2.3.3 Waxes that are not exported in *abcg* mutants accumulate in ER-derived inclusions

In *abcg11* or *abcg12* mutants, membranous lipid inclusions accumulate in stem epidermal cells (Pighin et al., 2004; Bird et al., 2007; Panikashvili et al., 2007). Here, we demonstrate that the inclusions in *abcg11* mutants contain markers of the ER but not

markers of the Golgi apparatus or the plasma membrane. In *Saccharomyces cerevisiae*, the ER can increase in size to accommodate defective proteins, independent of the unfolded protein response (Schuck et al., 2009). Therefore, it is possible that ER expansion is a stress response to sequester insoluble cuticular lipids from the rest of the endomembrane system.

Alternatively, the inclusions could reflect the nature of lipid traffic during cuticular lipid secretion. All of the enzymes that have been characterized in wax synthesis have been localized to the ER (Zheng et al., 2005; Greer et al., 2007; Bach et al., 2008; Li et al., 2008). If intermediate secretory compartments, such as the Golgi apparatus, are required for wax secretion to the cell surface, then wax accumulation in these compartments might be predicted occur when transport is blocked. However, Golgi, vesicle, and plasma membrane morphology appeared unaffected in TEM of *abcg11* knockout mutants. While the subcellular compartments involved in wax secretion are not known, accumulation of waxes only in the ER is consistent with wax moving directly from the ER to the plasma membrane via nonvesicular lipid traffic, by analogy to yeast lipid transport systems (Levine and Loewen, 2006).

In summary, Arabidopsis ABCG11 is capable of flexible dimerization *in vivo* to form either a heterodimer or a homodimer at the plasma membrane. In contrast, ABCG12 forms an obligate heterodimer with ABCG11, and heterodimerization is required for its normal trafficking to the plasma membrane. Based on these data and on previous ABCG studies, there are two emerging paradigms: 1) flexible pairing of one ABCG gene product with multiple partners to perform diverse functions and 2) formation of obligate ABCG heterodimers for specialized functions. These paradigms have been formerly deduced but not experimentally tested in the canonical WHITE/BROWN/ SCARLET complex in Drosophila. In mammalian cells, cases of flexible ABCG transporter partnering have not been described *in vivo*, although several lines of evidence hint that this is possible (Graf et al., 2002; Cserepes et al., 2004). This study demonstrates that mechanisms of ABCG transporter dimerization are conserved across biological kingdoms, despite the divergent functions played by these transporters.

2.4 Methods

2.4.1 Plant material

Seedlings were sown on AT medium and grown in an environmental growth chamber at 21°C, at roughly 80% humidity, and 24 h light (~100 $\mu E\ m^{-2}\ s^{-1}$) for roughly 10 d before transfer to Sunshine Mix 5 soil. The *cer5-2, wbc11-3, cer5-2+CER5pro:GFP-CER5,* and *wbc11-3+35Spro:YFP-WBC11* lines (all in the Columbia-0 (Col-0) background) have been previously described (Pighin et al., 2004; Bird et al., 2007), Col-0 seeds carrying the *35Spro:GFP-HDEL* ER marker were a generous gift from H. Zheng (Batoko et al., 2000), Landsberg seeds carrying *CER6pro::ST-mRFP* were a generous gift from P. Lam and L. Kunst, and Col-0 seeds carrying *35S:GFP-LTI6b* were a generous gift from S. Cutler (Cutler et al 2000).

2.4.2 BiFC transgene construction and protoplast transformation

ABCG12 cDNA was amplified from the *GFP:CER5* vector (Pighin et al., 2004), and *XmaI* and *EcoRI* sites were added using the primers ABCG12.P3 and ABCG12.P4 (Table 2.1). *ABCG11* cDNA was amplified from *YFP:WBC11* (Bird et al., 2007), and *XmaI* and *EcoRI* sites were added using the primers ABCG11.P3 and ABCG11.P4 (Table 2.1). The resulting products were ligated into the *EcoRI* and *XmaI* sites of *pSAT4-cEYFP-C1-B* and *pSAT4-nEYFP-C1* (Citovsky et al., 2006) and verified by sequencing. Control BiFC vectors containing components of the Arabidopsis nitrate transport machinery were a generous gift from Z. Kotur and A. Glass (Yong et al., 2010). Plasmid DNA was purified from *Escherichia coli* cultures using an endotoxin-free plasmid maxiprep kit (Qiagen). Protoplasts from Col-0 leaves were prepared and transformed as described (Tiwari et al., 2006) with 10 μg of each vector used in each protoplast transformation. The number of fluorescent protoplasts was scored out of the total number of live protoplasts (i.e., those with an intact plasma membrane when viewed with bright-field microscopy) and presented as a percentage relative to the number of fluorescent protoplasts in the positive control (*pSAT6+35Spro:EYFP)* as an estimation of transformation efficiency. Data from converse transformations (e.g., *cYFP-ABCG11+nYFP-ABCG12* and *cYFP-ABCG12+nYFP-ABCG11)* were grouped. To meet the assumptions of analysis of variance (ANOVA)

(Whitlock and Schluter, 2009), data from eight independent experiments were natural log (ln) transformed and corrected for variations in transformation efficiency among experiments by subtracting the mean transformation efficiency of that experiment from each value. Means were compared using analysis of variance and a Tukey post-hoc test using SPSS (IBM).

2.4.3 Confocal microscopy

Transformed protoplasts were mounted in WI solution from the protoplast preparation (Tiwari et al., 2006), or dissected stem segments from the top 3 cm from the shoot apical meristem (where cuticle synthesis and secretion is the highest; Suh et al., 2005) were mounted in distilled water and immediately imaged. Stem segments were stained with 1 μg/mL propidium iodide (Sigma-Aldrich) or 10 μM FM4-64 (Molecular Probes) for 10 minutes. Images were collected using a Zeiss 510 Meta scan head on a Zeiss Axiovert 200 M with a Zeiss AxioCam HRm CCD camera or using a Quorum Wave FX spinning-disk scan head on a Leica DMI6000 microscope with a Hamamatsu ImagEM CCD camera. On the Zeiss microscope, GFP was detected using a 488 nm laser with a 505 to 530 nm filter, YFP was detected using a 514 nm laser with a 535 to 580 nm filter, and propidium iodide and FM4-64 were detected using a 514 nm laser with a 600 to 650 nm filter. On the Quorum system, GFP and YFP were detected using a 491 nm laser with a 528 to 566 nm filter. To allow comparison of the relative brightness between different BiFC treatments, all protoplasts (except the YFP overexpressing positive control) were imaged under identical conditions, including detector gain and exposure time. Images were processed using Volocity (Improvision) or ImageJ, and Adobe Illustrator.

2.4.4 High-pressure freezing, TEM, and immunogold labeling

Stem tissue from the top 1 to 3 cm from the shoot apical meristem was frozen in 0.2 M sucrose in B sample holders (Ted Pella) using a Leica HPM-100 high-pressure freezer. Freeze substitution, resin infiltration, sectioning, post-staining, and imaging were performed as described in McFarlane et al. (2008). Immunolabeling of high-pressure frozen material was performed as described in McFarlane et al. (2008). Primary antibodies were 1/50 polyclonal anti-GFP (A6455 from Molecular Probes); 1/20 polyclonal anti-

calreticulin, generated against calreticulin from castor bean (*Ricinus communis* cv Hale), a generous gift from Sean Coughlan (Coughlan et al., 1997); and 1/50 polyclonal anti-PIP2, generated against PIP2 from tobacco (*Nicotiana tabacum* cv Petit Havana SR1), a generous gift from Ralf Kaldenhoff, (Bots et al., 2005). Secondary antibody was 1/100 10 nm gold-conjugated goat-anti-rabbit (Ted Pella). Images were processed using ImageJ and Adobe Illustrator.

2.4.5 Gene expression analysis

Total RNA was extracted using TRIzol reagent (Invitrogen) from stem segments 1 to 3 cm from the shoot apical meristem or from 10-day-old seedlings grown in liquid AT medium plus 1% sucrose, with and without 5 mM DTT (as positive and negative controls for the unfolded protein response, respectively). cDNA was synthesized from 15 µg of RNA using an oligo dT-18 primer and SuperScript III reverse transcriptase (Invitrogen). RT-PCR was performed for 20 cycles using 1 µL of cDNA with intron-flanking, gene-specific primers for *HSP90.7, BiP1/BiP2* (not specific to either gene alone, since these are 97% identical), *CALNEXIN1, CALRETICULIN2,* and *PDI-LIKE9* (Table 2.1). cDNA levels were normalized using primers for the *UBC10* ubiquitin conjugating enzyme gene for 20 cycles. PCR products were visualized using SYBRSafe (Invitrogen).

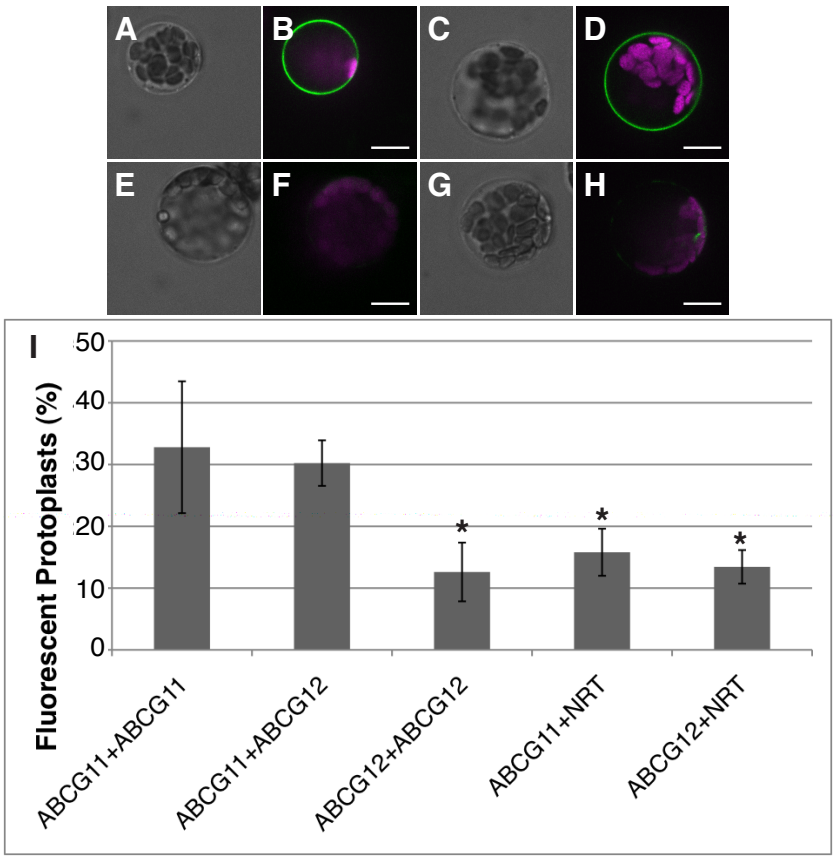

Figure 2.1: ABCG11 and ABCG12 heterodimerize and ABCG11 homodimerizes in the BiFC system. Only protoplasts with intact plasma membranes, shown with bright-field light microscopy (A, C, E, G), were tested for the presence of yellow fluorescence, indicating protein–protein interaction due to assembly of split YFP, shown with confocal microscopy (B, D, F, and H). Co-transformation of *cYFP-ABCG11* and *nYFP-ABCG11* into protoplasts with intact plasma membranes (A) generates yellow fluorescence (false-colored green) at the plasma membrane, surrounding chloroplast autofluorescence (false-colored magenta) in confocal (B). Co-transformation of *cYFP-ABCG11* and *nYFP-ABCG12* also generates yellow fluorescence at the plasma membrane (C and D). However, co-transformation of *cYFP-ABCG12* and *nYFP-ABCG12* (E and F) or *cYFP-ABCG11* and *NRT3.1-nYFP* (G and H) generated only faint yellow fluorescence in a low proportion of protoplasts. Results were quantified as the percentage of fluorescent protoplasts, relative to the percentage of fluorescent protoplasts in the positive control (full-length YFP) (I). n = 8 independent experiments (total of >1300 protoplasts scored per treatment), bars represent SE, * denotes statistically significant differences between samples ($p < 0.05$, ANOVA), and scale bars represent 10 μm. All protoplasts (except for the overexpressing YFP control) were imaged at the same exposure time and detector gain to allow for comparisons of relative fluorescence. Reproduced with permission from McFarlane et al., 2010; Copyright American Society of Plant Biologists © 2010 (www.plantcell.org).

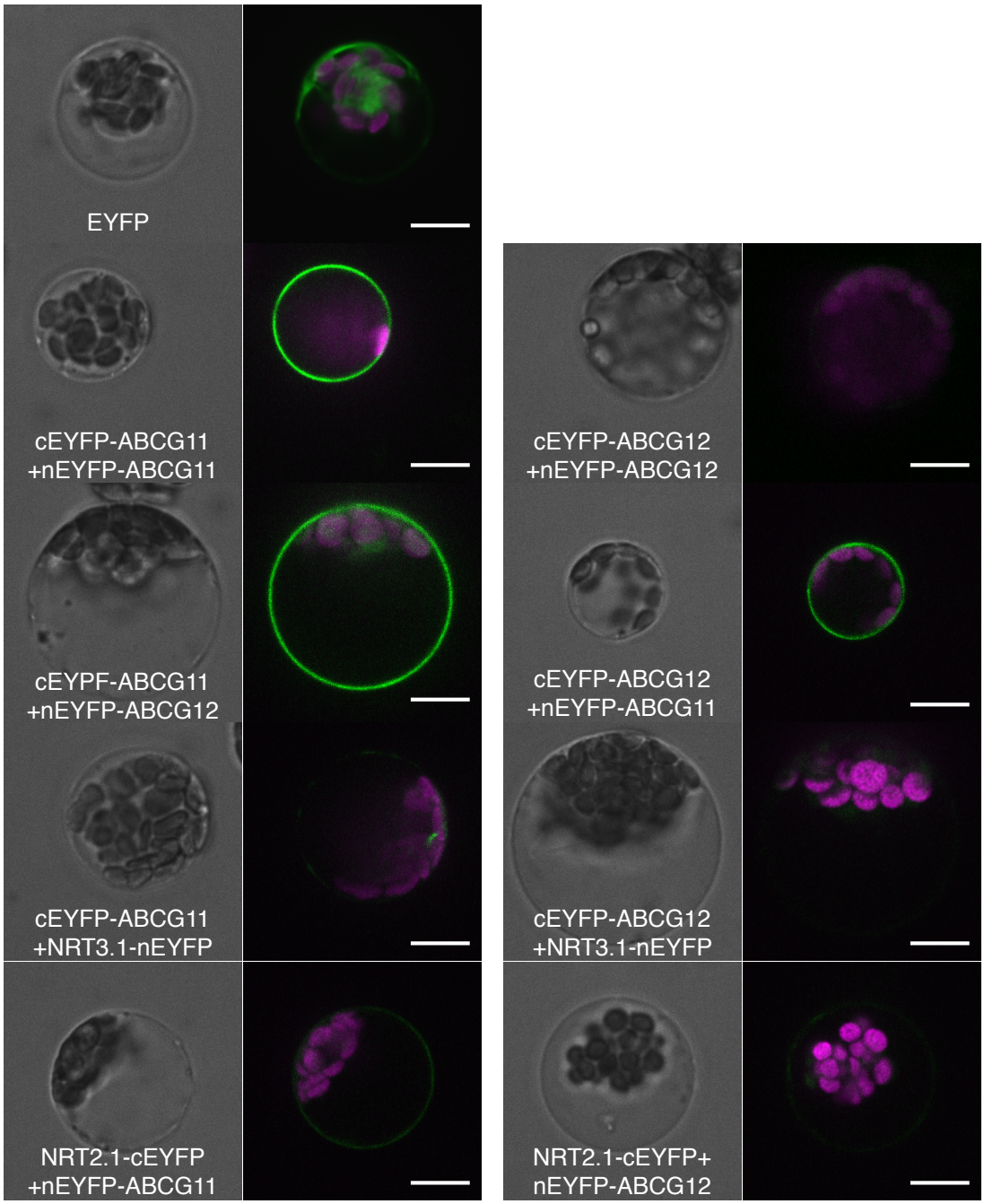

Figure 2.2: Controls for BiFC protein–protein interaction assay. All combinations of the *ABCG11, ABCG12, NRT2.1*, and *NRT3.1* constructs were transformed into Arabidopsis protoplasts. Only healthy protoplasts, indicated by an intact plasma membrane in brightfield microscopy, were scored. Significant yellow fluorescence, indicating a positive interaction, was only observed in *cYFP-ABCG11 + nYFP-ABCG11, cYFP-ABCG11 + nYFP-ABCG12, and cYFP-ABCG12 + nYFP-ABCG11* treatments. All protoplasts (except the over-expressing EYFP control) were imaged at the same exposure to allow for comparisons of relative fluorescence. YFP is false coloured green, chloroplast are false coloured magenta. Scale bars represent 10 μm. Reproduced with permission from McFarlane et al., 2010; Copyright American Society of Plant Biologists © 2010 (www.plantcell.org).

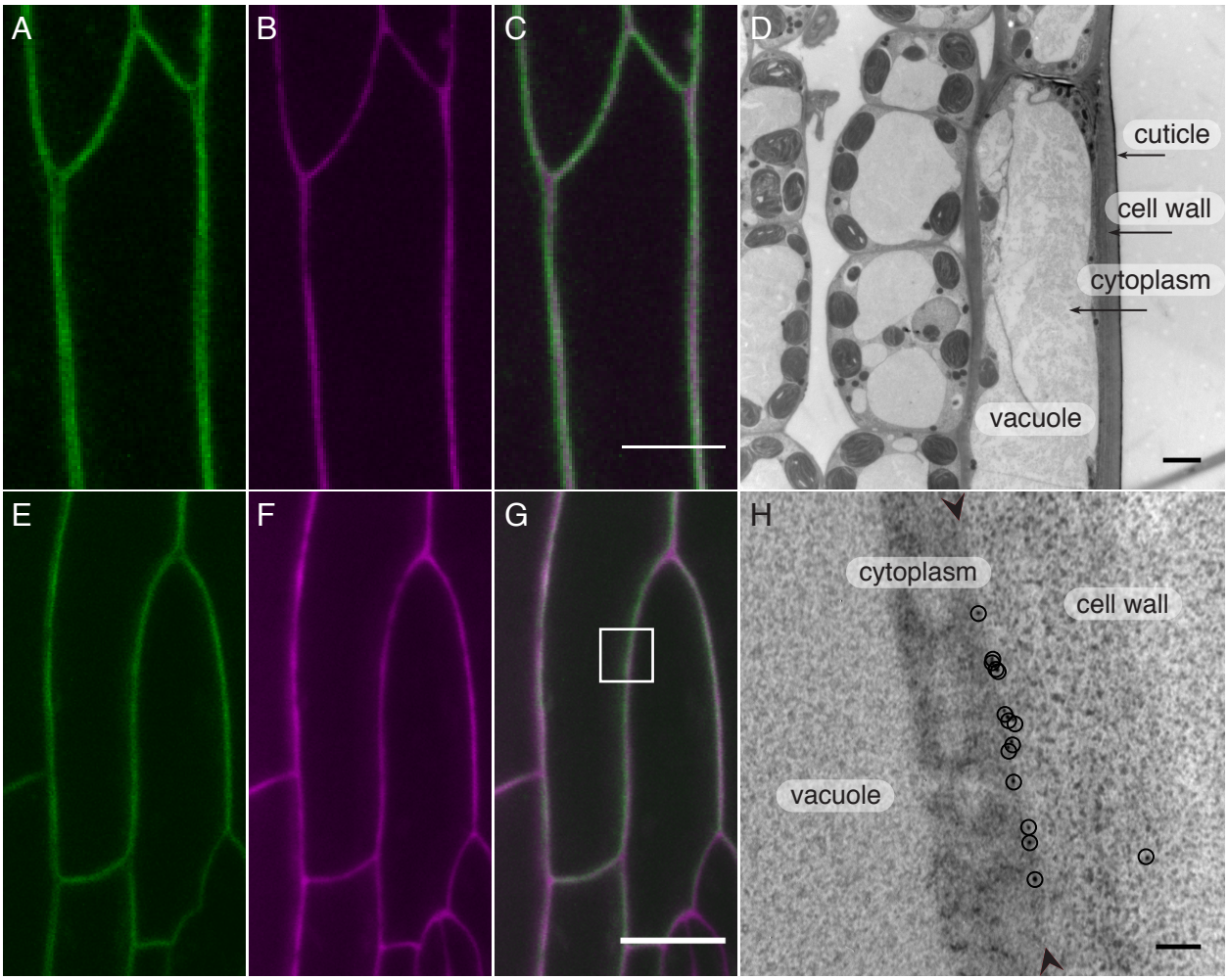

Figure 2.3: ABCG11 trafficking to the plasma membrane is independent of ABCG12. In *abcg11* mutants (A to C), YFP-ABCG11 is localized to the plasma membrane (A), as shown by counterstaining with propidium iodide (B) and merge (C). TEM of the wild-type stem illustrates epidermal cell morphology (D). In *abcg11 abcg12* double mutants (E to H), YFP-ABCG11 is also localized to the plasma membrane (E), where it colocalizes with FM4-64 (F) in the merge (G). TEM immunogold localization with anti-GFP confirms YFP-ABCG11 localization to the plasma membrane (H). The white box in (G) highlights an area that is representative of the field of view in (H). Circles highlight gold particles, and arrowheads denote the plasma membrane. Scale bars represent 10 mm in confocal images, 5 μm in (D), and 200 nm in (H). Reproduced with permission from McFarlane et al., 2010; Copyright American Society of Plant Biologists © 2010 (www.plantcell.org).

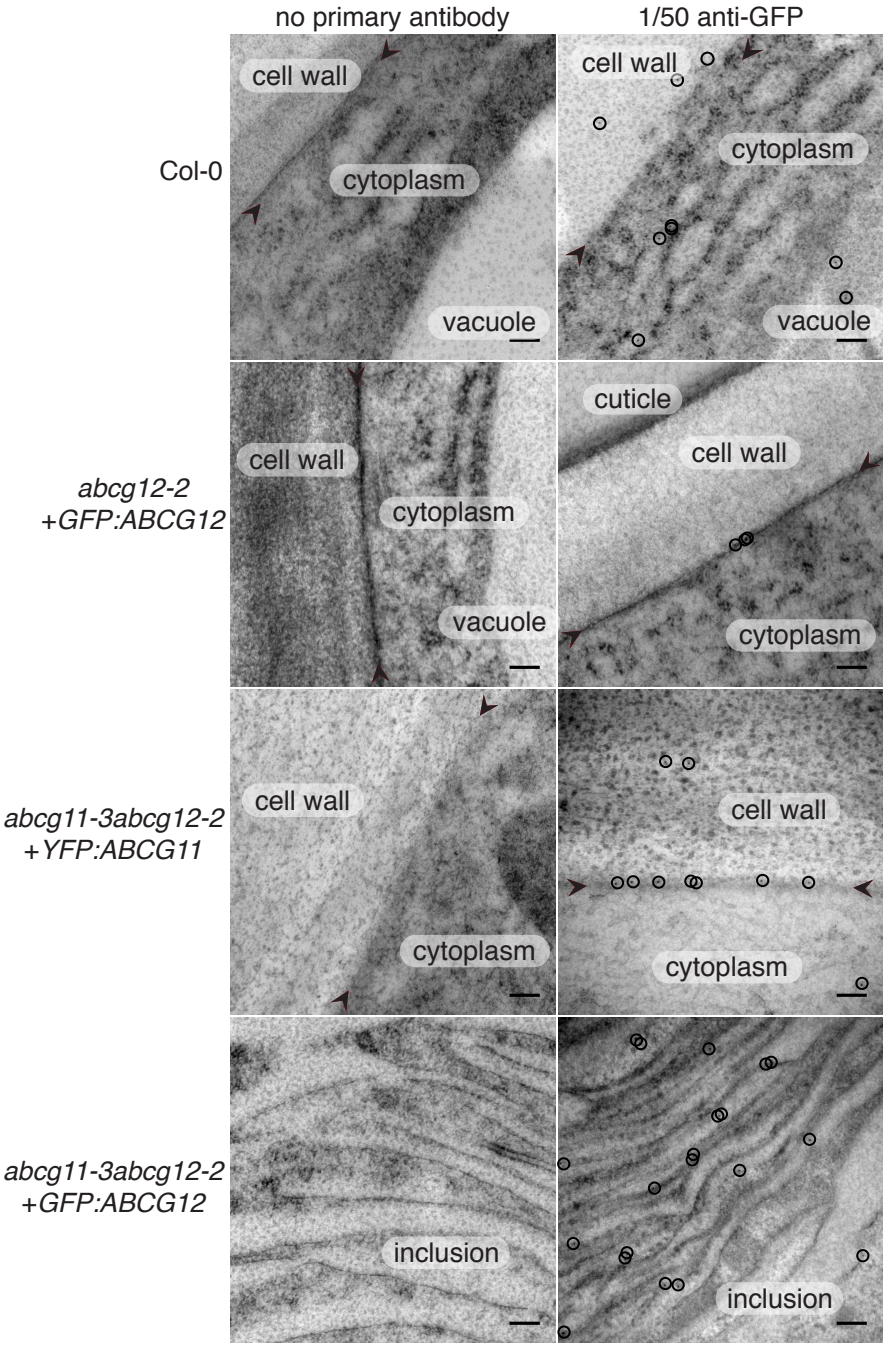

Figure 2.4: Controls for anti-GFP immunogold TEM. No significant labeling was detected when sections were probed without a primary antibody, as a negative control. Some anti-GFP signal was detected in the cytoplasm, vacuole, and cell wall of wild-type cells. However, signal was significantly enriched above background at the plasma membranes of *abcg12* mutants expressing GFP-ABCG12 and *abcg12 abcg11* double mutants expressing YFP-ABCG11. In *abcg11 abcg12* double mutants expressing GFP-ABCG12, most signal was restricted to the intracellular inclusions. Circles highlight gold particles and arrowheads denote the plasma membrane. Scale bars represent 200 nm. Reproduced with permission from McFarlane et al., 2010; Copyright American Society of Plant Biologists © 2010 (www.plantcell.org).

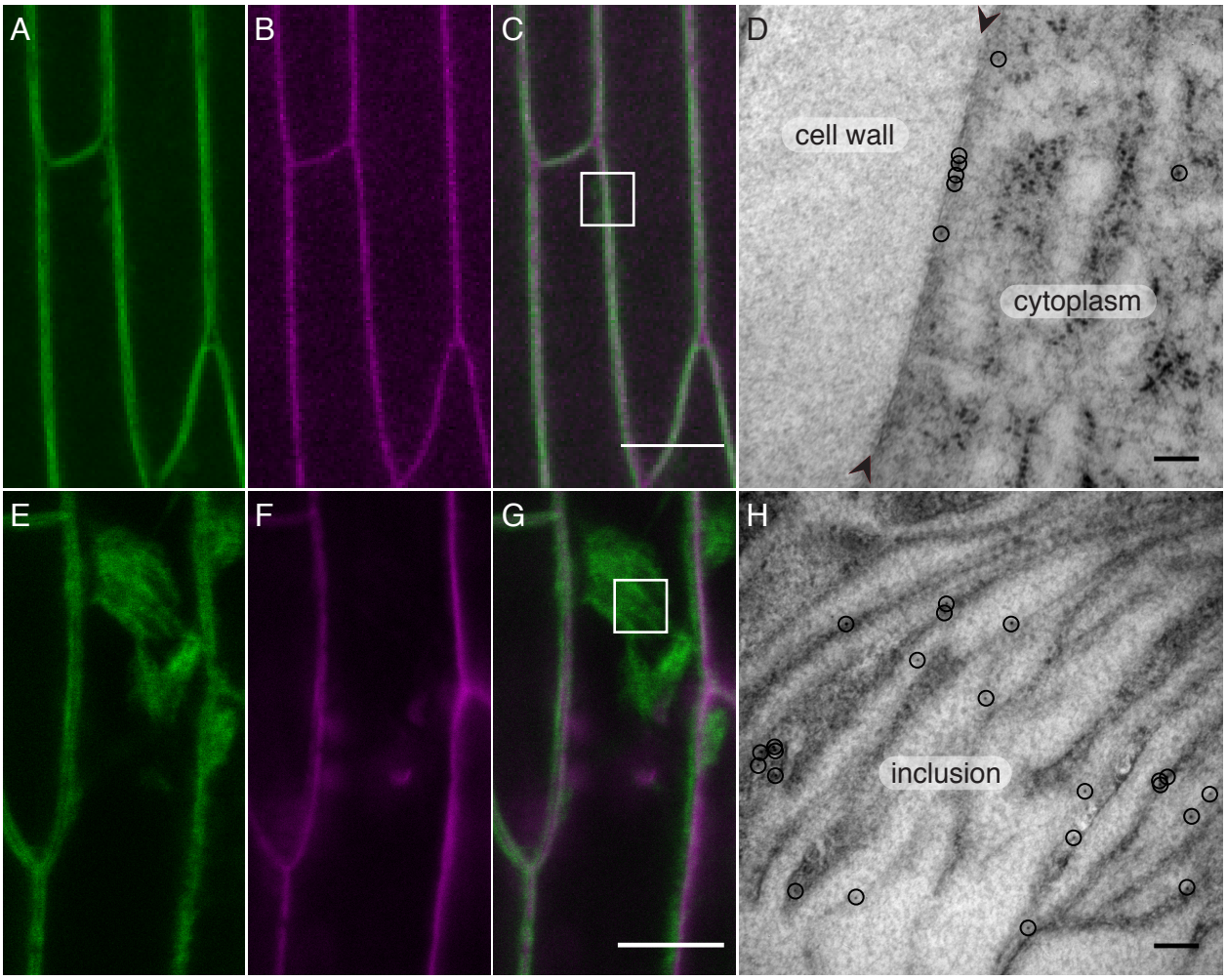

Figure 2.5: ABCG12 trafficking to the plasma membrane is dependent upon ABCG11. In *abcg12* mutants (A to D), GFP-ABCG12 is localized to the plasma membrane (A), as shown by counterstaining with the cell wall dye propidium iodide (B), merge (C), and TEM immunogold localization with anti-GFP (D). In *abcg11 abcg12* double mutants (E to H), GFP-ABCG12 is retained within the ER and in lipid inclusions of these mutants (E) and fails to colocalize with the plasma membrane dye FM4-64 (F) in the merge (G). TEM immunogold localization with anti-GFP confirms GFP-ABCG12 localization to inclusions (H). White boxes in (C) and (G) highlight an area that is representative of the field of view in (D) and (H), respectively, circles highlight gold particles, and arrowheads denote the plasma membrane. Scale bars represent 10 μm in confocal images and 200 nm in TEM. Reproduced with permission from McFarlane et al., 2010; Copyright American Society of Plant Biologists © 2010 (www.plantcell.org).

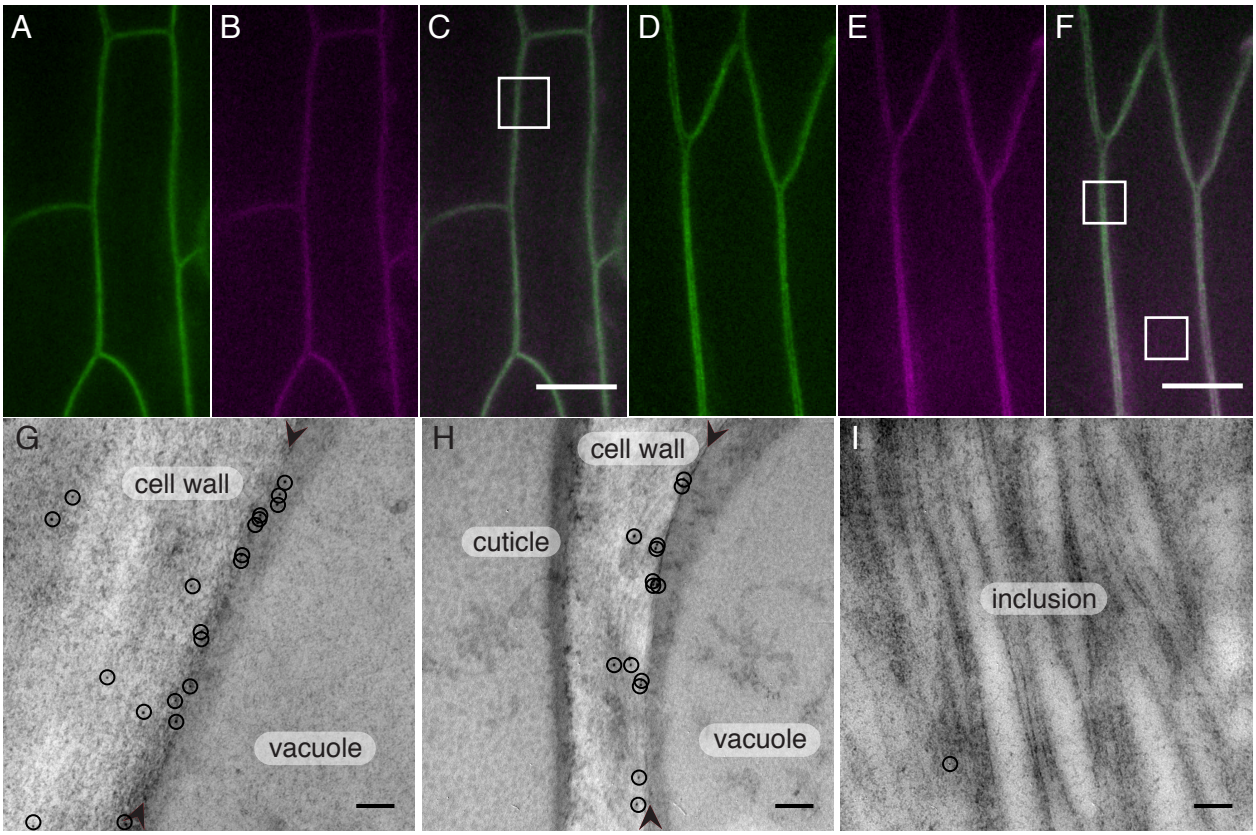

Figure 2.6: Trafficking of proteins to the plasma membrane is independent of ABCG11. In wild-type stem epidermal cells, GFP-LTI6b is localized to the plasma membrane (A), as shown by counterstaining with FM4-64 (B), and the merge (C). In *abcg11* mutants (E-H), GFP-LTI6b is also localized to the plasma membrane (D), where it colocalizes with FM4-64 (E) in the merge (F). Similarly, in wild type the PIP2 aquaporin is localized to the plasma membrane (G). PIP2 is also localized to the plasma membrane in *abcg11* mutants (H), and is not retained within the *abcg11* mutant inclusions (I). White boxes in confocal images highlight an area that is representative of the field of view in the TEM images, circles highlight gold particles, and arrowheads denote the plasma membrane. Scale bars represent 10 μm in confocal images and 200 nm in TEM. Reproduced with permission from McFarlane et al., 2010; Copyright American Society of Plant Biologists © 2010 (www.plantcell.org).

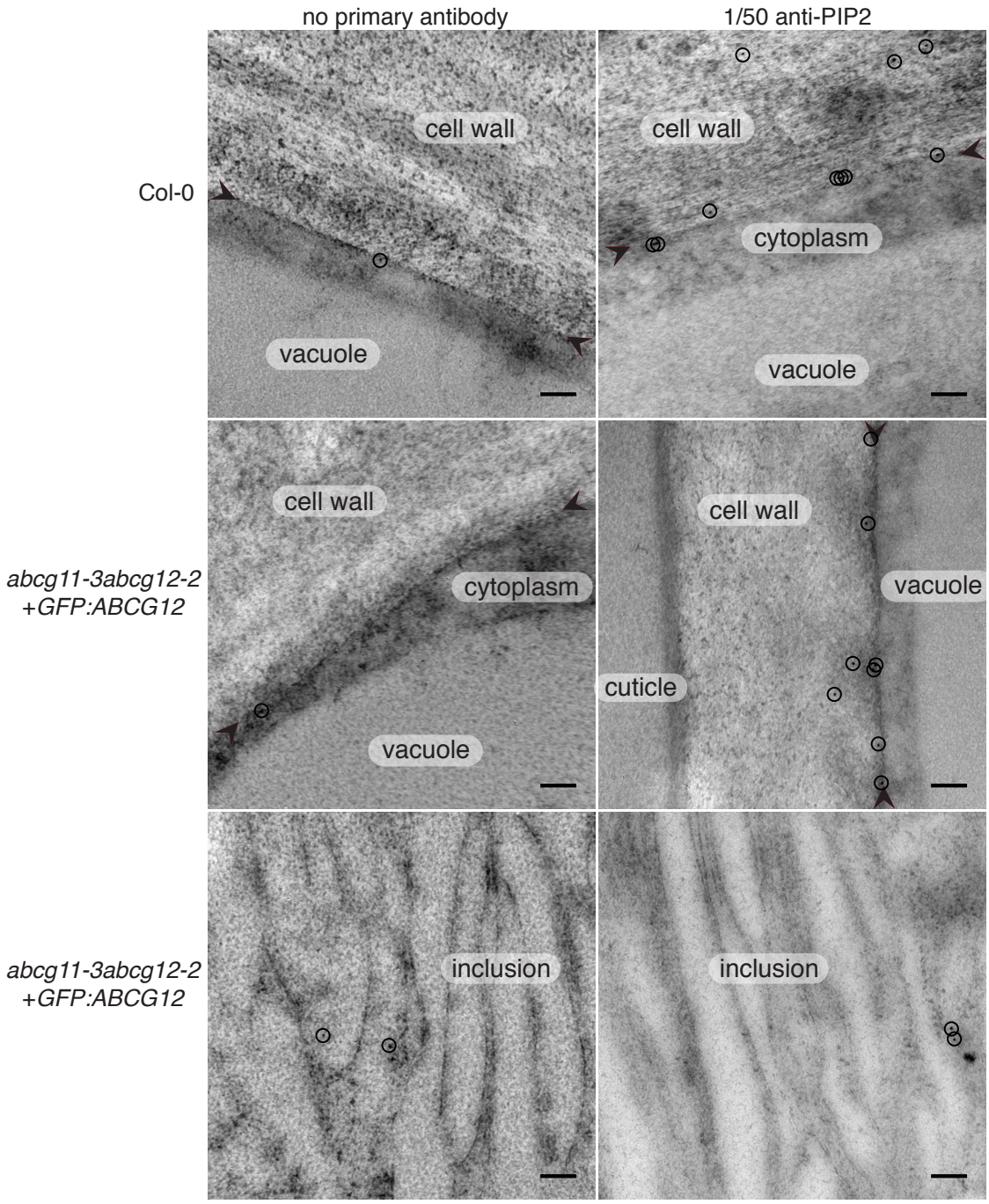

Figure 2.7: Controls for anti-PIP2 immunogold TEM. Anti-PIP2 signal accumulated in the plasma membrane of both wild-type and *abcg11 abcg12* mutants expressing GFP-ABCG12. No significant label was detected when sections were treated without the primary antibody, nor was significant label detected in the inclusions of *abcg11abcg12* mutants expressing GFP-ABCG12. Circles highlight gold particles, and arrowheads denote the plasma membrane. Scale bars represent 200 nm. Reproduced with permission from McFarlane et al., 2010; Copyright American Society of Plant Biologists © 2010 (www.plantcell.org).

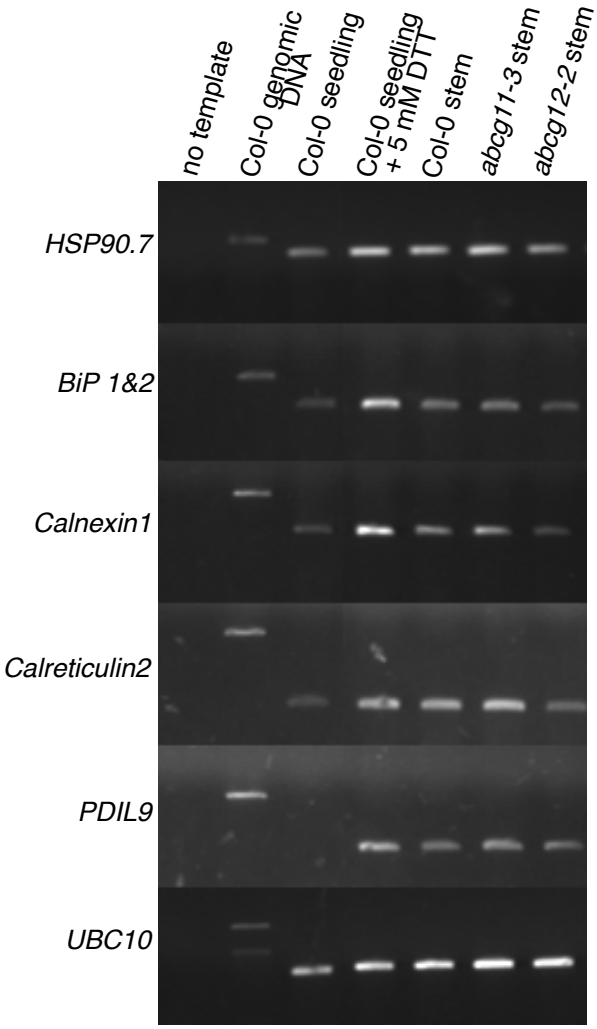

Figure 2.8: The unfolded protein response is not significantly upregulated in *abcg11* mutants with inclusions. UPR genes were induced in seedlings treated with DTT as a positive control, but not in untreated seedlings, as measured by RT-PCR. Wild-type, *abcg11*, and *abcg12* mutant stems showed similar levels of expression of all UPR genes tested. cDNA levels were normalized against transcript levels of the gene encoding an ubiquitin conjugating enzyme, *UBC10*. Reproduced with permission from McFarlane et al., 2010; Copyright American Society of Plant Biologists © 2010 (www.plantcell.org).

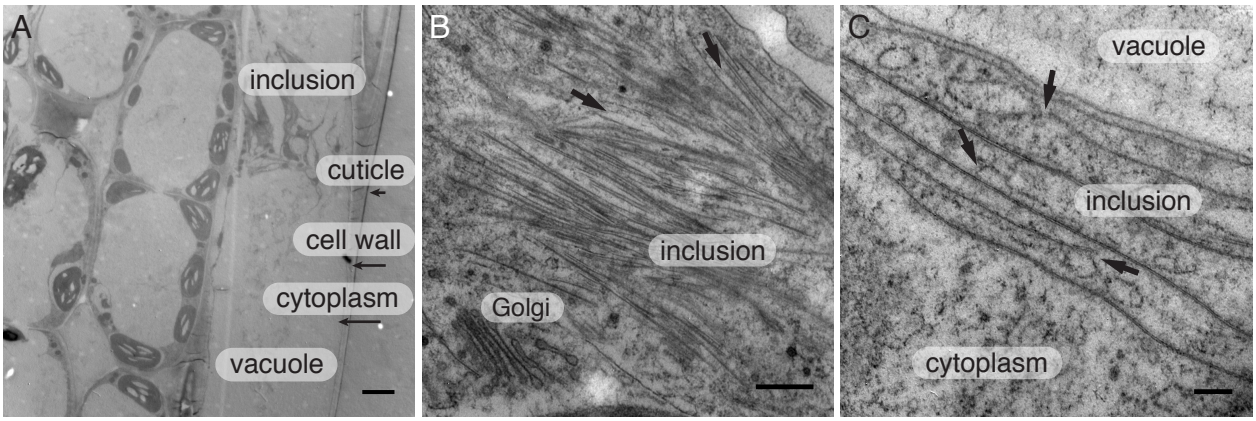

Figure 2.9: Membrane inclusions in *abcg11* mutants are closely associated with the ER. Stem epidermal cells of *abcg11* mutants accumulate inclusions that protrude into the large central vacuole (A). These inclusions are closely associated and interspersed with the electron-lucent ER (B and C); however, the morphology of the Golgi apparatus seems unaffected (B). Arrows in (B) and (C) highlight close associations between ER and inclusions. Scale bars represent 5 mm in (A), 500 nm in (B), and 200 nm in (C). Reproduced with permission from McFarlane et al., 2010; Copyright American Society of Plant Biologists © 2010 (www.plantcell.org).

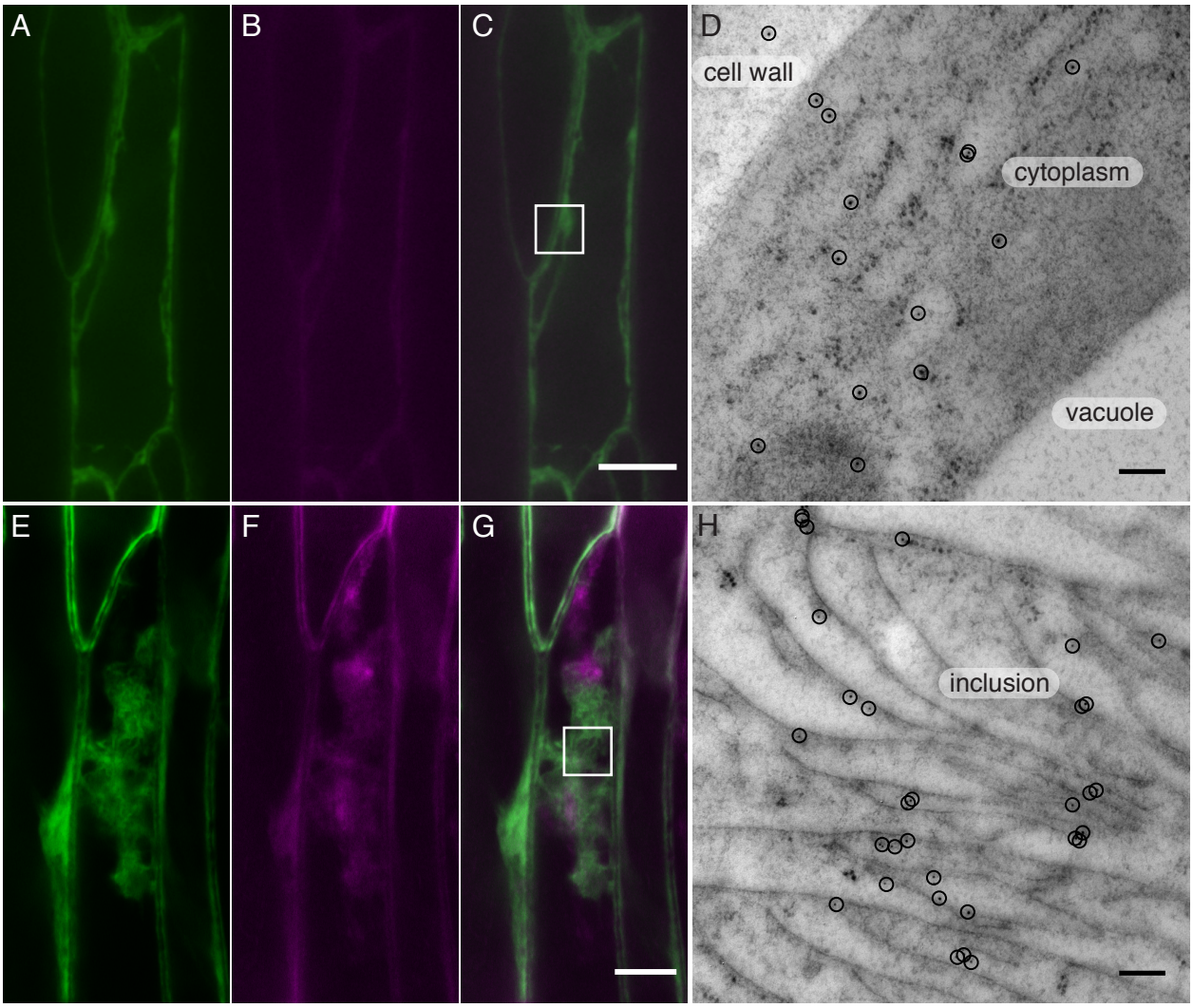

Figure 2.10: Membrane inclusions in *abcg11* mutants are contiguous with the ER. In wild-type stem epidermal cells (A to D), GFP-HDEL labels the ER network (A), and Nile red (a lipid dye) faintly labels cellular membranes (B), which partially colocalize with GFP-HDEL in the merge (C). TEM immunogold labeling with anti-calreticulin confirms the presence of this epitope in the wild-type electron-lucent ER (D). In *abcg11* mutants (E to H), GFP-HDEL labels the reticulate ER network as well as large aggregations in the center of the cells (E). Nile red signal indicates that these inclusions are lipidic (F), and GFP-HDEL and Nile red overlap in inclusions in the merge (G). TEM immunogold labeling with anti-calreticulin shows an accumulation of this ER epitope in inclusions (H). White boxes in (C) and (G) highlight an area that is representative of the field of view in (D) and (H), respectively, and circles highlight gold particles. Scale bars represent 10 μm in confocal images and 200 nm in TEM. Reproduced with permission from McFarlane et al., 2010; Copyright American Society of Plant Biologists © 2010 (www.plantcell.org).

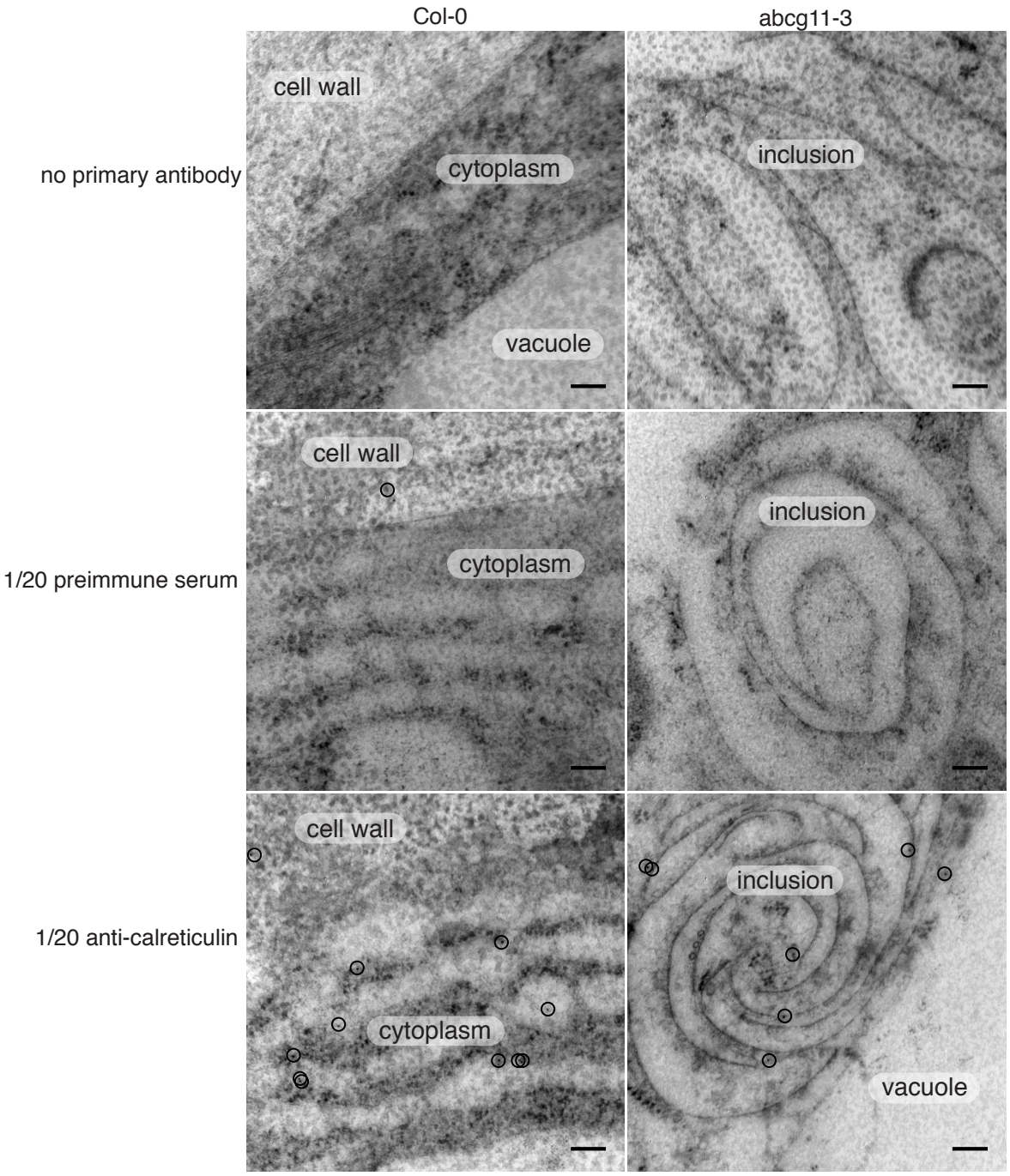

Figure 2.11: Controls for anti-calreticulin immunogold TEM. No significant labeling was detected when sections of each genotype (Col-0 wild-type and *abcg11* mutants) were probed without a primary antibody, or with pre-immune serum, as negative controls. Anti-calreticulin signal was detected within the electron-lucent ER of wild-type cells, but was prominent in inclusions in *abcg11* mutants. Circles highlight gold particles. Scale bars represent 200 nm. Reproduced with permission from McFarlane et al., 2010; Copyright American Society of Plant Biologists © 2010 (www.plantcell.org).

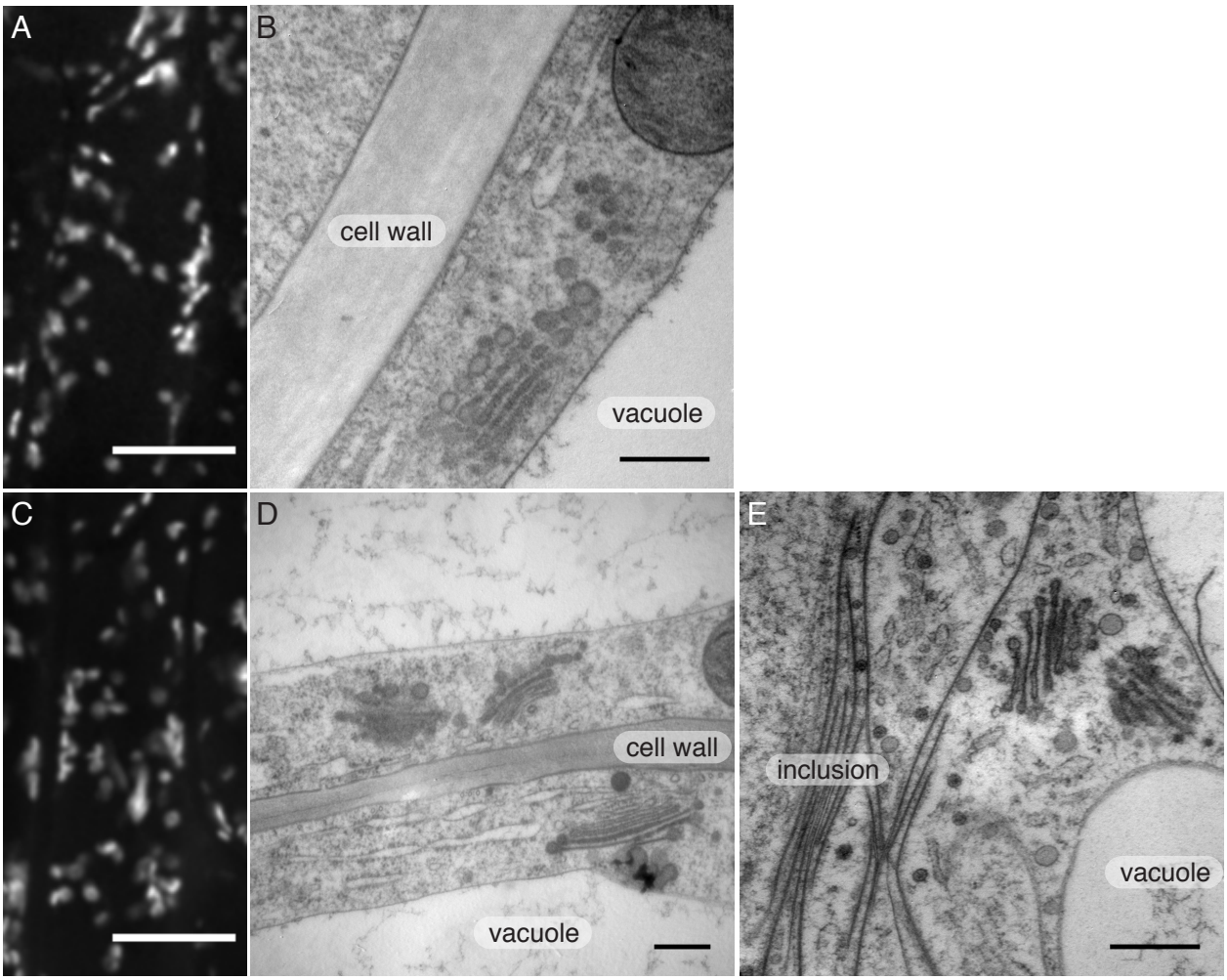

Figure 2.12: The Golgi apparatus is unaffected by membrane inclusions. In wild-type stem epidermal cells (A and B), ST-mRFP labels the Golgi apparatus (A). Distribution of ST-mRFP is unaffected in *abcg12* mutants (C). TEM reveals that the morphology of the Golgi apparatus in wild type (B) closely resembles the Golgi apparatus in *abcg12* and *abcg11* mutants (D and E), despite the presence of lipid inclusions. Scale bars represent 10 μm in confocal images and 500 nm in TEM.

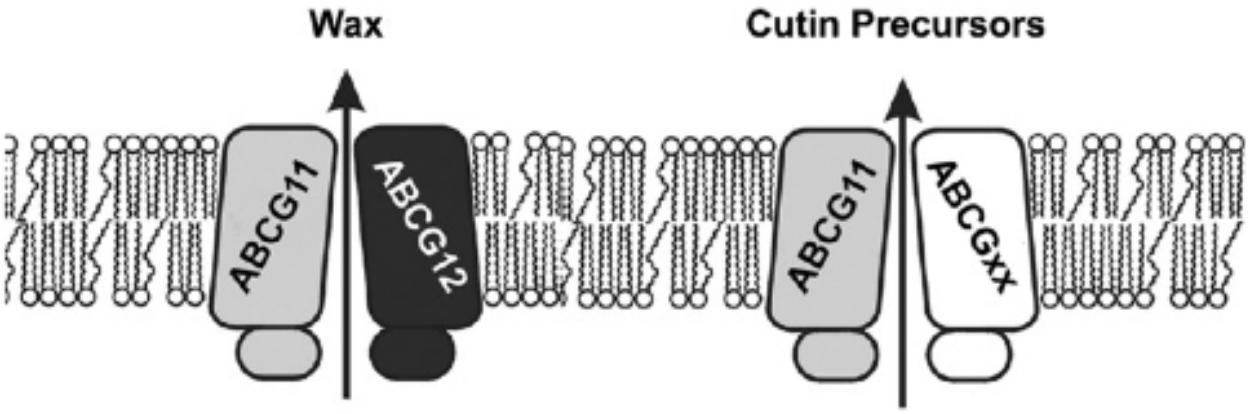

Figure 2.13: A model of the roles of ABCG11 and ABCG12 in cuticular lipid export. ABCG11 and ABCG12 are both required for wax export and ABCG12 forms an obligate heterodimer with ABCG11 in wax exporting stem epidermal cells. In contrast, ACBG11 is capable of forming flexible dimer partnerships, including homodimerization (represented by ABCG11-ABCGxx). Additionally, ABCG11 is required for cutin export from stem epidermal cells. Reproduced with permission from Bird, 2008; Copyright © 2008, Elsevier.

Name	Primer Sequence (5` -> 3`)	Purpose
ABCG11.P1	TCGAATGCAGTTCTTTGCAC	genotyping *abcg11-3* mutants
ABCG11.P2	AACAGATTGTCCCGGAGATG	genotyping *abcg11-3* mutants
ABCG11.P3	CAGGTTCGAGAATTCAATGGAGATAGAA-GCAAGCAGA	Cloning *ABCG11* for BiFC
ABCG11.P4	CTTAAAATATCCCGGGCCATCTGCGAGC-TCCATCTGT	Cloning *ABCG11* for BiFC
ABCG12.P1	GTGAAATTCCGTCCTGGTGT	genotyping *abcg12-2* mutants
ABCG12.P2	GCTTTGCTTGTATCGCCTTC	genotyping *abcg12-2* mutants
ABCG12.P3	CTTAAAATATCCCGGGTTAATTAATTGGAG-AGGTAAGAC	Cloning *ABCG12* for BiFC
ABCG12.P4	CAGGTTCGAGAATTCAATGGAGTTAGAGA-GTACGAGCA	Cloning *ABCG12* for BiFC
UBC10.P1	GGTAGCATTTGCCTCGACAT	RT-PCR for *UBC10* (At5g53300)
UBC10.P2	CTTCGTGCAGTGGACTCGTA	RT-PCR for *UBC10* (At5g53300)
HSP90.7.P1	GGATCATGCAGTCCCAAACT	RT-PCR for *HSP90.7* (At4g24190)
HSP90.7.P2	GATTTCCTCGTCGGCTACTG	RT-PCR for *HSP90.7* (At4g24190)
BiP1/2.P1	CCAAGGACTGCAGGCTACTC	RT-PCR for *BiP1/BiP2* (At5g28540)
BiP1/2.P2	GCCTTGTCCTCTGCTTTCAC	RT-PCR for *BiP1/BiP2* (At5g28540)
CNX1.P1	AAAGACGAGAAGGTCGCTGA	RT-PCR for *Calnexin 1* (At5g61790)
CNX1.P2	GTTGCTCGGCTTTCTCAATC	RT-PCR for *Calnexin 1* (At5g61790)
CRT2.P1	GAAACATGGGGAAAGCTCAA	RT-PCR for *Calreticulin 2* (At1g09210)
CRT2.P2	TCTCCTCGGCCTTAGATTCA	RT-PCR for *Calreticulin 2* (At1g09210)
PDIL9.P1	TCCAAAGCTGAAGGAAGGAA	RT-PCR for *PDI-like 9* (At2g32920)
PDIL9.P2	ATTTCCTTTTCCACCGGTTC	RT-PCR for *PDI-like 9* (At2g32920)

Table 2.1: A list of primers employed in Chapter 2. Reproduced with permission from McFarlane et al., 2010; Copyright American Society of Plant Biologists © 2010 (www.plantcell.org).

Chapter 3: Very long chain lipids are secreted via Golgi-TGN-mediated vesicle trafficking in Arabidopsis.

3.1 Introduction

The aerial, non-woody tissues of all land plants are covered by a waxy cuticle that protects the plant against non-stomatal water loss (Riederer and Schreiber, 2001). The cuticle represents the first barrier between the plant and its environment and mediates important biotic and abiotic interactions. Furthermore, evolution of the cuticle was one of the key adaptations that allowed plant colonization on land (Raven and Edwards, 2004). The cuticle has two main components: waxes and cutin. Cutin is a tough, cross-linked polyester matrix primarily composed of C16 and C18 oxygenated fatty acids and glycerol (Pollard et al., 2008). Wax is a heterogeneous mixture of very long chain fatty acid derivatives (primarily 29 alkane in *Arabidopsis thaliana*), which can also include terpenoids, phenolics, and other compounds, though these are a minor component of Arabidopsis wax (Samuels et al., 2008). Arabidopsis inflorescence stems have been a fruitful model system for studying very long-chain lipid synthesis because stem epidermal cells synthesize and export an extraordinary volume of cuticular waxes during their development (Suh et al., 2005). Recent characterization of key enzymes in plant alkane biosynthesis (Bernard et al., 2012, Haslam et al., 2012) has provided excellent potential to manipulate lipid synthesis in plants for industrial applications (Dyer and Mullen, 2008; Jetter and Kunst, 2008). However, simply expressing lipid synthesis enzymes in plants has often resulted in lower yields than expected (Snapp and Lu, 2012), highlighting the need to understand the cell biological context of these enzymes and of their substrates and products (Dyer and Mullen, 2008).

As a result of the combination of biochemical approaches, forward genetic screens yielding the *eceriferium* (*cer)* mutants (Koornneef et al., 1989), and reverse genetics approaches (Greer et al., 2007, Li et al., 2008), almost all of the enzymes in the wax biosynthesis pathway have been identified. Plastid-derived C16 or C18 fatty acids are transported to the endoplasmic reticulum (ER), where the elongase complex catalyzes sequential additions of two carbons at a time to increase the chain length to C28 (Figure

3.1). In Arabidopsis, the core elongase complex is composed of four enzymes: CER6, KCR1, PAS2, and CER10 (Millar et al., 1999; Zheng et al., 2005; Joubès et al., 2008; Bach et al., 2008; Beaudoin et al., 2009). Fatty acid elongation past C28 also requires CER2, although the mechanism underlying this requirement is not known (Figure 3.2; Haslam et al., 2012). The resulting products of the elongase complex are very long chain fatty acids of various lengths (primarily C26-C32 in Arabidopsis stems). These are further modified to form other wax components via two pathways: the alkane pathway and the primary alcohol pathway (Figure 3.2; Samuels et al., 2008). Alkanes are generated via an undefined mechanism involving CER1 and CER3 and an unidentified cytochrome b5 (Bernard et al., 2012). These alkanes may be modified by oxygenation by the midchain alkane hydroxylase cytochrome P450 (MAH1) to generate the midchain oxygenated components, secondary alcohols and ketones (Greer et al., 2007). Interestingly, all of the wax synthesis enzymes have been localized to the ER; it may be that these enzymes are organized into functional units to allow for metabolic channeling, as has been proposed for the enzymes involved in oil body synthesis (Shockey et al., 2006; Roudier et al., 2010; Gidda et al., 2011).

In contrast to wax synthesis, little is known about how waxes are trafficked to the cell surface. Two plasma membrane ATP-binding cassette transporters (ABCs) of the G subfamily are required for wax export (Pighin et al., 2004; Bird et al., 2007). These transporters form an obligate heterodimer, and when either half-transporter is disrupted, waxes accumulate in the ER (McFarlane et al., 2010; Chapter 2). Two extracellular glycosylphosphatidylinositol (GPI)-anchored lipid transfer proteins (LTPs) are further required for wax accumulation on the cell surface (DeBono et al., 2008; Lee et al., 2008; Kim et al., 2012). Thus, although several components of the molecular machinery of wax transport at the plasma membrane have been identified, the mechanisms by which waxes are transported from the ER to the plasma membrane remain undefined. This is a particularly interesting question because the cuticular waxes are predicted to partition into membrane bilayers (Coll et al., 2007), which makes them unusual secretory cargo for canonical vesicle trafficking.

Several hypotheses have been proposed for the transport of waxes from the ER to the plasma membrane (Samuels et al., 2008). The most obvious route is vesicular traffic. In this case, waxes would be incorporated into vesicles at the ER, travel to and through the

Golgi apparatus and the TGN, and then move to the plasma membrane via vesicle secretion. Although this model represents the simplest possible pathway, computational modeling of waxes in lipid bilayers indicates that alkanes partition entirely into the hydrophobic phase of the bilayer (Coll et al., 2007), which would make them difficult to detect via the typical receptor-cargo interaction. An alternative hypothesis to vesicle-mediated wax trafficking is non-vesicular trafficking, that is, intracellular movement that is independent of vesicle formation or fusion (Levine, 2004). This mechanism has been established in yeast and mammalian cells, but has yet to be ascertained in plant cells (Toulmay and Prinz, 2011). In this scenario, intracellular, soluble, lipid transfer proteins could shuttle waxes directly from their site of synthesis at the ER to the ABC transporters in the plasma membrane. Non-vesicular traffic typically occurs at sites of close contact between the donor and acceptor membranes, called membrane contact sites (Levine, 2004), which in the case of wax export would be between the ER and the plasma membrane (Samuels and McFarlane, 2011). To date, ER-plasma membrane contact sites have been identified in plants and implicated in lipid transfer and/or remodeling, but their functional components remain unknown (Larsson et al., 2007).

To determine the route by which cuticular waxes are transported from the ER to the plasma membrane, wax levels were examined in several secretion defective mutants, including *gnom like1-1* (*gnl1-1*; Richter et al., 2007; Teh and Moore et al., 2007), *transport particle protein subunit120-4* (*trs120-4*; Qi et al., 2011), and *echidna* (*ech;* Gendre et al., 2011). Both *gnl1-1* and *ech* mutants, but not *trs120-4* mutants, were defective in wax secretion. These results indicate that waxes travel from the ER to the plasma membrane via the Golgi apparatus and vesicle-mediated secretion, and that wax secretion is dependent upon the ECHIDNA complex, but independent of the TRAPP II complex. Interestingly, both *gnl1-1* and *ech* were also defective in wax biosynthesis and ER morphology. Furthermore, *root hair defective3 (rhd3-1)* mutants, which have defects in ER morphology but not secretion (Zheng et al., 2004; Chen et al., 2011c), were also defective in wax synthesis. Together, these data reveal a form and function relationship between ER morphology and wax synthesis, and demonstrate that a proportion of cuticular wax is secreted via the Golgi apparatus. These results have implications for our understanding of the synthesis, intracellular trafficking, and export of lipids from plant cells, which may be

applicable not only to cuticular lipids but also to a wide variety of plant metabolites and lipid-based industrial products.

3.2 Results

3.2.1 Several secretion mutants display defects in wax accumulation on the cell surface

In order to investigate the route by which cuticular waxes are secreted to the cell surface, a number of mutants with characterized defects in protein secretion at different points in the secretory pathway were tested for wax deficiency. For example, *gnl1-1* mutants are defective in an ADP-ribosylation factor guanine nucleotide exchange factor (ARF-GEF) that is required for COPI vesicle formation for retrograde traffic from the Golgi apparatus to the ER; this presumably has an impact on anterograde ER-Golgi traffic as well (Richter et al., 2007; Teh and Moore, 2007). Both *ech* and *trs120-4* are defective in trans-Golgi network (TGN) protein complexes. TRS120 is part of the transport protein particle II (TRAPP II) large GTPase complex, which is required for secretion to the cell wall and cell plate (Qi et al., 2011). ECHIDNA is a protein of unknown function that is part of the ECH/YIP (Ypt/Rab-interacting protein) complex, which is required specifically for secretion from the TGN to the plasma membrane (Gendre et al., 2011; Gendre et al., 2013). All of these mutants display cell elongation defects that result in reduced plant growth (Gendre et al., 2011; Qi et al., 2011; Figure 3.3A), reflecting the importance of secretion in cell wall production.

To compare secretory phenotypes of the different mutants, a secreted form of GFP (secGFP) was used as a qualitative secretion assay in Arabidopsis stem epidermal cells. In wild-type stem epidermal cells, secGFP is secreted via the ER and the Golgi apparatus to the apoplast where GFP signal is quenched by the low pH (Figure 3.3B; Batoko et al., 2000). In contrast to the faint secGFP fluorescence in wild-type cells, all three mutants retained secGFP inside stem epidermal cells (Figure 3.3B). This confirms that *gnl1-1*, *trs120-4*, and *ech* stem epidermal cells are defective in secretion in the cell type of interest for studying wax export.

If wax components are transported via the secretory pathway, then a decrease in cuticular waxes is predicted in these secretion mutants. Examination of wild-type and mutant stems using cryo-scanning electron microscopy (cryo-SEM) revealed a drastic reduction in stem wax crystals in *ech* mutants, relative to wild type, and a moderate reduction in *gnl1-1* (Figure 3.4A). To confirm this defect in cuticular lipid secretion, stem surface waxes were quantified using gas-liquid chromatography coupled to a flame ionization detector (GC-FID). Wild-type stem wax load (mean ± standard error = 17.29 ± 1.16 μg/cm^2) was not significantly different from *trs120-4* mutants (17.50 ± 0.86 μg/cm^2, p = 0.8865, t-test). However, wax loads were significantly reduced in the other two secretion mutants (9.48 ± 0.59 μg/cm^2, p < 0.0001 for *gnl1-1*; 3.21 ± 0.63 μg/cm^2, p < 0.0001 for *ech*; Figure 3.4B). These results reveal that of the three mutants that are defective in protein secretion (as established by the secGFP assay) only two mutants, *gnl1-1* and *ech,* are also defective in wax accumulation on the cell surface. This implies that wax is secreted to the plasma membrane via a Golgi-dependent mechanism that requires both GNL1 and ECH, but is independent of TRS120. Given that the phenotype of *trs120-4* plants is relatively mild compared to *gnl1-1* and *ech* (Figure 3.3A), it is possible that a wax phenotype might be observed in a stronger allele of *trs120*. Unfortunately, all of the more severe alleles are seedling- or embryo-lethal, likely because of their cell plate defects (Qi et al., 2011).

3.2.2 Components of the wax export machinery are correctly localized in *gnl1-1* and *ech*

Wax accumulation on the cell surface requires ABC transporters of the G-subfamily at the plasma membrane (Pighin et al., 2004; Bird et al., 2007). Since these transporters are trafficked through the ER to their site of action at the plasma membrane (McFarlane et al., 2010; Chapter 2), it is possible that the wax accumulation defects in *gnl1-1* and *ech* are due to the mislocalization of these ABCG transporters. To address this, fluorescently tagged 35S-driven YFP-ABCG11 (Bird et al., 2007) and native promoter-driven GFP-ABCG12 (Pighin et al., 2004) were crossed into *gnl1-1* and *ech*. In functionally wild-type stem epidermal cells, i.e. where *abcg11-3* mutants were complemented with the YFP-ABCG11 construct, YFP-ABCG11 signal is localized to the plasma membrane (Figure 3.5A). Similarly, GFP-ABCG12 is localized to the plasma membrane of functionally wild-type cells

(i.e. *abcg12-2* mutants complemented with the GFP-ABCG12 construct) (Figure 3.5B). Both YFP-ABCG11 and GFP-ABCG12, maintained in their respective mutant backgrounds, were primarily localized to the plasma membrane in *gnl1-1* and *ech* (Figure 3.5A and 3.5B). While some internal signal is detected in both mutants, this is negligible compared to the proportion of signal at the plasma membrane (Figure 3.5C). Consistent with the wild-type localization and function of the ABCG transporters, the chemical profiles of the wax secretion mutants are distinct from those of the *abcg* transporter and *ltpg* mutants. While all previously described wax transport mutants (*abcg11*, *abcg12, ltpg1*, and *ltpg2*) are primarily defective in alkane export (Pighin et al., 2004; Bird et al., 2007; DeBono et al., 2008; Kim et al., 2012), *gnl1-1* and *ech* mutants are preferentially defective in accumulation of midchain oxygenated compounds (Figure 3.6). Together, these data demonstrate that the wax accumulation defects in *gnl1-1* and *ech* are not due to mislocalization of the wax export machinery in these mutants.

3.2.3 *gnl1-1* and *ech* are defective in wax biosynthesis

Interestingly, the relative proportions of the waxes that accumulate on *gnl1-1* and *ech* stems are significantly altered compared to wild type (Figure 3.6). Both secretion mutants displayed a preferential decrease in midchain oxygenated compounds (secondary alcohols and ketones, i.e. MAH1 products; Figure 3.6A; Greer et al., 2007) and in exceptionally long chain waxes (compounds greater than 28 carbons long of all chemical species, i.e. CER2 products; Figure 3.6B; Haslam et al., 2012). These results imply that GNL1 and ECH are preferentially required for secretion of midchain oxygenated compounds and exceptionally long chain waxes. To test this hypothesis, the *mah1-1* mutation was crossed into both *gnl1-1* and *ech*, since *mah1* mutants produce nearly wild-type levels of wax, but lack midchain oxygenated compounds and produce higher than wild-type levels of alkanes as a result (Greer et al., 2007; Figure 3.7). Thus, if GNL1 and ECH are preferentially involved in secretion of midchain oxygenated compounds, then increasing alkane levels and reducing midchain oxygenated compounds by introducing the *mah1-1* mutation into *gnl1-1* and *ech* should partially rescue the total wax defect of these mutants. On the contrary, the increased alkane levels and decreased midchain oxygenated compound levels introduced by the *mah1-1* mutation did not result in significantly higher

total wax secretion in either *gnl1-1 mah1-1* ($p = 0.2227$, t-test) or *ech mah1-1* ($p = 0.1788$) double mutants, relative to their respective single mutants (Figure 3.7). Together, these data imply that the preferential decrease in some wax compounds in *gnl1-1* and *ech* mutants is not due to selective secretion of these cargos via GNL1 and ECH.

In order to generate a chemical profile of the waxes that accumulate on the cell surface plus the waxes that are not secreted and accumulate within the cell, stems were homogenized in chloroform to release both surface and intracellular waxes. Wild-type ground stems yielded slightly more wax than surface wax extraction via chloroform dip (17.58 ± 1.69 μg/cm^2 for ground stems, compared to 17.29 ± 1.16 μg/cm^2 for dipped stems). Consistent with the idea that biosynthetic intermediates would be recovered by assaying waxes from whole cells, slightly (<5%), but not significantly decreased levels of some of the end products of wax synthesis, including components longer than 28 carbons (i.e. CER2 products) and midchain oxygenated compounds (i.e. MAH1 products) were recovered (Figure 3.8). Similar to results from surface waxes, the total wild-type wax load (17.58 ± 1.69 μg/cm^2) was not significantly different from *trs120-4* mutants (18.70 ± 0.93 μg/cm^2, $p = 0.6110$). Interestingly, whole stem epidermal cells of both *gnl1-1* and *ech* mutants contained significantly less total wax than wild type (12.30 ± 1.11 μg/cm^2, $p = 0.0242$ for *gnl1-1*; 6.18 ± 0.64 μg/cm^2, $p < 0.0001$ for *ech*; Figure 3.8). This is in contrast to the *abcg12* transporter mutants, which synthesize wild-type levels of wax, despite their inability to export a significant proportion of these waxes (Pighin et al., 2004).

Consistent with this decrease in wax biosynthesis, there was no significant accumulation of waxes inside cells, as assayed by Nile red staining (Figure 3.9). *ech* mutant cells occasionally displayed large aggregations that stained with Nile red. However, these aggregations were extracellular, as defined by YFP-ABCG11 labeling of the plasma membrane (Figure 3.9). These aggregations also label with toluidine blue and FM4-64, implying that they may not be composed exclusively of wax. Given the decrease in total wax biosynthesis in *gnl1-1* and *ech* mutants, it is unsurprising that waxes do not significantly aggregate within these cells, despite the secretion defects of these mutants.

3.2.4 ER morphology defects correlate with the wax biosynthesis defects in *gnl1-1* and *ech*

Since, unlike ABC transporter mutants, the secretory mutants, *gnl1-1* and *ech*, did not accumulate wild-type levels of intracellular wax, the simplest explanation for their reduced wax levels is a biosynthetic defect. Previous studies of both *gnl1-1* and *ech* have revealed defects in ER morphology (Nakano et al., 2009; McFarlane et al., 2013). Therefore, it is possible that the wax biosynthesis defect in these mutants may be related to this ER disorganization phenotype. Consistent with this idea, ER defects were observed in *gnl1-1* and *ech* using confocal microscopy of the ER marker GFP-HDEL (Figure 3.10). Using three-dimensional surface rendering of the ER network in a single cell, the reticulate cortical network, trans-vacuolar strands, and the peri-nuclear region of wild type can be viewed in a single image. In *gnl1-1* and *ech* mutants, defects in GFP-HDEL distribution included ER fragmentation and aggregation (Figure 3.10B). The ER morphology of mutants and wild-type epidermal cells was also assessed using transmission electron microscopy (TEM). In wild type, tubular ER is largely confined to the peripheral cytoplasm. In *gnl1-1* and *ech* mutants, large dilations of the ER were observed, which were identified as ER-derived by their electron lucent appearance and by the presence of ribosomes on their cytoplasmic surface (Figure 3.10C). Unlike *gnl1-1* and *ech* mutants, which have decreased surface wax and ER morphology defects, *trs120-4* mutants, which had wild-type wax load by GC-FID, displayed no ER morphology defects when stained with hexyl rhodamine B, which labels both ER and mitochondria (Figure 3.10).

To test whether ER morphology defects, independent of vesicle traffic phenotypes, affect wax biosynthesis, wax levels were assayed in *rhd3-1* mutants. These mutants are defective in an ER-shaping protein similar to human Atlastins and yeast Sey1p and have defects in ER morphology but not secretion (Hu et al., 2003; Hu et al., 2009; Chen et al., 2011c; Figure 3.10). GC-FID indicated that *rhd3-1* mutants were also defective in wax synthesis relative to wild type (7.44 ± 0.52 μg/cm^2 for *rhd3-1* surface waxes compared to 17.29 ± 1.16 μg/cm^2 for wild type, $p < 0.0001$; 8.34 ± 0.78 μg/cm^2 for *rhd3-1* total waxes, compared to 17.58 ± 1.69 μg/cm^2 for wild type, $p < 0.0001$; Figure 3.11). This suggests that the defect in ER morphology is directly related to the decrease in wax synthesis, rather than being the result of some secondary defect in *gnl1-1* and *ech*. Indeed, there was a

correlation between the qualitative degree of disorganization of the ER (Figure 3.10) and the severity of the wax synthesis defect (Figure 3.8; Figure 3.11).

It is possible that these defects in ER morphology result in a decrease in wax synthesis via a down-regulation or a mislocalization of the wax synthesis enzymes. To address this first hypothesis, transcript levels of wax synthesis enzymes were monitored in wild-type and mutant stems. No drastic changes were observed in transcript levels of several key wax biosynthesis genes in *rhd3-1*, *trs120-4*, *gnl1-1*, or *ech* stems, relative to wild type (Figure 3.12), indicating that there was no negative feedback at the transcript level to regulate wax synthesis in these mutants. Because the most drastic biosynthesis decreases were observed for lipids longer than C28, the localization of CER2-GFP (Haslam et al., 2012) was examined in the complemented *cer2-5* mutant and in *gnl1-1* and *ech*. In *cer2-5* complemented with *CER2pro::CER2-GFP*, the fluorescently tagged enzyme was detected in the ER, with some signal in the cytoplasm and nucleus, as reported by Haslam et al. (2012). Preliminary results revealed no large-scale changes in CER2-GFP (maintained in the *cer2-5* mutant background) localization to the irregular ER in *gnl1-1* or *ech* mutants (Figure 3.13). These data suggest that the wax biosynthesis defects in *gnl1-1* and *ech* may be due to a disruption of the fine scale organization of enzymes within the ER membranes by analogy to triacylglycerol synthesis during oil body formation (Gidda et al., 2011).

3.2.5 Wax secretion is impaired in *gnl1-1* and *ech*

Understanding the profound effect of ER morphology defects on wax production in *rhd3-1*, *gnl1-1,* and *ech* mutants allowed the uncoupling of the wax biosynthesis phenotype from the wax secretion phenotype. By examining the ratio of the wax secreted to the cuticle (surface wax extracted by a brief chloroform dip) to total wax synthesized (wax from ground total stems including intracellular intermediates), the wax secretion defects of these mutants were assessed (Figure 3.14). In wild-type stems, the wax on the plant surface represented almost 93% of the total wax present in the stem, suggesting that at this snapshot in time, epidermal cells contained a pool representing less than 8% of the total wax, presumably representing waxes that were in the process of being synthesized and secreted. In *rhd3-1* stems, the wax on the plant surface represented 88% of the total wax present in the stem, confirming that *rhd3-1* mutants are not defective in wax secretion. In

gnl1-1 mutants, the amount of secreted wax/total wax was reduced to 78%, indicating that more of the 'total' pool came from waxes that were retained inside the cell and not secreted. This indicates that the Golgi to ER trafficking defect in *gnl1-1* mutants, independent of the biosynthetic defect, led to decreased wax at the cuticle. *ech* mutants, which are defective in post-Golgi trafficking had only 49% of the total wax at the cuticle, and therefore, increased wax retention inside stem epidermal cells, relative to wild type. While ectopic deposits of lipids were observed in *ech* epidermal cells (Figure 3.9C), it is expected that these extracellular lipids would be extracted in the chloroform dip for surface lipids. Thus, the decreased surface to total wax components phenotype indicates a role for ECH-mediated vesicle traffic in the export of cuticular lipids. In contrast, the *trs120-4* mutants did not have significantly less secreted wax relative to the total wax load, which suggests that the TRAPP II complex is not directly involved in wax export.

3.3 Discussion

While the biosynthesis of Arabidopsis cuticular waxes has been well defined, understanding of lipid export lags far behind. In order to examine the mechanism of cuticular wax secretion from the ER to the cell surface, several mutants in the secretory pathway, including *trs120*-4, *gnl1-1*, and *ech* were investigated. Mutant analysis via GC-FID indicated that waxes are secreted via a pathway that is dependent upon GNL1 and ECH, but independent of TRS120. Furthermore, these mutants, in addition to *rhd3-1*, revealed a relationship between the structure of the ER and its biosynthetic capacity.

3.3.1 ER structure is correlated with its biosynthetic capacity

Previous reports have shown that the structure of the endoplasmic reticulum is developmentally regulated, transitioning from a network dominated by sheet-like ER to a more tubular, reticulated network (Ridge et al., 1999). However, this was hypothesized to be the passive result of stretching and dispersion of the ER network during cell elongation to maintain an even distribution of ER membranes throughout development. Here, three-dimensional surface rendering of the ER network and TEM demonstrated that disruption of ER morphology in *rhd3-1, gnl1-1*, or *ech* mutants results in reduced wax biosynthesis,

which can account for at least some of the surface wax accumulation defects in these mutants. Because waxes are synthesized by ER-localized enzymes (Kunst and Samuels, 2009), it is likely that this reduction in wax biosynthesis occurs as a direct result of ER disorganization. Consistent with this hypothesis, wax biosynthetic genes were transcribed at wild-type levels in *rhd3-1, gnl1-1*, and *ech* mutants, suggesting that while wild-type levels of these enzymes were available, ER disorganization resulted in decreased wax biosynthesis efficiency. Interestingly, there was no change to the large-scale localization of the wax biosynthetic enzyme, CER2 in *gnl1-1* and *ech* mutants. A recent study of glutathione synthesis has linked defects in glutathione synthase to defects in ER morphology (Au et al., 2012). However, in this case, the ER morphology defects were the result of the biosynthetic defect, rather than the cause of it, since glutathione precursors accumulated in the ER of *glutathione synthase* mutants (Au et al., 2012). In contrast, Nile red staining of *gnl1-1* and *ech* revealed no significant lipid accumulation inside these mutants, implying that the ER morphology defects are not the result of wax accumulation. This is in contrast to *abcg* transporter mutants, which accumulate waxes in the ER (Pighin et al., 2004; McFarlane et al., 2010; Chapter 2).

Two possible mechanisms exist by which ER disorganization might cause a reduction in wax biosynthesis. First, it is possible that membrane contact sites between the ER and the plastid may be disrupted by the disorganization of the ER. Because wax precursors, i.e. C16 or C18 fatty acids, are synthesized in the plastid, and they are modified into waxes by ER-localized enzymes, these lipids must be transferred between the plastid and the ER during wax synthesis. Because there is no evidence for vesicle trafficking between the ER and endosymbiotic organelles, this transfer may rely on direct, non-vesicular lipid exchange between the plastid and the ER, which may occur at membrane contact sites between these organelles (Benning et al., 2006). Therefore, it is possible that ER disorganization in *rhd3-1, gnl1-1*, and *ech* mutants leads to reduced plastid-ER contact sites and a decrease in plastid to ER transfer of wax precursors, resulting in reduced wax biosynthesis.

Alternatively, it is possible that the fine-scale organization of wax biosynthetic enzymes is disrupted by ER disorganization. Previous studies of heterologously expressed enzymes for lipid droplet synthesis, which also occurs primarily via ER-bound enzymes,

have implied that these enzymes might organize within ER membranes to form enzyme clusters in specific subdomains of the ER, which would allow for metabolic channeling (Shockey et al., 2006; Gidda et al., 2011). A similar model has been proposed for wax biosynthesis; interestingly, the immunophilin-like protein, PAS1, is capable of interacting with all of the core components of the elongase complex and may serve as a scaffold for this multiprotein complex (Roudier et al., 2010). Curiously, CER2, which is required for fatty acid elongation past C28 (and therefore for the bulk of wax precursor synthesis in Arabidopsis stems), localizes to the ER but lacks any obvious targeting motif, suggesting that it could localize to the ER via interaction with the elongase complex (Haslam et al., 2012). In this way, it is possible that ER disorganization in *rhd3-1, gnl1-1*, and *ech* mutants results in disruption of these enzyme complexes and reduced metabolic channeling. However, because no changes were observed in CER2 localization in *gnl1-1* or *ech*, it seems that CER2 can still interact with its predicted ER-localized partner, despite the ER disorganization phenotypes of these mutants. This implies that if functional complexes of wax biosynthetic enzymes exist in the ER, they are not significantly affected by the large-scale ER disorganization observed in *gnl1-1* or *ech* to cause a change in CER2 localization that can be detected at light microscopy resolution.

3.3.2 Waxes are secreted via the Golgi apparatus by a GNOM-LIKE1/ECHIDNA-dependent, TRAPP II-independent mechanism

Despite the decrease in wax synthesis in *gnl1-1* and *ech* mutants, likely due to the disruption of ER morphology in these mutants, both *gnl1-1* and *ech* are also defective in wax export to the cell surface. Of the total wax that was synthesized in *gnl1-1* and *ech* cells, the proportion that was successfully secreted to the cell surface was significantly lower than wild type (Figure 3.14), indicating that these mutants are defective in both wax synthesis and secretion. The wax secretion defect in *gnl1-1* mutants implies that vesicle trafficking through the Golgi apparatus plays a key role in wax secretion to the cell surface.

Interestingly, two different mutations in TGN-localized complexes downstream of *gnl1-1* resulted in different wax phenotypes: while *ech* mutants were defective in both wax synthesis and secretion, *trs120-4* mutants were able to synthesize and secrete wild-type levels of wax. While it is possible that these differences are due to the subtlety of the

trs120-4 mutation and the severity of *ech* (Figure 3.3A), these results support the emerging model of the plant TGN as a complex, multifunctional organelle from which many pathways in the endomembrane system diverge. The TGN is a hub for several endomembrane trafficking routes, including secretion to the plasma membrane/cell wall, secretion to the vacuole, and endocytic recycling (Viotti et al., 2010). Thus, it is entirely possible that two TGN localized protein complexes may have completely different roles at the TGN. In support of this, VHA-a1, a TGN-localized vacuolar-type proton ATPase (Brüx et al., 2008), is mislocalized in *ech* (Gendre et al., 2011) but not in *trs120* (Qi et al., 2011). Furthermore, the ECH complex is specifically required for secretion to the cell wall, but not trafficking to the vacuole, or recycling via the TGN/early endosome compartment (Gendre et al., 2013). In contrast, the TRAPP II complex is required for trafficking to the cell wall and the cell plate, but it is not involved in recycling via the TGN/early endosome, and its role in TGN to vacuole trafficking has not been assessed (Qi et al., 2011). Furthermore, disruption of the ECH complex leads to accumulation of cell wall products inside the vacuole (Gendre et al., 2013; McFarlane et al., 2013), while defects in the TRAPP II complex do not result in this phenotype (Qi et al., 2011). Together, these data suggest that the ECH complex and the TRAPP II complex play distinct roles at the TGN. Thus, it is not surprising that these mutants secrete very different amounts of wax. The different *ech* and *trs120* phenotypes indicate that specific elements of the TGN machinery are required for wax secretion to the cell wall, i.e. waxes are trafficked through the TGN in an ECH complex dependent, TRAPP II complex-independent manner.

3.3.3 Other components of plant lipid trafficking remain to be defined

While these results have determined that at least some of the cuticular lipid secretion in Arabidopsis involves vesicle trafficking and a Golgi-mediated process that is dependent upon the GNOM-LIKE 1 at the ER-Golgi interface and the ECHIDNA complex at the TGN, many questions about plant lipid trafficking remain. For example, it is interesting that no mutants that are defective in wax trafficking to the cell surface are completely devoid of surface waxes. In the case of the ABC transporters and LTPs, this is likely due to genetic redundancy with other ABCs and LTPs that are expressed in the stem epidermis (Suh et al., 2005; Bird et al., 2007; Kim et al., 2012). For the secretion mutants examined

here, either they are mild alleles (*trs120-4*), or they are knockout mutants in which another gene product may be partially redundant (Richter et al., 2007; Gendre et al., 2011), since a total elimination of secretion would be lethal.

Nevertheless, it remains possible that some waxes also reach the plant surface via a route that is independent of vesicle trafficking through the Golgi. By analogy with yeast and animal systems, some wax components may be transported via non-vesicular trafficking at ER-plasma membrane contact sites (Samuels and McFarlane, 2012). The results described here do not exclude this possibility; because of the disruptions to ER morphology in all three wax deficient mutants, *rhd3-1, gnl1-1*, and *ech*, it is possible that some of the wax secretion defects may be due to disorganization of ER-plasma membrane contact sites.

In summary, mutant analysis combined with live cell imaging, electron microscopy and chemical phenotyping have demonstrated that Arabidopsis waxes, including very long chain fatty acids and their derivatives, are transported from their site of synthesis in the ER to their site of accumulation on the cell surface in part via the Golgi apparatus and the ECH complex at the TGN. Furthermore, disruption of ER morphology is tightly correlated with decreased wax synthesis, implying a close relationship between the structure of the ER and its biosynthetic capacity. Recent characterization of key enzymes in plant lipid biosynthesis, including very long chain alkane biosynthesis in Arabidopsis waxes (Bernard et al., 2012, Haslam et al., 2012), has provided excellent potential to manipulate lipid synthesis in plants for agricultural and/or industrial applications (Dyer and Mullen, 2008; Jetter and Kunst, 2008). However, biosynthetic enzyme overexpression has failed to increase yields as much as predicted (Snapp and Lu, 2012), demonstrating the need to understand the cell biological context and subcellular organization of wax biosynthesis enzymes and their substrates and products. Together, these results highlight the importance of maintaining the structure and function of the endomembrane system when manipulating lipid synthesis in plants for industrial applications.

3.4 Methods

3.4.1 Plant material

Arabidopsis thaliana seeds were sown on AT media plates (Haughn and Somerville, 1986) and grown at 21°C, 70-80% humidity, constant light (~100 μE m^{-2} s^{-1}) in an environmental growth chamber (Conviron). After 7-14 days, seedlings were transferred to Sunshine mix 5 soil and returned to the same growth conditions. Plant lines were in the Col-0 background and included: *echidna* (Gendre et al., 2011), *abcg11-3 + 35S::YFP-ABCG11* (Bird et al., 2007), *abcg12-2 + ABCG12pro::GFP-ABCG12* (Pighin et al., 2004), Col-0 *+ 35S::GFP-HDEL* and *Col-0 + 35S::secGFP* (Batoko et al., 2000), *gnl1-1* (Richter et al., 2007), *rhd3-1* (Zheng et al., 2004), *trs120-4* (Qi et al., 2011), *cer2-5 + CER2pro::CER2-GFP* (Haslam et al., 2012). All fluorescently tagged proteins (except secGFP and GFP-HDEL which are markers) were maintained in the mutant background to avoid overexpression artifacts and/or complications between the tagged protein and the endogenous protein. Crosses were genotyped using T-DNA specific primers plus the primers indicated in Table 3.1.

3.4.2 GC-FID

For surface waxes, samples were prepared as described by Lam et al. (2012): 10 cm segments from 4-6 week old stems were photographed, then immersed in HLPC grade chloroform, with 10 μg 24-alkane as an internal standard, for 30 seconds. Extracted waxes were resuspended in 100 μL chloroform, dried at 45°C under nitrogen, resuspended in 10 μL each pyridine (Sigma) and *N,O*-bis(trimethylsilyl) trifluoroacetamide with 1% trimethylchlorosilane (Sigma). Samples were derivatized at 75°C for 1 hour, dried at 45°C under nitrogen, and resuspended in 50 μL chloroform.

For total waxes (surface and intracellular), sample preparation and GC-FID was the same except fresh stems were ground with 10 μg 24-alkane as an internal standard, and waxes were extracted from the homogenate by washing three times with chloroform. The washes were pooled, dried under nitrogen, derivatized, and resuspended as above.

Waxes were analyzed on an Agilent 7890A gas-liquid chromatography (CG) system coupled to a flame ionization detector (FID) with a 30 m by 320 μm HP-1 methyl siloxane

column, and hydrogen as the carrier gas; 1 μL of each sample was injected using a 2.7:1 split. The program ran at 50°C for 2 minutes, increased by 40°C/minute to 200°C, held for 1 minute at 200°C, increased by 3°C/minute to 320°C and held for 15 minutes at 320°C. Chromatogram peaks were identified by comparing their retention time to that of known standards. Because wax esters and free fatty acids are very low abundance wax constituents of the Arabidopsis stem (Li et al., 2008), they were difficult to detect in wild type and often absent in *gnl1-1* and *ech*, so they were not included in further analyses. Total wax levels were determined by comparing the area of each peak to the 10 μg 24-alkane standard peak, and then correcting for the surface area of the stem. Stem surface areas were measured by determining the area of the photographed stem in ImageJ, then multiplying by π. Means are representative of three independent experiments. Statistically significant differences between means were determined using a students' t-test for each mutant, compared to wild type.

3.4.3 Confocal microscopy

Stem segments from the first 3 cm below the shoot apical meristem (where wax synthesis and secretion is most active; Suh et al., 2005) were mounted in water and viewed under a Leica DMI6000 inverted microscope equipped with a PerkinElmer UltraView VoX spinning-disk system and an Hamamatsu 9100-02 CCD camera. GFP was detected using 488 nm laser and 525/36 nm emission filter. YFP was detected using the 514 nm laser and 540/30 nm emission filter. Nile red (Sigma; diluted 1/1000 in water from a 1 mg/mL stock in DMSO), hexyl rhodamine B (Invitrogen; diluted 1/1000 in water from a 1.6 mM stock in DMSO), and propidium iodide (Invitrogen; 1 μg/mL in water) were detected with 561 nm laser and 595/50 emission filter. Images were processed using ImageJ, and 3-dimensional surface rendering of ER was performed using Osirix (Rosset et al., 2004). Localization of YFP-ABCG11 was quantified by measuring normalized pixel intensity at three random cross sections in cells (in ImageJ) and by comparing internal signal to PM-localized signal. Statistically significant differences between means were determined using a Students' t-test for each mutant, compared to wild type.

3.4.4 Scanning electron microscopy

Mature stems were mounted on stubs in colloidal graphite Aquadag E (Canemco), frozen on liquid nitrogen, and transferred to the Emitech K1250 Cryo-System. Water was sublimed at -100°C for 30 minutes, then samples were viewed on a Hitachi S4700 field emission-SEM at -130°C with an accelerating voltage of 5 kV, beam current of 10 μA, and a working distance of 15 mm, using a mix of both the upper and lower detectors.

3.4.5 High-pressure freezing and transmission electron microscopy

TEM sample preparation, including high-pressure freezing, freeze-substitution sectioning, poststaining, and imaging was performed as described in McFarlane et al. (2008). Briefly, stem segments from the first 3 cm below the shoot apical meristem (where wax synthesis and secretion is most active; Suh et al., 2005) were high-pressure frozen in B-type sample holders (Ted Pella) with hexadecane as a cryoprotectant using a Leica HPM-100. Samples were freeze substituted in 2% osmium tetroxide and 8% dimethoxypropane and infiltrated with Spurr's resin (Spurr, 1969) over 10 days. Samples were sectioned using a Leica Ultracut UCT and a Dimatome diamond knife, mounted on copper grids (Gilder), and post stained with 2% uranyl acetate in 70% methanol and Reynolds lead citrate (Reynolds, 1963). Samples were viewed using a Hitachi H7600 TEM at 80kV accelerating voltage with an ATM Advantage CCD camera (Hamamatsu).

3.4.6 Gene expression analysis

Total RNA was extracted, using TRIzol reagent (Invitrogen), from stem segments 1-3 cm below the shoot apical meristem. cDNA was synthesized from 5 μg of RNA using an oligo dT_{18} primer and SuperScript III Reverse Transcriptase (Invitrogen). RT-PCR was performed for 22-28 cycles using intron-flanking, gene-specific primers (Table 3.1). cDNA levels were normalized using primers for the *UBC10* ubiquitin conjugating enzyme gene for 22 cycles.

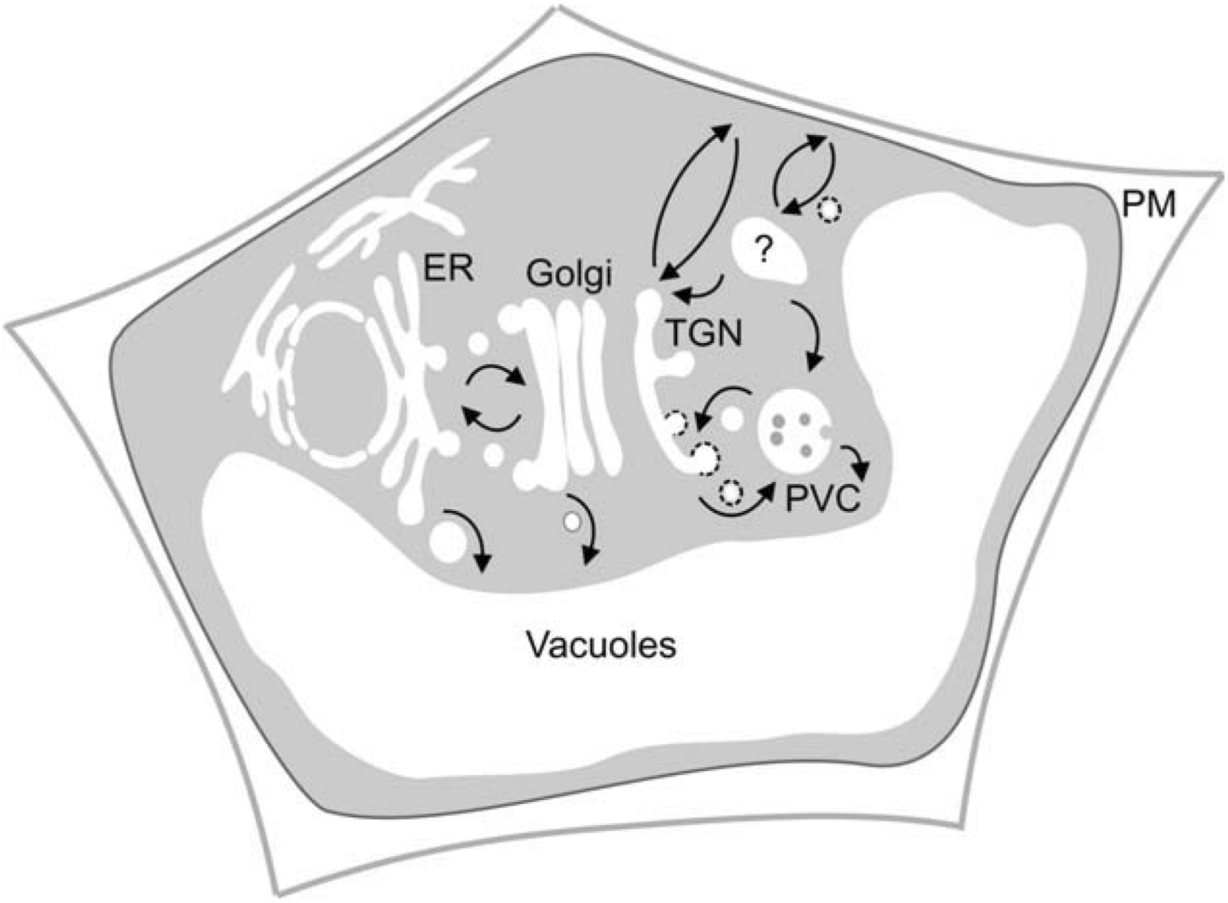

Figure 3.1: A diagram of the plant secretory pathway. ER = endoplasmic reticulum, TGN = trans-Golgi Network, PM = plasma membrane, PVC = pre-vacuolar compartment. Reproduced with permission from Foresti and Denecke, 2008; Copyright John Wiley and Sons © 2008.

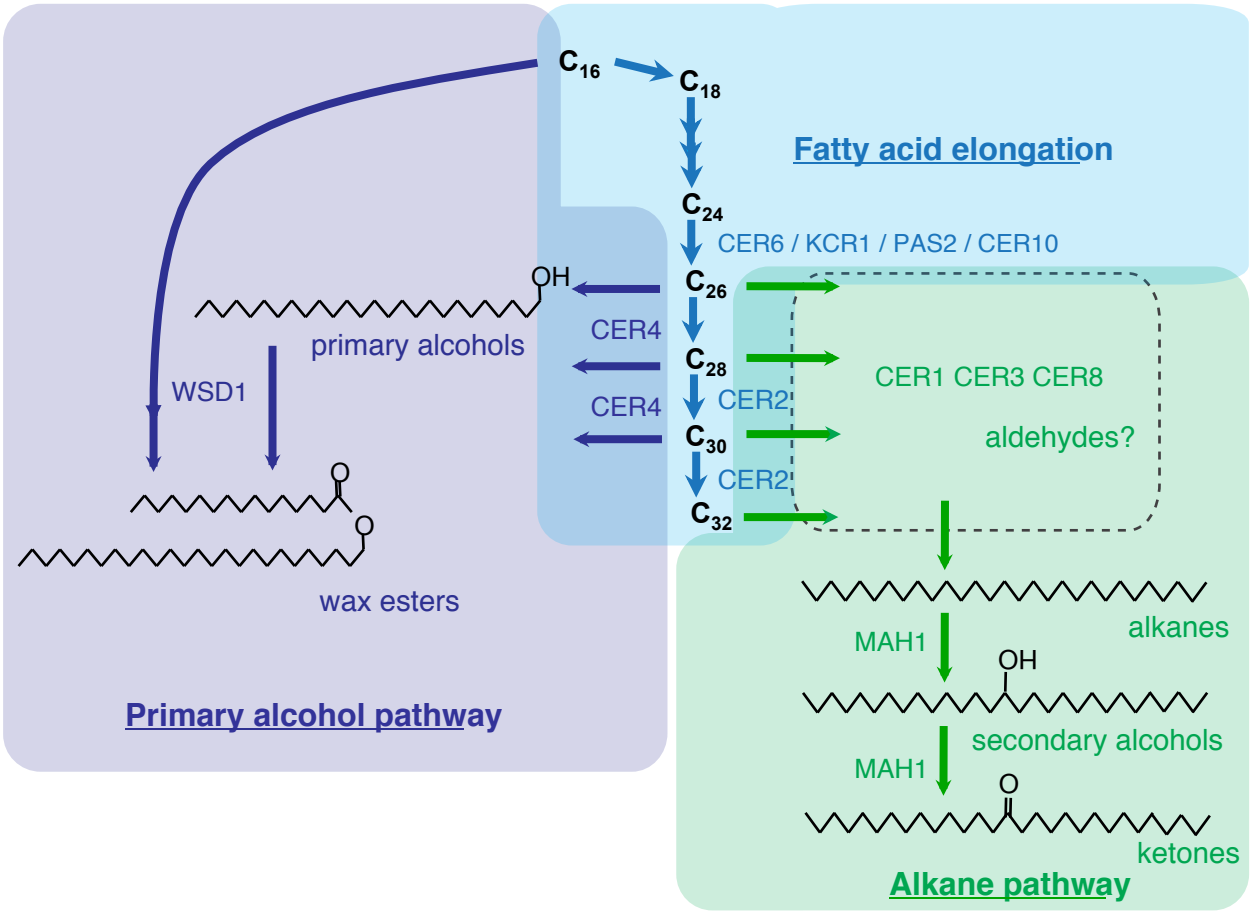

Figure 3.2: A diagram of the ER-localized wax biosynthetic pathway. Starting from 16-carbon (C16) fatty acids, fatty acid elongation (blue) occurs via the elongase complex (CER6, KCR1, PAS2, and CER10) to C28 fatty acid. Past C28, CER2 is also required for elongation. Very long chain fatty acids (primarily C26-C32) are modified to waxes in two pathways. In the primary alcohol pathway (purple), CER4 catalyzes reduction of fatty acids to alcohols and WSD1 condenses a fatty acid to this alcohol to produce a wax ester. In the alkane pathway (green), CER1, CER3, and CER8 are all required to form alkanes, possibly via an aldehyde intermediate. MAH1 may oxygenate the middle carbon of these alkane chains to produce secondary alcohols and ketones. All of these enzymes are localized to the ER.

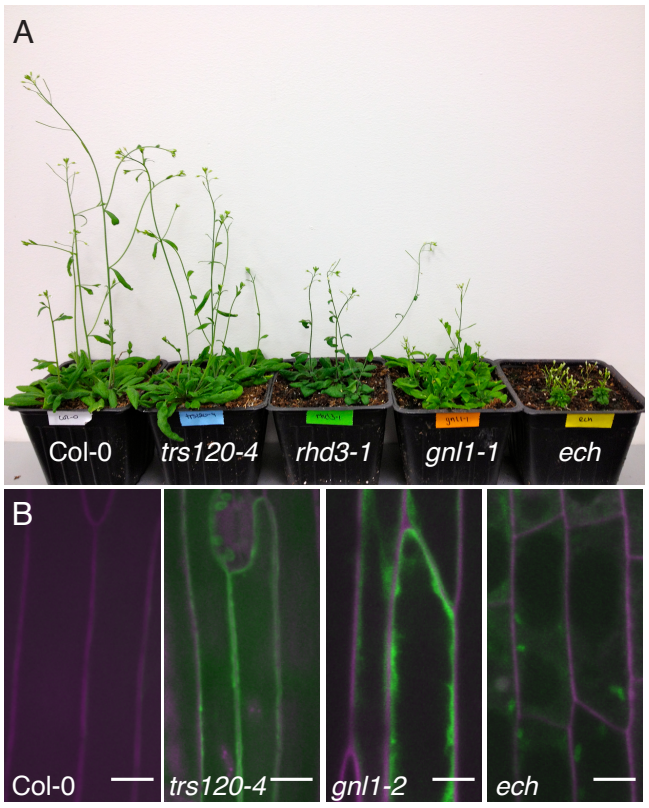

Figure 3.3: *trs120-4, gnl1-1*, and *ech* are defective in secretion. All mutants in this study are defective in cell elongation to varying degrees as indicated by their reduced growth after six weeks, compared to wild type (A). In stem epidermal cells, the secreted fluorescent protein, secGFP (green), faintly labels the secretory pathway and is secreted to the apoplast, labeled with propidium iodide (magenta), where fluorescence is quenched in wild-type cells. In *trs120-4*, *gnl1*, and *ech* mutants, secGFP accumulates inside stem epidermal cells, indicating a defect in protein secretion (B). Scale bars represent 10 μm.

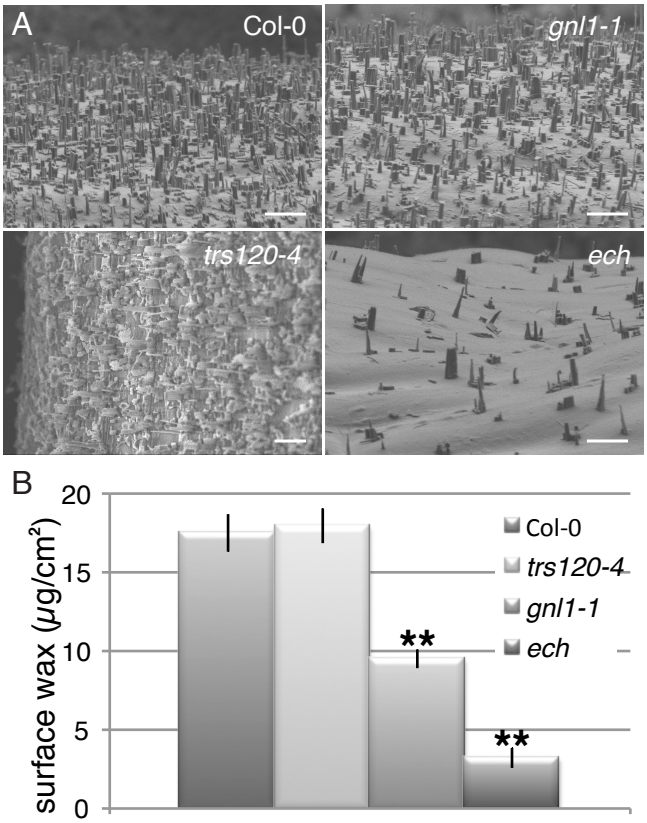

Figure 3.4: *gnl1-1* and *ech*, but not *trs120-4* are defective in wax accumulation on the cell surface. Cryo-SEM of mature stems reveals dense wax crystals on wild-type and *trs120-4* stems while *gnl1-1* and *ech* mutants have reduced wax crystals (A). Quantification of surface wax load via GC-FID reveals a significant decrease in surface waxes in *gnl1-1* and *ech*, but not *trs120-4*, relative to wild type (B). Values are means of 3 experiments of 3 biological replicates each (i.e. n=9), bars represent SE, stars indicate statistically significant differences between wild type and mutant (t-test, ** for $p < 0.01$). Scale bars represent 5 µm.

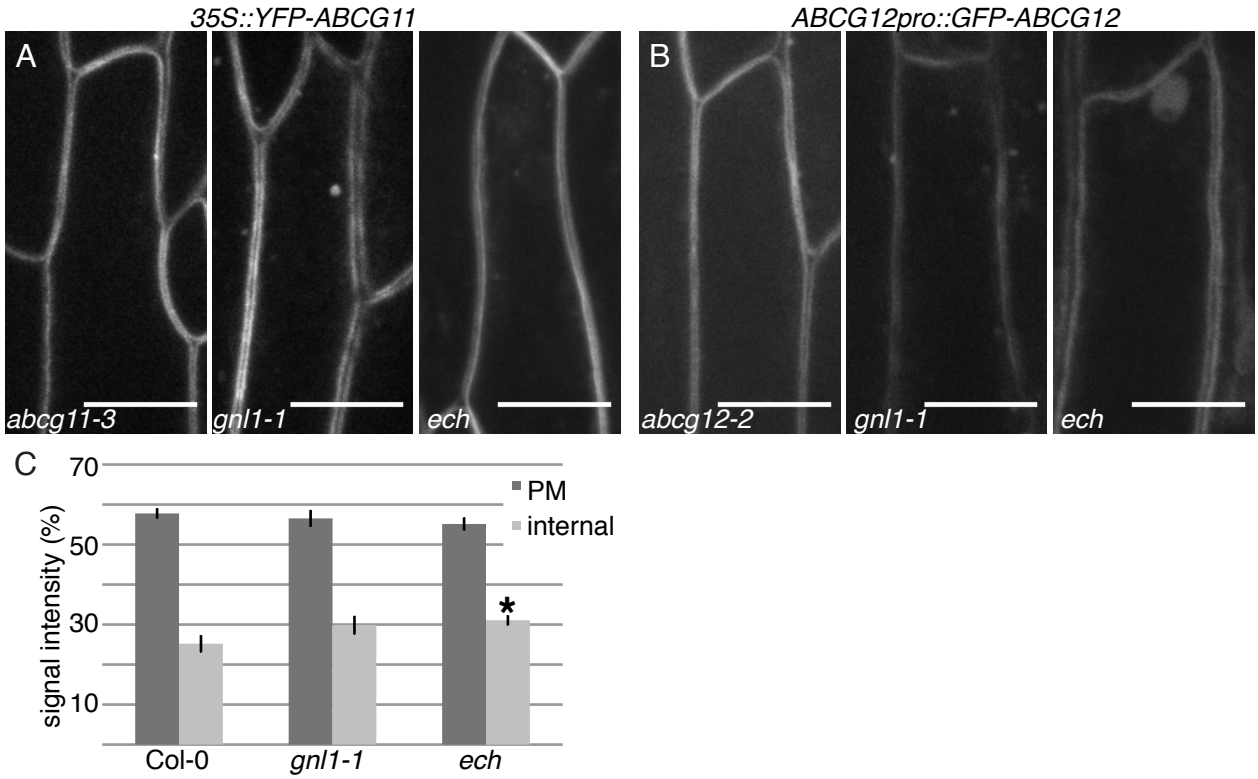

Figure 3.5: ABCG11 and ABCG12 are correctly localized in *gnl1-1* and *ech*. In *abcg11-3* stem epidermal cells complemented with YFP-ACBG11, the transporter is localized to the plasma membrane. Despite their secretion defects, the majority of the YFP-ABCG11 signal is localized to the plasma membrane in *gnl1-1* and *ech* mutants (A). Similarly, GFP-ABCG12 is also localized to the plasma membrane in complemented *abcg12-2* mutants, *gnl1-1*, and *ech* stem epidermal cells. Quantification of relative signal intensity of YFP-ABCG11 (C) confirms no significant change to the localization ABCG11 in *gnl1-1* and *ech* mutants at the plasma membrane (PM), relative to wild type. However, *ech* mutants do accumulate significantly more internal signal than wild type. Values are means from 18 individual cells (i.e. n=18), bars represent SE, stars indicate statistically significant differences between wild type and mutant (t-test, * for $p < 0.05$). Scale bars represent 10 μm.

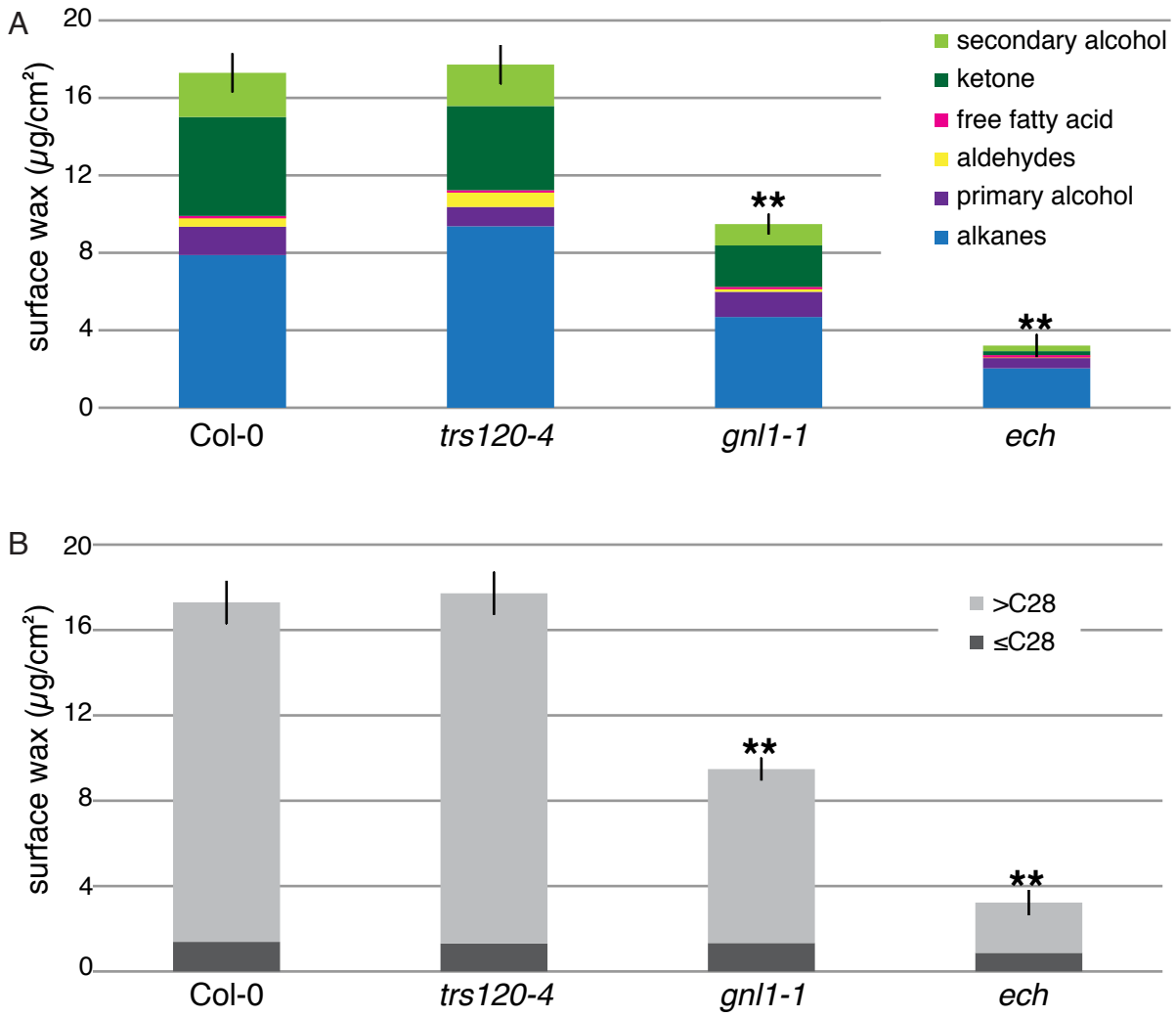

Figure 3.6: Wax composition is altered in *gnl1-1* and *ech*, but not *trs120-4* mutants. Quantification of surface wax composition via GC-FID reveals a significant overall change to the composition of surface waxes in *gnl1-1* and *ech*, but only subtle changes to *trs120-4*, relative to wild type. In particular, *gnl1-1* and *ech* have decreased levels of MAH1 products (green), relative to alkanes (blue) (A). Furthermore, *gnl1-1* and *ech* show a greater reduction in exceptionally long (>C28) wax components (B). Values are means of 3 experiments of 3 biological replicates each (i.e. n=9), bars represent SE of total surface wax load, stars indicate statistically significant differences between wild type and mutant (t-test, ** for $p < 0.01$).

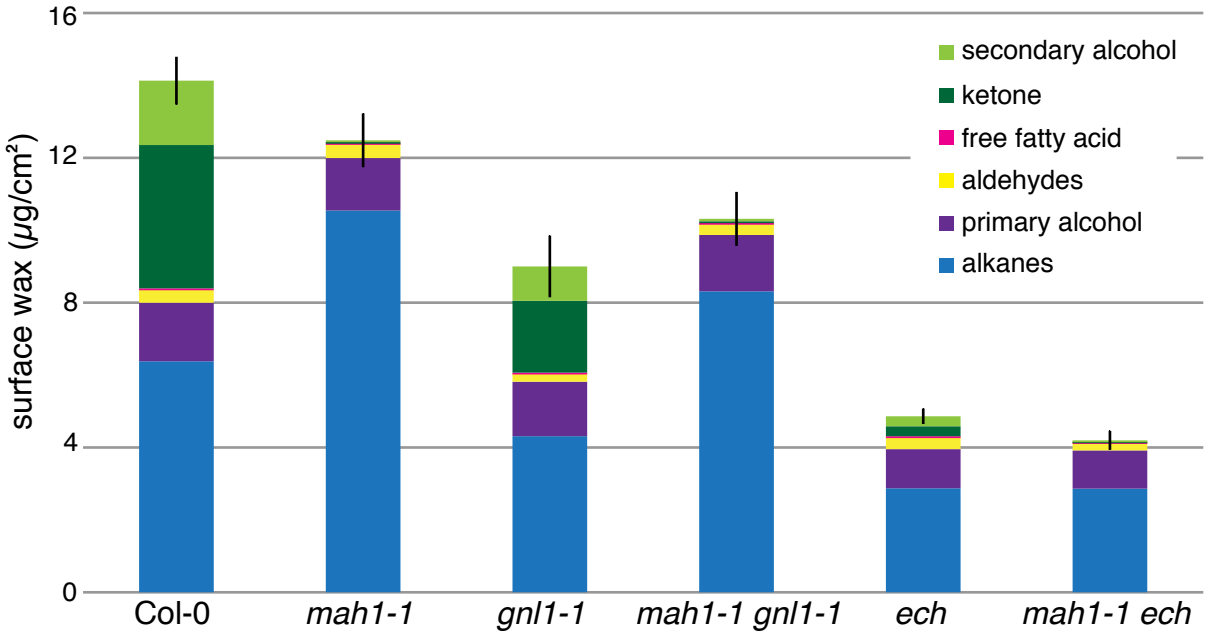

Figure 3.7: *gnl1-1* and *ech* wax accumulation phenotypes cannot be rescued by altering the chemical composition of surface waxes. Changing the chemical composition of *gnl1*-1 and *ech* wax by introducing the *mah1-1* mutation, which eliminates secondary alcohols and ketones (green) and increases alkane levels (blue), fails to increase the amount of total wax secreted in these mutants. Values are means of 3 experiments of at least 3 biological replicates each (i.e. n≥9), bars represent SE. There were no statistically significant differences between single mutant controls and *mah1-1* double mutants (t-test, p≥0.05).

Figure 3.8: *gnl1-1* and *ech* are defective in wax biosynthesis. Quantification of total waxes, including intracellular and cuticular waxes, from ground stems via GC-FID reveals that *gnl1-1* and *ech* but not *trs120-4* mutants have a defect in wax synthesis, relative to wild type. Note also the relatively larger decrease in midchain oxygenated compounds (secondary alcohols and ketones) and in all compounds with chain lengths ≥C28 in *gnl1-1* and *ech* mutants, but not *trs120-4* mutants. Values are means of 3 experiments of 3 biological replicates each (i.e. n=9), bars represent SE of total wax load, stars indicate statistically significant differences between wild-type and mutant total waxes (t-test, * for $p < 0.05$, ** for $p < 0.01$).

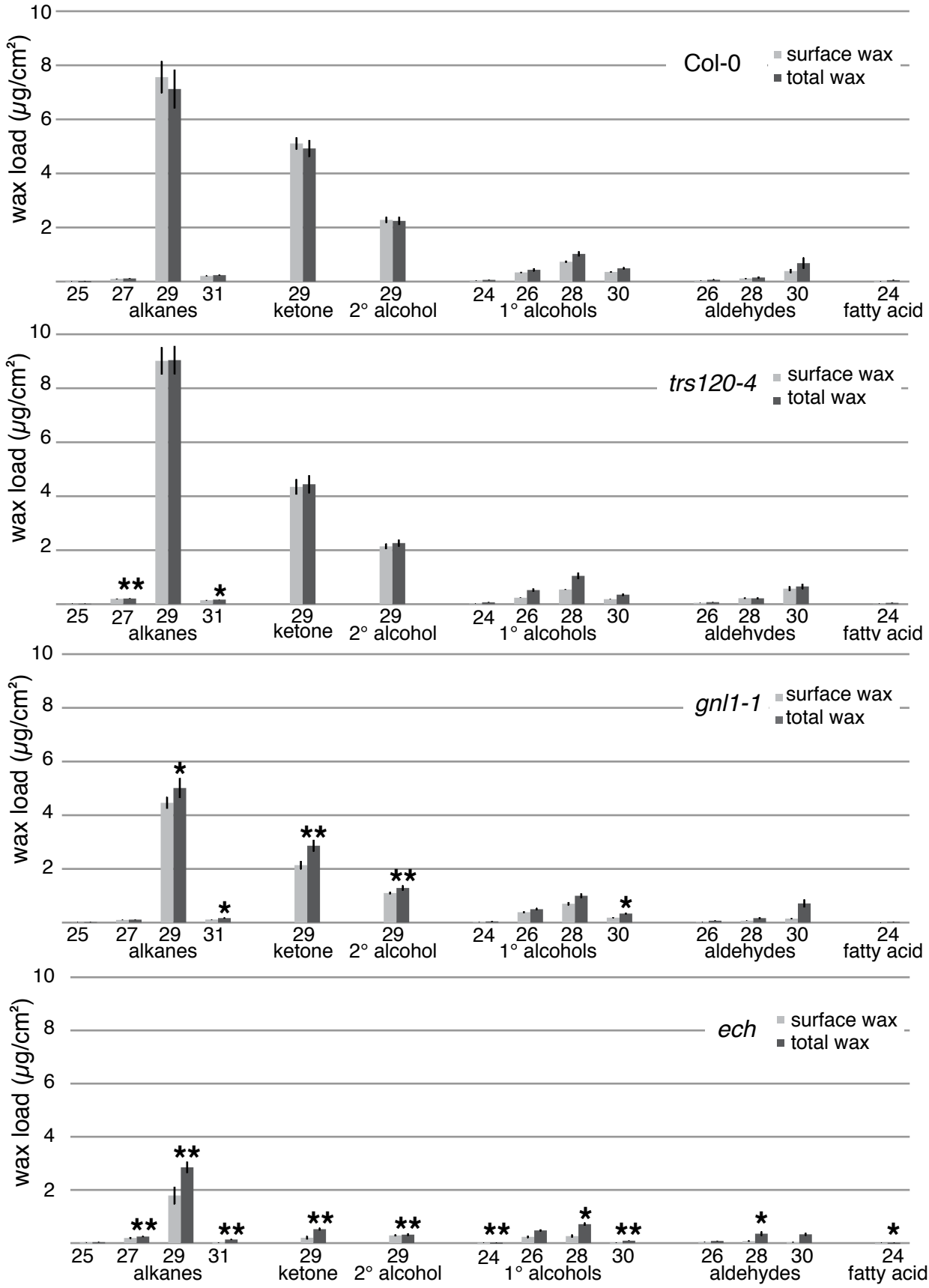
Col-0
surface wax
total wax
wax load (μg/cm²)
10
8
6
4
2
25 27 29 31 29 29 24 26 28 30 26 28 30 24
alkanes ketone 2° alcohol 1° alcohols aldehydes fatty acid
trs120-4
surface wax
total wax
wax load (μg/cm²)
**
*
alkanes ketone 2° alcohol 1° alcohols aldehydes fatty acid
gnl1-1
surface wax
total wax
wax load (μg/cm²)
*
**
**
*
*
alkanes ketone 2° alcohol 1° alcohols aldehydes fatty acid
ech
surface wax
total wax
wax load (μg/cm²)
**
**
**
**
**
**
*
*
*
alkanes ketone 2° alcohol 1° alcohols aldehydes fatty acid

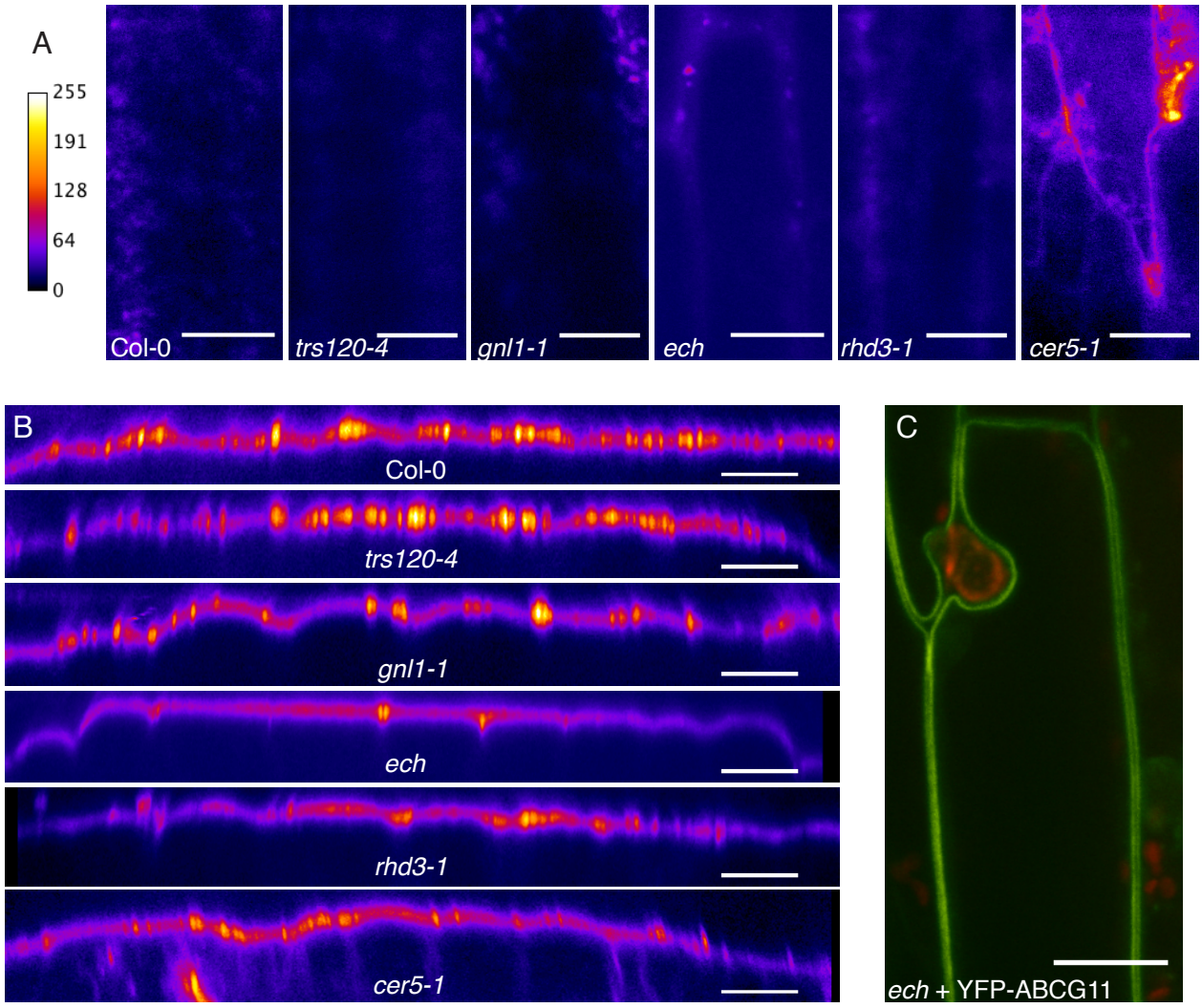

Figure 3.9: Waxes do not significantly aggregate in *trs120-4*, *gnl1-1*, or *ech* mutants. In wild-type stem epidermal cells, the lipophillic dye, Nile red, does not significantly label any internal structures (A), but strongly labels the cuticle, as seen in a xz plane view of confocal stacks (B). Similarly, no intracellular lipid accumulation is detected in *trs120-4*, *gnl1-1*, *ech*, or *rhd3-1*, compared to *abcg12-2* (A), and extracellular cuticular lipid label is correlated with wax levels determined by GC-FID (B). *ech* mutants occasionally display large aggregations of cuticular lipids (C, false coloured red), but these are extracellular, as demonstrated by plasma membrane visualization using YFP-ABCG11 (C, false-coloured green). Scale bars represent 10 μm.

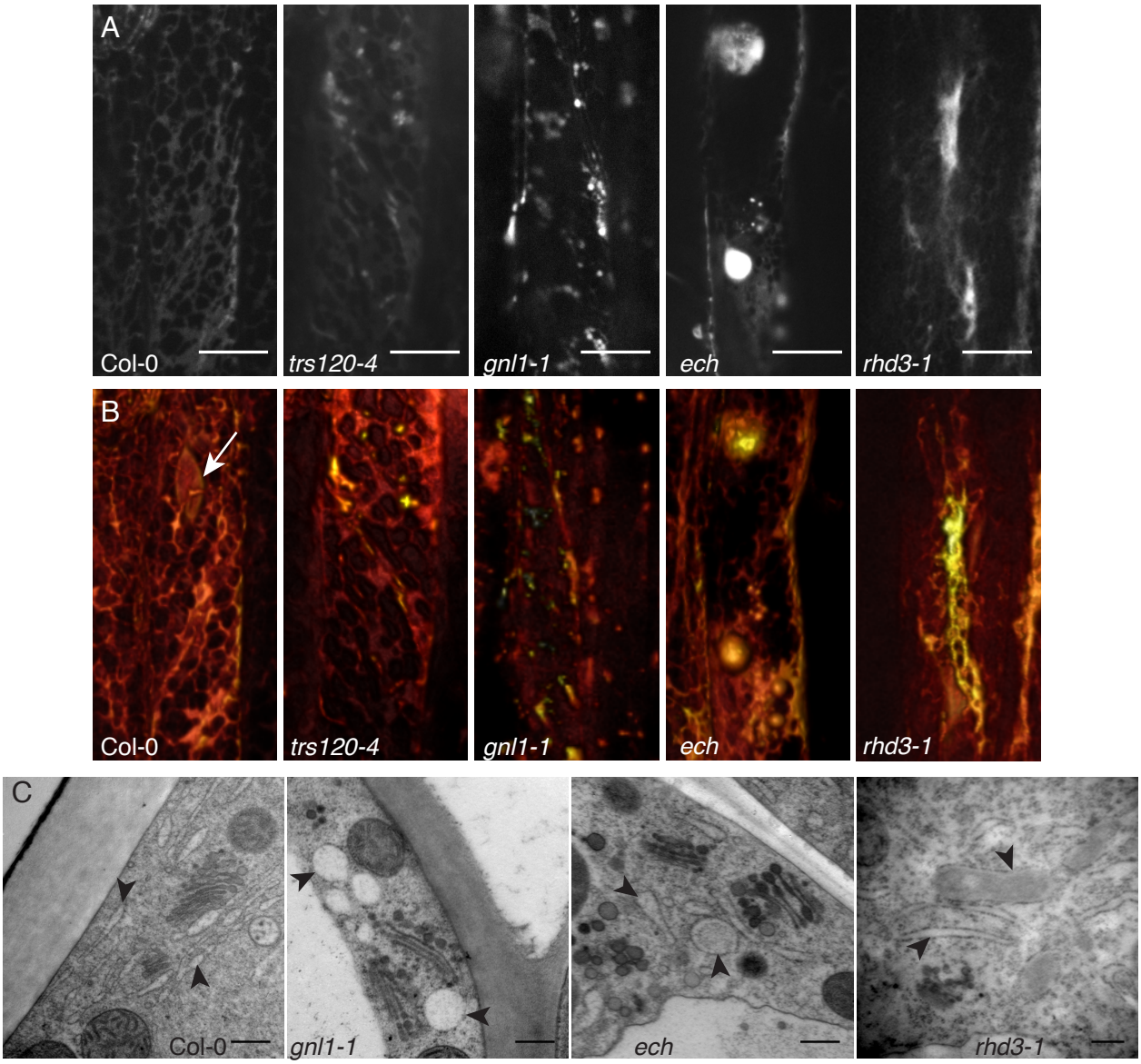

Figure 3.10: *gnl1-1*, *ech*, and *rhd3-1* are defective in ER morphology. In wild-type stem epidermal cells, the ER marker GFP-HDEL is localized to a reticulate cortical network, trans-vacuolar strands, and the peri-nuclear region (arrow). *gnl1-1*, *ech,* and *rhd3-1* mutants display defects in GFP-HDEL distribution, including ER fragmentation and aggregation in both single confocal images (A) and 3-dimensional surface rendering of the ER network in the same single cell (B). Hexyl rhodamine B staining of *trs120-4* mutant ER and mitochondria confirms that these mutants are not defective in ER morphology. TEM reveals large dilations of the ER in *gnl1-1*, *ech,* and *rhd3-1* mutants, relative to the tubular network observed in wild-type cells (C). Arrowheads point to ER in TEM. Scale bars represent 10μm in A and 200 nm in C.

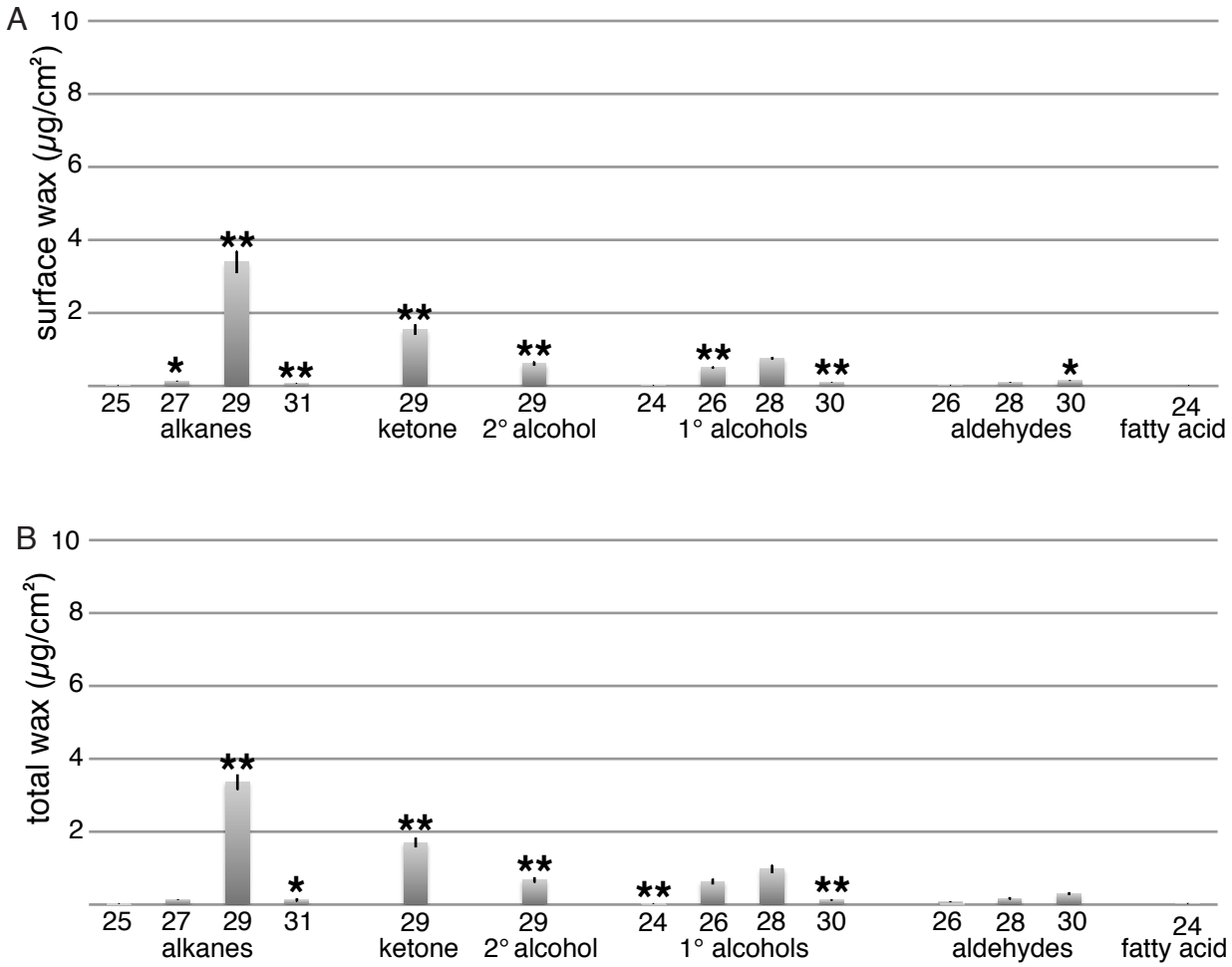

Figure 3.11: *rhd3-1* mutants are defective in wax synthesis, but not secretion. Quantification of surface waxes from stems briefly dipped in chloroform (A) and total waxes from ground stems (B) via GC-FID reveals that *rhd3-1* mutants have a defect in wax synthesis, relative to wild type since both secreted and total waxes are decreased. Values are means of 3 experiments of 3 biological replicates each (i.e. n=9), bars represent SE of total wax load, stars indicate statistically significant differences between wild type (see Figure 3.7) and *rhd3-1* (t-test, * for $p < 0.05$, ** for $p < 0.01$).

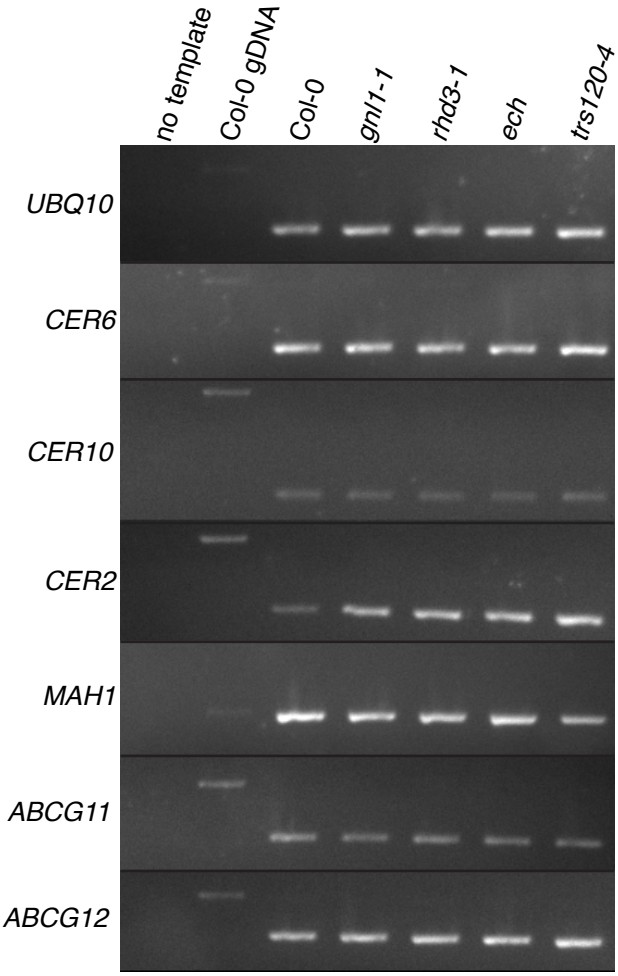

Figure 3.12: Transcript levels of wax biosynthetic genes are not affected in *gnl1-1*, *rhd3-1, ech,* or *trs120-4* mutants. Semi-quantitative RT-PCR of wax biosynthesis genes (*CER6*, *CER10*, *CER2*, *MAH1*) and wax transport genes (*ABCG11*, *ABCG12*) reveals no changes to transcript levels in *gnl1-1*, *rhd3-1*, *ech*, or *trs120-4*, stems relative to wild type. cDNA levels were normalized to transcript levels of the gene encoding an ubiquitin conjugating enzyme, UBC10; genomic DNA served as a positive control, and amplification without template DNA served as a negative control.

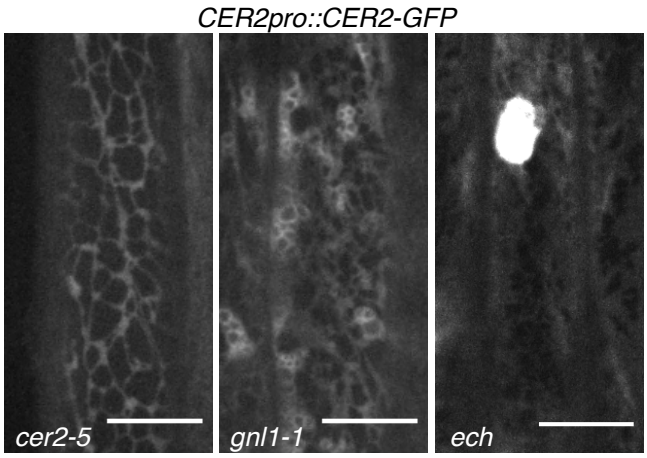

Figure 3.13: The localizations of the CER2 wax biosynthetic enzyme is not affected in *gnl1-1* or *ech* mutants. In *cer2-5* stem epidermal cells complemented with GFP-CER2, the enzyme is primarily localized to the ER. GFP-CER2 is also primarily localized to the ER in *gnl1-1* and *ech* mutants, despite their ER morphology defects. Scale bars represent 10 μm.

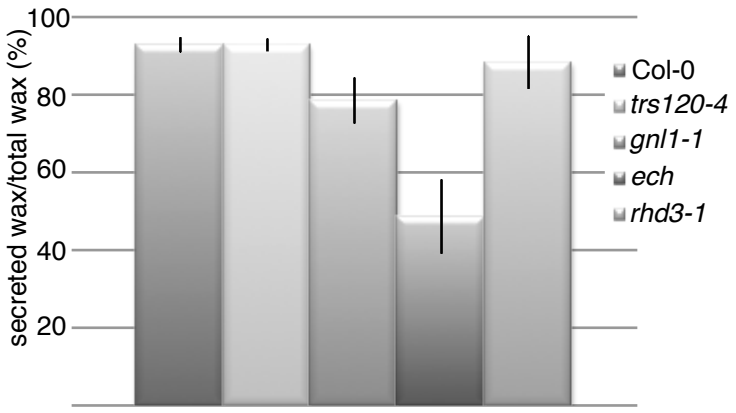

Figure 3.14: *gnl1-1* and *ech*, but not *trs120-4* or *rhd3-1* are defective in wax secretion. The amount of secreted wax extracted by a short chloroform dip is expressed as a percent of the total amount of wax that is extracted from homogenized stems; that is, secreted waxes are represented as a proportion of the total waxes synthesized. Values are means of 3 experiments of 3 biological replicates each (i.e. n=9), bars represent SE.

Name	Primer Sequence (5` -> 3`)	Purpose
ECH.P1	TCATTGATCTCGTTCCACCA	genotyping *ech* mutants
ECH.P1	CCACAACGGAGAAGGTGTTT	genotyping *ech* mutants
GNL1.P1	GGAATGGCGAAATCAAGGCAT	genotyping *gnl1-1* mutants
GNL1.P2	GCGGTGGCGTCCATGATTA	genotyping *gnl1-1* mutants
GNL1.P3	TCGGATCCCAGTCCACTGTTC	genotyping *gnl1-1* mutants
TRS120.P1	AAACCGATCAACGATTTCCTC	genotyping *trs120-4* mutants
TRS120.P2	CACCAAGCACAAATTTGAACC	genotyping *trs120-4* mutants
ABCG11.P1	TCGAATGCAGTTCTTTGCAC	genotyping *abcg11-3* mutants
ABCG11.P2	AACAGATTGTCCCGGAGATG	genotyping *abcg11-3* mutants
ABCG12.P1	GTGAAATTCCGTCCTGGTGT	genotyping *abcg12-2* mutants
ABCG12.P2	GCTTTGCTTGTATCGCCTTC	genotyping *abcg12-2* mutants
MAH1.P1	TCAAATCACGCCCTATTCCA	genotyping *mah1-1* mutants
MAH1.P2	ATCTGGCTTCGCAGGAGACT	genotyping *mah1-1* mutants
CER2.P1	GCTGGAAACGCAACGTTATT	genotyping *cer2-5* mutants
CER2.P2	CAAACTCCGGCACTCTCTTC	genotyping *cer2-5* mutants
UBC10.P1	GGTAGCATTTGCCTCGACAT	RT-PCR for *UBC10* (At5g53300)
UBC10.P2	CTTCGTGCAGTGGACTCGTA	RT-PCR for *UBC10* (At5g53300)
CER2.P3	CCAACGTCGAAGAGTTCACA	RT-PCR for *CER2* (At4g24510)
CER2.P4	ATGACCCGATACCAGCTGTC	RT-PCR for *CER2* (At4g24510)
CER6.P1	CACGTTGGCATCAACTTGTC	RT-PCR for *CER6* (At1g68530)
CER6.P2	CTGCGTGAATGCAAAAGTGT	RT-PCR for *CER6* (At1g68530)
CER10.P1	TCTGCAAGAAGCGTTTCATAA	RT-PCR for *CER10* (At3g55360)
CER10.P2	TGTGCGGTAGGAAACTTGTG	RT-PCR for *CER10* (At3g55360)
MAH1.P3	GTTGTGGGAGGAGATGAGGA	RT-PCR for *MAH1* (At1g57750)
MAH1.P4	CTCCACAAGATCACCGGTTT	RT-PCR for *MAH1* (At1g57750)
ABCG11.P3	CCAAATGACATCCCAAAACC	RT-PCR for *ABCG11* (At1g17840)
ABCG11.P4	CGATGCAAGTCGATCTGAAA	RT-PCR for *ABCG11* (At1g17840)
ABCG12.P3	CGATTTCCTTCATGAGTTATGGT	RT-PCR for *ABCG12* (At1g51500)
ABCG12.P4	GCTTTGCTTGTATCGCCTTC	RT-PCR for *ABCG12* (At1g51500)

Table 3.1: A list of primers employed in Chapter 3.

Chapter 4: Isolation and characterization of ER-PM contact sites

4.1 Introduction

In all eukaryotes the endoplasmic reticulum (ER) forms a complex network that reaches throughout the cell, including the nuclear envelope, endoplasmic tubules and cisternae, and a subnetwork of ER at the cell cortex, called the cortical ER (Staehelin, 1997; West et al., 2011). The ER network is shaped by a variety of proteins. Tubules are formed by reticulons and members of the Yop1p family, while Atlastins/Sey1p/RHD3 small GTPases are required for forming three-way junctions between tubules (Voeltz et al., 2006; Tolley et al., 2008; Chen et al., 2011c; Liu et al., 2012). The ER plays a central role in secretory pathway protein synthesis, folding, glycosylation, and quality control and is also involved in lipid synthesis, and calcium and redox homeostasis (Staehelin, 1997; Sparkes et al., 2009a). The cortical ER, in particular, is implicated in important functions such as calcium exchange during animal cell excitation–contraction coupling and division plane selection in fission yeast (Luik et al., 2006; Wu et al., 2006; Zhang et al., 2010). In plant cells the function of the cortical ER, relative to the rest of the ER network, has not been established.

In most eukaryotes the cortical ER often comes into very close contact (15 nm or less) with the plasma membrane (PM) (Staehelin, 1997; Levine, 2004). This creates an ER-plasma membrane (ER-PM) contact site, which excludes ribosomes from the surface of the ER and allows short-range, targeted exchange of small molecules between the ER and the PM (Toulmay and Prinz, 2011; West et al., 2011). In excitable animal cells (e.g. neurons and muscle cells), Ca^{2+} release is confined to these regions, presumably to channel Ca^{2+} directly to its receptors and to limit Ca^{2+} diffusion into the rest of the cytoplasm (Carrasco and Meyer, 2011; Asghari et al., 2012). In *Saccharomyces cerevisiae*, ER-PM contact sites participate in sterol uptake from the extracellular medium, channeling these lipids into the ER to be incorporated into lipid bodies (Li and Prinz, 2004; Raychaudhuri et al., 2006). These ER-PM contact sites bring the two membranes so close together that enzymes are able to act in *trans*; that is, an ER-localized lipid-modifying enzyme can act on PM-localized lipids (Stefan et al., 2011). Consistent with this model, a membrane fraction from budding yeast that is enriched in ER-PM contact sites has increased lipid biosynthesis and

remodeling capacity, compared to either bulk ER membrane or isolated PM (Pichler et al., 2001). Despite their broad importance in eukaryotes, very few proteins have been specifically localized to ER-PM contact sites (Manford et al., 2012).

The presence of ER-PM contact sites has been documented in plant cells but their functions have not been well characterized (Staehelin, 1997; Larsson et al., 2007). It is speculated that in plants, as in yeast, these contact sites may be regions of lipid recycling or lipid remodeling (Staehelin and Chapman, 1987; Larsson et al., 2007; Samuels and McFarlane, 2012). Indeed, like the ER-PM contact sites isolated from yeast, isolated plant ER-PM contact sites have increased lipid modification activity, relative to either ER or PM alone (Larsson et al., 2007). Plant cells also secrete a variety of lipid products, including cuticular lipids, which protect plants from non-stomatal water loss and essential oils, which can act as defense compounds (Mahmoud and Croteau, 2002; Samuels et al., 2008). By analogy to lipid uptake in yeast systems (Toulmay and Prinz, 2011) these plant lipid products might be secreted via ER-PM contact sites. Thus, in addition to the role that vesicular trafficking plays in lipid export (Chapter 3), ER-PM contact sites may also be avenues of lipid export from plant cells.

In order to investigate the roles of plant ER-PM contact sites, confocal microscopy, transmission electron microscopy (TEM), and transmission electron tomography were combined to describe the morphology and behaviour of the cortical ER network and of ER-PM contact sites at a variety of developmental stages. In order to determine the functional components of ER-PM contact sites and to elucidate their biological function in plants, attempts were made to isolate these membrane subcompartments by coupling differential centrifugation, aqueous two-phase partitioning, and free flow electrophoresis. High quality fractions of the plasma membrane obtained by this approach yielded interesting proteomic data on the Arabidopsis seedling plasma membrane which has provided promising candidate proteins for further investigation of plant ER-PM contact sites proteins.

4.2 Results

4.2.1 Cortical ER morphology and behaviour changes throughout plant development

In order to understand the function of ER-PM contact sites in plants, it is important to map their spatial and temporal distribution during different developmental and metabolic events. The Arabidopsis inflorescence stem epidermis provides a good experimental model for cells undergoing large amounts of elongation and lipid secretion. To document the distribution and dynamics of ER, live wild-type cells of plant lines expressing GFP-HDEL, an ER marker (Batoko et al., 2000), were imaged with spinning disc microscopy (Figure 4.1). To identify cortical versus endoplasmic ER, cells were also labeled with FM4-64, a steryl dye which initially labels the plasma membrane and then labels the trans-Golgi network (TGN)/early endosome and later, the vacuole (Bolte, et al., 2004). In young, rapidly elongating stem epidermal cells the cortical ER formed a dense, lamellar network that contained perforations of 0.5 to 1 μm (Figure 4.1A). Several transvacuolar strands connected this cortical ER network to the perinuclear ER (Figure 4.1B). Incubating elongating stem epidermal cells in FM4-64 for longer than 5 minutes allowed internalization of the dye into the endocytic pathway and demonstrated that the perforations in the cortical ER network contained elements of the endocytic pathway, which would include endosomes/TGN (Figure 4.1C). Interestingly, the cortical ER network in young stem epidermal cells was relatively stable and did not exhibit the same rapid remodeling and cytoplasmic streaming that have been observed in other cell types (Ridge et al., 1999; Sparkes et al., 2009b; Figure 4.1D). In mature stem epidermal cells, which are no longer undergoing rapid cell elongation, the cortical ER formed a complex network of tubules (Figure 4.1E, F). Tubules tended to intersect at three-way junctions and were rapidly remodeled over time. The cortical ER, transvacuolar strands, and some of the perinuclear ER of mature stem epidermal cells also underwent rapid cytoplasmic streaming (Figure 4.1G). Neither young, rapidly elongating, nor mature stem epidermal cells contained ER fusiform bodies, which have been described in roots, hypocotyls, and leaves (Ridge et al., 1999; Hawes et al., 2001).

In order to determine whether this dense, lamellar cortical ER network was specific to young stem epidermal cells with high lipid secretion rates, GFP-HDEL was imaged in young, rapidly elongating and mature cells of hypocotyls and roots (Figure 4.2). These tissues represent both a gradient of elongation (young, rapidly elongating cells versus non-elongating mature cells) and a gradient of lipid secretion activities: root epidermal cells do not have a thick cuticle, while stem epidermal cells synthesize and secrete a significant layer of cuticular lipids, and hypocotyls secrete an intermediate amount of lipid. Interestingly, dense, lamellar cortical ER, similar to the stem epidermal cortical ER, was observed in the elongation zone of both hypocotyls and roots (Figure 4.2A). The cortical ER network of mature root and hypocotyl cells also resembled that of mature stems except that the root and hypocotyl ER networks also contained fusiform bodies, which accumulate GFP-HDEL (Figure 4.2A). Quantification of cortical ER density revealed that there was no significant difference in the cortical ER density between different tissue types of young, rapidly elongating cells, nor were there significant differences in cortical ER density between mature cell types ($p < 0.0001$ for all tissue types of elongating cells, $p < 0.0001$ for all tissue types of mature cells; $n > 60$ measurements from 20 cells; ANOVA; Figure 4.2B). However, all three cell types had significantly denser cortical ER during their young, rapidly elongating stages, relative to mature cells ($p < 0.0001$ for young versus mature ER density for all three types; $n > 60$ measurements from 20 cells; t-test; Figure 4.2B). Together, these data indicate that a dense cortical ER network is correlated with cells undergoing rapid elongation, rather than high levels of lipid secretion.

4.2.2 ER-PM contact sites are correlated with cell elongation

The increased cortical ER density observed in young, rapidly elongating cells, relative to mature cells, implies that young cells could have more ER-PM contact sites. However, the resolution of confocal microscopy is not sufficiently high to differentiate between true contact sites (15 nm or less between the ER and PM) and cortical ER (> 15 nm between the ER and PM) (Figure 4.3A). To investigate these different cell types at higher resolution, high pressure frozen, freeze substituted stems, hypocotyls, and roots were examined by TEM. Contact sites were defined as regions where ribosomes were excluded from the ER membrane and the distance between the ER membrane and the inner

leaflet of the PM bilayer was 15 nm or less (Holthuis and Levine, 2005). In TEM, contact sites represented only a small proportion of the total ER that would have been identified as cortical ER in confocal microscopy (Figure 4.3B; compare total cortical ER in green to ER-PM contact sites in blue). The average contact site in elongating stem epidermal cells was 176 nm long ± 5 nm standard error (n=503 contact sites). The longest observed contact site was 746 nm, while the shortest was 28 nm, though most fell within the range of 50-300 nm (Figure 4.3C). In contrast to *S. cerevisiae*, in which the ER is in close contact with 20-45% of the PM (Pichler et al., 2001; West et al., 2011), less than 10% of the Arabidopsis PM was in close contact with the ER (Figure 4.3D). This discrepancy is likely due to the relatively strict definition of ER-PM contact site employed here and the very loose definition employed in other studies (30 nm or less between the ER and the PM in Pichler et al., 2001; up to 65 nm, with a mean of 33 nm in West et al., 2011). If contact sites of only 15nm or less were counted in yeast, their frequency would be reduced to less than 10% (West et al., 2011). These data imply that the frequency of ER-PM contact sites is relatively conserved among eukaryotes. It is likely that the remainder of the plasma membrane must remain accessible for other functions, such as vesicle budding and fusion, and cytoskeleton anchoring.

To compare the high-resolution view from TEM with the overview given by live cell imaging, the frequency of ER-PM contact sites in TEM was correlated with the density of the cortical ER in confocal microscopy. ER-PM contact site occurrence was measured as the proportion of PM that was participating in a contact site, relative to the total surface area of the plasma membrane. Consistent with confocal microscopy of GFP-HDEL labeled ER (Figure 4.2), there were significantly more ER-PM contact sites in young, rapidly elongating cells ($p < 0.001$, $n > 500$ measurements in > 20 cells; t-test), compared to mature cells of the same tissue (Figure 4.3D). These results indicate that in these tissues, cortical ER density is correlated with the ER-PM contact site density and that ER-PM contact sites are regulated through development in a manner that is correlated with the rate of cell elongation.

The two dimensional nature of TEM makes it difficult to understand the three-dimensional nature of ER-PM contact sites. Therefore, in order to examine the three-dimensional architecture of ER-PM contact sites, electron tomography was employed. Dual

axis tomograms were collected of the cortical cytoplasm from young, rapidly elongating stem epidermal cells. Visualization and modeling of reconstructed tomograms revealed the complex and highly variable structure of the plant cortical ER (Figure 4.4). While ER morphology is typically characterized in terms of tubules or sheets, the plant cortical ER resembled a highly interconnected network that could equally be described as a tubular network or fenestrated sheet. Similar to ER-PM contact sites in yeast (West et al., 2011) the cortical ER came in and out of close contact with the PM over a wide area, though individual contact sites were relatively small (~50-150 nm), which is consistent with the measurements taken in TEM (Figure 4.4, inserts). Thus tomography revealed the complex substructure of the ER at the nanoscale that was not apparent in live cell imaging or TEM.

To test whether cortical ER density and ER-PM contact sites are correlated with lipid secretion, the cortical ER density and ER-PM contact site density was measured in wild-type cells overexpressing the *WAX INDUCER1 (WIN1)* transcription factor. Since these plants produce higher than wild-type levels of cuticular lipids (Broun et al 2004; Kannangara et al., 2007), an increase in cortical ER and ER-PM contact site density would be expected if cuticular lipids are being exported via non-vesicular trafficking from their site of synthesis in the ER to the PM. There was no significant increase in cortical ER density (Figure 4.5A and 4.5B) or ER-PM contact sites (Figure 4.5C and 4.5D) in *WIN1* overexpressing stem epidermal cells, relative to wild type ($p = 0.1510$, $n > 75$ measurements from 25 cells for cortical ER; $p = 0.3695$, $n > 500$ measurements from > 20 cells for ER-PM contact sites; t-test; Figure 4.5).

As a second line of genetic investigation as to whether ER-PM contact sites are involved in cuticular lipid secretion, ER-PM contact sites were quantified in *root hair defective3* (*rhd3-1*) mutant stem epidermal cells. RHD3 is a GTPase that is implicated in ER shaping, analogous to mammalian Atlastins and yeast Sey1p (Hu et al., 2009; Chen et al., 2011c; Liu et al., 2012). *rhd3-1* mutants are defective in ER morphology; ER aggregates in the centre of the cell around the nucleus, similar to yeast mutants in which ER-PM tethering proteins have been deleted (Chen et al., 2011c; Manford et al., 2012). However, despite the dramatic decrease in cortical ER density in *rhd3-1* mutants observed with live cell imaging (Chapter 3; Figure 4.5C and 4.5D) there was no significant difference in the density of ER-PM contact sites at the TEM level between *rhd3-1* mutants and wild type (p =

0.4658, n > 500 measurements from > 20 cells for ER-PM contact sites; t-test Figure 4.5D). This is consistent with chemical analyses of *rhd3-1* cuticular lipids, which revealed a decrease in lipid biosynthesis (possibly due to the defects in ER morphology and organization), but no defect in lipid secretion in these mutants (Chapter 3). Together with the correlation of cortical ER density and ER-PM contact site frequency with cell elongation and not with lipid export (Figure 4.3D), these data suggest that ER-PM contact sites in plants may be involved in lipid recycling during vesicular traffic during cell wall secretion or in lipid remodeling during development, rather than in lipid secretion.

4.2.3 Isolation of ER-PM contact sites

Clearly, a better understanding of the proteins found at plant ER-PM contact sites could elucidate their function. Since few ER-PM contact site proteins have been identified in yeast or animals (Manford et al., 2012), and fewer still have homologues in plants (Altschul et al., 1997), biochemical isolation and proteomic analysis of these ER-PM contact sites allows an unbiased approach, compared to investigation of candidate genes selected based on similarity to other eukaryotes.

To this end, plasma membranes were isolated from young pea (*Pisum sativum*) seedlings using aqueous two-phase partitioning according to an established protocol (Larsson et al., 2007). ER-PM contact sites were further enriched compared to the bulk plasma membrane by separation on a sucrose density gradient (Figure 4.6A; Larsson et al., 2007). Comparison of denatured, coomassie blue-stained total proteins from bulk microsomes and the post-two-phase partitioning plasma membrane fraction with the ER-PM contact site fraction demonstrated a specific enrichment of some proteins and depletion of other proteins in the ER-PM contact site fraction, relative to microscomes or PM (Figure 4.6B). This differential change in proteins has been previously described for both plant and yeast ER-PM contact sites (Pichler et al., 2001; Larsson et al., 2007). Since the Arabidopsis genome is far more complete than genomic resources for pea, attempts were made to adjust this protocol for Arabidopsis seedlings or cell cultures. Wild-type seedlings expressing the ER marker, GFP-HDEL (Batoko et al., 2000), were used in these experiments to allow for visual identification of ER membranes. ER-PM contact sites were isolated using a modified version of two-phase partitioning (Larsson et al., 1984) coupled

to separation on a sucrose density gradient (Larsson et al., 2007). Fluorescence microscopy of the ER-PM contact site fraction from GFP-HDEL seedlings, stained with FM4-64 (which does not label ER membranes; van Gisbergen et al., 2008) to visualize the plasma membrane, revealed GFP-HDEL in close association with the plasma membranes in these fractions (Figure 4.6C). Unfortunately, this method did not yield significant amounts of ER-PM contact sites for proteomic analysis and the technical challenges in reproducing continuous sucrose gradients prohibited pooling of independent experiments to increase the total amount of ER-PM contact site proteins available for analysis.

Since insufficient amounts of ER-PM contact sites were isolated using the previously published protocol, an alternative approach was developed to isolate ER-PM contact sites for proteomics. As above, plasma membranes were isolated from young Arabidopsis seedlings expressing GFP-HDEL using aqueous two-phase partitioning (Larsson et al., 1984). Plasma membranes were then further separated into 96 fractions by free-flow electrophoresis (FFE), which separates membranes primarily based on their surface charge (Sandelius et al., 1986; Brady et al., 2005; Parsons et al., 2012; Figure 4.7A). While technical considerations intrinsic to FFE can cause some variation in migration between experiments, fractions can be combined across experiments by comparing the absorbance at 280 nm (A_{280}), as a proxy for protein concentration (Figure 4.7B; Parsons et al., 2012). Comparison of the GFP-HDEL signal intensity of one experiment with the A_{280} signal revealed no significant concentration of ER GFP-HDEL fluorescence within any population of subfractions of the plasma membrane (Figure 4.7B). Fractions from two of the three peaks (fractions 50-64, and fractions 86-88) were collected for further analysis. The earliest peak (fractions 10-17) was not collected as it corresponds to Golgi membrane and other contaminants (Parsons et al., 2012). Western blotting with anti-GFP, anti-calreticulin (as an ER maker), and anti-AHA (as a PM marker) (Figure 4.7C) and microscopy of FM4-64 stained fractions (Figure 4.7D) confirmed that FFE failed to enrich ER-PM contact sites from bulk plasma membrane in any subset of fractions.

4.2.4 High quality-PM proteomics reveals promising ER-PM contact site candidate proteins

Despite the challenges in isolating ER-PM contact sites, high quality plasma membrane fractions were obtained by coupling two-phase partitioning and free-flow electrophoresis. Given that almost 10% of the plasma membrane participates in ER-PM contact sites in young tissues (Figure 4.3D), it is likely that many ER-PM contact site proteins exist in these isolated PMs. Therefore, each fraction of interest from three independent experiments was analyzed via LC-MS/MS and compared against The Arabidopsis Information Resource (TAIR) release 10 protein data set. For each experiment, only proteins that were detected by at least 5 spectral counts were included in further analyses (Lundgren et al., 2010). These totaled 936 proteins, 589 of which were identified in more than one experiment (Figure 4.8A).

To determine the quality of PMs isolated by coupling two-phase partitioning to FFE, subcellular localizations of the identified proteins were identified using MASCP-Gator (Joshi et al., 2011), which aggregates information from the SUBA database, including fluorescent protein localizations, previous proteomics analyses, and protein localization predictions (Heazlewood et al., 2007). Localization data revealed that 81.7% of proteins in the post-two phase partitioning fraction were annotated as plasma membrane proteins, compared to only 35.5% in the microsomal fraction (Figure 4.8B and 4.8C). Furthermore, of the fractions obtained from FFE, 88.9% proteins were annotated as PM proteins (Figure 4.8D). These include proteins such as the plasma membrane proton pumps (AHAs), a variety of glycosylphosphatidylionsitol (GPI) anchored proteins (e.g. fasciclin-like arabinogalactan proteins and COBRA), ATP-binding cassette transporters (including ABCG11 and ABCG12) and various transmembrane receptor kinases.

The primary contaminants in the FFE fractions were cytosolic proteins (6.3%). However, at least some of these may represent PM-associated peripheral proteins. ER proteins were also a contaminant in the post-two phase partitioning fraction and in the FFE fractions (1.1%), which likely represent ER-PM contact sites. Finally, a significant proportion of the detected proteins (9.6%) were proteins of unknown localization, many of which may be PM proteins. Compared to other efforts to purify PMs for proteomic analysis, which typically result in ~80% PM proteins (Nelson et al., 2006), these results represent a

high quality data set and demonstrate the power of coupling two-phase partitioning with FFE.

In order to determine whether any specific proteins are differentially eluted across the FFE fractions, spectral counts were compared across these fractions. Because of technical limitations intrinsic to free-flow electrophoresis, proteins do not always elute in the exact same FFE fraction across experiments, but the relationship between fractions remains relatively reproducible (Parsons et al., 2012). To reduce this variability, data were grouped into four bins, based on their relative position in the FFE fractions: bin1 corresponds to the first third of the wide middle peak, bin2 to the middle third, bin3 of the last third of the wide middle peak, and bin4 to the narrow late peak (Figure 4.7B and 4.7C). The average percent of spectral counts in each bin was $\log_2$ transformed and data were clustered using the K-means module of Multi-Experiment Viewer (Saeed et al., 2003; Figure 4.9). Consistent with the dispersion of GFP-HDEL throughout all of the PM fractions, GFP was included in a cluster that showed little variation across the four bins (Figure 4.9). Interestingly, proteins that are GPI anchored (Sherrier et al., 1999) or localized to detergent resistant membranes (Borner et al., 2005) did not show a differential distribution across the FFE fraction bins (M. Meents, H. McFarlane, and L. Samuels; unpublished data).

Among the PM proteins detected in these experiments were several proteins with homology to ER-PM contact site proteins in other organisms (Table 4.1). Synaptotagmin (SYT) proteins in Arabidopsis share homology to *S. cerevisiae* Tcb1p, Tcb2p, and Tcb3p. In yeast, these Tcb proteins have been localized specifically to ER-PM contact sites, and they are required for lipid modification at contact sites (Tolumay and Prinz, 2012; Manford et al., 2012). Although there are six SYTs in Arabidopsis (SYTA-SYTF), only two of these, SYTA and STYE, were detected in these experiments (Table 4.1). A third protein with low homology to the Tcbs, BONZAI2 (BON2) was also detected (Table 4.1). A second family of proteins involved in ER-PM contact sites in yeast are the VAPs, which are also required for lipid modification at these sites (Loewen et al., 2007; Stefan et al., 2011; Manford et al., 2012). Of the seven Arabidopsis VAPs, also called plant VAP homologues (PVAs), only two were detected in these proteomics experiments: PVA12 and VAP27-1 (Table 4.1). Interestingly, although oxysterol binding proteins (OSBPs) have been detected at ER-PM

contact sites in yeast (Raychaudhuri et al., 2006; Stefan et al., 2011) no OSBPs were detected in these experiments. Consistent with the analysis of GFP-HDEL across FFE fractions (Figure 4.7), there was no evidence that any of these potential ER-PM contact site proteins were enriched in any subset of FFE fractions (Figure 4.9).

4.3 Discussion

In plants, sites of close contact between the ER and the PM have been hypothesized to play a number of important roles including secretion of protective lipids, lipid remodeling during development and under nutrient limitation, and lipid recycling during periods of intense vesicle secretion (Staehelin and Chapman, 1987; Larsson et al., 2007; Samuels et al., 2008; Tjellström et al., 2010). However, a comprehensive characterization of their frequency, morphology, regulation, composition, and function was lacking. Here, live cell imaging combined with high-resolution electron microscopy and electron tomography has demonstrated that in Arabidopsis the ER is in close (<15 nm) contact with roughly 10% of the PM in young, rapidly expanding cells. Furthermore, these ER-PM contact sites are correlated with the rate of cell expansion but not with lipid export. While ER-PM contact site purification was insufficient for proteomic analysis, high quality PM proteomics revealed several ER-PM contact site proteins that are conserved between yeast and plants. Together with the developmental correlation between the frequency of ER-PM contact sites and cell elongation, these results suggest a role for plant ER-PM contact sites in lipid remodeling or recycling during development.

4.3.1 The frequency of ER-PM contact sites is developmentally regulated

Here, the morphology of the cortical ER has been described at different developmental stages in different tissues using live cell imaging of the ER marker GFP-HDEL. In young, rapidly elongating cells the cortical ER appears as a dense network of fenestrated cisternae. Further examination revealed that at least some of these gaps in the ER network contain TGN/early endosome components, highlighting the importance of regulating cortical ER distribution to allow other subcellular components access to the PM. Closer examination of the cortical ER using high-resolution TEM and electron tomography

revealed that the cortical ER more closely resembles a dense tubular network than would be expected based upon the cisternae observed with light microscopy. In mature cells, which are no longer rapidly elongating, the cortical ER network is significantly less dense and is primarily comprised of tubules connected at three-way junctions. These developmental changes were consistent across stems, hypocotyls, and roots, which implies that the morphology of the cortical ER network is developmentally regulated in a common fashion across tissue types.

Using TEM, ER-PM contact sites were quantified at representative developmental stages for both rapidly elongating cells and mature cells that are no longer rapidly elongating. Roughly 10% of the PM was in close contact with the ER in young stem epidermal cells. Interestingly, this percentage is much lower than what has been reported for *S. cerevisiae* (20-45%) (Pichler et al., 2001; West et al., 2011). The most obvious explanation for this discrepancy is that both studies in yeast employed a much more generous definition of ER-PM contact sites; while this work only counted sites where ER and PM are 15 nm or less apart, Pichler et al. (2001) counted sites with up to 30 nm between the ER and the PM, and West et al. (2011) used up to 65 nm. Alternatively, it is possible that this difference in the frequency of ER-PM contact sites may be due to a fundamental difference between plants and yeast. For example, in plants ER-PM contact sites have been hypothesized to play a role in lipid recycling (Staehelin and Chapman, 1987). As plant cells grow they must secrete large amounts of cell wall polysaccharides to maintain a consistent cell wall, thus vesicle mediated secretion plays a key role in plant growth. However, if most of the lipids that are added to the PM by vesicle fusion were not recycled, the rate of PM expansion would vastly outweigh the rate of cell wall expansion. Thus, in order to match PM growth with cell wall growth, lipids must be rapidly recycled during cell wall secretion. While some of this recycling will occur via endocytosis, mediated by clathrin-coated vesicles (Dhonukshe et al., 2007), it is unclear whether the rate of endocytosis is sufficient to match the rate of secretion (Ketelaar et al., 2008). The correlation between ER-PM contact sites and the rate of cell elongation implies that plant ER-PM contact sites may play a role in lipid recycling during cell expansion. However, if ER-PM contact sites play this lipid-recycling role in plants, then plants might have more contact sites than yeast, rather than fewer, as reported here.

Electron tomography of the plant cortical ER has revealed the fascinating complexity of this network. What appears as sheets of ER in confocal microscopy and tubules in TEM, is actually a complex reticulated network that could equally be described as either highly fenestrated sheets or a highly interrelated network of tubules. These data highlight the utility of electron tomography. While confocal microscopy gives excellent temporal resolution and allows three-dimensional examination of the cortical ER, and TEM allows high-resolution examination of the cortical ER, both techniques have their limitations. Confocal microscopy is limited by the resolution of the light microscope, which cannot resolve individual ER membranes. TEM, on the other hand, provides essentially two-dimensional information about the cell at a single time point. In contrast, tomography can provide high-resolution three-dimensional images. Thus, while tomography is a laborious technique, it can be highly useful in relating four-dimensional confocal data to high-resolution electron microscopy.

4.3.2 The frequency of ER-PM contact sites is not correlated with lipid synthesis or secretion

Previous studies have speculated that ER-PM contact sites may be involved in lipid secretion during cuticle development (McFarlane et al., 2010). To test this hypothesis, the density of the cortical ER and the frequency of ER-PM contact sites was measured in cells at comparable developmental stages undergoing a range of levels of lipid secretion. There was no significant difference in the frequency of ER-PM contact sites between root epidermal cells, which do not secrete a lipidic cuticle, stem epidermal cells, which secrete a significant cuticular layer, and stem epidermal cells overexpressing WIN1, which produce even more cuticular lipid than wild type (Broun et al 2004; Kannangara et al., 2007). This correlation suggests that cuticular lipids may not be transported at ER-PM contact sites. Indeed, these data are in agreement with the role of Golgi-mediated vesicle secretion in cuticular lipid export (Chapter 3). However, these experiments assume that the frequency of ER-PM contact sites is related to their functional capacity. A similar correlation between contact site density and function has been observed in lipid remodeling in budding yeast; when sites of close contact between the ER and the PM are disrupted, lipid remodeling cannot occur very efficiently because the enzyme is localized to the ER, but its substrates

are localized to the PM (Stefan et al., 2011; Manford et al., 2012). Despite this lack of correlation between ER-PM contact sites and lipid export, it is still possible that some cuticular lipids may be exported via non-vesicular trafficking via ER-PM contact sites. In order to directly test this hypothesis, it is first necessary to isolate mutants with defects in ER-PM contact sites so that their cuticular lipid levels can be assayed.

4.3.3 PM proteomics reveals potential ER-PM contact site proteins

In an attempt to define the functional components of ER-PM contact sites, efforts were made to isolate these contact sites from pea seedlings, Arabidopsis seedlings, and Arabidopsis cell cultures. Although ER-PM contact sites could not be consistently isolated from Arabidopsis with sufficient yield for proteomics, a high-quality proteomic analysis of Arabidopsis seedling plasma membrane proteins revealed several proteins with homology to ER-PM contact site proteins in other organisms (Table 4.1).

Due to the difficulties in isolating PMs, relative to other endomembrane compartments, high quality studies of the plant PM have been limited. Typically, PM isolations contain significant contamination from the tonoplast, the ER, endosomes, and the Golgi apparatus. Thus, reported values of PM purity are highly variable and range from 50% (Santoni et al., 1999) to over 90% (Sandelius et al., 1986; Alexandersson et al., 2004; Marmagne et al., 2004). However, some reports do not describe how purity was assessed (Alexandersson et al., 2004), or use methods that do not differentiate between PM and tonoplast (e.g. vannadate-sensitive ATPase activity; Marmagne et al., 2004). Therefore, the true purity of many previously reported PM fractions is likely well below these values (Nelson et al., 2006; Zhang and Peck, 2011). Other techniques, especially localization of organelle proteins by isotope tagging (LOPIT), have been employed to identify PM proteins with high confidence, but these studies have identified only a small number of proteins (e.g 92 proteins in Dunkley et al., 2006, 72 proteins in Nelson et al., 2006), many of which had already been confidently predicted to be PM proteins, such as receptor kinases, ABC transporters, and GPI-anchored proteins (Dunkley et al., 2006; Nelson et al., 2006). By coupling aqueous two-phase partitioning and free flow electrophoresis, highly pure PMs have been isolated for proteomics. The strength in this combination is that the two methods rely on different properties of the plasma membrane, and are therefore

complementary. Two-phase partitioning separates PM based upon the properties of the extracellular surface (Larsson et al., 1984; Palmgren et al., 1990); the similarity between the tonoplast and the PM causes contamination of PMs with vacuolar components, but provides good separation of ER and Golgi membranes from the PM (Larsson et al., 1984). FFE, on the other hand, separates membranes based on their surface charge (Sandelius et al., 1986; Parsons et al., 2012). While FFE is usually insufficient to separate PM from endosomes and Golgi, it provides good resolution between tonoplast and PM (Sandelius et al., 1986; Bardy et al., 2005). Thus, the combination of two techniques yields significantly more purified PM fractions and has allowed proteomic analysis of PM fractions that are 88.9% pure, and identification of over 500 proteins.

In contrast to many previous studies (Santoni et al., 1999; Alexandersson et al., 2004; Marmagne et al., 2004), the primary contaminants in this proteomic analysis of the PM were cytoplasmic proteins. It is somewhat surprising that soluble cytoplasmic proteins could persist throughout the membrane isolation protocol. However, many of these proteins are often closely associated with the plasma membrane. For instance, various isoforms of tubulin represented 10.5% of spectral counts from the cytoplasmic contaminants. In the form of microtubules, tubulin can associate with the cell cortex, which would explain tubulin co-isolation with PM fractions. This association is partially dependent upon Class II-associated invariant chain peptide (CLIP)-associated protein (CLASP) (Ambrose and Wasteneys, 2008); CLASP was detected in PM fraction proteomics, but not above threshold levels. Similarly, several vesicle budding and fusion related proteins, such as clathrin, are soluble proteins that may interact with the PM (Dhonukshe et al., 2007; Konopka et al., 2008). Co-isolation of these cytosolic, potentially PM-binding proteins with PM fractions highlights the complex and dynamic nature of the cortical cytoplasm at the PM. In the context of ER-PM contact sites, it is clear that a proportion of the PM is reserved for other functions, such as cytoskeleton anchoring, cell wall synthesis, and vesicle budding and fusion, so it is unsurprising that ER-PM contact sites occupy only about 10% of the PM.

Within this proteomic study of the PM, several homologous proteins to yeast ER-PM contact site components were identified. In *S. cerevisiae*, three tricalbin proteins, Tcb1, Tcb2p, and Tcb3p, which all contain a synaptotagmin-like-mitochondrial-lipid binding

protein (SMP) domain, have been localized to ER-PM contact sites (Tolumay and Prinz, 2012; Manford et al., 2012). These are most similar to Arabidopsis synaptotagmin-like proteins (SYTs); although other Arabidopsis proteins also contain SMP domains, only the SYT proteins share a similar domain structure to the yeast Tcb proteins, including a transmembrane domain, the SMP domain, and several calcium-dependent lipid binding motifs (C2 domains) (Lee and Hong, 2006). There are six SYT proteins in Arabidopsis (SYTA-SYTF), though only two of these, SYTA and STYE, were detected in these experiments. Only SYTA has been partially characterized in Arabidopsis. Mutants in *SYTA* are defective in salt tolerance (Schapire et al., 2008), freezing tolerance (Yamazaki et al., 2008), and viral spread between cells (Lewis and Lazarowitz, 2010). Similar to the tricalbins in yeast (Manford et al., 2012), the localization of SYTA is unclear, though various reports describe SYTA as localized to the ER including some puncta of cortical ER that appear non-motile (Schapire et al., 2008), which may correspond to ER-PM contact sites, as well as the PM (Schapire et al., 2008; Yamazaki et al., 2008), and endosomes (Lewis and Lazarowitz, 2010). Consistent with the idea that SYTA may play a similar role to the Tcb proteins in yeast, recombinant SYTA can bind liposomes composed of mixed phospholipids in a Ca^{2+}-dependent manner (Schapire et al., 2008). Different groups have deduced widely different gene functions for SYTA from these mutant phenotypes, including participating in membrane repair during osmotic stress, membrane fluidity during freezing, and viral movement via endocytosis (Schapire et al., 2008; Yamazaki et al., 2008; Lewis and Lazarowitz, 2010). However, a role for SYTA in lipid remodeling at ER-PM contact sites would be consistent with all of these phenotypes as well.

A third C2-domain protein, BONZAI2 (BON2) was also detected. Although a BLASTp search indicates that BON2 shares similarity to the yeast Tcb proteins, BON2 is more similar to Copine family proteins, which are found exclusively in multicellular organisms (Cruetz et al., 1998). Copine family proteins have been associated with vesicle trafficking, protein ubiquitination, and lipid signaling, though their exact function remains unclear (Cruetz et al., 1998). In plants, the three BON family members (BON1-BON3) have all been implicated in repression of a disease resistance (*R*) gene (Yang et al., 2006). Triple mutants for all three BONs are seedling-lethal and display necrotic lesions, though these phenotypes can be partially rescued by mutations in some *R* genes (Yang et al., 2006). However, the

mechanism by which BON genes repress *R* genes is unknown, and it is acknowledged the possibility that these genes may play a more general role in plant growth and development (Yang et al., 2006). Although the Copine family proteins have not yet been investigated as potential ER-PM contact site proteins, their domain structure, consisting of a transmembrane region plus a long cytoplasmic tail containing repeated lipid-binding motifs, makes them excellent candidates to anchor two membranes together at a membrane contact site (Toulmay and Prinz, 2012).

Other studies in *S. cerevisiae* have implicated the vesicle associated membrane protein (VAMP)-associated proteins (VAPs), Scs2p and Scs22p, in ER-PM interactions (Loewen et al., 2007; Stefan et al., 2011; Manford et al., 2012). Of the seven Arabidopsis VAPs, also called plant VAP homologues (PVAs), two were detected in these proteomics experiments: PVA12 and VAP27-1. Neither of these VAPs have been functionally investigated in plants. Interestingly, although oxysterol binding proteins (OSBPs) have been detected at ER-PM contact sites in yeast (Raychaudhuri et al., 2006; Stefan et al., 2011), and the plant OSBP ORP3a can interact with PVA12 (Saravanan et al. 2009), none of the 12 Arabidopsis OSBPs were detected in these experiments.

ER-PM contact sites have been described in a variety of eukaryotes, including plants. Previous studies have implicated plant ER-PM contact sites in diverse processes, including lipid recycling, lipid remodeling during development or under stress conditions, and/or lipid secretion. Here, the developmental correlation between cell elongation and the frequency of ER-PM contact sites suggests that plant ER-PM contact sites may be developmentally regulated and could play a role in lipid remodeling or lipid recycling during cell elongation. Furthermore, no correlation was apparent between the frequency of ER-PM contact sites and the level of lipid secretion in a cell, implying that plant ER-PM contact sites are not involved in anterograde lipid transport. One of the challenges of studying ER-PM contact sites is the difficulty in defining their functional components. While mutant screens have proven very powerful for defining other processes in Arabidopsis, it is unclear what phenotype could be used in a screen to discover ER-PM contact site mutants. Reverse genetic approaches can be used to evaluate the role of several plant homologues to recently characterized ER-PM contact site genes from yeast, but cannot be used to discover new genes or plant-specific genes. A combination of

proteomics and reverse genetics can be a powerful tool to identify ER-PM contact site components and to infer their function in plants. Further experiments should be able to refine ER-PM contact site isolation and to define these functional components.

4.4. Methods

4.4.1 Plant material

Arabidopsis thaliana seeds were sown on AT medium plates (Haughn and Somerville, 1986) and grown at 21°C, 70-80% humidity, constant light (~100 μE m^{-2} s^{-1}) in an environmental growth chamber (Conviron). After 7-14 days, seedlings were transferred to Sunshine mix 5 soil and returned to the same growth conditions. Plant lines were the Col-0 wild-type background, Col-0 + *35S::GFP-HDEL* (Batoko et al., 2000), Col-0 + *35S::WIN1* (a generous gift from P. Lam and L. Kunst), and *rhd3-1* (Chen et al., 2011c). Dark-grown hypocotyls were treated with white light for 4 hours, then incubated in darkness at 21°C for 5 days. For membrane isolation experiments, 7-day old seedlings were grown in half-strength Murashige and Skoog medium (Sigma) with 1% sucrose. Pea seedlings (*Pisum sativum* L., cv Kelvedon Wonder) were sewn directly on soil and grown in greenhouse conditions with 16 hours light and 8 hours of darkness. *Arabidopsis thaliana* T87 tissue cultures (obtained from the Arabidopsis Biological Resource Centre) were grown in NT-1 medium (ABRC) at 200 rpm and 21°C in darkness.

4.4.2 Confocal microscopy

Stem, root, or hypocotyl segments were mounted in water and immediately viewed under a Leica DMI6000 inverted microscope equipped with a PerkinElmer UltraView VoX spinning-disk system and an Hamamatsu 9100-02 CCD camera. GFP was detected using 488 nm laser and 525/36 nm emission filter. FM4-64 (Invitrogen; diluted 1/1000 in water from a 10 mM stock in DMSO) was detected with 514 nm laser and 650/75 nm emission filter. Because ER geometry is difficult to quantify (Bouchekhima and Frigerio, 2009), cortical ER density was quantified by measuring the normalized fluorescent intensity (i.e.

grey level, from 0-255) in randomly selected regions of interest. Images were processed using ImageJ.

4.4.3 High-pressure freezing, transmission electron microscopy, and electron tomography

TEM sample preparation, including high-pressure freezing, freeze-substitution, sectioning, post-staining, and imaging was performed as described in McFarlane et al. (2008). Briefly, stem, root, and hypocotyl segments were high-pressure frozen in B-type sample holders (Ted Pella) with hexadecane or 200 mM sucrose as a cryoprotectant using a Leica HPM-100. Samples were freeze substituted in 2% osmium tetroxide and 8% dimethoxypropane and infiltrated with Spurr's resin (Spurr, 1969) over 10 days. Samples were sectioned using a Leica Ultracut UCT and a Dimatome diamond knife, mounted on copper grids (Gilder), and post stained with 2% uranyl acetate in 70% methanol and Reynolds lead citrate (Reynolds, 1963). Samples were viewed using a Hitachi 7600 TEM at 80kV accelerating voltage with an ATM Advantage HR digital CCD camera (Advanced Microscopy Techniques).

For tomography, thick sections (200-300 nm) were placed on formvar-coated copper-rhodium slot grids, post stained with 2% uranyl acetate in 70% methanol and Reynolds lead citrate (Reynolds, 1963), and coated with 15 nm colloidal gold (Ted Pella) as a fiducial marker. Dual axis tomograms were collected from +65° to -65° using 2° per image from +20° to -20° and 1° per image thereafter, using a Technai G2 Twin (FEI) equipped with an FEI Eagle 4K camera at an accelerating voltage of 200kV . Tomograms were reconstructed with Inspect 3D software (FEI) using 12 iterations of Simultaneous Iterative Reconstruction Technique (SIRT) and dual axis tomograms were merged with Amira software (Visualization Sciences Group) using Lanczos interpolation. Models were generated in Amira; ER was identified by grey-level thresholding, while other structures were manually assigned by segmentation analysis (Donohoe et al., 2006).

4.4.4 Membrane purification via two-phase partitioning and sucrose gradient centrifugation

For plasma membrane isolations, microsomes were prepared from the aerial tissues of 7 day old pea seedlings grown in soil by homogenizing seedlings in 50 mM HEPES buffer (pH 7.6) with 400 mM sucrose, 10mM KCl, 3 mM ethylene glycol tetraacetic acid (EGTA), 3 mM Na-ethylenediaminetetraacetic acid (EDTA), 0.1% fatty acid free bovine serum albumin (Sigma), 1.5 mM dithiothreitol (DTT), and 1 mM Na-ascorbate, filtrating the homogenate through Miracloth (Calbiochem), centrifuging out large contaminants (6000g for 15 minutes at 4°C), and centrifuging the supernatant at 60 000 g_{max} for 30 minutes at 4°C. Microsomes were resuspended in 5 mM potassium phosphoate buffer (pH 7.8) and 2 g were applied to a 20 g, one sample, two wash aqueous two phase partitioning system consisting of 6.20 g Dextran T-500 (Amersham Pharmacia Biotech) and 3.10 g PEG 3350 (Sigma) (Larsson et al., 1984). Aqueous two phase partitioning was performed according to Larsson et al. (1984). Plasma membranes were recovered by centrifuging the upper phase of the second wash of the two phase partitioning system in 10 mM HEPES buffer (pH 7.5) with 250 mM sucrose, and 20 mM KCl at 100 000 g_{max} for 30 minutes and washing the pellet twice with the same buffer.

To isolate ER-PM contact sites, a method modified from Pichler (2001) was employed (Larsson et al., 2007). PM fractions were suspended in 10 mM MES-KOH buffer (pH 6.0) with 300 mM sucrose, frozen in liquid nitrogen and thawed three times to invert vesicles. Samples were loaded onto continuous gradients of 20-50% (w/v) sucrose in the same buffer, and centrifuged at 100 000 g_{max} in a swing out rotor at 4°C for 1 hour, with no brake applied at the end. The top band corresponded to ER-PM contact sites, as described by Larsson et al. (2007).

4.4.5 Membrane purification via two-phase partitioning and free flow electrophoresis

Microsomes were prepared from 7 day old Arabidopsis seedlings expressing GFP-HDEL grown in liquid culture by homogenizing seedlings in 100 mM HEPES buffer (pH 7.5), 0.2% N-Z-amine B (Sigma), 200 mM sorbitol, 10% glycerol, 5 mM EDTA, 5 mM Na-ascorbate, 0.6% polyvinylpyrrolidone K-25 (Sigma), 1 mM DTT, and protease inhibitor

(Roche), filtrating the homogenate through Miracloth (Calbiochem), centrifuging out large contaminants (6000g for 15 minutes at 4°C), and centrifuging the supernatant at 60 000 g_{max} for 30 minutes at 4°C. Microsomes resuspended in 5 mM potassium phosphate buffer (pH 7.5) with 330 mM sucrose, 3 mM KCl, 0.1 mM EDTA, 1 mM DTT, and protease inhibitor (Roche), and applied to a 20 g, one sample, two wash aqueous two phase partitioning system consisting of 6.20 g Dextran T-500 (Sigma) and 3.10 g PEG 3350 (Sigma) (Larsson et al., 1984). Aqueous two phase partitioning was performed according to Larsson et al. (1984). Plasma membranes were recovered by centrifuging the upper phase of the second wash of the two phase partitioning system at 100 000 g_{max} for 1 hour.

Free flow electrophoresis was performed according to Parsons et al. (2012), using a Becton-Dickinson FFE apparatus. All FFE buffers were prepared as described in Eubel et al. (2007) but adjusted to pH 7.1 (separation and counter flow buffer) or pH 6.5 (stabilization and circuit buffers) with NaOH. A voltage of 700 V was applied for a current of ~150 mA. Sample injection speed was 1500 µL/h. Fractions were collected on precooled 96-well plates. Membranes were pooled from fractions by centrifugation at 100 000 g_{max} for 1 hour at 4°C and resuspended in 10 mM Tris-HCl, (pH 7.5). Absorbance at 280 nm (A_{280}) (as a proxy for protein concentration) and GFP were detected using a SpectraMax M2 plate reader (Molecular Devices). Protein concentrations were confirmed using a BioRad Protein Assay kit according to the manufacturers' directions.

4.4.6 Proteomic analysis of membrane fractions

10 µg of protein from each sample was digested with 1 µg trypsin in 50% methanol overnight at 37°C. Solvents were evaporated in a speed-vac for 40 minutes at room temperature, and then samples were suspended in 20 uL of 2% acetonitrile with 0.1% formic acid. 1 µg of protein was analyzed using an Eksigent nano-LC system with an electrospray ionization QSTAR Elite Hybrid quadrupole time-of-flight (Q-TOF) mass spectrometer (AB Sciex) with the settings described in Parsons et al (2012). Peptides were queried against the TAIR10 database (35,397 sequences; 14,487,047 residues) using Mascot search engine version 2.3.02 (Matrix Science) as described in Parsons et al. (2012) except the peptide tolerance was ±50 ppm, the MS/MS tolerance was ±0.1 Da; the variable modification was Oxidation (M); a maximum of one missed cleavage for trypsin was

permitted, and the instrument type was set to electrospray ionization-Q-TOF. The ion score or expect cut-off of was 32. For each experiment, only proteins that were detected by at least 5 spectral counts were included in further analyses (Lundgren et al., 2010).

Subcellular localizations of the identified proteins were determined using MASCP-Gator (Joshi et al., 2011), which aggregates information from the SUBA database, including fluorescent protein localizations, previous proteomics analyses, and protein localization predictions (Heazlewood et al., 2007). Because of limitations intrinsic to free-flow electrophoresis, proteins do not always elute in the exact same fraction across experiments, but the relationship between fractions remains relatively reproducible (Parsons et al., 2012). To reduce this variability, data were grouped into four bins based on their relative position in the FFE fractions: bin1 corresponds to the first third of the wide middle peak, bin2 to the middle third, bin3 of the last third of the wide middle peak, and bin4 to the narrow late peak (Figure 4.7B and 4.7C). For hierarchical data clustering, the average percent of spectral counts in each bin was $\log_2$ transformed (with 0 set to 0.0009) and data were clustered using the K-means module of Multi-Experiment Viewer (Saeed et al., 2003).

4.4.7 SDS-PAGE and immunodetection of proteins via western blotting

5 μg of protein was loaded per lane on a 12% SDS-PAGE denaturing gel. For total protein, gels were stained with Coomassie Blue-Silver (Candiano et al., 2004). For western blotting, proteins were transferred to PVDF membrane using the MiniTransBlot wet transfer system (BioRad) and Towbin buffer (25 mM Tris buffer (pH 7.4), 192 mM glycine, and 20% methanol). Membranes were blocked with 5% skim milk in Tris-buffered saline (pH 7.4) with 1% Tween-20 (TBST), washed in TBST, incubated in primary antibody for 1 hour, washed in TBST, incubated in secondary antibody for 1 hour, washed, and developed in 1/3000 NBT/BCIP (Sigma). Primary antibodies were 1/1000 anti-GFP (Invitrogen, A-6455), anti-BIP (Cosmobio, COP-COP-080017), anti-AHA (Cosmobio, COP-COP-080006), and anti-vacuolar V-PPase (Cosmobio, COP-COP-080001); secondary antibody was 1/1500 goat-anti-rabbit conjugated to alkaline phosphatase (Sigma).

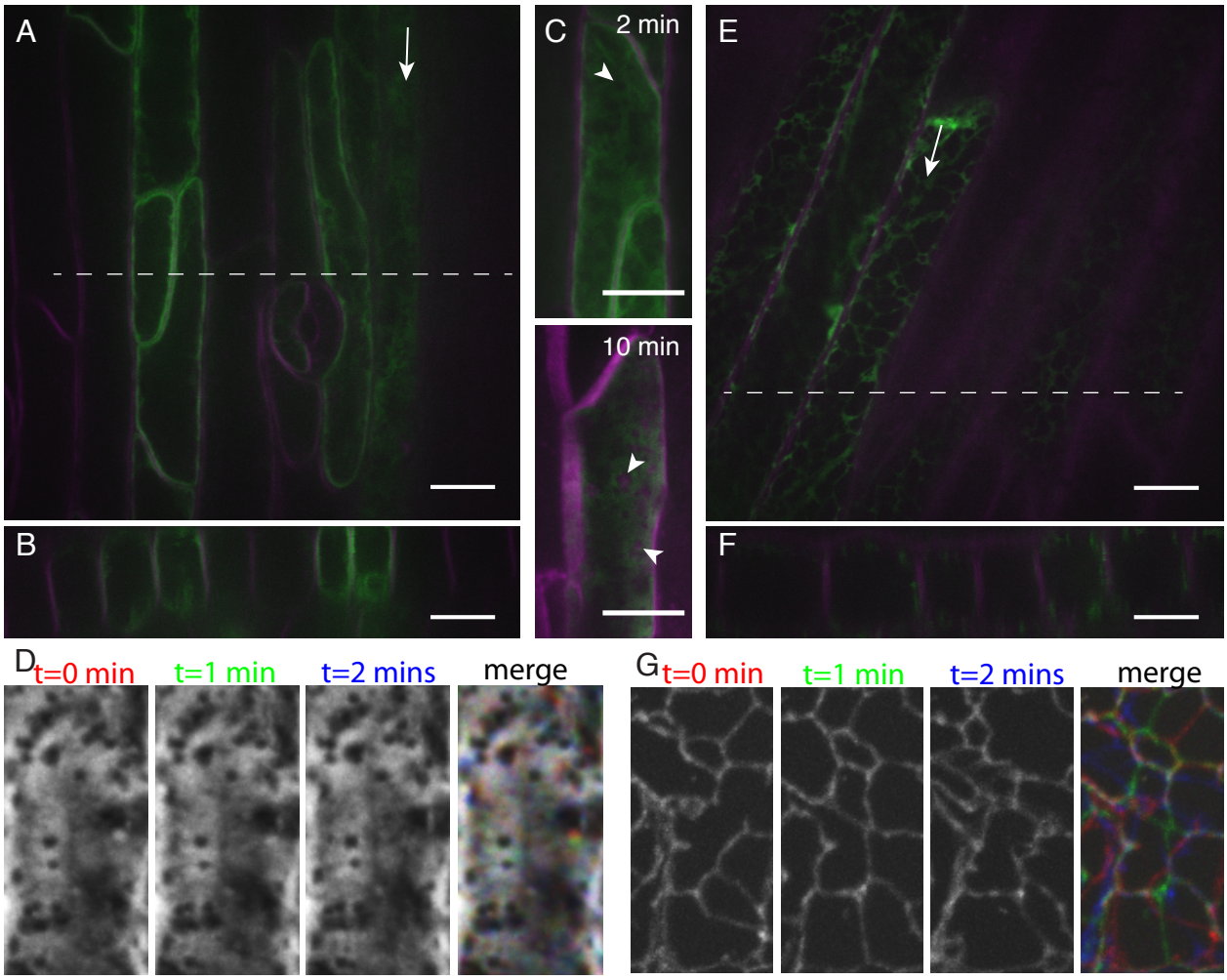

Figure 4.1: ER morphology and behaviour changes through development. In young, rapidly elongating stem epidermal cells (A-D), GFP-HDEL (green) labels the cortical ER network (arrow), visualized in relation to the plasma membrane labeled with FM4-64 (magenta) (A). A cross section of the confocal plane indicated by the dotted line shows that most GFP-HDEL is localized to the cell cortex (B). Fenestrations in the cortical ER network (arrowhead) are rapidly labeled by FM4-64, implying that they may surround endosomes/TGN (C). The cortical ER of young stem epidermal cells is relatively stable over two minutes, as demonstrated by time-lapse imaging of GFP-HDEL, where in the merge, white indicates regions of ER that have not been remodeled (D). In mature stem epidermal cells (E-G) the cortical ER network (arrow) is much more tubular (E, F). The network is rapidly remodeled over two minutes, as demonstrated by the coloured tubules which have moved during time-lapse imaging (G). Scale bars represent 10 µm.

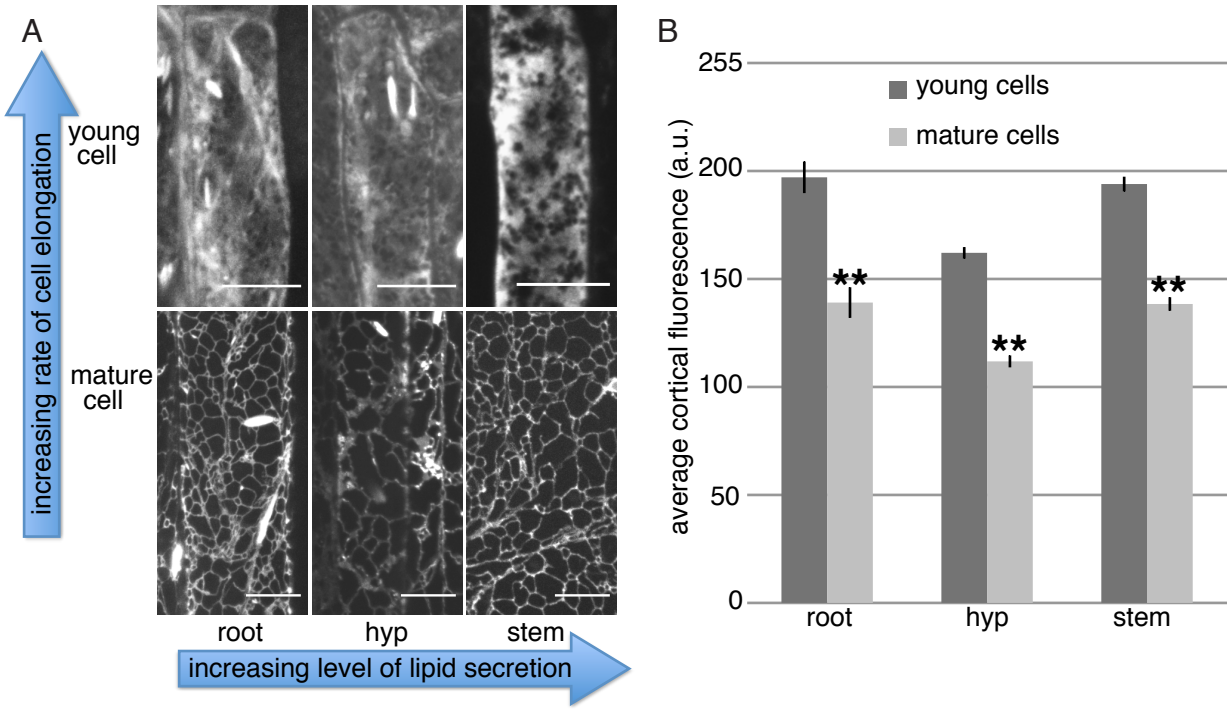

Figure 4.2: Changes in ER morphology are correlated with cell expansion. In young, rapidly elongating cells from roots, hypocotyls (hyp) and stems, GFP-HDEL imaging reveals a dense lamellar network of cortical ER, while mature cells display a more fenestrated tubular network. Quantification of the ER network density by measuring normalized grey levels, from 0-255, (B) revealed no significant differences in ER density between various tissues at comparable developmental stages, but statistically significant differences existed between different developmental stages of the same tissue. Values are means of > 60 measurements from 20 cells, bars represent SE, stars indicate statistically significant differences between developmental stages (t-test, ** for $p < 0.01$).

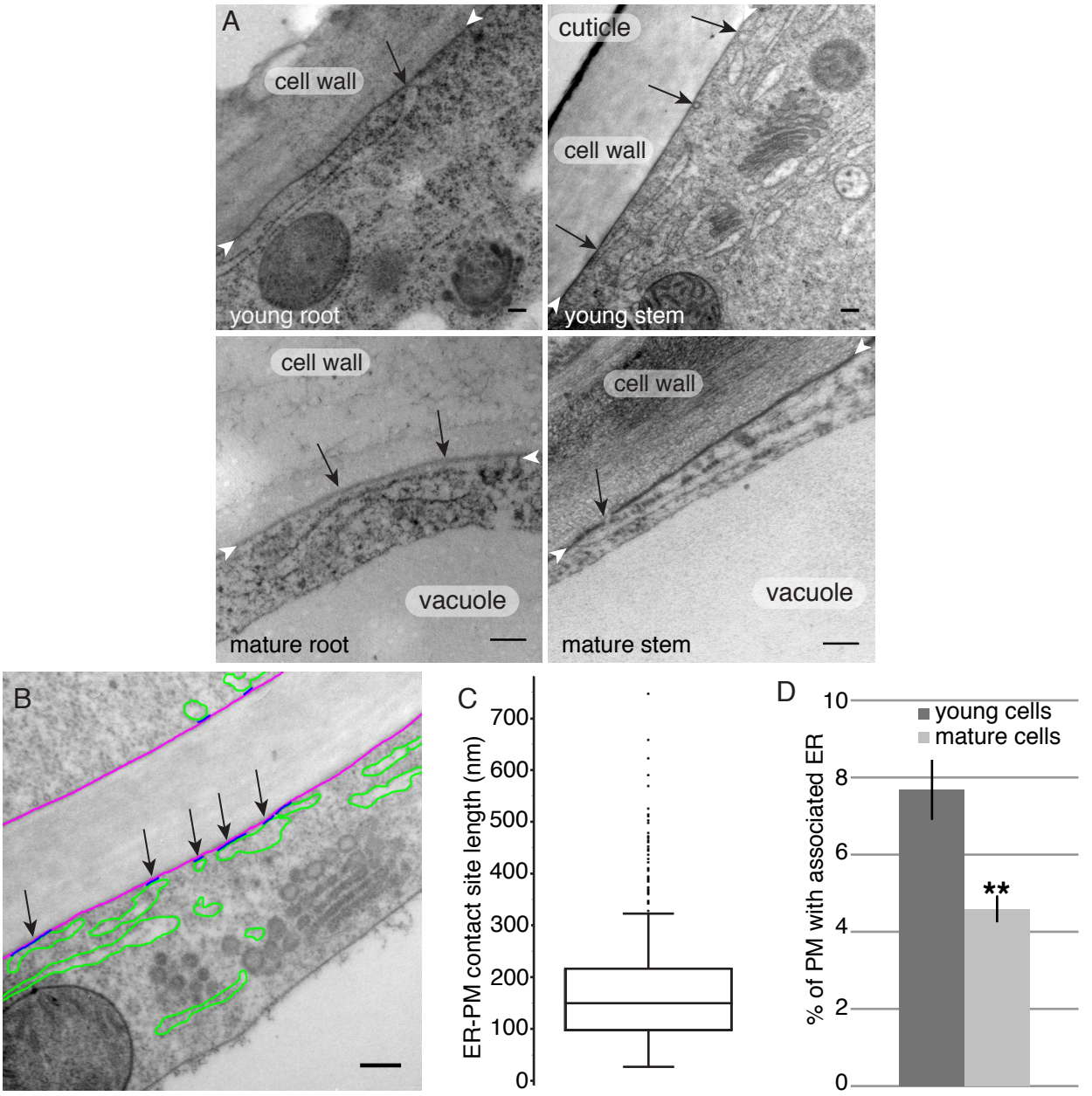

Figure 4.3: ER-PM contact site density is correlated with cortical ER density in rapidly elongating cells. TEM of ER-PM contact sites in young and mature stem and root cells (A). Measurement of ER-PM contact sites (blue), relative to total ER (green) and total PM (magenta) reveals that only a small proportion of the cortical ER participates in contact sites of 15 nm or less between the two membranes (B). Contact sites have a mean length of 176 nm, and range from 746 nm to 28 nm (C). Quantification of the proportion of PM that participates in ER-PM contact sites, relative to the total area of PM, reveals that almost 10% of the PM participates in contact sites in young stem epidermal cells, while significantly less of the PM participates in ER-PM contact sites in mature stem epidermal cells (D). Values are means of > 500 measurements in > 20 cells, bars represent SE, stars indicate statistically significant differences (t-test, ** for $p < 0.01$). Arrows highlight ER-PM contact sites and arrowheads denote the plasma membrane. Scale bars represent 200 nm.

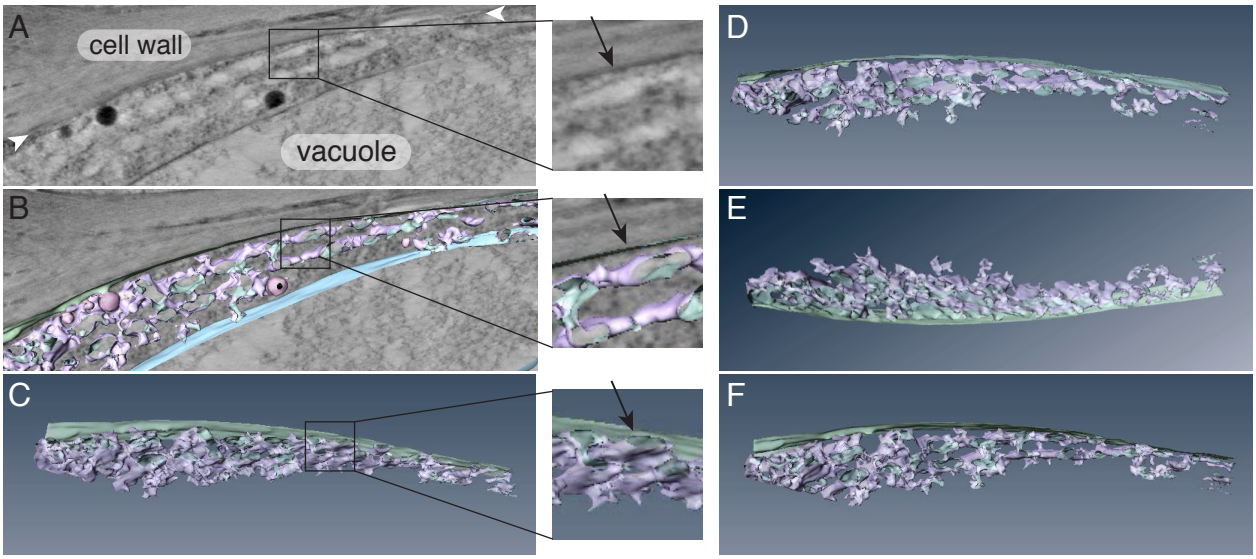

Figure 4.4: Tomography of ER-PM contact sites illustrates the complex nature of the cortical ER in relation to the PM. After reconstruction (A) a tomogram can be modeled (B) to highlight regions of interest from different angles, with the tonoplast omitted from this view (C-F). Plasma membrane is green, tonoplast is blue, vesicles are pink, ER is purple. Arrows in inserts indicate a single ER-PM contact site.

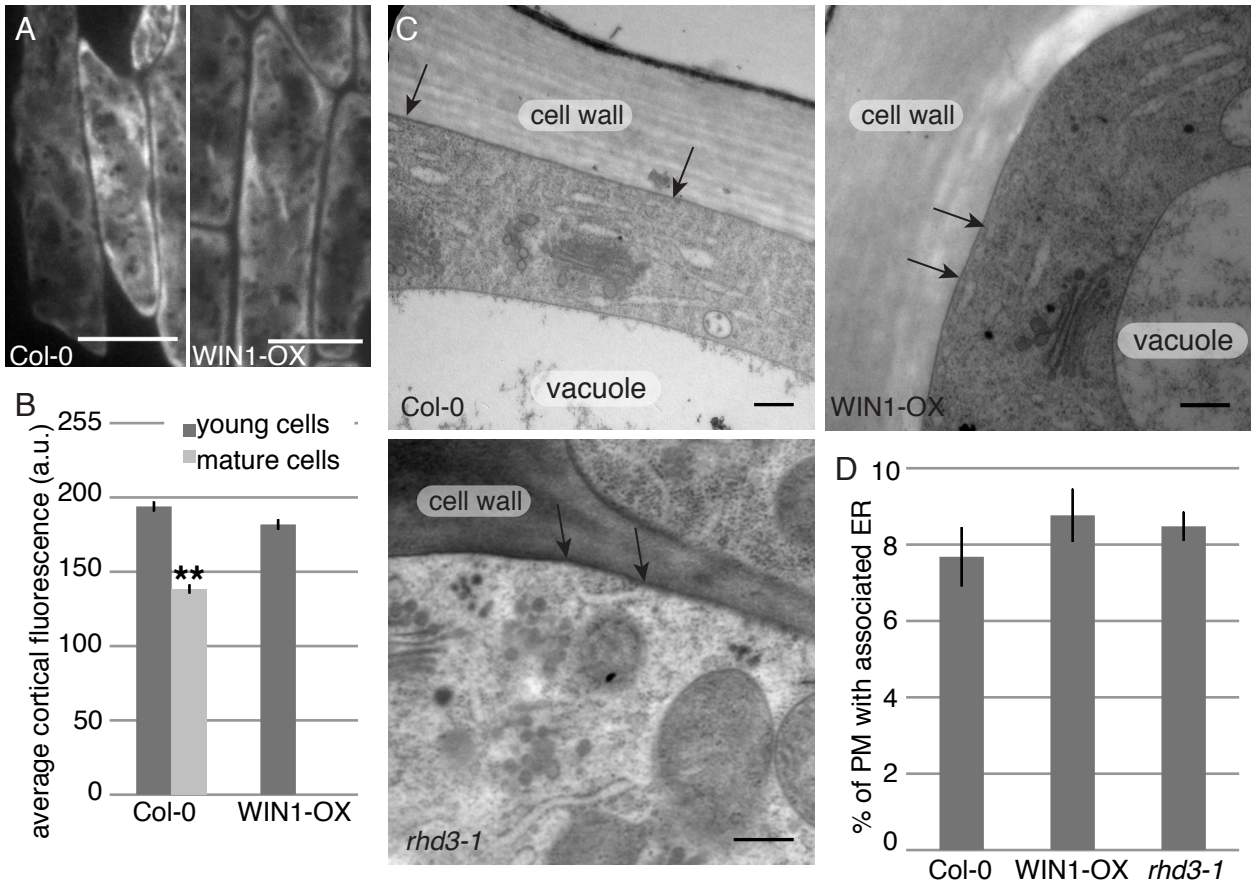

Figure 4.5: ER-PM contact sites are not correlated with lipid secretion. Young stem epidermal cells overexpressing the WIN1 transcription factor (WIN1-OX) display dense, lamellar cortical ER, similar to wild type (A). There is no significant difference between the cortical ER density of young wild-type and WIN1-OX cells (B). Consistent with this, ER contact sites are observed in WIN1-OX and *rhd3-1* mutants, similar to wild type (C) and there is no significant difference in the number of ER-PM contact sites (measured as a proportion of the PM that is within 15 nm of ER) observed in WIN1-OX or *rhd3-1* young stem epidermal cells. Values in B are means of > 60 measurements from > 20 cells, bars represent SE, stars indicate statistically significant differences between wild type and WIN1-OX (t-test, ** for $p < 0.01$). Values in D are means of > 500 measurements from > 20 cells, bars represent SE, stars indicate statistically significant differences between wild type and mutant (t-test, ** for $p < 0.01$). Scale bars represent 10 μm in A and 200 nm in C.

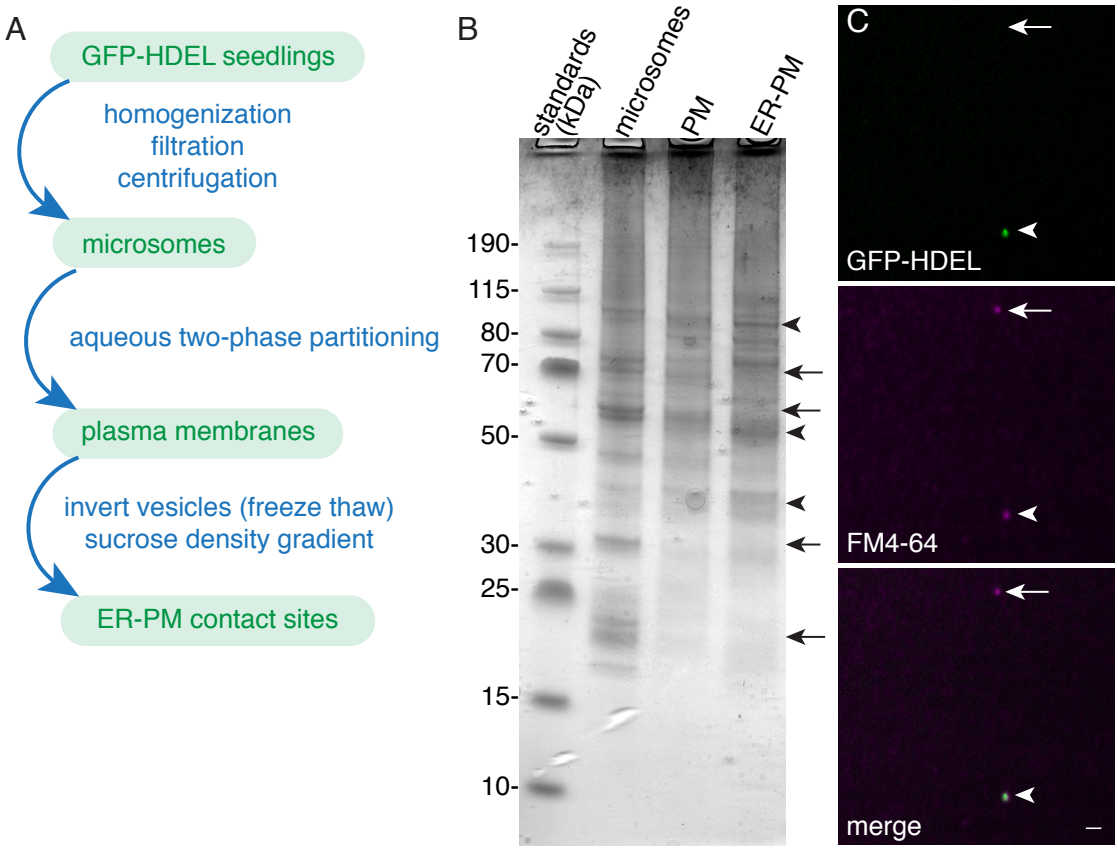

Figure 4.6: Two-phase partitioning coupled to sucrose gradients can enrich a fraction for ER-PM contact sites. A combination of aqueous two-phase partitioning and sucrose gradient centrifugation (A) is sufficient to enrich ER-PM contact sites from pea seedlings, as shown by their differential bulk protein composition in SDS-PAGE, compared to microsomes and PMs (B). Arrows denote proteins depleted in ER-PM contact site fractions while arrowheads denote proteins enriched in contact sites. ER-PM contact sites can also be isolated from GFP-HDEL expressing seedlings by this method, as demonstrated by confocal microscopy of the ER-PM contact site fraction (C). Arrows point to membrane vesicles that are PM (i.e. that stain with FM4-64) but are GFP-HDEL negative, while arrowheads point to ER-PM contact sites, which are positive for both FM4-64 and GFP-HDEL. Scale bars represent 10 µm.

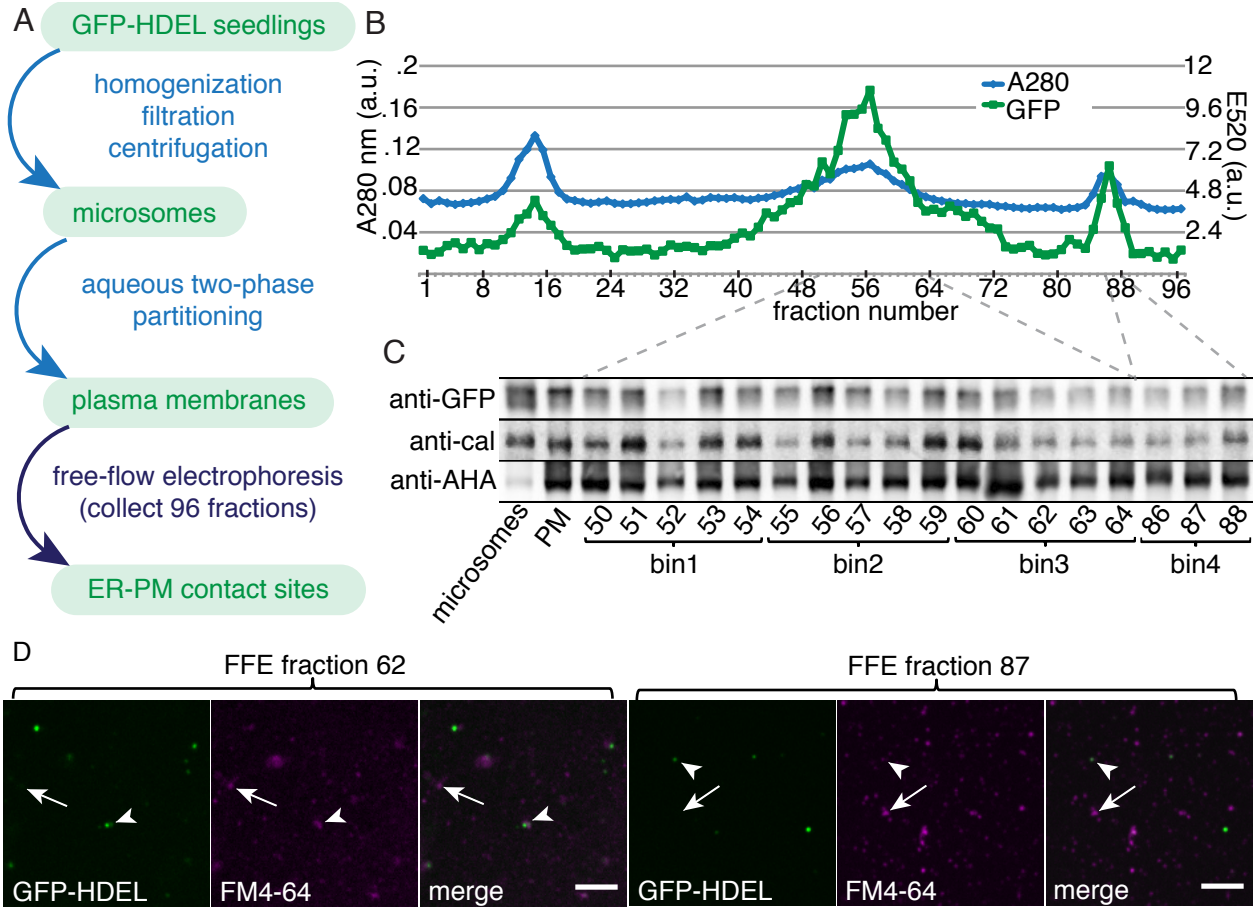

Figure 4.7: Two-phase partitioning coupled to free-flow electrophoresis cannot enrich a fraction for ER-PM contact sites. A combination of aqueous two-phase partitioning and free flow electrophoresis (FFE) (A) is insufficient to enrich ER-PM contact sites from GFP-HDEL expressing seedlings, as shown by the even distribution of GFP-HDEL across the fractions in fluorescence, relative to total protein content (B). Western blotting with anti-GFP, anti-calreticulin (an ER marker), and anti-AHA (a PM marker) confirm that GFP-HDEL (and therefore ER) is distributed throughout the fractions. Confocal microscopy of two fractions confirms that ER-PM contact sites exist across the FFE fractions (D). Arrows point to membrane vesicles that are PM (i.e. that stain with FM4-64) but are GFP-HDEL negative, while arrowheads point to ER-PM contact sites, which are positive for both FM4-64 and GFP-HDEL. Scale bars represent 10 µm.

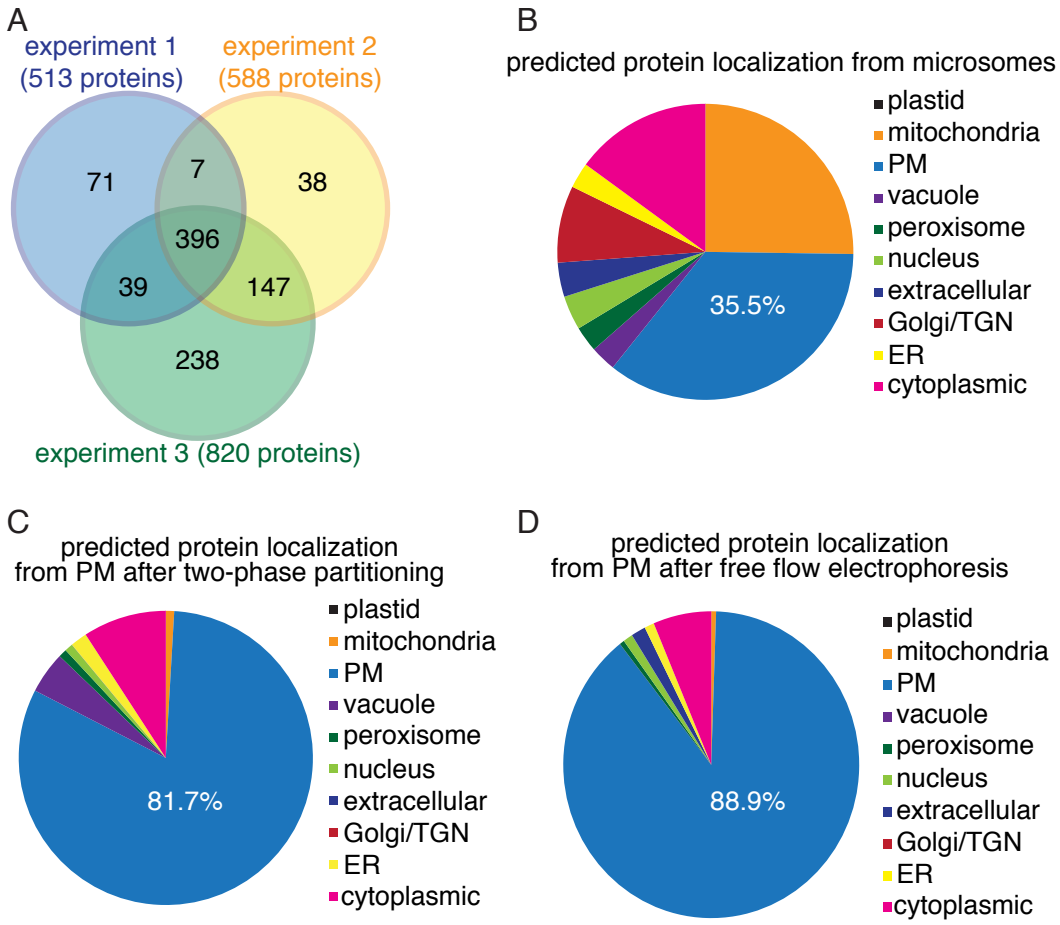

Figure 4.8: Two-phase partitioning coupled to free-flow electrophoresis yields high quality PM fractions. A Venn diagram of total proteins identified above cutoff (> 4 spectral counts within each experiment) shows moderate overlap between all three experiments, and especially between experiments 2 and 3 (A). Predicted subcellular localizations of these proteins from SUBA (Heazlewood et al., 2007) demonstrate the increasing enrichment of PM proteins in microsomes (B), post-two phase partitioning (C), and post-FFE fractions (D).

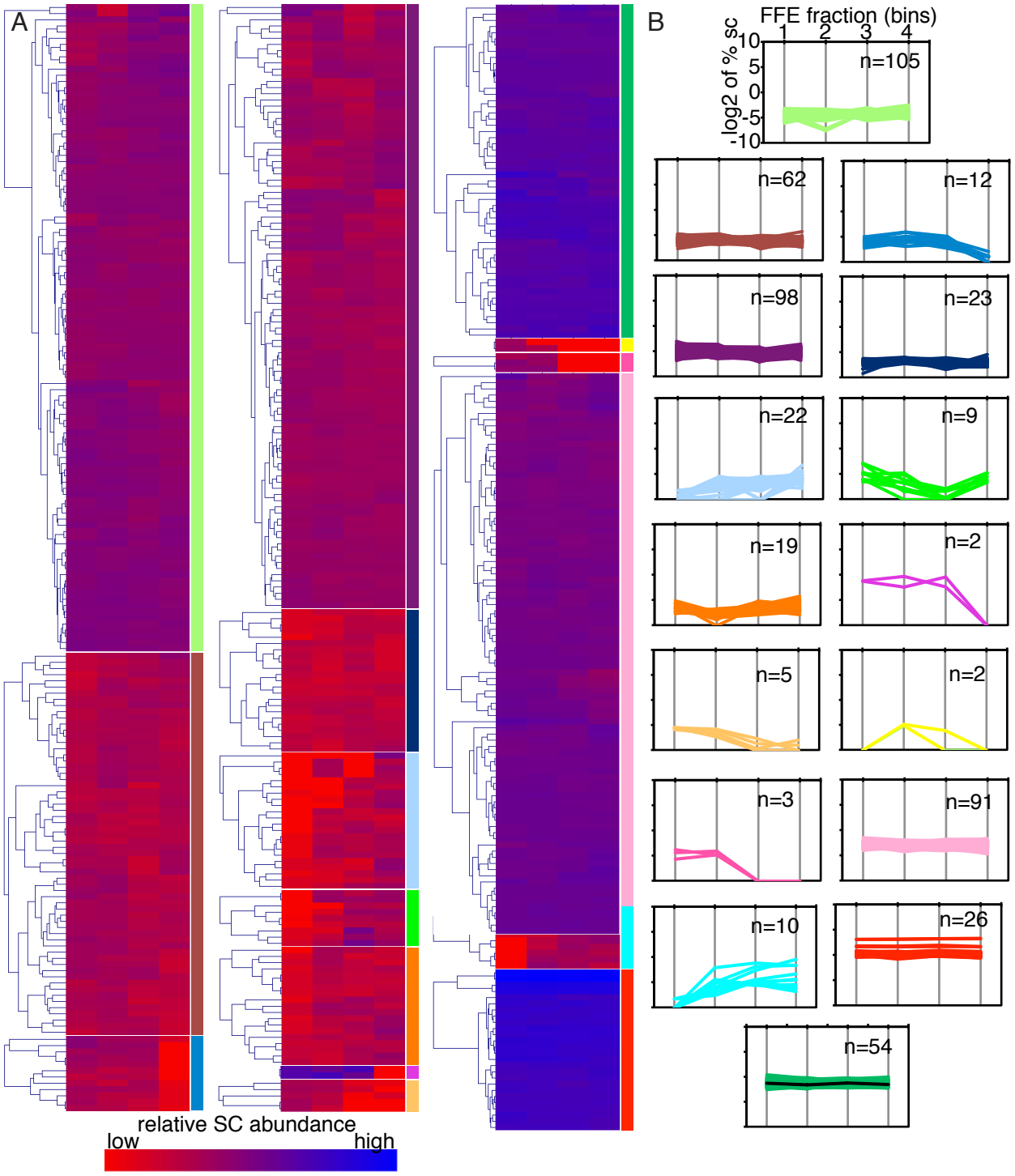

Figure 4.9: ER-PM contact site candidate proteins do not cluster together across FFE fractions. Heat maps (A) and graphs (B) of MEV clustered, $\log_2$ transformed average percent spectral counts (SC) for all proteins above the cutoff values from experiment 2 and 3 display different profiles across the four bins. GFP is indicated in the lowest graph in (B) as a black line and shows no differential distributions across the bins. The colour legend below the heat map corresponds to the colour used in the graph.

Table 4.1: ER-PM contact site candidate proteins detected in PM proteomics experiments. The number of spectral counts is displayed as the number observed in experiment 1/experiment 2/experiment 3.

AGI number	TAIR Annotation	*S. cerevisiae* Homologue	Number of SC	References
AT2G20990.1	Synaptotagmin A (SYTA)	Tcb1, Tcb2, Tcb3	62/335/471	Schapire et al., 2008 Yamazaki et al., 2008; Lewis and Lazarowitz, 2010
AT1G05500.1	Synaptotagmin E (SYTE)	Tcb1, Tcb2, Tcb3	2/33/36	
AT5G07300.1	Bonzai 2 (BON2)	Tcb1, Tcb2, Tcb3	6/33/51	Yang et al., 2006
AT2G45140.1	Plant VAP homolog 12 (PVA12)	Scs2, Scs22	18/56/103	Saravanan et al. 2009
AT3G60600.1	Vesicle associated protein (VAP27-1)	Scs2, Scs22	0/8/28	

Chapter 5: Conclusion

5.1: Major findings of this work

The broad goal of this research was to determine the pathway of cuticular lipid export in plant cells, using the stem epidermal cells of *Arabidopsis thaliana* as a model system for lipid export (Figure 5.1). In Chapter 1, several key questions were posed about cuticular lipid export, based upon a review of current literature. First: how do the ATP-binding cassette transporters, ABCG11 and ABCG12, interact in the context of cuticular lipid export? Secondly: how are lipids trafficked from their site of synthesis in the endoplasmic reticulum (ER) to the plasma membrane (PM) for export by ABC transporters? Previous work had implied that cuticular lipids may travel to the cell surface by vesicle trafficking, or by trafficking that is independent of vesicle formation and fusion, i.e. non-vesicular trafficking. Below, each of these key questions will be revisited with regards to the findings presented in Chapters 2 to 4.

5.1.1: ABCG transporters can form different dimers, which are required for export of different substrates

In Chapter 2, the physical interactions between ABCG11 and ABCG12 were investigated to determine possible pairings that could lead to different functional transporter complexes. Previous studies had implicated these ABC transporters in wax export (ABCG12; Pighin et al., 2004) and both wax and cutin export (ABCG11; Bird et al., 2007). However, double *abcg11 abcg12* mutants had the same wax defects as each single mutant, indicating that the two transporters likely acted in the same complex or pathway in wax export (Bird et al., 2007). Since these ABCGs are half transporters, they must dimerize in order to function (Higgins, 2001). Therefore, it was predicted that ABCG11 might dimerize with ABCG12 to function in wax export, while ABCG11 might dimerize with some other ABCG in cutin precursor export (Bird et al., 2007; Bird, 2008).

Using bimolecular fluorescence complementation (BiFC), I demonstrated a physical interaction between ABCG11 and ABCG12. I also showed that ABCG11 is capable of forming a homodimer, while ABCG12 is not. Furthermore, in the context of the stem epidermal cell, I employed complementary light and immunoelectron microscopy

approaches to demonstrate that, similar to mammalian ABCG transporters (Graf et al., 2002; Graf et al., 2003), dimerization of ABCGs in the ER was a prerequisite for trafficking of these transporters to the PM in stem epidermal cells. That is, in *abcg11* mutants, GFP-ABCG12 was retained in the ER, indicating that it could not dimerize with any other ABCG that is expressed in stem epidermal cells (e.g. ABCG1, ABCG18, or ABCG19; Suh et al., 2005). In *abcg12* mutants, YFP-ABCG11 was still localized to the PM because ABCG11 can homodimerize, and it may be able to pair with other ABCGs that are expressed in stem epidermal cells. Thus, ABCG12 forms an obligate heterodimer with ABCG11 that is required for wax export, while ABCG11 can form promiscuous dimers and plays multiple roles in cuticular lipid export.

In addition to these studies on the dimerization and localization of ABCG transporters, I also showed that waxes that are synthesized, but not exported, in *abcg11* and *abcg12* mutants accumulated in the ER, but not in the Golgi apparatus. These results implied that cuticular lipids might be trafficked to the PM independent of the Golgi apparatus, for example, via non-vesicular trafficking, directly from the ER to the PM. However, ER expansion is also a general stress response.

These results have important implications for studies on all ABCG transporters in prokaryotes and eukaryotes. Although the influence of dimerization on substrate specificity had been previously predicted in several systems, physical interactions between ABCGs had not successfully been demonstrated *in vivo* in the context of the export system. Accordingly, these results were published in McFarlane et al. (2010) and have been widely cited by groups working on a variety of plant, animal, and bacterial ABC transporters (e.g. Bessire et al., 2011; Chen et al., 2011a; Haider et al., 2011; Boncoeur et al., 2012).

5.1.2 Cuticular lipids are secreted to the plasma membrane in part by vesicular trafficking via the Golgi apparatus

A review of the current literature leads to two hypotheses of cuticular lipid export: cuticular lipids might be secreted via Golgi-mediated vesicular secretion, or cuticular lipids might be transported to the PM directly from the ER via non-vesicular trafficking. Given the accumulation of lipids associated with the ER, but not with the Golgi apparatus in *abcg*

mutants (Chapter 2), I postulated that at least some cuticular lipid export might be mediated via non-vesicular trafficking.

To directly test whether vesicular trafficking is also required for wax export I exploited several previously characterized mutants in the Arabidopsis secretory pathway in Chapter 3. Cryo-scanning electron microscopy of stems and quantitative analysis of cuticular waxes by gas chromatography demonstrated that two secretory pathway mutants, *gnl1-1* and *ech,* were defective in wax accumulation on the plant surface. GNL1 is required for Golgi-ER trafficking (Richter et al., 2007; Teh and Moore, 2007), while ECH is required for secretion from the trans-Golgi network (TGN) (Gendre et al., 2011; Gendre et al., 2013). Interestingly, a second mutant that is defective in post-Golgi trafficking, *trs120-4* (Qi et al., 2011) was not defective in wax accumulation on the cell surface, implying that TRS and ECH play divergent roles at the TGN. However, further analyses of these mutants via confocal microscopy and transmission electron microscopy demonstrated that *gnl1-1* and *ech* mutations cause alterations to ER morphology, which likely resulted in defects in wax synthesis. Using *rhd3-1* mutants, which also have abnormal ER morphology, but are not impaired in secretion (Chen et al., 2011c), I was able to show that defects in ER morphology are correlated with defects in wax synthesis, implying a structure and function relationship between the ER and its biosynthetic capacity. Finally, by examining the proportion of waxes that were successfully secreted in *gnl1-1* and *ech*, relative to the total amount that these mutants were able to synthesize, I was able to demonstrate that the loss of normal vesicle traffic in these mutants was correlated with defective wax secretion. Thus, these results imply that at least some cuticular lipids are secreted to the cell surface via vesicular trafficking.

These findings will contribute to our understanding of lipid biosynthesis in plants, including cuticular lipids and commercially important essential oils. The strong decrease in wax production in mutants with altered ER structure suggests metabolic enzymes have some strict, and presently unknown, requirements for particular ER morphologies. This may have implications for other ER-derived plant products, including seed storage oil (Dyer and Mullen, 2008), essential oils (Mahmoud and Croteau, 2002), and cell wall monolignols (Schuetz et al., 2012). Finally, these results represent a cautionary tale for studying mutants of the endomembrane system; often, mutants in the secretory system

display pleiotrophic defects throughout the secretory pathway, and it can be challenging to deduce the primary biological function of a gene product from a number of interrelated mutant phenotypes.

5.1.3: ER-PM contact sites may play a role in lipid recycling or lipid remodeling during plant development

ER-PM contact sites have been observed in a variety of eukaryotic cells. In animals, they play an important role in Ca^{2+} signaling during excitation-contraction coupling (Carrasco and Meyer, 2011; Asghari et al., 2012), while in yeast, they are involved in non-vesicular lipid trafficking and lipid remodeling (Li and Prinz, 2004; Raychaudhuri et al., 2006; Stefan et al., 2011; Manford et al., 2012). Despite their potential importance in similar processes in plant cells, the frequency, morphology, regulation, protein composition, and function of ER-PM contact sites in plants had not been investigated. In Chapter 4, I undertook a comprehensive characterization of ER-PM contact sites in Arabidopsis using a combination of light and electron microscopy, electron tomography, biochemical isolation, and proteomic analysis.

By tracking the morphology of the ER, using both the fluorescently-tagged ER reporter, GFP-HDEL (Batoko et al., 2000), and transmission electron microscopy, I was able to characterize the nature of the cortical ER and of ER-PM contact sites at multiple developmental stages in a variety of cell types. I demonstrated that the cortical ER is significantly denser in young, rapidly elongating cell types than in mature cells that are no longer undergoing rapid elongation. Similarly, in young elongating cells, ER-PM contact sites occupied nearly 10% of the PM, while they occupied less than half as much of the PM in mature cells. This developmental correlation between ER-PM contact sites and the rate of cell elongation suggests that ER-PM contact sites are regulated throughout development and that they may play a larger role in young, rapidly elongating cells than in mature cells.

To test the hypothesis that ER-PM contact sites are involved in non-vesicular lipid export, I compared the density of the cortical ER and the frequency of ER-PM contact sites in rapidly elongating cells that were secreting different amounts of cuticular lipids. The density of the cortical ER was not significantly different between root epidermal cells, which secrete low amounts of lipid; hypocotyl epidermal cells, which secrete moderate

levels of cuticular lipids; stem epidermal cells, which secrete high levels of cuticular lipids; and WIN1-overexpressing stem epidermal cells, which secrete higher than wild-type levels of cuticular lipids (Broun et al., 2004; Kannangara et al., 2007). Similarly, when assayed with TEM, there is no change in the frequency of ER-PM contact sites in WIN1-overexpressing stem epidermal cells, relative to wild type. Together, these data demonstrate no correlation between cuticular lipid secretion and ER-PM contact sites, implying that ER-PM contact sites may not be involved in lipid secretion in plants.

In order to further investigate the role of ER-PM contact sites in plants, I attempted to biochemically isolate these membrane fractions for proteomic analysis. While I was able to isolate ER-PM contact sites from pea seedlings according to a previously published protocol (Larsson et al., 2007), this procedure yielded insufficient amounts from Arabidopsis for proteomic analysis. Using a new approach, I coupled components of the previous isolation protocol with free-flow electrophoresis (FFE). While there was no preferential distribution of ER-PM contact sites across the FFE fractions, this method yielded high-quality PM, which was subjected to proteomic analysis. Results from this experiment include several potential ER-PM contact site candidates for further investigation.

5.2: Outstanding questions and future directions

Taken together, the results described above beg a number of further questions, many of which can be addressed by a series of future experiments, outlined below.

5.2.1: What other dimerization partners might ABCG11 have, and what other roles might these dimers play in Arabidopsis?

One of the outstanding questions from work on ABCG11 is what other roles this ABC transporter might play in plants (Bird et al., 2007). Genetic evidence implies that ABCG11 may function in other processes besides cuticular lipid export: severe *abcg11* mutants display defects in cuticular lipids but they are also dwarf and sterile (Bird et al., 2007), and both microarray data (Toufighi et al., 2005) and promoter:reporter fusions (Bird et al., 2007) indicate that ABCG11 is expressed in emerging roots, particularly in lateral roots, and in flowers, especially in young anthers within the flower. Furthermore,

the capacity of ABCG11 to form flexible dimer combinations implies that it could form different dimers to play multiple roles.

abcg11 mutants have reduced fertility (Bird et al., 2007). This fertility defect is common to several cuticular lipid mutants and can be partially rescued by growing plants at high humidity (Preuss et al., 1993; Sieber et al., 2000; D. Bird, unpublished). Scanning electron microscopy has revealed that *abcg11* pollen grains may be defective in either the pollen wall, made of sporopollenin, or the pollen coat, made of very long chain lipids (T. Quilichini and H. McFarlane, unpublished). Given the similarities between sporopollenin plus the pollen coat, and the cuticle plus the epicuticular waxes (Li et al., 2010; Beisson et al., 2012), it is possible that ABCG11 may be involved in export of sporopollenin precursors or pollen coat lipids. Consistent with this hypothesis, another ABCG half transporter, ABCG26, has been implicated in sporopollenin transport from the tapetum to the developing pollen wall (Quilichini et al., 2010) and is a strong candidate for interaction with ABCG11 (T. Quilichini, unpublished).

The expression of ABCG11 in the root expansion zone and emerging lateral roots is also consistent with ABCG11 playing another role in Arabidopsis besides cuticular lipid export. The Casparian strip forms an impermeable barrier in roots and is an important part of solute uptake regulation (Alassimone et al., 2012). The Casparian strip is first made of a matrix of lignin-containing polymers, and then enhanced with suberin, which, like wax, is composed of very long-fatty acid derivatives (Beisson et al., 2012; Naseer et al., 2012). Given its expression in suberizing tissues in roots, and in emerging lateral roots, which must remodel the Casparian strip during development (Alassimone et al., 2012), ABCG11 might function in either lignin or suberin export in roots for Casparian strip formation. Recently, ABCG29, a full-length ABCG transporter that does not need to dimerize to function, has been characterized as a monolignol transporter (Alejandro et al., 2012). Although no ABCG half-transporters have been implicated in monolignol transport, the expression pattern of *ABCG11* is consistent with this possibility. Alternatively, ABCG11 might be involved in suberin export following Casparian strip development in roots.

Finally, although ABCG11 can homodimerize *in planta*, it is possible that it may interact with other ABCG half transporters in cutin export. Indeed, ABCG13, which is also a half transporter, has been implicated in cutin export, but its expression is primarily

restricted to petals (Panikashvili et al., 2011). Three other ABCG half-transporter genes, *ABCG1*, *ABCG18*, and *ABCG19* are also expressed in the stem epidermis during cuticle development (Suh et al., 2005). While these represent possible dimerization partners with ABCG11, it is likely that some of these ABCGs act independently of ABCG11, since in the absence of ABCG11, there remains some cutin and some wax on the cell surface (Bird et al., 2007). Consistent with this, the full-length ABCG32 has been implicated in export of hydroxyl-fatty acids early in cutin development (Bessire et al., 2011).

In all cases described above, there seems to be a close relationship between ABCG11 and various protective coatings that plant cells secrete. There is symmetry between these coatings as well: the cuticle, the pollen wall and coat, and the Casparian strip, are all composed of a tough polymer network with a lipid component (Beisson et al., 2012; Alassimone et al., 2012). It may be that ABCG11 plays a general role in export of all of these protective products, and that the tissue-specific expression of its partners (e.g. ABCG12; Pighin et al., 2004) and hypothesized partners (e.g. ABCG26; Quilichini et al., 2010) define its substrate specificity in these tissues. Further experiments to directly test this hypothesis include a more detailed examination of *abcg11* mutant phenotypes in roots and flowers and systematic analysis of all ABCG dimer combinations in Arabidopsis using pairwise BiFC experiments *in vivo*, followed by single and double mutant analyses of ABCG11 interactors.

5.2.2: How do cuticular lipids accumulate only on the outer epidermal surface?

Previous studies on ABCG11 reported that it is polarly localized in stem epidermal cells (Panikashvili et al., 2007). While this localization is consistent with the polar accumulation of waxes on the apical surface of stem epidermal cells, these studies were conducted on dissected stem segments, which can cause disruption of the cell and result in misinterpretation of the fluorescent signal. Localization of 35S promoter-driven YFP-ABCG11 and native promoter-driven GFP-ABCG12, both of which can complement their respective mutants (Pighin et al, 2004; Bird et al., 2007), by confocal microscopy and by immuno-transmission electron microscopy, has demonstrated that these transporters are localized evenly throughout the plasma membrane (Chapter 2; McFarlane et al., 2010). This begs the question: how do cuticular lipids accumulate only on the outer epidermal

surface of the cell? Given that these ABCGs are evenly distributed throughout the entire PM, two possible mechanisms exist for polar wax accumulation on the cell surface. Either the intracellular transport of wax to the ABCG transporters is polarized, or the extracellular transport of wax from the ABCG transporter through the cell wall is polarized.

Neither of extracellular glycosylphosphatidly inositol (GPI) anchored lipid transfer proteins (LTPs) that are required for wax export are polarly localized at the plasma membrane (DeBono et al., 2009; Kim et al., 2012). However, it is possible that this anchor may be cleaved by phospholipases in a polar fashion (DeBono et al., 2009), or that they may transfer waxes to other soluble lipid transfer proteins in the cell wall, that may be polarly distributed. The interactions between ABCGs and LTPs are also an interesting avenue for future investigation. Non-vesicular trafficking of sterols from the PM to the ER in yeast requires both ABC transporters and intracellular LTPs, though the mechanism by which these proteins function together remains unclear (Li and Prinz, 2004; Raychaudhuri et al., 2006). By analogy to ABCA1-mediated transport of cholesterols to apolipoprotein acceptors in high-density lipoprotein formation in humans (Coleman et al., 2012), it is possible that the plant extracellular LTPs could dock to an ABCG dimer and accept the cargo into the hydrophobic pocket, thus shielding the highly hydrophobic wax from the aqueous environment of the cell wall.

Alternatively, wax secretion may be polarized to the apical surface of the cell via polar transport of waxes to the cell surface. Unfortunately, the mechanisms of polar secretion in Arabidopsis remain unclear, and results from Chapter 3 imply that some, but not all components of post-Golgi trafficking are required for wax export to the cell surface. Furthermore, because lipids do not contain canonical localization motifs, such as those found within proteins, it is unclear how they might be accurately partitioned into vesicles for polar secretion. This is further complicated by the fact that waxes are predicted to partition into the hydrophobic center of bilayers, making them inaccessible to classical vesicle cargo binding and sorting proteins (Coll et al., 2007; see 5.2.6 below). Based on this hydrophobicity, it is possible that waxes may partition into lipid microdomains, which contain higher levels of sphingolipids and sterols and begin to form in the Golgi apparatus (Fischer et al., 2004). In plant mutants defective in very long chain sphingolipid synthesis, polar secretion of auxin efflux carriers to the PM is disrupted, implying a role for

sphingolipids, and possibly lipid microdomains, in polar secretion (Markham et al., 2011). If waxes are also secreted to the PM via non-vesicular trafficking at ER-PM contact sites, then there might be a polar distribution of these sites within stem epidermal cells. However, quantification of ER-PM contact sites at the apical surface of the stem epidermal plasma membrane, relative to the basolaterial domains, revealed no significant difference between the density of ER-PM contact sites between these regions of the PM (H. McFarlane, unpublished). Assuming that, as in yeast (Stefan et al., 2011; Manford et al., 2012), the density of ER-PM contact sites is correlated with their function, these data imply that ER-PM polarization of cuticular lipids is not achieved at the level of ER-PM contact site polarization.

Interestingly, another ABCG that is required for cutin export, ABCG32 is polarly localized to the outer face of stem epidermal cells (Bessire et al., 2011). This implies that at least some cuticular lipid export is polarized by the restricted localization of ABCG transporters, rather than at the intracellular or extracellular level. Further investigation of these questions will involve genetic characterization of the other LTPs and ABC transporters that are required for cuticular lipid export and testing whether they may interact with the ABCGs that are also required for cuticular lipid export.

5.2.3: What is the relationship between ER morphology, ER stress, and ER biosynthetic capacity?

From Chapter 2 and Chapter 3, confounding data concerning the relationship between ER morphology, ER stress, and the biosynthetic capacity of the ER have arisen. In Chapter 2, cuticular waxes that were synthesized but not secreted, accumulated in the ER of *abcg11* and *abcg12* mutants. These lipid accumulations resulted in large ER aggregations within an otherwise normal ER network (McFarlane et al., 2010). In contrast, in Chapter 3 it was demonstrated that three mutants with defects in ER morphology, *rhd3-1*, *gnl1-1*, and *ech*, were all defective in wax biosynthesis and did not accumulate waxes in the ER. Investigating the relationship between the morphology of the ER, ER stress, and the biosynthetic capacity of the ER has become a topic of interest for a number of research groups, although the exact nature of these relationships remains elusive. However, the three most likely causes for these differences are: 1) a difference in the ER stress response

activation, 2) alterations to ER association with other organelles, or 3) defects in metabolic cluster organization within the ER.

The best studied form of ER stress is the unfolded protein response (UPR). The UPR is induced when unfolded, misfolded, or misglycosylated proteins accumulate in the ER in response to stress (e.g. heat or oxidative stress) (Martinez and Chrispeels, 2003; Kamauchi et al., 2005). Activation of a signaling cascade results in increased expression of chaperones to aid in refolding of these proteins, and increased expression of the ubiquitination and protein degradation pathways to degrade unfolded proteins (Martinez and Chrispeels, 2003; Kamauchi et al., 2005). However, recent studies of ER stress in yeast have revealed important relationships between ER stress and ER morphology. In some cases, it seems that the ER can expand to accommodate cargo, independent of the UPR, presumably to sequester cargo from the rest of the endomembrane system (Schuck et al., 2009). In other cases, lipid stress (i.e. disruption of lipid ratios and/or gradients within the cell) can induce the UPR, presumably to remodel the protein composition of membranes in response to this change in lipid composition (Thibault et al., 2012). Similarly, in Arabidopsis, defects in glutathione synthesis lead to an accumulation of glutathione precursors in ER membranes and in dilations of the ER (Au et al. 2012). In another study, defects in polysaccharide secretion resulted in cargo accumulation in ER dilations (McFarlane et al., 2013). In the case of wax accumulation in the ER of *abcg11* and *abcg12* mutants, the UPR is not induced and ER membranes appear to expand to accommodate the excess lipid cargo while maintaining an otherwise normal ER network (Chapter 2; McFarlane et al., 2010). In contrast, the *cer9* mutant, which was originally isolated based on its *eceriferum* phenotype, is defective in an E3 ubiquitin ligase that is homologous to a yeast protein involved in targeting ER associated degradation of proteins (Lü et al., 2012). Although CER9 potentially links the unfolded protein response to wax production, the E3 ubiquitin ligase activity of CER9 has not been tested, nor have its protein targets been identified (Lü et al., 2012). Whether the UPR is induced in response to the ER morphology changes in *rhd3-1*, *gnl1-1*, and *ech* has not yet been determined (Chapter 3), though this would be relatively easy to test using quantitative or semi-quantitative reverse transcriptase PCR for genes induced by the UPR (Martinez and Chrispeels, 2003; Kamauchi et al., 2005; McFarlane et al., 2010). It is possible that differences in UPR induction might

explain the differences in wax synthesis between the ER morphology mutants in Chapter 3, which synthesize significantly less wax than wild type, and the *abcg* transporter mutants in Chapter 2, which also display ER aggregations but synthesize wild-type levels of wax.

Alternatively, it is also possible that these differences in wax synthesis between the ER morphology mutants and the *abcg* mutants are due to differences in precursor trafficking to the ER. In plants, the ER often comes in close contact (15 nm or less) with the plastid at an ER-plastid contact site (Andersson et al., 2007). Since most fatty acids are produced by the plastid, these ER-plastid contact sites may represent sites of lipid exchange between the two organelles, especially since there is no evidence of vesicular trafficking between the ER and the plastid (Benning et al., 2006). At least some of the galactolipids that compose plastid photosynthetic membranes are synthesized by a pathway that requires lipid trafficking between the plastid and the ER (Ohlrogge and Browse, 1995; Benning et al., 2006; Xu et al., 2008; Wang et al., 2012; Kim et al., 2013). Extensions of the plastid outer membrane, called stromules, come in close contact with the ER, possibly to increase the surface area available for lipid exchange between these organelles (Schattat et al., 2011). Under phosphate-limited conditions, there is evidence that lipids are transported from the PM to the plastid, remodeled via this same ER-plastid dependent pathway, and replaced at the PM (Andersson et al., 2005; Tjellström et al., 2010). In cells undergoing wax secretion, fatty acids synthesized in the plastid must be transported to the ER for elongation into very long chain fatty acids and modification into wax components via ER-localized enzymes (Samuels et al., 2008). Indeed, cells overexpressing the WIN1 transcription factor, which results in increased wax production (Broun et al., 2004; Kannangara et al., 2007), have an increase in ER-plastid association visible by light microscopy (H. McFarlane, unpublished). Thus, if trafficking of fatty acid wax precursors occurs at ER-plastid contact sites, then disruption of ER morphology may lead to a decrease in ER-plastid contact sites and decreased wax synthesis. While light microscopy lacks the resolution to accurately quantify contact sites (Chapter 4), transmission electron microscopy of *abcg11*, *abcg12*, *rhd3-1*, *gnl1-1*, and *ech* stem epidermal cells could determine whether defects in ER-plastid contact sites might underlie the wax synthesis defects in *rhd3-1*, *gnl1-1*, and *ech* mutants, but not *abcg11* or *abcg12* mutants.

Thirdly, it is possible that defects in ER morphology lead to disruption of the fine-scale organization of enzymes within the ER membranes. During oil body formation, it is hypothesized that enzymes required for oil synthesis may localize to specific subdomains of the ER to concentrate oil synthesis at the forming oil body (Dyer and Mullen, 2008). Furthermore, to avoid loss of oil intermediates, the biosynthetic enzymes have been proposed to form a metabolic cluster, within which precursors may pass directly from one enzyme to another (Dyer and Mullen, 2008). Consistent with this hypothesis, a heterologously expressed diacylglycerol acyltransferase (DGAT) localizes to specific subdomains of the ER, where it colocalizes with two glycerol-3-phosphate acyltransferases (GPATs) (Gidda et al., 2011). A similar model of enzyme clustering for metabolic channeling has been proposed in the context of lignin biosynthesis (Chen et al., 2011b; Bassard et al., 2012a; Bassard et al., 2012b), soluble cell wall polysaccharide synthesis (Atmodjo et al., 2011; Oikawa et al., 2013), and wax synthesis. In yeast, a component of the elongase complex is localized to a specific subdomain of the ER, the nuclear-vacuolar junction (NVJ) (Pan et al., 2000; Elbaz and Schuldiner, 2011). When the analogous component of the Arabidopsis elongase complex, CER10, is expressed in yeast, it is also localized to the NVJ (Zheng et al., 2005). However, in Arabidopsis, CER10 and other components of the elongase complex are evenly distributed throughout the ER at the resolution of light microscopy (Zheng et al., 2005). While there is no obvious heterogeneity to wax synthesis enzyme distribution apparent at the light microscopy level, it remains possible that they are organized into metabolic clusters. Consistent with this hypothesis, several components of the elongase complex and two components required for alkane formation, CER1 and CER3, can physically interact *in planta* (Bach et al., 2008; Roudier et al., 2010; Bernard et al., 2012), and all components of the elongase complex can interact with the immunophilin-like protein, PAS1, which may act as a scaffold for this multienzyme complex (Roudier et al., 2010). Furthermore, CER2, which does not have a transmembrane-spanning domain, is partially localized to ER membranes, implying that it must interact with a protein that is anchored in the ER membrane, possibly a component of the elongase complex (Haslam et al., 2012). Together, these data suggest that wax synthesis occurs at metabolic clusters that are organized within ER membranes, and that defects in ER morphology may lead to defects in wax synthesis as a result of

disorganization of these complexes. Interestingly, *rhd3* mutants, which are defective in ER morphology and wax biosynthesis (Chapter 3) also have secondary cell wall phenotypes (Hu et al., 2003), possibly as a result of decreased monolignol synthesis at the ER. Preliminary results revealed no mislocalization of CER2 in *gnl1-1* or *ech* mutants at the light microscopy level (Chapter 3), implying that interactions between CER2 and other ER-localized components of wax synthesis are not altered and suggesting that fine-scale organization of wax synthesis enzymes in the ER is not affected in these mutants. A more sensitive system, such as the BiFC system employed to demonstrate PAS2-CER10 (Bach et al., 2008) and CER1-CER3 (Bernard et al., 2012) interactions, or investigation of CER2 localization using high resolution immuno-TEM, is required to determine whether metabolic clusters exist in wild-type plants during wax synthesis. Then, this system could also be employed to determine whether metabolic clusters are disorganized in *rhd3-1*, *gnl1-1*, and *ech* mutants.

5.2.4: Why are two TGN-localized complexes differentially required for wax secretion?

Initially, it was surprising that two different mutants in TGN-localized complexes required for protein secretion, *trs120-4* and *echidna*, displayed different wax phenotypes (Chapter 3). While *ech* mutants show roughly an 80% reduction in wax relative to wild type, *trs120-4* mutants have wild-type wax levels. There are several hypotheses that may explain these differences. First, these two mutants are of different severities, which could explain the differences in the wax phenotypes. Secondly, the pleiotrophic defects in *ech* may be contributing to the wax phenotype of these plants. Thirdly, and potentially most interestingly, these results may imply a divergence of functions at the TGN.

While *ech* mutants display very severe phenotypes, including dwarfism, partial sterility, and bushiness (Gendre et al., 2011), *trs120-4* mutants are only slightly stunted (Qi et al., 2011). It is possible that the different wax phenotypes of these mutants are simply the result of the different severities of these mutations; while *ech* is a knockout mutant, *trs120-4* is a knockdown. The simplest way to test this hypothesis would be to assay the wax load of weaker *ech* alleles and/or stronger *trs120* alleles to determine whether the strength of the allele (i.e. of the whole plant phenotype) is correlated with the wax

phenotype. Unfortunately, there are no other characterized alleles of *ech* available (Gendre et al., 2011), and the other alleles of *trs120* mutants, including transcriptional knockouts and dominant negative mutants, are all seedling lethal and do not grow enough for cuticular waxes to be assayed (Qi et al., 2011). It may be possible to cross a heterozygous plant for the knockout of *trs120* to a *trs120-4* homozygous mutant to create a hemizygous mutant in the F1 generation, which might be of intermediate severity. Recently, two ECH interacting proteins, YPT/RAB interacting protein 1 (YIP1) and YIP2 have been characterized and *yip1 yip2* mutants display many of the same phenotypes as *ech* mutants, though they are significantly less severe (Gendre et al., 2013). Thus, the *yip1 yip2* double mutants seem to behave in a fashion that would be predicted for weak alleles of *ech.* Preliminary analysis of surface waxes on *yip1 yip2* double mutants has shown that these mutants have very similar wax profiles to *ech* mutants (Y. Watanabe and H. McFarlane, unpublished), implying that any disruption in the ECH/YIP complex leads to an 80% decrease in surface wax and the difference in wax defects is not due to a difference in the severity of the whole plant phenotype.

The differences between *trs120-4* and *ech* mutants could also be due to a difference in the cell biological phenotypes of these mutants. *ech* mutants display many endomembrane defects, including mislocalization of the vacuolar H^+ ATPase subunit, VHA-a1 (Gendre et al., 2011; Gendre et al., 2013). While some isoforms of this proton pump are localized to the vacuole, the VHA-a1 containing isoform is actually localized to the TGN/early endosome, where it plays a key role in acidifying the secretory and endocytic pathways (Dettmer et al., 2006; Brüx et al., 2008). In contrast to *ech,* VHA-a1 is correctly localized to the TGN/early endosome in *trs120* mutants (Qi et al., 2011). One of the main challenges of studying *ech* mutants is the difficulty in separating the primarily phenotypes, due to the loss of the ECH-YIP complex, from the secondary phenotypes, e.g. from the depletion of VHA-a1 at the TGN/early endosome. The simplest way to separate these phenotypes would be to examine the wax load of *vha-a1* mutants, but these are embryo-lethal (Brüx et al., 2008). However, the fact that another secretory pathway mutant, *gnl1-1*, has decreased wax secretion, but no reported defect in VHA-A1 localization (Richter et al., 2007; Teh and Moore, 2007) implies that the wax defect in *ech* is a primary phenotype due

to altered vesicle traffic, rather than a secondary phenotype due to the depletion of VHA-a1 at the TGN/early endosome.

Finally, it is most likely that the differences in the wax phenotypes of *ech* and *trs120-4* mutants are due to a divergence of functions at the TGN. The plant TGN is a highly complex organelle that can exist in association with or independent of a Golgi stack, and both the Golgi stack and the TGN are highly motile (Viotti et al., 2010). Depending on the secretory versus endocytic flux of a cell, the TGN may vary from a cluster of large, dense secretory vesicles to a small, thin network of tubules (Staehelin and Kang, 2008; Kang et al., 2011). In plants, the TGN acts as both a hub for secretion of Golgi products to the PM, cell wall, and vacuole, and as an early endosome for receiving and re-secreting recycled material from the PM (Viotti et al., 2010). Because of the complex and highly dynamic nature of the TGN, many regulatory and trafficking proteins must act in concert at this organelle. Recent work has demonstrated that the ECH/YIP1/YIP2 complex is required specifically for secretion from the TGN to the cell wall, but not for trafficking from the TGN to the vacuole or for endocytic trafficking (Gendre et al., 2013; McFarlane et al., 2013). In contrast, the phenotypes of *trs120* mutants imply that the TRAPP II complex plays an important role in trafficking from the TGN to the cell plate and a relatively smaller role in secretion to the PM/cell wall (Qi et al., 2011). Furthermore, while the TRAPP II complex is not required for endocytic trafficking, its role in TGN to vacuole trafficking has not been tested (Qi et al., 2011). Thus, the ECH complex and the TRAPP II complex seem to play different roles at the TGN, which is consistent with their different wax secretion phenotypes.

5.2.5: How are waxes sorted into vesicles?

Given that some wax is trafficked to the PM via vesicular trafficking through the Golgi apparatus (Chapter 3), this leads to questions about how waxes are sorted into vesicles and how these wax-containing vesicles are targeted. Unlike proteins, most lipids lack specific motifs for targeting. For example, the main wax component in Arabidopsis stems is a C29 alkane, and this wax compound, in particular, lacks any distinct sorting signal, as it is simply a linear 29-carbon long, fully saturated hydrocarbon. Furthermore, molecular modeling predicts that C29 alkanes will partition into the hydrophobic bilayer of

membranes, thereby masking them from typical cargo binding molecules (Coll et al., 2007). While midchain oxygenated compounds may more closely resemble membrane lipids by exposing the oxygen group to the cytoplasm and exposing the two C14 "tails" of each half of the alkyl chain to the hydrophobic region of the bilayer, they still lack sorting motifs (Coll et al., 2007). Genetically altering the composition of waxes that were synthesized in *ech* and *gnl1-1* mutants using *mah1* double mutant combinations did not alter the total amount of secreted waxes, suggesting that both alkanes and midchain oxygenated compounds are secreted via the same pathway (Chapter 3).

Based on the aggregations of ER membranes observed when waxes accumulate in the ER of *abcg11* or *abcg12* mutants (Chapter 2; McFarlane et al., 2010), it is predicted that wax molecules will tend to aggregate together to form an insoluble mass that could disrupt the secretory pathway, including the Golgi apparatus. Therefore, waxes must be carefully sorted and trafficked to the PM to avoid disruption of the endomembrane system. It is possible that specific lipid-binding proteins could accomplish these sorting and trafficking tasks by acting as cargo binding molecules during vesicle formation. Although transcriptomic analyses of wax-secreting cells have failed to unveil obvious candidates for this process (Suh et al., 2005), it may be that some of the transmembrane proteins of unknown function, which were identified in these microarrays, include a hydrophobic pocket domain that could bind lipids and serve this role.

5.2.6: How are cutin monomers trafficked to the plasma membrane?

Results in Chapter 3 indicate that at least some cuticular waxes are trafficked from their site of synthesis to the ABC transporters in the PM via vesicular trafficking. However, the question of cutin monomer trafficking was out of the scope of this thesis. This was partially because of the technical challenges in assaying cutin, which is relatively difficult to extract compared to waxes. Additionally, since cutin components polymerize into the cutin matrix in the cell wall, the nature of the cutin precursors that are synthesized and transported is generally unknown (Pollard et al., 2008). Studies in *Solanum lycopersicum* (tomato) have recently demonstrated that a glycine-aspartic acid-serine-leucine motif (GDSL) lipase/hydrolase, Cutin Deficient 1 (CD1), is required for cutin formation and that it can catalyze sequential additions of mono-acylglycerols to form a cutin-like polymer *in*

vitro (Yeats et al., 2012). These results imply that at least one of the precursors to cutin is mono-acylglycerol (Yeats et al., 2012), though the exact structure of this precursor in Arabidopsis remains unclear because of the significant differences between the chemical composition of the cuticles of Arabidopsis and tomato (Pollard et al., 2008; Yeats et al., 2012). Regardless, the last step of mono-acylglycerol cutin precursor synthesis is transfer of acyl chains to glycerol, which is catalyzed by ER-localized glycerol-3-phosphate acyltransferases, and these precursors must be transported to the cell wall localized-GDSL hydrolase for polymerization into the cutin network (Gidda et al., 2009; Yeats et al., 2012). Interestingly, the cell wall localization of the GDSL hydrolase could also explain how the cuticle is polarly formed on only the outer apical surface of Arabidopsis stem epidermal cells. If the GDSL hydrolase is polarly localized within the cell wall, cutin precursors will only be incorporated into the cuticle in this region. Additionally, assuming that cutin precursors can move freely within the apoplast, the GDSL hydrolase activity could act as a sink for apoplastic cutin precursors (Yeats et al., 2012). Unfortunately, these hypotheses cannot yet be tested, as the GDSL hydrolase(s) required for cutin polymerization in Arabidopsis have not yet been identified, and in the context of the tomato fruit epidermis in which CD1 was originally characterized, the cuticle is formed around the entire cell in an apolar fashion (Yeats et al., 2012). Nevertheless, equipped with this new knowledge of cutin precursor synthesis, the study of cutin precursor secretion is now far more accessible.

The structure of the mono-acylglycerol cutin precursors, especially those lacking midchain or omega hydroxylation, more closely resemble membrane lipids than any of the cuticular waxes, thus cutin precursors could be more easily transported via vesicle secretion. However, while testing whether the secretion mutants examined in Chapter 3 were defective in cutin accumulation on the cell surface was outside the scope of this work, several lines of evidence suggest that these mutants are not defective in cutin secretion. First, neither *gnl1-1* nor *ech* mutants, which are defective in wax secretion, display characteristic cutin-defective phenotypes, including organ fusions (Chapter 3; Sieber et al., 2000). Furthermore, neither of these mutants displays permeability to toluidine blue, a dye that can permeate plants with a compromised cuticle (H. McFarlane, unpublished; Tanaka et al., 2003). Together, these data suggest that cutin precursors are not secreted by the same pathway as cuticular waxes; either they may be secreted by vesicular trafficking

via a pathway that is independent of *trs120-4*, *gnl1-1*, and *ech*, or they may be transported via non-vesicular trafficking. However, it is important to note that organ fusions and permeability to toluidine blue are both qualitative phenotypes of severe cutin mutants. Therefore, the cutin levels of these secretion mutants must be quantitatively assessed before drawing any conclusions as to their involvement in cutin precursor trafficking.

5.2.7: Is some wax export mediated via non-vesicular trafficking?

Although the question of whether some waxes are exported via vesicular trafficking has been directly addressed in this thesis (Chapter 3), the question of whether some waxes may be exported via non-vesicular trafficking at membrane contact sites remains open, and conflicting evidence exists both for and against non-vesicular wax trafficking.

Studies of lipid trafficking between the PM and the ER of yeast initially lead to the hypothesis that cuticular lipids are exported via non-vesicular trafficking from their site of synthesis in the ER to the ABCG transporters at the PM. Circumstantial evidence supported this hypothesis. For example, there is a strong correlation between ER proliferation and wax synthesis during light-induced wax production in *Sorghum bicolor*, but there is no corresponding proliferation of the Golgi apparatus (Jenks et al., 1994). In contrast, Golgi proliferation is observed in cells undergoing intense polysaccharide synthesis and secretion (Young et al., 2008). Together, these morphological changes suggest that the ER plays a more important role in wax synthesis and secretion than the Golgi apparatus, though this may simply be a result of the increased biosynthetic demands placed on the ER during wax synthesis. Similarly, waxes accumulate in the ER, but not the Golgi apparatus of *abcg11* and *abcg12* mutants (Chapter 2; McFarlane et al., 2010), which synthesize wild-type levels of wax, but cannot secrete most of this wax (Pighin et al., 2004), suggesting that wax transport may not occur via the Golgi apparatus. Consistent with the notion that waxes might be transported via non-vesicular trafficking, long chain acyl CoA synthase (LACS) 1, 2, and 3, are required for wax synthesis (Lü et al., 2009) and have recently been shown to have both acyl-CoA synthase activity and lipid transfer activity in yeast (Pulsifer et al., 2012). Because it is unclear how LACS activity might be required for wax synthesis (Lü et al., 2009), it may be that these proteins act as lipid transfer proteins during non-

vesicular wax transport or that the CoA esterification that they mediate changes fatty acid solubility and serves to trap lipids in subcellular locations.

Although it was demonstrated in Chapter 3 that defects in the secretory pathway result in decreased wax secretion, these data do not eliminate the possibility of non-vesicular wax secretion. Indeed, these secretion mutants still accumulated some surface waxes. This could be because the secretion mutants examined here were either leaky alleles (*trs120-4*; Qi et al., 2011), or they were knockout mutants and another gene product may be partially redundant (*gnl1-1* and *ech*; Richter et al., 2007; Gendre et al., 2011), since a total elimination of secretion would be lethal. Alternatively, some of the wax that accumulates on the cell surface of secretion mutants may be the result of non-vesicular trafficking. These hypotheses are not mutually exclusive and the two mechanisms may act together in wax export. Previous experiments to determine the route of wax trafficking provided evidence that waxes are present in the Golgi apparatus (Bertho et al., 1991). However, these experiments also detected activity of several ER enzymes (including the fatty acid elongase complex) in the "Golgi" fraction, indicating that this fraction was significantly contaminated with ER membranes (Bertho et al., 1991). Due to recent advances in Golgi isolation techniques, it is now possible to isolate Golgi membrane fractions that are over 80% pure (Parsons et al., 2012). Preliminary experiments have confirmed that a GC-FID protocol to quantify surface waxes can also be applied to detect waxes in microsome membrane fractions (H. McFarlane, unpublished); it will be interesting to determine whether these Golgi fractions also contain waxes.

While the frequency of ER-PM contact sites was predicted to be correlated with their function (Stefan et al., 2011; Manford et al., 2012), quantification of both cortical ER using light microscopy, and of ER-PM contact sites using TEM revealed no significant differences in tissues undergoing low, moderate, high, or extremely high levels of cuticular lipid secretion (Chapter 4). Furthermore, *rhd3-1* mutants, which have GFP-HDEL defects similar to the sextuple yeast mutants that are defective in ER-PM contact sites (Chapter 3; Chen et al., 2011c; Manford et al., 2012), did not display any defect in wax trafficking to the cell surface (Chapter 3). However, examination of *rhd3-1* ER by TEM revealed no significant change to the density of ER-PM contact sites in these mutants relative to wild type (Chapter 4). Thus, while *rhd3-1* mutants appeared to be defective in cortical ER when

visualized by light microscopy, the small amount of cortical ER that remained was sufficient to form ER-PM contact sites with the same frequency as wild type. Therefore, the lack of a wax secretion phenotype in *rhd3-1* mutants cannot eliminate the possibility that waxes are secreted via non-vesicular trafficking.

While there is evidence both for and against non-vesicular trafficking of waxes from the ER to the PM at ER-PM contact sites, it is extremely difficult to differentiate between these possibilities without first identifying mutants defective in non-vesicular trafficking, or in ER-PM contact site morphology. While LACS1, 2, and 3 have lipid transfer activity in yeast, this activity has not yet been demonstrated *in planta*, nor have these proteins been localized to ER-PM contact sites (Pulsifer et al., 2012). Several other possible components of ER-PM contact sites exist in Arabidopsis (Chapter 4), but the functions of these proteins in ER-PM contact sites have not yet been investigated. The first step to conclusively determining whether waxes may be transported via non-vesicular trafficking at ER-PM contact sites is to determine the functional components of these contact sites.

5.2.8: What are the functions of ER-PM contact sites in plants?

The major outstanding question from Chapter 4 concerns the function of ER-PM contact sites in plants. Three hypotheses have been presented throughout this thesis: 1) ER-PM contact sites may be involved in lipid export, including cuticular lipid export (Samuels et al., 2008); 2) ER-PM contact sites may be involved in lipid recycling following vesicle fusion with the PM, especially during cell wall secretion during phases of rapid cell elongation (Staehelin and Chapman, 1987); 3) ER-PM contact sites may be involved in lipid remodeling during development and under certain stress conditions (Larsson et al., 2007). It is important to note that there are several lines of evidence that support the notion that, regardless of their function, ER-PM contact sites play an important role in plant cells. First, these contact sites are observed in all plant species and cell types examined (Chapter 4; Staehelin 1997). Second, ER-PM contact sites contain a distinct complement of proteins compared to either ER membranes or PM, indicating that they likely have a specialized function, relative to either the ER or the PM (Chapter 4; Larsson et al., 2007). Third, ER-PM contact sites are developmentally regulated in plant cells, suggesting that they play specific roles in plant growth and development (Chapter 4).

In yeast, non-vesicular uptake of sterols requires ABC transporters and lipid transfer proteins of the oxysterol binding protein subfamily (OSHs) (Li and Prinz, 2004; Raychaudhuri et al., 2006). Although there is no evidence that sterol uptake necessarily occurs at ER-PM contact sites, OSH4 can simultaneously bind two membranes and both membrane binding sites are required for its sterol transport activity (Schulz et al., 2009). Plant cells require significant retrograde lipid trafficking during cell elongation (Ketelaar et al., 2008). As cells expand, soluble cell wall polysaccharides are secreted to the plasma membrane by vesicle trafficking (Gendre et al., 2013). As polysaccharides are added to the cell wall by vesicle fusion, lipids are also added to the PM. Because much more cell wall material than PM is required for cell expansion, excess PM lipids must be recycled (Ketelaar et al., 2008). While some of this lipid recycling certainly occurs via clathrin-mediated endocytosis (Dhonukshe et al., 2007; Ketelaar et al., 2008), it is unclear whether the rate of endocytosis is sufficient to recycle all of the lipids that are added to the PM during cell wall secretion, especially in rapidly elongating cell types, which may need to recycle up to 90% of the vesicle membrane that fuses with the PM (Ketelaar et al., 2008). Thus, ER-PM contact sites may play a role in non-vesicular lipid recycling during cell expansion, especially since clathrin coated vesicle budding into the cytoplasm may be very energetically costly under turgor pressure in plant cells (Cram, 1980). While the hypothesis that ER-PM contact sites are involved in lipid recycling is consistent with the correlation between the rate of cell expansion and the frequency of ER-PM contact sites in Arabidopsis, there is no evidence to directly support it.

In addition to the requirement for retrograde lipid recycling, plants also secrete significant volumes of lipids in the form of protective coatings (e.g. cuticular lipids, suberin, pollen coat) and defense compounds (e.g. essential oils) (Mahmoud and Croteau, 2002; Samuels et al., 2008; Choi et al., 2012). In contrast to soluble cell wall material, which is synthesized in the Golgi apparatus, or secreted proteins, which are glycosylated in the Golgi apparatus, secreted lipid products are synthesized by ER-bound enzymes and need not pass through the Golgi apparatus (Samuels et al., 2008). Thus, it is possible that these lipid products are secreted by non-vesicular trafficking. As discussed (see section 5.2.7 above), there is no direct evidence that supports non-vesicular lipid export at ER-PM contact sites. However, given the data presented here, this possibility cannot be eliminated either.

By analogy to recent studies in yeast, it is also possible that lipid remodeling occurs at ER-PM contact sites. In yeast, an ER-localized phosphatase can convert PM-localized phosphatidylinositol-4-phosphate (PIns4P) to phosphatidylinositol (PI) at ER-PM contact sites (Stefan et al., 2011). In plants, PIns4P is localized to the plasma membrane, particularly to the tips of growing cells and to nascent cell plates (Vermeer et al., 2008). Both a PI kinase, which creates PIns4P, and a PIns4P phosphatase, which metabolizes PIns4P, have been localized to the Golgi/TGN and the PM in Arabidopsis. Together with a RabA4 family member, PIns4P has been implicated in targeted secretion from the TGN via an unknown mechanism (Preuss et al., 2006; Kang et al., 2011). Thus, unlike yeast, in which the PIns4P phosphatase is localized to the ER and acts at the PM (Stefan et al., 2011), at least one Arabidopsis PIns4P phosphatase is localized to the same membranes as its lipid substrate; therefore, ER-PM contact sites may not be required for PIns4P metabolism in plants.

However, there are other lipid remodeling processes, specific to plants, which may occur at ER-PM contact sites. For example, under phosphate-limited conditions, the plasma membrane is rapidly remodeled to replace phospholipids with galactolipids. Since galactolipids are synthesized in the plastid, phosphate must be scavenged from PM lipids and galactolipids must be transported from the plastid to the PM. Since there is no evidence of vesicular traffic between the ER and the plastid, it is speculated that non-vesicular trafficking occurs between the plastid and the ER (Benning et al., 2006). Furthermore, the initial remodeling of PM lipids to scavenge phosphate likely requires membrane lipid conversion to diacylglycerol, and there is evidence that diacylglycerol is rapidly transported to the ER (Grabski et al., 1993), possibly via direct PM to ER transfer. Because of the sessile nature of plants, lipid remodeling may also be an important part of plant responses to pathogen infection and abiotic stress. A role for ER-PM contact sites in lipid remodeling under stress would be consistent with the stress-sensitive phenotypes of several of the ER-PM contact site candidates discussed in Chapter 4 (Schapire et al., 2008; Yamazaki et al., 2008; Lewis and Lazarowitz, 2010).

In order to determine which of these roles ER-PM contact sites may play in plants, a comprehensive analysis of the components in ER-PM contact sites is required. Initial proteomic experiments on the PM have revealed several interesting candidates for ER-PM

contact site proteins (Chapter 4). Determining the subcellular localization of these candidates (e.g. via fluorescent fusion proteins) will demonstrate whether they are localized to ER-PM contact sites. Once mutants have been isolated for these proteins (e.g. by obtaining T-DNA insertional mutants from available libraries), it will be possible to test whether they are required for maintaining ER-PM contact sites and whether they play a role in any of the processes discussed above. If any of these candidates are localized to ER-PM contact sites, they could be used to isolate ER-PM contact sites for proteomics via an immunological approach (Drakakaki et al., 2011).

While reverse genetic screens are very useful in Arabidopsis, they rely on preexisting knowledge and thus represent a biased approach that cannot be used to identify novel components. However, a forward genetic screen for ER-PM contact site components is challenging because, without a defined function for these contact sites, it is unclear what phenotype to screen for, and screening for fewer ER-PM contact sites via TEM would be unrealistically laborious. Although it is possible to screen a mutant population for changes in GFP-HDEL distribution (Nakano et al., 2009), studies on *rhd3-1* mutants have demonstrated that significant defects in ER morphology detected by confocal microscopy do not necessarily result in defects in ER-PM contact sites (Chapter 3; Chapter 4). However, given that only a small amount of cortical ER remains in *rhd3-1* mutants, yet there are wild-type levels of ER-PM contact sites, it may be that most or all of this cortical ER is participating in ER-PM contact sites. Thus, an enhancer screen of *rhd3-1* mutants that carry GFP-HDEL might reveal mutants that are defective in the remaining cortical ER in *rhd3-1*, that is, mutants that are defective in ER-PM contact sites.

In summary, the broad goal of this research was to determine the pathway of cuticular lipid export in plant cells, using the stem epidermal cells of *Arabidopsis thaliana* as a model system for lipid export. In Chapter 2, interaction studies of two ABCG transporters, ABCG11 and ABCG12, combined with chemical analysis of their mutants, were used to generate a model of ABCG function in cuticular lipid export in which different dimer combinations may influence the substrate specificity of the resulting transporter. In Chapter 3, analysis of wax trafficking in several well-characterized secretory pathway mutants revealed that some cuticular lipids are secreted from the ER to the cell surface via vesicle trafficking through the Golgi apparatus. These studies also revealed a close

relationship between the morphology of the ER and its biosynthetic capacity. In Chapter 4, ER-PM contact sites were examined as a possible alternate route of cuticular lipid export, but the frequency of these contact sites was not correlated with cuticular lipid synthesis and secretion. Proteomic analysis of high quality PM fractions reveals several candidates for ER-PM contact site proteins, and developmental regulation of ER-PM contact sites implies a role in lipid remodeling or recycling during development, rather than in cuticular lipid export. Together, these results contribute to a model of cuticular lipid export from the site of synthesis, the ER, to the site of accumulation on the cell surface (Figure 5.1).

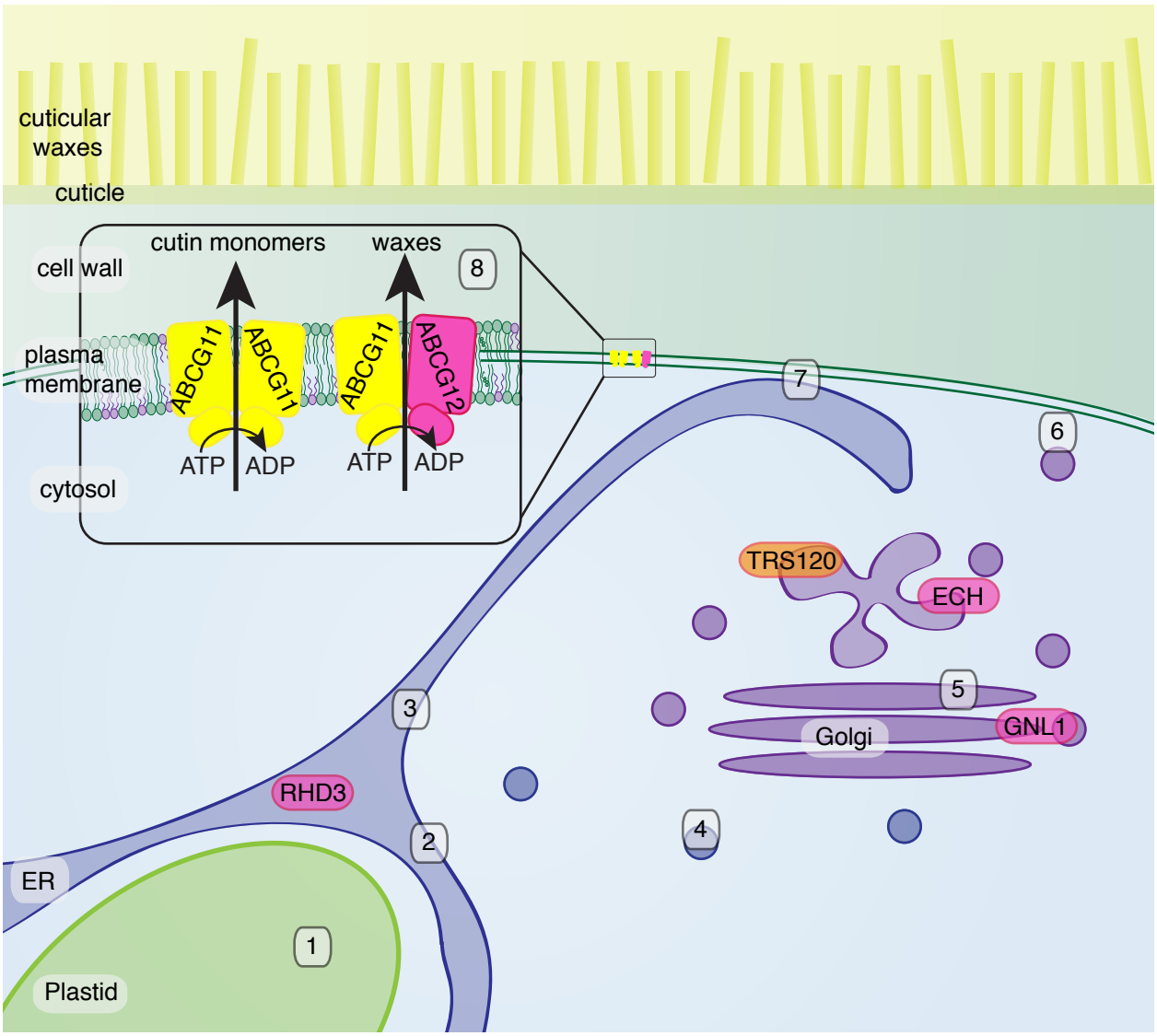

Figure 5.1: A model of wax transport from the ER to the cell surface. Fatty acids are synthesized in the plastid (1) then transported to the ER where they undergo fatty acid elongation (2) and modification into waxes (3). This synthesis is dependent upon ER morphology, which is maintained by proteins including RHD3. Waxes are transported to the Golgi apparatus (4) then trafficked through the Golgi apparatus and trans-Golgi network (5) in a GNL1-dependent manner. Waxes are secreted to the plasma membrane via trans-Golgi network-derived vesicles (6) in an ECH-dependant, TRS120-independent fashion. Waxes may also be transported directly from the ER to the plasma membrane at membrane contact sites (7). Waxes are exported from the cell via an ABCG11-ABCG12 heterodimer (8) while the ABCG11 homodimer is required for cutin monomer export.

References

Achleitner, G., Gaigg, B., Krasser, A., Kainersdorfer, E., Kohlwein, S.D., Perktold, A., Zellnig, G., and Daum, G. 1999. Association between the endoplasmic reticulum and mitochondria of yeast facilitates interorganelle transport of phospholipids through membrane contact. *European Journal of Biochemistry* 264: 545-553.

Alassimone, J., Roppolo, D., Geldner, N., and Vermeer, J.E. 2012. The endodermis—development and differentiation of the plant's inner skin. *Protoplasma* 249: 433-443.

Alejandro, S., Lee, Y., Tohge, T., Sudre, D., Osorio, S., Park, J., Bovet, L., Lee, Y., Geldner, N., Fernie, A., and Martinoia, E. 2012. AtABCG29 is a monolignol transporter involved in lignin biosynthesis. *Current Biology* 22: 1207-1212.

Alexandersson, E., Saalbach, G., Larsson, C., and Kjellbom, P. 2004. Arabidopsis plasma membrane proteomics identifies components of transport, signal transduction and membrane trafficking. *Plant and Cell Physiology* 45: 1543-1556.

Alfaro, G., Johansen, J., Dighe, S.A., Duamel, G., Kozminski, K.G., and Beh, C.T. 2011. The sterol-binding protein Kes1/Osh4p is a regulator of polarized exocytosis. *Traffic* 12: 1521-1536.

Altschul, S.F., Madden, T.L., Schäffer, A.A., Zhang, J., Zhang, Z., Miller, W., and Lipman, D.J. 1997. Gapped BLAST and PSI-BLAST: a new generation of protein database search programs. *Nucleic Acids Research* 25: 3389-3402.

Ambrose, J.C. and Wasteneys, G.O. 2008. CLASP modulates microtubule-cortex interaction during self-organization of acentrosomal microtubules. *Molecular Biology of the Cell* 19: 4730-4737.

Andersson, M.X., Goksör, M., and Sandelius, A.S. 2007. Optical manipulation reveals strong attracting forces at membrane contact sites between endoplasmic reticulum and chloroplasts. *Journal of Biological Chemistry* 282: 1170-1174.

Andersson, M.X., Larsson, K.E., Tjellström, H., Liljenberg, C., and Sandelius, A.S. 2005. Phosphate-limited oat: the plasma membrane and the tonoplast as major targets for phospholipid-to-glycolipid replacement and stimulation of the phospholipases in the plasma membrane. *Journal of Biological Chemistry* 280: 27578-27586.

Andersson, M.X., Stridh, M H., Larsson, K.E., Liljenberg, C., and Sandelius, A.S. 2003. Phosphate-deficient oat replaces a major portion of the plasma membrane phospholipids with the galactolipid digalactosyldiacylglycerol. *FEBS Letters* 53*:* 128-132.

Aniento, F. and Robinson, D.G. 2005. Testing for endocytosis in plants. *Protoplasma 226*: 3-11.

Antonny, B. and Schekman, R. 2001. ER export: public transportation by the COPII coach. *Current Opinion in Cell Biology* 12: 438-443.

Asghari, P., Scriven, D.R., Hoskins, J., Fameli, N., van Breemen, C., and Moore, E.D. 2012. The structure and functioning of the couplon in the mammalian cardiomyocyte. *Protoplasma* 249: 31-38.

Atmodjo, M.A., Sakuragi, Y., Zhu, X., Burrell, A.J., Mohanty, S.S., Atwood III, J.A., Orlando, R, Scheller, H.V., and Mohnen, D. 2011. Galacturonosyltransferase (GAUT) 1 and GAUT7 are the core of a plant cell wall pectin biosynthetic homogalacturonan:galacturonosyltransferase complex. *Proceedings of the National Academy of Sciences*, *USA* 108: 20225-20230.

Au, K.K.C., Pérez-Gómez, J., Neto, H., Müller, C., Meyer, A.J., Fricker, M.D. and Moore, I. 2012. A perturbation in glutathione biosynthesis disrupts endoplasmic reticulum morphology and secretory membrane traffic in *Arabidopsis thaliana*. *The Plant Journal* 71: 881–894.

Awai, K., Xu, C., Lu, B., and Benning, C. 2006a. Lipid trafficking between the endoplasmic reticulum and the chloroplast. *Biochemical Society Transactions* 34: 395-398.

Awai, K., Xu, C., Tamot, B., and Benning, C. 2006b. A phosphatidic acid-binding protein of the chloroplast inner envelope membrane involved in lipid trafficking. *Proceedings of the National Academy of Sciences, USA* 103: 10817-10822.

Bach, L., Michaelson, L.V., Haslam, R., Bellec, Y., Gissot, L., Marion, J., Da Costa, M., Boutin, J.P., Miquel, M., Tellier, F., Domergue, F., Markham, J.E., Beaudoin, F., Napier, J.A, and Faure, J.D. 2008. The very-long-chain hydroxy fatty acyl-CoA dehydratase PASTICCINO2 is essential and limiting for plant development. *Proceedings of the National Academy of Sciences, USA* 105: 14727-14731.

Bandmann, V. and Homann, U. 2012. Clathrin-independent endocytosis contributes to uptake of glucose into BY-2 protoplasts. *The Plant Journal* 70: 578–584.

Bardy, N., Carrasco, A., Galaud, J.P., Pont-Lezica, R., and Canut, H. 2005. Free-flow electrophoresis for fractionation of *Arabidopsis thaliana* membranes. *Electrophoresis* 19: 1145-1153.

Bassard, J.E., Mutterer, J., Duval, F., and Werck-Reichhart, D. 2012a. A novel method for monitoring the localization of cytochromes P450 and other endoplasmic reticulum membrane associated proteins: a tool for investigating the formation of metabolons. *FEBS Journal* 279: 1576-1583.

Bassard, J.E., Richert, L., Geerinck, J., Renault, H., Duval, F., Ullmann, P., Schmitt, M., Mayer, E., Mutterer, J., Boerjan, W., De Jaeger, G., Meley, Y., Goossens, A., and Werck-Reichhart,

D. 2012b. Protein–protein and protein–membrane associations in the lignin pathway. *The Plant Cell* 24: 4465-4482.

Bassil, E., Ohto, M.A., Esumi, T., Tajima, H., Zhu, Z., Cagnac, O., Belmonte, M., Peleg, Z., Yamaguchi, T., and Blumwald, E. 2011. The Arabidopsis intracellular Na+/H+ antiporters NHX5 and NHX6 are endosome associated and necessary for plant growth and development. *The Plant Cell* 23: 224-239.

Batoko, H., Zheng, H.Q., Hawes, C., and Moore, I. 2000. A Rab1 GTPase is required for transport between the endoplasmic reticulum and Golgi apparatus and for normal Golgi movement in plants. *The Plant Cell* 12: 2201-2218.

Beaudoin, F., Wu, X., Li, F., Haslam, R.P., Markham, J.E., Zheng, H., Napier, J.A., and Kunst, L. 2009. Functional characterization of the Arabidopsis beta-ketoacyl-coenzyme A reductase candidates of the fatty acid elongase. *Plant Physiology* 150: 1174-1191.

Beh, C.T., Alfaro, G., Duamel, G., Sullivan, D.P., Kersting, M.C., Dighe, S., Kosminski, K.G., and Menon, A.K. 2009. Yeast oxysterol-binding proteins: sterol transporters or regulators of cell polarization? *Molecular and Cellular Biochemistry 326*: 9-13.

Beisson, F., Li-Beisson, Y., and Pollard, M. 2012. Solving the puzzles of cutin and suberin polymer biosynthesis. *Current Opinion in Plant Biology* 15: 329-337.

Benning, C., Xu, C., and Awai, K. 2006. Non-vesicular and vesicular lipid trafficking involving plastids. *Current Opinion in Plant Biology* 9: 241-247.

Berendzen, K., Böhmer, M., Wallmeroth, N., Peter, S., Vesić, M., Zhou, Y., Tiesler, F., Schleifenbaum, F., and Harter, K. 2012. Screening for *in planta* protein-protein interactions combining bimolecular fluorescence complementation with flow cytometry. *Plant Methods* 8: 25.

Berge, K.E., Tian, H., Graf, G.A., Yu, L., Grishin, N.V., Schultz, J., Kwiterovich, P., Shan, B., Barnes, R., and Hobbs, H.H. 2000. Accumulation of dietary cholesterol in sitosterolemia caused by mutations in adjacent ABC transporters. *Science* 290: 1771-1775.

Bernard, A., Domergue, F., Pascal, S., Jetter, R., Renne, C., Faure, J.D., Haslam, R.P., Napier, J.A., and Joubès, J. 2012. Reconstitution of plant alkane biosynthesis in yeast demonstrates that Arabidopsis ECERIFERUM1 and ECERIFERUM3 are core components of a very-long-chain alkane synthesis complex. *The Plant Cell* 24: 3106-3118.

Bertho, P., Moreau, P., Morré, D.J., and Cassagne, C. 1991. Monensin blocks the transfer of very long chain fatty acid containing lipids to the plasma membrane of leek seedlings. Evidence for lipid sorting based on fatty acyl chain length. *Biochimica et Biophysica Acta* 1070: 127-134.

Bessire, M., Chassot, C., Jacquat, A.C., Humphry, M., Borel, S., Petétot, J.M., Métraux, J.P., and Nawrath, C. 2007. A permeable cuticle in Arabidopsis leads to a strong resistance to *Botrytis cinerea*. *The EMBO Journal* 26: 2158-2168.

Bessire M., Borel, S., Fabre, G., Carraça., L., Efremova, N., Yephermov, A., Cao, Y., Jetter, R., Jacquat, A.C., Métraux, J.P., and Nawrath, C. 2011. A member of the PLEIOTROPIC DRUG RESISTANCE family of ATP-binding cassette transporters is required for the formation of a functional cuticle in Arabidopsis. *The Plant Cell* 23: 1958-1970.

Bird, D.A. 2008. The role of ABC transporters in cuticular lipid secretion. *Plant Science* 174: 563-569.

Bird, D.A., Beisson, F., Brigham, A., Shin, J., Greer, S., Jetter, R., Kunst, L., Wu, X., Yephremov, A., and Samuels, A.L. 2007. Characterization of Arabidopsis ABCG11/WBC11, an ATP binding cassette (ABC) transporter that is required for cuticular lipid secretion. *The Plant Journal* 52: 485-498.

Boevink, P., Oparka, K., Santa Cruz, S., Martin, B., Betteridge, A., and Hawes, C. 1998. Stacks on tracks: the plant Golgi apparatus traffics on an actin/ER network. *The Plant Journal* 15: 441-447.

Bolte, S., Talbot, C., Boutte, Y., Catrice, O., Read, N.D., and Satiat-Jeunemaitre, B. 2004. FM-dyes as experimental probes for dissecting vesicle trafficking in living plant cells. *Journal of Microscopy* 214: 159-173.

Boncoeur, E., Durmort, C., Bernay, B., Ebel, C., Di Guilmi, A.M., Croizé, J., Vernet, T., and Jault, J.M. 2012. PatA and PatB form a functional heterodimeric ABC multidrug efflux transporter responsible for the resistance of *Streptococcus pneumoniae* to fluoroquinolones. *Biochemistry* 51: 7755-7765.

Borner, G.H.H., Sherrier, D.J., Weimar, T., Michaelson, L.V., Hawkins, N.D., MacAskill, A., Napier, J.A., Beale, M.H., Lilley, K.S., and Dupree, P. 2005. Analysis of detergent-resistant membranes in Arabidopsis. Evidence for plasma membrane lipid rafts. *Plant Physiology* 137: 104-116.

Bots, M., Feron, R., Uehlein, N., Weterings, K., Kaldenhoff, R., and Mariani, T. 2005. PIP1 and PIP2 aquaporins are differentially expressed during tobacco anther and stigma development. *Journal of Experimental Botany* 56: 113–121.

Bouchekhima, A.N. and Frigerio, L. 2009. Geometric quantification of the plant endoplasmic reticulum. *Journal of Microscopy* 234: 158-172.

Broun, P., Poindexter, P., Osborne, E., Jiang, C.Z., and Riechmann, J.L. 2004. WIN1, a transcriptional activator of epidermal wax accumulation in Arabidopsis. *Proceedings of the National Academy of Sciences, USA*101: 4706-4711.

Brüx, A., Liu, T.Y., Krebs, M., Stierhof, Y.D., Lohmann, J.U., Miersch, O., Wasternack, C., and Schumacher, K. 2008. Reduced V-ATPase activity in the trans-Golgi network causes oxylipin-dependent hypocotyl growth inhibition in Arabidopsis. *The Plant Cell* 20: 1088-1100.

Candiano, G., Bruschi, M., Musante, L., Santucci, L., Ghiggeri, G.M., Carnemolla, B., Orecchia, R., Zardi, L., and Righetti, P.G. 2004. Blue silver: a very sensitive colloidal Coomassie G-250 staining for proteome analysis. *Electrophoresis* 25: 1327-1333.

Carrasco, S. and Meyer, T. 2011. STIM proteins and the endoplasmic reticulum-plasma membrane junctions. *Annual Review of Biochemistry* 80: 973-1000.

Chatre, L., Brandizzi, F., Hocquellet, A., Hawes, C., and Moreau, P. 2005. Sec22 and Memb11 are v-SNAREs of the anterograde endoplasmic reticulum-Golgi pathway in tobacco leaf epidermal cells. *Plant Physiology* 139: 1244-1254.

Cheesbrough, T.M. and Kolattukudy, P.E. 1984. Alkane biosynthesis by decarbonylation of the aldehydes catalyzed by a particulate preparation from *Pisum sativum*. *Proceedings of the National Academy of Sciences, USA* 81: 6613-6617.

Chen, M., Han, G., Dietrich, C.R., Dunn, T.M., and Cahoon, E.B. 2006. The essential nature of sphingolipids in plants as revealed by the functional identification and characterization of the Arabidopsis LCB1 subunit of serine palmitoyltransferase. *The Plant Cell* 18: 3576-3593.

Chen, M., Markham, J.E., Dietrich, C.R., Jaworski, J.G., and Cahoon, E.B. 2008. Sphingolipid long-chain base hydroxylation is important for growth and regulation of sphingolipid content and composition in Arabidopsis. *The Plant Cell* 20: 1862-1878.

Chen, G., Komatsuda, T., Ma, J.F., Nawrath, C., Pourkheirandish, M., Tagiri, A., Hu, Y.G., Sameri, M., Li, X., Zhao, X., Liu, Y., Li, C., Ma, X., Wang, A., Nair, S., Wang, N., Sakuma, S., Yamaji, N., Zheng, X., and Nevo, E. 2011a. An ATP-binding cassette subfamily G full transporter is essential for the retention of leaf water in both wild barley and rice. *Proceedings of the National Academy of Sciences*, *USA* 108: 12354-12359.

Chen, H.C., Li, Q., Shuford, C.M., Liu, J., Muddiman, D.C., Sederoff, R.R., and V.L. Chiang. 2011b. Membrane protein complexes catalyze both 4- and 3-hydroxylation of cinnamic acid derivatives in monolignol biosynthesis. *Proceedings of the National Academy of Sciences*, *USA* 108: 21253-21258.

Chen, J., Stefano, G., Brandizzi, F., and Zheng, H. 2011c. Arabidopsis RHD3 mediates the generation of the tubular ER network and is required for Golgi distribution and motility in plant cells. *Journal of Cell Science* 124: 2241-2252.

Choi, H., Jin, J.Y., Choi, S., Hwang, J.U., Kim, Y.Y., Suh, M.C., and Lee, Y. 2011. An ABCG/WBC-type ABC transporter is essential for transport of sporopollenin precursors for exine formation in developing pollen. *The Plant Journal* 65: 181-193.

Choi, Y.E., Lim, S., Kim, H.J., Han, J.Y., Lee, M.H., Yang, Y., Kim, J.A., and Kim, Y.S. 2012. Tobacco NtLTP1, a glandular-specific lipid transfer protein, is required for lipid secretion from glandular trichomes. *The Plant Journal* 70: 480-491.

Citovsky, V., Lee, L.Y., Vyas, S., Glick, E., Chen, M.H., Vainstein, A., Gafni, Y., Gelvin, S.B., and Tzfira, T. 2006. Subcellular localization of interacting proteins by bimolecular fluorescence complementation *in planta. Journal of Molecular Biology* 362: 1120–1131.

Coleman, J.A., Quazi, F., and Molday, R.S. 2012. Mammalian P4-ATPases and ABC transporters and their role in phospholipid transport. *Biochimica et Biophysica Acta - Molecular and Cell Biology of Lipids* In Press: DOI: dx.doi.org/10.1016/j.bbalip.2012.10.006

Coll, E.P., Kandt, C., Bird, D.A., Samuels, A.L., and Tieleman, D.P. 2007. The distribution and conformation of very long-chain plant wax components in a lipid bilayer. *The Journal of Physical Chemistry* 111: 8702-8704.

Cominelli, E., Sala, T., Calvi, D., Gusmaroli, G., and Tonelli, C. 2008. Over-expression of the Arabidopsis *AtMYB41* gene alters cell expansion and leaf surface permeability. *The Plant Journal* 53: 53–64.

Cosgrove, D.J. 2005. Growth of the plant cell wall. *Nature Reviews Molecular Cell Biology* 6: 850-861.

Coughlan, S.J., Hastings, C., and Winfrey, R., Jr. 1997. Cloning and characterization of the calreticulin gene from *Ricinus communis* L. *Plant Molecular Biology* 34: 897–911.

Cram, W.J. 1980. Pinocytosis in plants. *New Phytologist* 84: 1-17.

Creutz, C.E., Tomsig, J.L., Snyder, S.L., Gautier, M.C., Skouri, F., Beisson, J., and Cohen, J. 1998. The copines, a novel class of C2 domain-containing, calciumdependent, phospholipid-binding proteins conserved from Paramecium to humans. *Journal of Biological Chemistry* 273: 1393-1402.

Cserepes, J., Szentpétery, Z., Seres, L., Ozvegy-Laczka, C., Langmann, T., Schmitz, G., Glavinas, H., Klein, I., Homolya, L., Váradi, A., Sarkadi, B., and Elkind, N.B. 2004. Functional expression and characterization of the human ABCG1 and ABCG4 proteins: indications for heterodimerization. *Biochemical and Biophysical Research Communications* 320: 860–867.

Cutler, S.R., Ehrhardt, D.W., Griffiths, J.S., and Somerville, C.R. 2000. Random GFP::cDNA fusions enable visualization of subcellular structures in cells of Arabidopsis at a high frequency. *Proceedings of the National Academy of Sciences, USA* 97: 3718-3723.

D'Angelo, G., Polishchuk, E., Di Tullio, G., Santoro, M., Di Campli, A., Godi, A., West, G., Bielawski, J., Chuang, C.C., van der Spoel, A.C., Platt, F.M., Hannun, Y.A., Polishchuck, R., Mattjus, P., and De Matteis, M.A. 2007. Glycosphingolipid synthesis requires FAPP2 transfer of glucosylceramide. *Nature* 449: 62-67.

D'Angelo, G., Vicinanza, M., and De Matteis, M.A. 2008. Lipid-transfer proteins in biosynthetic pathways. *Current Opinion in Cell Biology* 20: 360-370.

De Brito, O.M. and Scorrano, L. 2008. Mitofusin2 tethers endoplasmic reticulum to mitochondria. *Science* 456: 605-610.

De Caroli, M., Lenucci, M. S., Di Sansebastiano, G.P., Dalessandro, G., De Lorenzo, G., and Piro, G. 2011. Protein trafficking to the cell wall occurs through mechanisms distinguishable from default sorting in tobacco. *The Plant Journal* 65: 295–308.

DeBono, A., Yeats, T.H., Rose, J.K., Bird, D.A., Jetter, R., Kunst, L., and Samuels, A.L. 2009. Arabidopsis LTPG Is a glycosylphosphatidylinositol-anchored lipid transfer protein required for export of lipids to the plant surface. *The Plant Cell* 21: 1230-1238.

Denic, V. and Weissman, J.S. 2007. A molecular caliper mechanism for determining very long-chain fatty acid length. *Cell* 130: 663-677.

Dettmer, J., Hong-Hermesdorf, A., Stierhof, Y.D., and Schumacher, K. 2006. Vacuolar H^+-ATPase activity is required for endocytic and secretory trafficking in Arabidopsis. *The Plant Cell* 18: 715-730.

Dhonukshe, P., Aniento, F., Hwang, I., Robinson, D.G., Mravec, J., Stierhof, Y.D., and Friml, J. 2007. Clathrin-mediated constitutive endocytosis of PIN auxin efflux carriers in Arabidopsis. *Current Biology 17*: 520-527.

Dietrich, C.R., Han, G., Chen, M., Berg, R.H., Dunn, T.M., and Cahoon, E.B. 2008. Loss-of-function mutations and inducible RNAi suppression of Arabidopsis LCB2 genes reveal the critical role of sphingolipids in gametophytic and sporophytic cell viability. *The Plant Journal* 54: 284-298.

Donohoe, B.S., Kang, B.H., and Staehelin, L.A. 2007. Identification and characterization of COPIa- and COPIb-type vesicle classes associated with plant and algal Golgi. *Proceedings of the National Academy of Sciences, USA* 104: 163-168.

Donohoe, B.S., Mogelsvang, S., and Staehelin, L.A. 2006. Electron tomography of ER, Golgi and related membrane systems. *Methods* 39: 154-162.

Dou, X.Y., Yang, K.Z., Zhang, Y., Wang, W., Liu, X.L., Chen, L.Q., Zhang, X.Q., and Ye, D. 2011. WBC27, an adenosine tri-phosphate-binding cassette protein, controls pollen wall formation and patterning in Arabidopsis. *Journal of Integrative Plant Biology* 53: 74-88.

Drakakaki, G., van de Ven, W., Pan, S., Miao, Y., Wang, J., Keinath, N.K., Weatherly, B., Jiang, L., Schumacher, K., Hicks, G., and Raikhel, N. 2011. Isolation and proteomic analysis of the SYP61 compartment reveal its role in exocytic trafficking in Arabidopsis. *Cell Research* 22: 413-424.

Dunkley, T.P., Hester, S., Shadforth, I.P., Runions, J., Weimar, T., Hanton, S.L., Griffin, J.L., Bessant, C., Brandizzi, F., Hawes, C., Watson, R.B., Dupree, P., and Lilley, K.S. 2006. Mapping the Arabidopsis organelle proteome. *Proceedings of the National Academy of Sciences*, *USA* 103: 6518-6523.

Dyer, J.M. and Mullen, R.T. 2008. Engineering plant oils as high-value industrial feedstocks for biorefining: the need for underpinning cell biology research. *Physiologia Plantarum* 132: 11–22.

Elbaz, Y. and Schuldiner, M. 2011. Staying in touch: the molecular era of organelle contact sites. *Trends in Biochemical Sciences* 36: 616-623.

El-Kasmi, F., Pacher, T., Strompen, G., Stierhof, Y.-D., Müller, L. M., Koncz, C., Mayer, U., and Jürgens, G. 2011. Arabidopsis SNARE protein SEC22 is essential for gametophyte development and maintenance of Golgi-stack integrity. *The Plant Journal* 66: 268–279.

English, A.R., Zurek, N., and Voeltz, G.K. 2009. Peripheral ER structure and function. *Current Opinion in Cell Biology* 21: 596-602.

Eubel, H., Lee, C.P., Kuo, J., Meyer, E.H., Taylor, N.L., and Millar, A.H. 2007. TECHNICAL ADVANCE: Free-flow electrophoresis for purification of plant mitochondria by surface charge. *The Plant Journal* 52: 583-594.

Evans, J.M., Day, J.P., Cabrero, P., Dow, J.A.T., and Davies, S.A. 2008. A new role for a classical gene: White transports cyclic GMP. *Journal of Experimental Biology* 211: 890–899.

Ewart, G.D., Cannell, D., Cox, G.B., and Howells, A.J. 1994. Mutational analysis of the traffic ATPase (ABC) transporters involved in uptake of eye pigment precursors in *Drosophila melanogaster.* Implications for structure-function relationships. *Journal of Biological Chemistry* 269: 10370–10377.

Esseling-Ozdoba, A., Houtman, D., Van Lammeren, A.A. M., Eiser, E., and Emons, A.M.C. 2008. Hydrodynamic flow in the cytoplasm of plant cells. *Journal of Microscopy* 231: 274-283.

Faso, C., Chen, Y. N., Tamura, K., Held, M., Zemelis, S., Marti, L., Saravanan, R.S., Hummel, E., Kung, E., Miller, E., Hawes, C., and Brandizzi, F. 2009. A missense mutation in the

Arabidopsis COPII coat protein Sec24A induces the formation of clusters of the endoplasmic reticulum and Golgi apparatus. *The Plant Cell* 21: 3655-3671.

Fischer, U., Men, S., and Grebe, M. 2004. Lipid function in plant cell polarity. *Current Opinion in Plant Biology* 7: 670–676.

Foresti, O. and Denecke, J. 2008. Intermediate organelles of the plant secretory pathway: identity and function. *Traffic* 9: 1599-1612.

Gaigg, B., Simbeni, R., Hrastnik, C., Paltauf, F., and Daum, G. 1995. Characterization of a microsomal subfraction associated with mitochondria of the yeast, *Saccharomyces cerevisiae*. Involvement in synthesis and import of phospholipids into mitochondria. *Biochimica et Biophysica Acta* 1234: 214-220.

Gao, D., Knight, M.R., Trewavas, A.J., Sattelmacher, B., and Plieth, C. 2004. Self-reporting Arabidopsis expressing pH and [$Ca2^{+}$] indicators unveil ion dynamics in the cytoplasm and in the apoplast under abiotic stress. *Plant Physiology* 134: 898-908.

Geisler, M. and Murphy, A.S. 2006 . The ABC of auxin transport: The role of p-glycoproteins in plant development. *FEBS Letters* 580: 1094–1102.

Geldner, N., Anders N., Wolters, H., Keicher, J., Kornberger, W., Muller, P., Delbarre, A., Ueda, T., Nakano, A., and Jürgens, G. 2003. The Arabidopsis GNOM ARF-GEF mediates endosomal recycling, auxin transport, and auxin-dependent plant growth. *Cell* 112: 219–230.

Gendre, D., Oh, J., Boutté, Y., Best, J.G., Samuels, L., Nilsson, R., Uemura, Y., Marchant, A., Bennett, M.J., Grebe, M., and Bhalerao, R. P. 2011. Conserved Arabidopsis ECHIDNA protein mediates trans–Golgi-network trafficking and cell elongation. *Proceedings of the National Academy of Sciences, USA* 108: 8048-8053.

Gendre, D., McFarlane, H.E., Johnson, E., Mouille, G., Sjödin, A., Oh, J., Levesque-Tremblay, G., Watanabe, Y., Samuels, A.L., and Bhalerao, R.P. 2013. TGN localised ECH and YIP proteins are required for cell wall polysaccharides secretion in *Arabidopsis thaliana*. In Review.

Gidda, S.K., Shockey, J.M., Falcone, M., Kim, P.K., Rothstein, S.J., Andrews, D.W., Dyer, J.M., and Mullen, R.T. 2011. Hydrophobic-domain-dependent protein–protein interactions mediate the localization of GPAT enzymes to ER subdomains. *Traffic* 12: 452–472.

Grabski, S., De Feijter, A.W., and Schindler, M. 1993. Endoplasmic reticulum forms a dynamic continuum for lipid diffusion between contiguous soybean root cells. *The Plant Cell* 5: 25-38.

Graça, J., Schreiber, L., Rodrigues, J., and Pereira, H. 2002. Glycerol and glyceryl esters of ω-hydroxyacids in cutins. *Phytochemistry* 61: 205-215.

Graf, G.A., Cohen, J.C., and Hobbs, H.H. 2004. Missense mutations in ABCG5 and ABCG8 disrupt heterodimerization and trafficking. *The Journal of Biological Chemistry* 279: 24881-24888.

Graf, G.A., Li, W.P., Gerard, R.D., Gelissen, I., White, A., Cohen, J.C., and Hobbs, H.H. 2002. Coexpression of ATP-binding cassette proteins ABCG5 and ABCG8 permits their transport to the apical surface. *Journal of Clinical Investigation* 110: 659-669.

Graf, G.A., Yu, L., Li, W.P., Gerard, R., Tuma, P.L., Cohen, J.C., and Hobbs, H.H. 2003 . ABCG5 and ABCG8 are obligate heterodimers for protein trafficking and biliary cholesterol excretion. *Journal of Biological Chemistry* 278: 48275–48282.

Gray, J.C., Hansen, M.R., Shaw, D.J., Graham, K., Dale, R., Smallman, P., Natesan, S.K.A., and Newell, C.A. 2012. Plastid stromules are induced by stress treatments acting through abscisic acid. *The Plant Journal* 69: 387–398.

Grebe, M., Xu, J., Möbius, W., Ueda, T., Nakano, A., Geuze, H.J., Rood, M.B., and Scheres, B. 2003. Arabidopsis sterol endocytosis involves actin-mediated trafficking via ARA6-positive early endosomes. *Current Biology* 13: 1378–1387.

Greer, S., Wen, M., Bird, D.A., Wu, X., Samuels, A.L., Kunst, L., and Jetter, R. 2007. The cytochrome P450 enzyme CYP96A15 is the midchain alkane hydroxylase responsible for formation of secondary alcohols and ketones in stem cuticular wax of Arabidopsis. *Plant Physiology* 145: 653-667.

Griffing, L.R. 2008. FRET analysis of transmembrane flipping of FM4–64 in plant cells: is FM4–64 a robust marker for endocytosis? *Journal of Microscopy* 231: 291-298.

Gutierrez, R., Lindeboom, J.J., Paredez, A.R., Emons, A.M.C., and Ehrhardt, D.W. 2009. Arabidopsis cortical microtubules position cellulose synthase delivery to the plasma membrane and interact with cellulose synthase trafficking compartments. *Nature Cell Biology* 11: 797-806.

Haider, A. J., Briggs, D., Self, T. J., Chilvers, H. L., Holliday, N. D., and Kerr, I.D. 2011. Dimerization of ABCG2 analysed by bimolecular fluorescence complementation. *PloS One* 6: e25818.

Hála, M., Cole, R., Synek, L., Drdová, E., Pečenková, T., Nordheim, A., Lamkemeyer, T., Madlung, J., Hochholdinger, F., Fowler, J.E., and Žárský, V. 2008. An exocyst complex functions in plant cell growth in Arabidopsis and tobacco. *The Plant Cell* 20: 1330-1345.

Halter, D., Neumann, S., Van Dijk, S.M., Wolthoorn, J., De Mazière, A.M., Vieira, O.V., Mattjus, P., Klumperman, J., Van Meer, G., and Sprong, H. 2007. Pre-and post-Golgi translocation

of glucosylceramide in glycosphingolipid synthesis. *The Journal of Cell Biology* 179: 101-115.

Hanada, K., Kumagai, K., Tomishige, N., and Yamaji, T. 2009. CERT-mediated trafficking of ceramide. *Biochimica et Biophysica Acta* 1791: 684-691.

Hanada, K., Kumagai, K., Yasuda, S., Miura, Y., Kawano, M., Fukasawa, M., and Nishijima, M. 2003. Molecular machinery for non-vesicular trafficking of ceramide. *Nature* 426: 803-809.

Haslam T.M., Fernández, A.M., Zhao, L., and Kunst, L. 2012. Arabidopsis ECERIFERUM2 is a component of the fatty acid elongation machinery required for fatty acid extension to exceptional lengths. *Plant Physiology* 160: 1164-1174.

Haughn, G.W. and Somerville, C. 1986. Sulfonylurea-resistant mutants of *Arabidopsis thaliana*. *Molecular and General Genetics* 204: 430-434.

Hawes, C., Osterrieder, A., Hummel, E., and Sparkes, I. 2008. The plant ER–Golgi interface. *Traffic* 9: 1571-1580.

Hawes, C., Saint-Jore, C., Martin, B., and Zheng, H. 2001. ER confirmed as the location of mystery organelles in Arabidopsis plants expressing GFP! *Trends in Plant Science* 6: 245-246.

Hawes, C. and Satiat-Jeunemaitre, B. 2005. The plant Golgi apparatus - going with the flow. *Biochimica et Biophysica Acta* 1744: 465-517.

Heazlewood, J.L., Verboom, R.E., Tonti-Filippini, J., Small, I., and Millar, A.H. 2007. SUBA: the Arabidopsis subcellular database. *Nucleic Acids Research* 35 (supplement 1): D213-D218.

Hepler, P.K., Palevitz, B.A., Lancelle, S.A., McCauley, M.M., and Lichtscheidl, I. 1990. Cortical endoplasmic reticulum in plants. *Journal of Cell Science* 96: 355-373.

Higgins, C.F. 2001. ABC transporters: physiology, structure and mechanism - an overview. *Research in Microbiology* 152: 205-210.

Hinz, G., Hillmer, S., Bäumer, M., and Hohl, I. 1999. Vacuolar storage proteins and the putative vacuolar sorting receptor BP-80 exit the Golgi apparatus of developing pea cotyledons in different transport vesicles. *The Plant Cell* 11: 1509-1524.

Hohl, I., Robinson, D.G., Chrispeels, M.J., and Hinz, G. 1996 . Transport of storage proteins to the vacuole is mediated by vesicles without a clathrin coat. *Journal of Cell Science* 109: 2539-2550.

Holthuis, J.C.M. and Levine, T.P. 2005. Lipid traffic: floppy drives and a superhighway. *Nature Reviews Molecular Cell Biology* 6: 209-220.

Hooker, T. S., Lam, P., Zheng, H., and Kunst, L. 2007. A core subunit of the RNA-processing/degrading exosome specifically influences cuticular wax biosynthesis in Arabidopsis. *The Plant Cell* 19*:* 904-913.

Hu, J., Shibata, Y., Zhu, P.P., Voss, C., Rismanchi, N., Prinz, W.A., Rapoport, T.A., and Blackstone, C. 2009. A class of dynamin-like GTPases involved in the generation of the tubular ER network. *Cell* 138: 549-561.

Hu, Y., Zhong, R., Morrison III, W.H., and Ye, Z.H. 2003. The Arabidopsis RHD3 gene is required for cell wall biosynthesis and actin organization. *Planta* 217: 912-921.

Jeffree, C.E*. The fine structure of the plant cuticle* in Riederer, M. and Müller, C. (eds.) *Biology of the Plant Cuticle*. Blackwell Publishing. p. 12-125

Jelínková, A., Malínská, K., Simon, S., Kleine-Vehn, J., Pařezová, M., Pejchar, P., Kubeš, M., Martinec, J., Friml, J., Zažímalová, E., and Petrášek, J. 2010. Probing plant membranes with FM dyes: tracking, dragging or blocking? *The Plant Journal* 61: 883–892.

Jenks, M.A., Rich, P.J., and Ashworth, E.N. 1994. Involvement of cork cells in the secretion of epicuticular wax filaments on *Sorghum bicolor* (L.) Moench. *International Journal of Plant Science* 155: 506-518.

Jetter, R. and Kunst, L. 2008. Plant surface lipid biosynthetic pathways and their utility for metabolic engineering of waxes and hydrocarbon biofuels. *The Plant Journal* 54: 670–683.

Jetter, R., Kunst, L., and Samuels, A.L. 2006. *Composition of plant cuticular waxes* in Riederer, M. and Müller, C. (eds.) *Biology of the Plant Cuticle*. Blackwell Publishing. p. 145-181

Jetter, R., Schäffer, S., and Riederer, M. 2000. Leaf cuticular waxes are arranged in chemically and mechanically distinct layers: evidence from *Prunus laurocerasus* L. *Plant Cell and Environment* 23: 619-628.

Jonikas, M.C., Collins, S.R., Cenic, V., Oh, E., Quan, E.M., Schmid, V., Weibezahn, J., Schwappach, B., Walter, P., Weissman, J.S., and Schuldiner, M. 2009. Comprehensive characterization of genes required for protein folding in the endoplasmic reticulum. *Science Signalling* 323: 1693-1697.

Joshi, H.J., Hirsch-Hoffmann, M., Baerenfaller, K., Gruissem, W., Baginsky, S., Schmidt, R., Schulze, W.X., Sun, Q., van Wijk, K.J., Egelhofer, V., Wienkoop, S., Weckwerth, W., Bruley, C., Rolland, N., Toyoda, T., Nakagami, H., Jones, A.M., Priggs, S.P., Castleden, I., Tanz, S.K.,

Millar, A.H., and Heazlewood, J.L. 2011. MASCP Gator: an aggregation portal for the visualization of Arabidopsis proteomics data. *Plant Physiology* 155: 259-270.

Joubès, J., Raffaele, S., Bourdenx, B., Garcia, C., Laroche-Traineau, J., Moreau, P., Domergue, F., and Lessire, R. 2008. The VLCFA elongase gene family in *Arabidopsis thaliana*: phylogenetic analysis, 3D modelling and expression profiling. *Plant Molecular Biology* 67: 547-566.

Kader, J.C. 1997. Lipid-transfer proteins: a puzzling family of plant proteins. *Trends in Plant Science* 2: 66-70.

Kamauchi, S., Nakatani, H., Nakano, C., and Urade, R. 2005. Gene expression in response to endoplasmic reticulum stress in *Arabidopsis thaliana. FEBS Journal* 272: 3461–3476.

Kang, B.-H., Nielsen, E., Preuss, M. L., Mastronarde, D. and Staehelin, L. A. 2011. Electron tomography of RabA4b- and PI-4Kβ1-labeled *trans* Golgi network compartments in Arabidopsis. *Traffic* 12: 313–329.

Kannangara, R., Branigan, C., Liu, Y., Penfield, T., Rao, V., Mouille, G., Höfte, H., Pauly, M., Riechmann, J.L., and Broun, P. 2007. The transcription factor WIN1/SHN1 regulates cutin biosynthesis in *Arabidopsis thaliana*. *The Plant Cell* 19: 1248-1294.

Ketelaar, T., de Ruijter, N.C., and Emons, A.M.C. 2003. Unstable F-actin specifies the area and microtubule direction of cell expansion in Arabidopsis root hairs. *The Plant Cell 15*: 285-292.

Ketelaar, T., Galway, M.E., Mulder, B.M., and Emons, A.M.C. 2008. Rates of exocytosis and endocytosis in Arabidopsis root hairs and pollen tubes. *Journal of Microscopy*, 231: 265-273.

Kim, H., Lee, S.B., Kim, H.J., Min, M.K., Hwang, I., and Suh, M.C. 2012. Characterization of glycosylphosphatidylinositol-anchored lipid transfer protein 2 (LTPG2) and overlapping function between LTPG/LTPG1 and LTPG2 in cuticular wax export or accumulation in Arabidopsis thaliana. *Plant and Cell Physiology* 53:1391-403.

Kim, S., Yamaoka, Y., Ono, H., Kim, H., Shim, D., Maeshima, M., Martinoia, E., Cahoon, E.B., Nishida, I., and Lee, Y. 2013. AtABCA9 transporter supplies fatty acids for lipid synthesis to the endoplasmic reticulum. *Proceedings of the National Academy of Sciences, USA* 110: 773-778.

Kleine-Vehn, J., Dhonukshe, P., Swarup, R., Bennett, M., and Friml, J. 2006. Subcellular trafficking of the Arabidopsis auxin influx carrier AUX1 uses a novel pathway distinct from PIN1. *The Plant Cell* 18: 3171-3181.

Konopka, C.A., Backues, S.K., and Bednarek, S.Y. 2008. Dynamics of Arabidopsis dynamin-related protein 1C and a clathrin light chain at the plasma membrane. *The Plant Cell* 20: 1363-1380.

Koornneef, M., Hanhart, C.J., and Thiel, F. 1989. A genetic and phenotypic description of *eceriferum* (*cer*) mutants in *Arabidopsis thaliana*. *Journal of Heredity* 80: 118-122.

Kornmann, B., Currie, E., Collins, S.R., Schuldiner, M., Nunnari, J., Weissman, J.S., and Walter, P. 2009. An ER-mitochondria tethering complex revealed by a synthetic biology screen. *Science* 325: 477-481.

Kosma, D.K., Bourdenx, B., Bernard, A., Parsons, E.P., Lü, S., Joubès, J., and Jenks, M A. 2009. The impact of water deficiency on leaf cuticle lipids of Arabidopsis. *Plant Physiology* 151: 1918-1929.

Kuerschner, L., Ejsing, C.S., Ekroos, K., Shevchenko, A., Anderson, K.I., and Thiele, C. 2004. Polyene-lipids: a new tool to image lipids. *Nature Methods* 2: 39-45.

Kulich, I., Cole, R., Drdová, E., Cvrčková, F., Soukup, A., Fowler, J., and Žárský, V. 2010. Arabidopsis exocyst subunits SEC8 and EXO70A1 and exocyst interactor ROH1 are involved in the localized deposition of seed coat pectin. *New Phytologist* 188: 615–625.

Kunst, L., Browse, J., and Somerville, C. 1988. Altered regulation of lipid biosynthesis in a mutant of Arabidopsis deficient in chloroplast glycerol-3-phosphate acyltransferase activity. *Proceedings of the National Academy of Sciences, USA* 85: 4143-4147.

Kunst L. and Samuels, A.L. 2009. Plant cuticles shine: advances in wax biosynthesis and export. *Current Opinion in Plant Biology 12*: 721-727.

Kuromori, T., Miyaji, T., Yabuuchi, H., Shimizu, H., Sugimoto, E., Kamiya, A., Moriyama, Y., and Shinozaki, K. 2010. ABC transproter AtABCG25 is involved in abscisic acid transport and responses. *Proceedings of the National Academy of Sciences*, *USA* 107: 2361-2366.

Kuromori, T., Ito, T., Sugimoto, E., and Shinozaki, K. 2011. Arabidopsismutant of *AtABCG26*, an ABC transporter gene, is defective in pollen maturation. *Journal of Plant Physiology* 168: 2001-2005.

Kusano, H., Testerink, C., Vermeer, J.E.M., Tsuge, T., Shimada, H., Oka, A., Munnik, T., and Aoyama, T. 2008. The Arabidopsis phosphatidylinositol phosphate 5-kinase PIP5K3 is a key regulator of root hair tip growth. *The Plant Cell* 20: 367-380.

Lam, P., Zhao, L., McFarlane, H.E., Aiga, M., Lam, V., Hooker, T.S., and Kunst, L. 2012. RDR1 and SGS3, components of RNA-mediated gene silencing, are required for the regulation of cuticular wax biosynthesis in developing inflorescence stems of Arabidopsis. *Plant Physiology* 159: 1385-1395.

Larsson, C., Kjellbom, P., Widell, S., and Lundborg, T. 1984. Sidedness of plant plasma membrane vesicles purified by partitioning in aqueous two-phase systems. *FEBS Letters* 171: 271-276.

Larsson, K.E., Kellberg, J.M., Tjellström, H., and Sandelius, A.S. 2007. LysoPC acyltransferase/PC transacylase activities in plant plasma membrane and plasma membrane-associated endoplasmic reticulum. *BMC Plant Biology* 7: 64-75.

Lavieu, G., Orci, L., Shi, L., Geiling, M., Ravazzola, M., Wieland, F., Cosson, P., and Rothman, J.E. 2010. Induction of cortical endoplasmic reticulum by dimerization of a coatomer-binding peptide anchored to endoplasmic reticulum membranes. *Proceedings of the National Academy of Sciences*, USA 107: 6876-6881.

Lee, I. and Hong, W. 2006. Diverse membrane-associated proteins contain a novel SMP domain. *The FASEB Journal* 20: 202-206.

Lee, S.B., Go, Y.S., Bae, H.J., Park, J.H., Cho, S.H., Cho, H.J., Lee, D.S., Park, O.K., Hwang, I., Suh, M.C. 2009. Disruption of glycosylphosphatidylinositol-anchored lipid transfer protein gene altered cuticular lipid composition, increased plastoglobules, and enhanced susceptibility to infection by the fungal pathogen *Alternaria brassicicola*. *Plant Physiology* 150: 42-54.

Levine, T. 2004. Short-range intracellular trafficking of small molecules across endoplasmic reticulum junctions. *Trends in Cell Biology* 14: 483-490.

Levine, T. 2007. A lipid transfer protein that transfers lipid. *The Journal of Cell Biology* 179: 11-13.

Levine T. and Loewen, C.J. 2006. Inter-organelle membrane contact sites: through a glass, darkly. *Current Opinion in Cell Biology* 18: 371-378.

Lewis, J.D. and Lazarowitz, S.G. 2010. Arabidopsis synaptotagmin SYTA regulates endocytosis and virus movement protein cell-to-cell transport. *Proceedings of the National Academy of Sciences*, *USA* 107: 2491-2496.

Li, Y., Beisson, F., Koo, A.J., Molina, I., Pollard, M., and Ohlrogge, J. 2007. Identification of acyltransferases required for cutin biosynthesis and production of cutin with suberin-like monomers. *Proceedings of the National Academy of Sciences*, *USA* 104: 18339-18344.

Li, R., Liu, P., Wan, Y., Chen, T., Wang, Q., Mettbach, U., Baluška, F., Šamaj, J., Fang, X., Lucas, W.J., and Lin, J. 2012. A membrane microdomain-associated protein, Arabidopsis Flot1, is involved in a clathrin-independent endocytic pathway and is required for seedling development. *The Plant Cell* 24: 2105-2122.

Li, H., Pinot, F., Sauveplane, V., Werck-Reichhart, D., Diehl, P., Schreiber, L., Franke, R., Zhang, P., Chen, L., Gao, Y., Liang, W., and Zhang, D. 2010. Cytochrome P450 family member CYP704B2 catalyzes the ω-hydroxylation of fatty acids and is required for anther cutin biosynthesis and pollen exine formation in rice. *The Plant Cell* 22: 173-190.

Li, Y. and Prinz, W.A. 2004. ATP-binding cassette (ABC) transporters mediate nonvesicular, raft-modulated sterol movement from the plasma membrane to the endoplasmic reticulum. *The Journal of Biological Chemistry* 279: 45226-45234.

Li, F., Wu, X., Lam, P., Bird, D.A., Zheng, H., Samuels, A.L., Jetter, R., and Kunst, L. 2008. Identification of the wax ester synthase/acyl-CoA:diacylglycerol acyltransferase WSD1 required for stem wax ester biosynthesis in *Arabidopsis thaliana*. *Plant Physiology* 148: 97-107.

Lisboa, S., Scherer, G.E., and Quader, H. 2008. Localized endocytosis in tobacco pollen tubes: visualisation and dynamics of membrane retrieval by a fluorescent phospholipid. *Plant Cell Reports 27*: 21-28.

Liu, T.Y., Bian, X., Sun, S., Hu, X., Klemm, R.W., Prinz, W.A., Rapoport, T.A., and Hu, J. 2012. Lipid interaction of the C terminus and association of the transmembrane segments facilitate atlastin-mediated homotypic endoplasmic reticulum fusion. *Proceedings of the National Academy of Sciences, USA* 109: E2146-E2154.

Loewen, C.J. and Levine, T.P. 2005. A highly conserved binding site in vesicle-associated membrane protein-associated protein (VAP) for the FFAT motif of lipid-binding proteins. *Journal of Biological Chemistry* 280: 14097-14104.

Loewen, C.J., Roy, A., and Levine, T.P. 2003. A conserved ER targeting motif in three families of lipid binding proteins and in Opi1p binds VAP. *The EMBO Journal* 22: 2025-2035.

Loewen, C.J., Young, B.P., Tavassoli, S., and Levine, T.P. 2007. Inheritance of cortical ER in yeast is required for normal septin organization. *The Journal of Cell Biology* 179: 467-483.

Lou, B., Xue, X.Y., Hu, W.L., Want, L.J., and Chen, X.Y. 2007. An ABC transporter gene of *Arabidopsis thaliana*, *AtWBC11*, is involved in cuticle development and prevention of organ fusion. *Plant and Cell Physiology* 48: 1790-1802.

Lu, B., Xu, C., Awai, K., Jones, A.D., and Benning, C. 2007. A small ATPase protein of Arabidopsis, TGD3, involved in chloroplast lipid import. *The Journal of Biological Chemistry* 282: 35945-35953.

Lü, S., Song, T., Kosma, D.K., Parson, E.P., Rowland, O., and Jenks, M.A. 2009. Arabidopsis CER8 encodes a Long-Chain Acyl CoA Synthetase 1 (LACS1) and has overlapping functions with LACS2 in plant wax and cutin synthesis. The Plant Journal 59: 553-564.

Luik, R.M., Wu, M.M., Buchanan, J., and Lewis, R.S. 2006. The elementary unit of store-operated Ca2+ entry: local activation of CRAC channels by STIM1 at ER–plasma membrane junctions. *The Journal of Cell Biology* 174: 815-825.

Lundgren, D.H., Hwang, S.I., Wu, L., and Han, D.K. 2010. Role of spectral counting in quantitative proteomics. *Expert Review of Proteomics* 7: 39-53.

Mackenzie, S.M., Brooker, M.R., Gill, T.R. Cox, G.B., Howells, A.J., and Ewart, G.D. 1999. Mutations in the WHITE gene in *Drosophila melanogaster* affecting ABC transporters that determine eye coloration. *Biochmiica et Biophysica Acta* 1419: 173-185.

Mackenzie, S.M., Howells, A.J., Cox, G.B., and Ewart, G.D. 2000. Sub-cellular localisation of the white/scarlet ABC transporter to pigment granule membranes within the compound eye of *Drosophila melanogaster. Genetica* 108: 239–252.

Mahmoud, S.S. and Croteau, R.B. 2002. S trategies for transgenic manipulation of monoterpene biosynthesis in plants. *Trends in Plant Science* 7: 366-373.

Manford, A.G., Stefan, C.J., Yuan, H.L., MacGurn, J.A., and Emr, S.D. 2012. ER-to-Plasma Membrane Tethering Proteins Regulate Cell Signaling and ER Morphology. *Developmental Cell* 23: 1129-1140.

Markham, J.E., Molino, D., Gissot, L., Bellec, Y., Hématy, K., Marion, J., Belcram, K., Palauqui, J.C., Satiat-JeuneMaître, B., and Faure, J.D. 2011. Sphingolipids containing very-long-chain fatty acids define a secretory pathway for specific polar plasma membrane protein targeting in Arabidopsis. *The Plant Cell* 23: 2362-2378.

Marmagne, A., Rouet, M. A., Ferro, M., Rolland, N., Alcon, C., Joyard, J., Garin, J., Barbier-Brygoo, H., and Ephritikhine, G. 2004. Identification of new intrinsic proteins in Arabidopsis plasma membrane proteome. *Molecular and Cellular Proteomics* 3: 675-691.

Martínez, I.M., and Chrispeels, M.J. 2003. Genomic analysis of the unfolded protein response in Arabidopsis shows its connection to important cellular processes. *The Plant Cell* 15: 561–576.

Mayer, U., Buttner, G., and Jürgens, G. 1993. Apical-basal pattern formation in the Arabidopsis embryo: studies on the role of the gnom gene. *Development* 117: 149-162.

McFarlane, H.E., Shin, J.J., Bird, D.A., and Samuels, A.L. 2010. Arabidopsis ABCG transporters, which are required for export of diverse cuticular lipids, dimerize in different combinations. *The Plant Cell* 22: 3066-3075.

McFarlane, H.E., Watanabe, Y., Gendre, D., Carruthers, K., Levesque-Tremblay, G., Haughn, G.W., Bhalerao, R.P. and Samuels, A.L. 2013. The *echidna* mutant demonstrates that

pectic polysaccharides and proteins require distinct post-Golgi vesicle traffic machinery. In Preparation.

McFarlane, H.E., Young, R.E., Wasteneys, G.O., and Samuels, A.L. 2008. Cortical microtubules mark the mucilage secretion domain of the plasma membrane in Arabidopsis seed coat cells. *Planta* 227: 1363-1375.

Men, S., Boutté, Y., Ikeda, Y., Li, X., Palme, K., Stierhof, Y.D., Hartmann, M.A., Moritz, T., and Grebe, M. 2008. Sterol-dependent endocytosis mediates post-cytokinetic acquisition of PIN2 auxin efflux carrier polarity. *Nature Cell Biology* 10: 237-244.

Mentewab, A., and Stewart, C.N., Jr. 2005. Overexpression of an *Arabidopsis thaliana* ABC transporter confers kanamycin resistance to transgenic plants. *Nature Biotechnology* 23: 1177–1180.

Millar, A.A., Clemens, S., Zachgo, S., Giblin, E.M., Taylor, D.C., and Kunst, L. 1999. CUT1, an Arabidopsis gene required for cuticular wax biosynthesis and pollen fertility, encodes a very-long-chain fatty acid condensing enzyme. *The Plant Cell* 11: 825-838.

Moreau, P., Bessoule, J.J., Mongrand, S., Testet, E., Vincent, P., and Cassagne, C. 1998. Lipid trafficking in plant cells. *Progress in Lipid Research* 37: 371-391.

Moscatelli, A., Ciampolini, F., Rodighiero, S., Onelli, E., Cresti, M., Santo, N., and Idilli, A. 2007. Distinct endocytic pathways identified in tobacco pollen tubes using charged nanogold. *Journal of Cell Science* 120*:* 3804–3819*.*

Munnik, T. and Nielsen, E. 2011. Green light for polyphosphoinositide signals in plants. *Current Opinion in Plant Biology* 14: 489-497.

Nakano, R.T., Matsushima, R., Ueda, H., Tamura, K., Shimada, T., Li, L., Hayashi, Y., Kondo, M., Nishimura, M., and Hara-Nishimura, I. 2009. GNOM-LIKE1/ERMO1 and SEC24a/ERMO2 are required for maintenance of endoplasmic reticulum morphology in Arabidopsis thaliana. *The Plant Cell* 21: 3672-3685.

Naseer, S., Lee, Y., Lapierre, C., Franke, R., Nawrath, C., and Geldner, N. 2012. Casparian strip diffusion barrier in Arabidopsis is made of a lignin polymer without suberin. *Proceedings of the National Academy of Sciences*, USA 109: 10101-10106.

Nawrath, C. 2006. Unraveling the complex network of cuticular structure and function. *Current Opinion in Plant Biology* 9: 281-287.

Nebenführ, A., Gallagher, L.A., Dunahay, T.G., Frohlick, J.A., Mazurkiewicz, A.M., Meehl, J.B., and Staehelin, L.A. 1999. Stop-and-go movements of plant Golgi stacks are mediated by the acto-myosin system. *Plant Physiology* 121: 1127-1141.

Nebenführ, A. and Staehelin, L.A. 2001. Mobile factories: Golgi dynamics in plant cells. *Trends in Plant Science* 6: 160-167.

Nelson, C.J., Hegeman, A.D., Harms, A.C., and Sussman, M.R. 2006. A quantitative analysis of Arabidopsis plasma membrane using trypsin-catalyzed ^{18}O labeling. *Molecular and Cellular Proteomics* 5: 1382-1395.

Nielsen, E., Cheung, A.Y., and Ueda, T. 2008. The regulatory RAB and ARF GTPases for vesicular trafficking. *Plant Physiology* 147: 1516-1526.

Nishi, T., and Forgac, M. 2002. The vacuolar H^+-ATPases—nature's most versatile proton pumps. *Nature Reviews Molecular Cell Biology* 3: 94-103.

Ohlrogge, J. and Browse, J. 1995. Lipid biosynthesis. *The Plant Cell* 7: 957-970.

Oikawa, A., Lund, C.H., Sakuragi, Y., and Scheller, H.V. 2013. Golgi-localized enzyme complexes for plant cell wall biosynthesis. *Trends in Plant Science* 18: 49-58

Orci, L., Ravazzola, M., Le Coadic, M., Shen, W.W., Demaurex, N., and Cosson, P. 2009. STIM1-induced precortical and cortical subdomains of the endoplasmic reticulum. *Proceedings of the National Academy of Sciences*, *USA* 106: 19358-19362.

Palmgren, M.G., Askerlund, P., Fredrikson, K., Widell, S., Sommarin, M., and Larsson, C. 1990. Sealed inside-out and right-side-out plasma membrane vesicles: optimal conditions for formation and separation. *Plant Physiology* 92: 871-880.

Pan, X., Roberts, P., Chen, Y., Kvam, E., Shulga, N., Huang, K., Lemmon, S., and Goldfarb, D. S. 2000. Nucleus–vacuole junctions in *Saccharomyces cerevisiae* are formed through the direct interaction of Vac8p with Nvj1p. *Molecular Biology of the Cell* 11: 2445-2457.

Panikashvili, D., Savaldi-Goldstein, S., Mandel, T., Yifhar, T., Franke, R.B., Höfer, R., Schreiber, L., Chory, J., and Aharoni, A. 2007. The Arabidopsis DESPERADO/AtWBC11 transporter is required for cutin and wax secretion. *Plant Physiology* 145: 1345-1360.

Panikashvili, D., Shi, J.X., Bocobza, S., Franke, R.B., Schreiber, L., and Aharoni, A. 2010. The Arabidopsis DSO/ABCG11 transporter affects cutin metabolism in reproductive organs and suberin in roots. *Molecular Plant* 3: 563–575.

Panikashvili, D., Shi, J.X., Schreiber, L., and Aharoni, A. 2011. The Arabidopsis ABCG13 transporter is required for flower cuticle secretion and patterning of the petal epidermis. *New Phytologist* 190: 113-124.

Parsons, H.T., Christiansen, K., Knierim, B., Carroll, A., Ito, J., Batth, T.S., Smith-Moritz, A.M., Morrison, S., McInerney, P., Hadi, M.Z., Auer, M., Mukhopadhyay, A., Petzold, C.J., Scheller, H.V., Loqué, D., and Heazlewood, J. L. 2012. Isolation and proteomic

characterization of the Arabidopsis Golgi defines functional and novel components involved in plant cell wall biosynthesis. *Plant Physiology* 159: 12-26.

Pascal, S., Bernard, A., Sorel, M., Pervent, M., Vile, D., Haslam, R. P., Napier, J.A., Lessire, R., Domergue, F., and Joubès, J. 2013. The Arabidopsis *cer26* mutant, like the *cer2* mutant, is specifically affected in the very long chain fatty acid elongation process. *The Plant Journal* 73: 733–746.

Peremyslov, V.V., Prokhnevsky, A.I., Avisar, D., and Dolja, V.V. 2008. Two class XI myosins function in organelle trafficking and root hair development in Arabidopsis. *Plant Physiology* 146: 1109-1116.

Pichler, H., Gaigg, B., Hrastnik, C., Achleitner, G., Kohlwein, S.D., Zellnig, G., Perktold, A., and Daum, G. 2001. A subfraction of the yeast endoplasmic reticulum associates with the plasma membrane and has a high capacity to synthesize lipids. *European Journal of Biochemistry* 268: 2351-2361.

Pighin, J.A., Zheng, H., Balakshin, L.J., Goodman, I.P., Western, T.L., Jetter, R., Kunst, L., and Samuels, A.L. 2004. Plant cuticular lipid export requires an ABC transporter. *Science* 306: 702-704.

Pollard, M., Beisson, F., Li, Y., and Ohlrogge, J.B. 2008. Building lipid barriers: biosynthesis of cutin and suberin. *Trends in Plant Science* 13: 236-246.

Preuss D., Lemieux B., Yen G., and Davis R.W. 1993. A conditional sterile mutation eliminates surface components from Arabidopsis pollen and disrupts cell signaling during fertilization. *Genes and Development* 7: 974–985.

Preuss, M.L., Schmitz, A.J., Thole, J.M., Bonner, H.K., Otegui, M.S., and Nielsen, E. 2006. A role for the RabA4b effector protein PI-4Kbeta1 in polarized expansion of root hair cells in Arabidopsis thaliana. *The Journal of Cell Biology* 172: 991-998.

Pulsifer, I.P., Kluge, S., and Rowland, O. 2012. Arabidopsis LONG-CHAIN ACYL-COA SYNTHASE 1 (LACS1), LACS2, and LACS3 facilitate fatty acid uptake in yeast. *Plant Physiology and Biochemistry* 51: 31-39.

Qi, X., Kaneda, M., Chen, J., Geitmann, A., and Zheng, H. 2011. A specific role for Arabidopsis TRAPPII in post-Golgi trafficking that is crucial for cytokinesis and cell polarity. *The Plant Journal* 68: 234–248.

Quilichini T.D., Friedmann, M., Samuels, A.L., and Douglas, C.J. 2010. ATP-binding cassette transporter G26 (ABCG26) is required for male fertility and pollen exine formation in Arabidopsis. *Plant Physiology* 154: 678-690.

Raffaele, S., Vailleau, F., Léger, A., Joubès, J., Miersch, O., Huard, C., Blée, E., Mongrand, S., Domergue, F., and Roby, D. 2008. A MYB transcription factor regulates very-long-chain

fatty acid biosynthesis for activation of the hypersensitive cell death response in Arabidopsis. *The Plant Cell* 20: 752-767.

Raven, J. A., and Edwards, D. (2004). *Physiological evolution of lower embryophytes: adaptations to the terrestrial environment* in Hemsley, A. and Poole, I. (eds.) *The Evolution of Plant Physiology: From Whole Plants to Ecosystems.* Elsevier Publishing. p. 17-41.

Raychaudhuri, S., Im, Y.J., Hurley, J.H., and Prinz, W.A. 2006. Nonvesicular sterol movement from plasma membrane to ER requires oxysterol-binding protein-related proteins and phosphoinositides. *The Journal of Cell Biology* 173: 107-119.

Raychaudhuri, S. and Prinz, W.A. 2008. Nonvesicular phospholipid transfer between peroxisomes and the endoplasmic reticulum. PNAS 105: 15785-15790.

Reynolds, E.S. 1963. The use of lead citrate at high pH as an electron-opaque stain in electron microscopy. *The Journal of Cell Biology* 17: 208-212.

Richter, S., Geldner, N., Schrader, J., Wolters, H., Stierhof, Y.D., Rios, G., Robinson, D.G., and Jürgens, G. 2007. Functional diversification of closely related ARF-GEFs in protein secretion and recycling. *Nature* 448: 488-492.

Ridge, R.W., Uozumi, Y., Plazinski, J., Hurley, U.A., and Williamson, R.E. 1999. Developmental transitions and dynamics of the cortical ER of Arabidopsis cells seen with green fluorescent protein. *Plant and Cell Physiology 40*: 1253-1261.

Riederer, M. 2006. *Introduction: biology of the plant cuticle* in Riederer, M. and Müller, C. (eds.) *Biology of the Plant Cuticle*. Blackwell Publishing. p. 1-10.

Riederer, M. and Schreiber, L. 2001. Protecting against water loss: analysis of the barrier properties of plant cuticles. *Journal of Experimental Botany* 52: 2023-2032.

Robinson, D.G., Jaing, L., and Schumacher, K. 2008. The endosomal system of plants: charting new and familiar territories. Plant Physiology 147: 1482-1492.

Rosset, A., Spadola, L., and Ratib, O. 2004. OsiriX: an open-source software for navigating in multidimensional DICOM images. *Journal of Digital Imaging* 17: 205-216.

Roston, R.L., Gao, J., Murcha, M.W., Whelan, J., and Benning, C. 2012. TGD1,-2, and-3 proteins involved in lipid trafficking form ATP-binding cassette (ABC) transporter with multiple substrate-binding broteins. *Journal of Biological Chemistry 287*: 21406-21415.

Roston, R., Gao, J., Xu, C., and Benning, C. 2011. Arabidopsis chloroplast lipid transport protein TGD2 disrupts membranes and is part of a large complex. *The Plant Journal* 66: 759–769.

Roudier, F., Gissot, L., Beaudoin, F., Haslam, R., Michaelson, L., Marion, J., Molino, D., Lima, A, Back, L., Morin, H., Tellier, F., Palauqui, J.C., Bellec, Y., Renne, C., Miquel, M., DaCosta, M., Vignard, J., Rochat, C., Markham, J.E., Moreau, P., Napier, J., and Faure, J.D. 2010. Very-long-chain fatty acids are involved in polar auxin transport and developmental patterning in Arabidopsis. *The Plant Cell* 22: 364-375.

Rowland, O., Zheng H., Hepworth, S.R., Lam, P., Jetter, R., and Kunst, L. 2006. *CER4* encodes an alcohol-forming fatty acyl-coenzyme A reductase involved in cuticular wax production in Arabidopsis. *Plant Physiology* 142: 866-877.

Saeed, A.I., Bhagabati, N.K., Braisted, J.C., Liang, W., Sharov, V., Howe, E.A., Li, J., Thiagarajan, M., White, J.A., and Quackenbush, J. 2006. TM4 Microarray Software Suite. *Methods in Enzymology* 411: 134-193.

Sakuradani, E., Zhao, L., Haslam, T.M., and Kunst, L. 2012 . The CER22 gene required for the synthesis of cuticular wax alkanes in Arabidopsis thaliana is allelic to CER1. *Planta* In Press: DOI 10.1007/s00425-012-1791-y

Sampathkumar, A., Gutierrez, R., McFarlane, H.E., Bringmann, M., Lindeboom, J.J., Emons, A.M., Ehrardt, D.W., Samuels, A.L., Ketelaar, T., and Persson, S. 2013. Impairment of the actin cytoskeleton leads to uneven cell wall distribution and to perturbations in cellulose synthase insertions into the plasma membrane. In Review.

Samuel, M.A., Chong, Y.T., Haasen, K.E., Aldea-Brydges, M.G., Stone, S.L., and Goring, D.R. 2009. Cellular pathways regulating responses to compatible and self-incompatible pollen in Brassica and Arabidopsis stigmas intersect at Exo70A1, a putative component of the exocyst. *The Plant Cell* 21: 2655-2671.

Samuels, A.L., Kunst, L., and Jetter, R. 2008. Sealing plant surfaces: cuticular wax formation by epidermal cells. *Annual Review of Plant Biology* 59: 683-707.

Samuels, A.L., and McFarlane, H.E. 2012. Plant cell wall secretion and lipid traffic at membrane contact sites of the cell cortex. *Protoplasma* S1: 19-23.

Sánchez-Fernández, R., Davies, T.E., Coleman, J.O., and Rea, P.A. 2001 . The Arabidopsis thaliana ABC protein superfamily, a complete inventory. *Journal of Biological Chemistry* 276: 30231-30244.

Sandelius, A.S., Penel, C., Auderset, G., Brightman, A., Millard, M., and Morré, D.J. 1986. Isolation of highly purified fractions of plasma membrane and tonoplast from the same homogenate of soybean hypocotyls by free-flow electrophoresis. *Plant Physiology* 81: 177-185.

Sanderfoot, A.A., Kovaleva, V., Bassharm, D.C., and Raikhel, N.V. 2001. Interactions between syntaxins identify at least five SNARE complexes within the Golgi/prevacuolar system of the Arabdipsis cell. *Molecular Biology of the Cell* 12: 3733-3743.

Sanderfoot, A.A. and Raikhel, N.V. 2003. *The secretory system of Arabidopsis* in Somerville, C.R. and Meyerowitz, E.M. (eds.) *The Arabidopsis Book*. American Society of Plant Biologists.

Santoni, V., Kieffer, S., Desclaux, D., Masson, F., and Rabilloud, T. 2000. Membrane proteomics: use of additive main effects with multiplicative interaction model to classify plasma membrane proteins according to their solubility and electrophoretic properties. *Electrophoresis* 21: 3329-3344.

Saravanan, R.S., Slabaugh, E., Singh, V.R., Lapidus, L.J., Haas, T., and Brandizzi, F. 2009. The targeting of the oxysterol-binding protein ORP3a to the endoplasmic reticulum relies on the plant VAP33 homolog PVA12. *The Plant Journal* 58: 817-830.

Schapire, A.L., Voigt, B., Jasik, J., Rosado, A., Lopez-Cobollo, R., Menzel, D., Salinas, J., Mancuso, S., Valpuesta, V., Baluska, F., and Botella, M.A. 2008. Arabidopsis Synaptotagmin 1 is required for the maintenance of plasma membrane integrity and cell viability. *The Plant Cell* 20: 3374-3388.

Schattat, M., Barton, K., Baudisch, B., Klösgen, R.B., and Mathur, J. 2011. Plastid stromule branching coincides with contiguous endoplasmic reticulum dynamics. *Plant Physiology* 155: 1667-1677.

Schneider-Belhaddad, F. and Kolattukudy, P.E. 2000. Solubilization, partial purification and characterization of a fatty aldehyde decarbonylase from a higher plant, *Pisum sativum*. *Archives of Biochemistry and Biophysics 377*: 341-349.

Schuck, S., Prinz, W.A., Thorn, K.S., Voss, C., and Walter, P. 2009. Membrane expansion alleviates endoplasmic reticulum stress independently of the unfolded protein response. *Journal of Cell Biology* 187: 525–536.

Schuetz, M., Smith, R., and Ellis, B. 2012. Xylem tissue specification, patterning, and differentiation mechanisms. *Journal of Experimental Botany* 64: 11-31.

Schulz, T.A., Choi, M.G., Raychaudhuri, S., Mears, J.A., Ghirlando, R., Hinshaw, J.E., and Prinz, W.A. 2009. Lipid-regulated sterol transfer between closely apposed membranes by oxysterol-binding protein homologues. *The Journal of Cell Biology* 187: 889-903.

Seo, P.J., Lee, S.B., Suh, M.C., Park, M.J., Go, Y.S., and Park, C.M. 2011. The MYB96 transcription factor regulates cuticular wax biosynthesis under drought conditions in Arabidopsis. *The Plant Cell* 23: 1138-1152.

Sherrier, D.J., Prime, T.A., and Dupree, P. 1999. Glycosylphosphatidylinositol-anchored cell-surface proteins from Arabidopsis. *Electrophoresis* 20: 2027-2035.

Shockey, J.M., Gidda, S.K., Chapital, D.C., Kuan, J.C., Dhanoa, P.K., Bland, J.M., Rothstein, S.J., Mullen, R.T., and Dyer, J.M. 2006. Tung tree DGAT1 and DGAT2 have nonredundant functions in triacylglycerol biosynthesis and are localized to different subdomains of the endoplasmic reticulum. *The Plant Cell* 18: 2294-2313.

Sieber, P., Schorderet, M., Ryser, U., Buchala, A., Kolattukudy, P., Métraux, J.P., and Nawrath, C. 2000. Transgenic Arabidopsis plants expressing a fungal cutinase show alterations in the structure and properties of the cuticle and postgenital organ fusions. *The Plant Cell* 12: 721-737.

Signore, G., Nifosì, R., Albertazzi, L., Storti, B., and Bizzarri, R. 2010. Polarity-sensitive coumarins tailored to live cell imaging. *Journal of the American Chemical Society* 132: 1276-1288.

Skirpan, A.L., Dowd, P.E., Sijacic, P., Jaworski, C.J., Gilroy, S., and Kao, T.H. 2006. Identification and characterization of PiORP1, a Petunia oxysterol-binding-protein related protein involved in receptor-kinase mediated signaling in pollen, and analysis of the ORP gene family in Arabidopsis. *Plant Molecular Biology* 61: 553-565.

Snapp, A.R., and Lu, C. 2012. Engineering industrial fatty acids in oilseeds. *Frontiers in Biology* DOI: 10.1007/s11515-012-1228-9: 1-10

Sparkes, I., Frigerio, L., Tolley, N., and Hawes, C. 2009a. The plant endoplasmic reticulum: a cell-wide web. *Biochemical J*ournal 423: 145-155.

Sparkes, I., Runions, J., Hawes, C., and Griffing, L. 2009b. Movement and remodeling of the endoplasmic reticulum in nondividing cells of tobacco leaves. *The Plant Cell* 21: 3937-3949.

Sparkes, I., Tolley, N., Aller, I., Svozil, J., Osterrieder, A., Botchway, S., Mueller, C., Frigerio, L., and Hawes, C. 2010. Five Arabidopsis reticulon isoforms share endoplasmic reticulum location, topology, and membrane-shaping properties. *The Plant Cell* 22: 1333-1343.

Sperling, P., Franke, S., Lüthje, S., and Heinz, E. 2005. Are glucocerebrosides the predominant sphingolipids in plant plasma membranes? *Plant Physiology and Biochemistry*, 43: 1031-1038.

Spurr, A.R. 1969. A low-viscosity epoxy resin embedding medium for electron microscopy. *Journal of Ultrastructure Research* 26: 31-43.

Staehelin, L.A. 1997. The plant ER: a dynamic organelle composed of a large number of discrete functional domains. *The Plant Journal* 11: 1151-1165.

Staehelin, L.A. and Chapman, R.L. 1987. Secretion and membrane recycling in plant cells: novel intermediary structures visualized in ultrarapidly frozen sycamore and carrot suspension-culture cells. *Planta* 171: 43-57.

Staehelin, L.A. and Kang, B.H. 2008. Nanoscale architecture of endoplasmic reticulum export sites and of Golgi membranes as determined by electron tomography. *Plant Physiology* 147: 1454-1468.

Staehelin, L.A. and Moore, I. 1995. The plant Golgi apparatus: structure, functional organization, and trafficking mechanisms. *Annual Review of Plant Physiology and Plant Molecular Biology* 46: 261-288.

Stefan, C.J., Manford, A.G., Baird, D., Yamada-Hanff, J., Mao, Y., and Emr, S. D. 2011. Osh proteins regulate phosphoinositide metabolism at ER-plasma membrane contact sites. *Cell* 144: 389-401.

Stradalova, V., Blazikova, M., Grossmann, G., Opekarová, M., Tanner, W., and Malinsky, J. 2012. Distribution of cortical endoplasmic reticulum determines positioning of endocytic events in yeast plasma membrane. *PloS One* 7: e35132.

Suh, M.C., Samuels, A.L., Jetter, R., Kunst, L., Pollard, M., Ohlrogge, J., and Beisson, F. 2005. Cuticular lipid composition, surface structure, and gene expression in Arabidopsis stem epidermis. *Plant Physiology* 139: 1649-1665.

Sullivan, D.T., Bell, L.A., Paton, D.R., and Sullivan, M.C. 1979. Purine transport by Malpighian tubules of pteridine-deficient eye color mutants of *Drosophila melanogaster*. *Biochemical Genetics* 17: 565-573.

Sullivan, D.T., Bell, L.A., Paton, D.R., and Sullivan, M.C. 1980. Genetic and functional analysis of tryptophan transport in Malpighian tubules of Drosophila. *Biochemical Genetics* 18: 1109–1130.

Sullivan, D.P., Georgiev, A., and Menon, A.K. 2009. Tritium suicide selection identifies proteins involved in the uptake and intracellular transport of sterols in *Saccharomyces cerevisiae*. *Eukaryotic Cell* 8: 161-169.

Sullivan, D.T. and Sullivan, M.C. 1975. Transport defects as the physiological basis for eye color mutants of Drosophila melanogaster. *Biochemical Genetics* 13: 603-613.

Takeuchi, M., Ueda, T., Sato, K., Abe, H., Nagata, T., and Nakano, A. 2000. A dominant negative mutant of Sar1 GTPase inhibits protein transport from the endoplasmic reticulum to the Golgi apparatus in tobacco and *Arabidopsis* cultured cells. *The Plant Journal* 23: 517–525.

Tanaka, T., Tanaka, H., Machida, C., Watanabe, M., and Machida, Y. 2004. A new method for rapid visualization of defects in leaf cuticle reveals five intrinsic patterns of surface defects in Arabidopsis. *The Plant Journal* 37: 139-146.

Tarr, P.T., Tarling, E.J., Bojanic, D.D., Edwards, P.A., and Baldán, A. 2009. Emerging new paradigms for ABCG transporters. *Biochimica et Biophysica Acta* 1791: 584-593.

Teh, O.K. and Moore, I. 2007. An ARF-GEF acting at the Golgi and in selective endocytosis in polarized plant cells. *Nature* 448: 493-496.

Thibault, G., Shui, G., Kim, W., McAlister, G.C., Ismail, N., Gygi, S.P., Wenk, M.R., and Ng, D.T. 2012. The membrane stress response buffers lethal effects of lipid disequilibrium by reprogramming the protein homeostasis network. *Molecular Cell* 48: 16-27.

Thole, J.M., Vermeer, J.E.M., Zhang, Y., Gadella, T.W.J., and Nielsen, E. 2008. Root hair defective4 encodes a phosphatidylinositol-4-phosphate phosphatase required for proper root hair development in *Arabidopsis thaliana*. *The Plant Cell* 20: 381-395.

Tiwari, S., Wang, S., Hagen, G., and Guilfoyle, T.J. 2006. Transfection assays with protoplasts containing integrated reporter genes. *Methods in Molecular Biology* 323: 237–244.

Tjellström, H., Andersson, M.X., Larsson, K.E., and Sandelius, A.S. 2008. Membrane phospholipids as a phosphate reserve: the dynamic nature of phospholipid-to-digalactosyl diacylglycerol exchange in higher plants. *Plant, Cell and Environment* 31: 1388-1398.

Tjellström, H., Hellgren, L.I., Wieslander, Å., and Sandelius, A.S. 2010 . Lipid asymmetry in plant plasma membranes: phosphate deficiency-induced phospholipid replacement is restricted to the cytosolic leaflet. *The FASEB Journal* 24: 1128-1138.

Tolley, N., Sparkes, I.A., Hunter, P.R., Craddock, C.P., Nuttall, J., Roberts, L.M., Hawes, C., Pedrazzini, E., and Frigerio, L. 2007. Overexpression of a plant reticulon remodels the lumen of the cortical endoplasmic reticulum but does not perturb protein transport. *Traffic* 9: 94-102.

Toufighi, K., Brady, S.M., Austin, R., Ly, E., and Provart, N.J. 2005. The Botany Array Resource: e-Northerns, expression angling, and promoter analyses. *The Plant Journal* 43: 153–163.

Toulmay, A. and Prinz, W.A. 2011. Lipid transfer and signaling at organelle contact sites: the tip of the iceberg. *Current Opinion in Cell Biology* 23: 458-463.

Toulmay, A. and Prinz, W.A. 2012. A conserved membrane-binding domain targets proteins to organelle contact sites. *Journal of Cell Science* 125: 49-58.

Toyooka, K., Goto, Y., Asatsuma, S., Koizumi, M., Mitsui, T., and Matsuoka, K. 2009. A mobile secretory vesicle cluster involved in mass transport from the Golgi to the plant cell exterior. *The Plant Cell* 21: 1212-1229.

Ukitsu, H., Kuromori, T., Toyooka, K., Goto, Y., Matsuoka, K., Sakuradani, E., Shimizu, S., Kamiya, A., Imura, Y., Yuguchi, M., Wada, T., Hirayama, T., and Shinozaki, K. 2007. Cytological and biochemical analysis of *cof1*, an Arabidopsis mutant of an ABC transporter gene. *Plant and Cell Physiology* 48: 1524-1533.

Van Gisbergen, P.A.C., Esseling-Ozdoba, A., and Vos, J.W. 2008. Microinjecting FM4–64 validates it as a marker of the endocytic pathway in plants. *Journal of Microscopy* 231: 284-290.

Vermeer, J.E.M., Thole, J.M., Goedhart, J., Nielsen, E., Munnik, T., and Gadella Jr, T.W.J. 2008. Imaging phosphatidylinositol 4-phosphate dynamics in living plant cells. *The Plant Journal* 57: 356-372.

Vermeer, J.E.M., Van Leeuwen, W., Tobeña-Santamaria, R., Laxalt, A.M., Jones, D.R., Divecha, N., Gadella Jr., T.W.J., and Munnik, T. 2006. Visualization of PtdIns3P dynamics in living plant cells. *The Plant Journal* 47: 687-700.

Verrier, P.J., Bird, D.A., Burla, B., Dassa, E., Forestier, C., Geisler, M., Klein, M., Kolukisaoglu, U., Lee, Y., Martinoia, E., Murphy, A., Rea, P.A., Samuels, A.L., Schulz, B., Spalding, E.J., Yazaki, K., and Theodoulou, F.L. 2008. Plant ABC proteins - a unified nomenclature and updated inventory. *Trends in Plant Science* 13: 151-159.

Vincent, P., Chua, M., Nogue, F., Fairbrother, A., Mekeel, H., Xu, Y., Allen, N., Bibikova, T.N., Gilroy, S., and Bankaitis, V.A. 2005. A Sec14p-nodulin domain phosphatidylinositol transfer protein polarizes membrane growth of Arabidopsis thaliana root hairs. *The Journal of Cell Biology* 168: 801-812.

Viotti, C., Bubeck, J., Stierhof, Y.D., Krebs, M., Langhans, M., van den Berg, W., van Dongen, W., Richter, S., Geldner, N., Takano, J., Jürgens, G., de Vries, S.C., Robinson, D.G., and Schumacher, K. 2010. Endocytic and secretory traffic in Arabidopsis merge in the trans-Golgi network/early endosome, an independent and highly dynamic organelle. *The Plant Cell 22*: 1344-1357.

Voeltz, G.K., Prinz, W.A., Shibata, Y., Rist, J.M., and Rapoport, T.A. 2006. A class of membrane proteins shaping the tubular endoplasmic reticulum. *Cell* 124: 573-586.

Voss, C., Lahiri, S., Young, B.P., Loewen, C.J., and Prinz, W.A. 2012. ER-shaping proteins facilitate lipid exchange between the ER and mitochondria in *S. cerevisiae. Journal of Cell Science* 125: 4791–4799.

Waizenegger, I., Lukowitz, W., Assaad, F., Schwarz, H., Jürgens, G., and Mayer, U. 2000. The Arabidopsis KNOLLE and KEULE genes interact to promote vesicle fusion during cytokinesis. *Current Biology* 10: 1371–1374.

Wang, J., Ding, Y., Wang, J., Hillmer, S., Miao, Y, Lo, S.W., Wang, X., Robinson, D.G., and Jiang, L. 2010. EXPO, an exocyst-positive organelle distinct from multivesicular endosomes

and autophagosomes, mediates cytosol to cell wall exocytosis in Arabidopsis and tobacco cells. *The Plant Cell* 22: 4009-4030.

Wang, J., Sun, F., Zhang, D.W., Ma, Y., Xu, F., Belani, J.D., Cohen, J.C., Hobbs, H.H., and Xie, X.S. 2005. Sterol transfer by ABCG5 and ABCG8: in vitro assay and reconstitution. *The Journal of Biological Chemistry* 281: 27894-27904.

Wang, Z., Xu, C., and Benning, C. 2012. TGD4 involved in endoplasmic reticulum-to-chloroplast lipid trafficking is a phosphatidic acid binding protein. *The Plant Journal* 70: 614–623.

Wellesen, K., Durst, F., Pinot, F., Benveniste, I., Nettesheim, K., Wisman, E., Steiner-Lange, S., Saedler, H., and Yephremov, A. 2001. Functional analysis of the LACERATA gene of Arabidopsis provides evidence for different roles of fatty acid ω-hydroxylation in development. *Proceedings of the National Academy of Science of the USA* 98: 9694-9699.

West, G., Viitanen, L., Alm, C., Mattjus, P., Salminen, T.A., and Edqvist, J. 2008. Identification of a glycosphingolipid transfer protein GLTP1 in *Arabidopsis thaliana*. *FEBS Journal* 275: 3421-3437.

West, M., Zurek, N., Hoenger, A., and Voeltz, G.K. 2011. A 3D analysis of yeast ER structure reveals how ER domains are organized by membrane curvature. *The Journal of Cell Biology* 193: 333-346.

Whitlock, M., and Schluter, D. 2009. *The Analysis of Biological Data*. (Greenwood Village, CO: Roberts and Co. Publishers).

Whittington, A.T., Vugrek, O., Wei, K.J., Hasenbein, N.G., Sugimoto, K., Rashbrooke, M.C., and Wasteneys, G.O. 2001. MOR1 is essential for organizing cortical microtubules in plants. *Nature* 411: 610-613.

Willemsen, V., Friml, J., Grebe, M., Van Den Toorn, A., Palme, K., and Scheres, B. 2003. Cell polarity and PIN protein positioning in Arabidopsis require STEROL METHYLTRANSFERASE1 function. *The Plant Cell* 15: 612-625.

Wolf, W., Kilic, A., Schrul, B., Lorenz, H., Schwappach, B., and Seedorf, M. 2012. Yeast Ist2 recruits the endoplasmic reticulum to the plasma membrane and creates a ribosome-free membrane microcompartment. *PloS One* 7: e39703.

Wu, M.M., Buchanan, J., Luik, R.M., and Lewis, R.S. 2006. Ca^{2+} store depletion causes STIM1 to accumulate in ER regions closely associated with the plasma membrane. *The Journal of Cell Biology* 174: 803-813.

Wu, R., Li, S., He, S., Waßmann, F., Yu, C., Qin, G., Schreiber, L., Qu, L.J., and Gu, H. 2011. CFL1, a WW domain protein, regulates cuticle development by modulating the function of

HDG1, a class IV homeodomain transcription factor, in rice and Arabidopsis. *The Plant Cell* 23: 3392-3411.

Xiao, F., Goodwin, S.M., Xiao, Y., Sun, Z., Baker, D., Tang, X., Jenks, M.A., and Zhou, J.M. 2004. Arabidopsis CYP86A2 represses Pseudomonas syringae type III genes and is required for cuticle development. *The EMBO Journal* 23: 2903-2913.

Xu, C., Fan, J., Riekhof, W., Froehlich, J.E., and Benning C. 2003. A permease-like protein involved in ER to thylakoid lipid transfer in Arabidopsis. *The EMBO Journal* 22: 2370-2379.

Xu, C., Fan, J., Cornish, A.J., and Benning C. 2008. Lipid trafficking between the endoplasmic reticulum and the plastid in Arabidopsis requires the extraplastidic TGD4 protein. *The Plant Cell* 20: 2190-2204.

Xu, C., Moellering, E.R., Muthan, B., Fan, J., and Benning, C. 2010. Lipid transport mediated by Arabidopsis TGD proteins is unidirectional from the endoplasmic reticulum to the plastid. *Plant and Cell Physiology* 51: 1019-1028.

Xu, J., Yang, C., Yuan, Z., Zhang, D., Gondwe, M.Y., Ding, Z., Liang, W., Zhang, D., and Wilson, Z.A. 2010. The ABORTED MICROSPORES regulatory network is required for postmeiotic male reproductive development in *Arabidopsis thaliana. The Plant Cell* 22: 91–107.

Yamazaki, T., Kawamura, Y., Minami, A., and Uemura, M. 2008. Calcium-dependent freezing tolerance in Arabidopsis involves membrane resealing via synaptotagmin SYT1. *The Plant Cell* 20: 3389-3404.

Yang, H. and Murphy, A.S. 2009. Functional expression and characterization of Arabidopsis ABCB, AUX 1 and PIN auxin transporters in *Schizosaccharomyces pombe*. *The Plant Journal* 59: 179-191.

Yang, Z. 2008 . Cell polarity signaling in Arabidopsis. *Annual Review of Cell and Developmental Biology 24*: 551.

Yang, S., Yang, H., Grisafi, P., Sanchatjate, S., Fink, G. R., Sun, Q. and Hua, J. 2006. The *BON/CPN* gene family represses cell death and promotes cell growth in Arabidopsis. *The Plant Journal* 45: 166–179.

Yeats, T.H., Martin, L.B., Viart, H.M., Isaacson, T., He, Y., Zhao, L., Matas, A.J., Buda, G.J., Domozych, D.S., Clausen, M.H. and Rose, J.K.C. 2012. The identification of cutin synthase: formation of the plant polyester cutin. *Nature Chemical Biology* 8: 609-611.

Yeats, T.H. and Rose, J.K.C. 2008. The biochemistry and biology of extracellular plant lipid transfer proteins (LTPs). *Protein Science* 17: 191-198.

Yong, Z., Kotur, Z., and Glass, A.D. 2010. Characterization of an intact two-component high-affinity nitrate transporter from Arabidopsis roots. *The Plant Journal* 63: 739–748.

Young, R.E., McFarlane, H.E., Hahn, M.G., Western, T.L., Haughn, G.W., and Samuels, A.L. 2008. Analysis of the Golgi apparatus in Arabidopsis seed coat cells during polarized secretion of pectin-rich mucilage. *The Plant Cell* 20: 1623-1638.

Zhang, Q., Blaylock, L.A., and Harrison, M.J. 2010. Two *Medicago truncatula* half-ABC transporters are essential for arbuscule development in arbuscular mycorrhizal symbiosis. *The Plant Cell* 22: 1483–1497.

Zhang, Z.J., and Peck, S.C. 2011. Simplified enrichment of plasma membrane proteins for proteomic analyses in *Arabidopsis thaliana*. *Proteomics* 11: 1780-1788.

Zhang, D., Vjestica, A., and Oliferenko, S. 2010. The cortical ER network limits the permissive zone for actomyosin ring assembly. *Current Biology* 20: 1029-1034.

Zhang, D., Vjestica, A., and Oliferenko, S. 2012. Plasma membrane tethering of the cortical ER necessitates its finely reticulated architecture. *Current Biology* 22: 2048–2052.

Zhao, Y., Yan, A., Feijó, J. A., Furutani, M., Takenawa, T., Hwang, I., Fu, Y., and Yang, Z. 2010. Phosphoinositides regulate clathrin-dependent endocytosis at the tip of pollen tubes in Arabidopsis and tobacco. *The Plant Cell* 22: 4031-4044.

Zheng, H., Kunst, L., Hawes, C., and Moore, I. 2004. A GFP-based assay reveals a role for RHD3 in transport between the endoplasmic reticulum and Golgi apparatus. *The Plant Journal* 37: 398-414.

Zheng, H., Rowland, O., and Kunst, L. 2005. Disruptions of the Arabidopsis enoyl-CoA reductase gene reveal an essential role for very-long-chain fatty acid synthesis in cell expansion during plant morphogenesis. *The Plant Cell* 17: 1467-1481.